EDITORIAL STAFF

R. M. Burns, *Chairman*
Norman Hackerman, *Technical Editor*
Ruth G. Sterns, *Managing Editor*
Cecil V. King, *Acting Editor*
U. B. Thomas, *News Editor*
Natalie Michalski, *Assistant Editor*
Eleanor Blair, *Assistant Editor*

DIVISIONAL EDITORS

W. C. Vosburgh, *Battery*
J. V. Petrocelli, *Corrosion*
John J. Chapman, *Electric Insulation*
Abner Brenner, *Electrodeposition*
H. C. Froelich, *Electronics*
Sherlock Swann, Jr., *Electro-Organic*
Irvin R. Kramer, *Electrothermics and Metallurgy, I*
A. U. Seybolt, *Electrothermics and Metallurgy, II*
W. C. Gardiner, *Industrial Electrolytic*
Carl Wagner, *Theoretical*

REGIONAL EDITORS

Howard T. Francis, *Chicago*
Joseph Schulein, *Pacific Northwest*
J. C. Schumacher, *Los Angeles*
G. W. Heise, *Cleveland*
Paul S. Brallier, *Niagara Falls*
Oliver Osborn, *Houston*
Earl A. Gulbransen, *Pittsburgh*
A. C. Holm, *Canada*
J. W. Cuthbertson, *Great Britain*
T. L. Rama Char, *India*

ADVERTISING OFFICE

Jack Bain
Advertising Manager
545 Fifth Avenue
New York 17, N. Y.
PHONE—*Murray Hill 2-3345*

Journal of the
Electrochemical Society

JUNE 1955 VOL. 102 • NO. 6

CONTENTS

Editorial

Sustaining Members Aid Publication 127C

Technical Papers

Resistance Studies on Various Types of Dry Cells. *Richard Glicksman and C. K. Morehouse* 273
Investigation of Storage Battery Failure by a Method of Plastic Impregnation. *A. C. Simon and E. L. Jones* 279
The Effect of Cobalt on the High Temperature Oxidation of Nickel. *S. F. Frederick and I. Cornet* 285
Reaction of Nitrogen with Uranium. *M. W. Mallett and A. F. Gerds* 292
Kinetics of Surface Reactions of Metals, I. Iron. *Donald M. Sowards and Norman Hackerman* 297
The Difference Effect on Aluminum Dissolving in Hydrofluoric and Hydrochloric Acids. *M. E. Straumanis and Y. N. Wang* 304
Recent Innovations in the Control and Operation of Zirconium Reduction Furnaces. *F. E. Block and A. D. Abraham* ... 311
A Metallurgical Evaluation of Iodide Chromium. *D. J. Maykuth, W. D. Klopp, R. I. Jaffee, and H. B. Goodwin* .. 316
Preparation of Titanium by Fluoride Electrolysis. *M. A. Steinberg, S. S. Carlton, M. E. Sibert, and E. Wainer* 332
Conductimetric and Viscometric Behavior of Lithium Bromide in 50-50 Weight Per Cent Methanol-Acetone at Temperatures within the Range 20° to −50°C. *Lyle R. Dawson, Richard A. Hagstrom, and Paul G. Sears* 341
Mathematical Studies of Galvanic Corrosion, II. Coplanar Electrodes with One Electrode Infinitely Large and with Equal Polarization Parameters. *James T. Waber and Marshall Rosenbluth* 344
Discussion Section 354

Technical Review

Review of Articles on Luminescence for 1953–1954. *Gorton R. Fonda* 129C

Current Affairs

Alcoa—ECS Sustaining Member 134C
Gordon Research Conferences, July 1955 ..... 134C
Section News 136C
Personals 136C
New Members 138C
ECS Membership Statistics 138C
Letters to the Editor 139C
News Items 141C
Meetings of Other Organizations 143C
Book Review 143C
Recent Patents 144C
Literature from Industry 145C
New Products 146C

Published monthly by The Electrochemical Society, Inc., Mount Royal and Guilford Aves., Baltimore 2, Md., combining the JOURNAL and TRANSACTIONS OF THE ELECTROCHEMICAL SOCIETY. Editorial offices: 216 West 102nd Street, New York 25, N. Y. Statements and opinions given in articles and papers in the JOURNAL OF THE ELECTROCHEMICAL SOCIETY are those of the contributors, and The Electrochemical Society assumes no responsibility for them. Nondeductible subscription to members $5.00; subscription to nonmembers $15.00. Single copies $1.25 to members, $1.50 to nonmembers. Copyright 1955 by The Electrochemical Society, Inc. Entered as second-class matter November 15, 1947, at the Post Office at Baltimore, Md., under the act of August 24, 1912.

FUTURE MEETINGS OF
The Electrochemical Society

Pittsburgh, October 9, 10, 11, 12, and 13, 1955

Headquarters at the William Penn Hotel

Sessions will be scheduled on

Batteries, Corrosion, Electrodeposition, Electro-Organics, and Electrothermics and Metallurgy

★ ★ ★

San Francisco, April 29 and 30, and May 1, 2, and 3, 1956

Headquarters at the Mark-Hopkins Hotel

Sessions probably will be scheduled on

Electric Insulation, Electronics, Electrothermics and Metallurgy, Industrial Electrolytics, and Theoretical Electrochemistry

★ ★ ★

Cleveland, October 28, 29, 30, and 31, and November 1, 1956

Headquarters at the Statler Hotel

★ ★ ★

Washington, D. C., May 12, 13, 14, 15, and 16, 1957

Headquarters at the Statler Hotel

★ ★ ★

Buffalo, October 6, 7, 8, 9, and 10, 1957

★ ★ ★

Papers are now being solicited for the meeting to be held in Pittsburgh. Triplicate copies of each abstract (not exceeding 75 words in length) are due at the Secretary's office, 216 West 102nd Street, New York 25, N. Y., *not later than June 15, 1955*. Complete manuscripts should be sent in triplicate to the Managing Editor of the JOURNAL at the same address.

Triplicate copies of abstracts of papers for the San Francisco Meeting must reach the Secretary's office not later than January 2, 1956.

JUST PUBLISHED
6th EDITION

...a practical refresher in chemical arithmetic

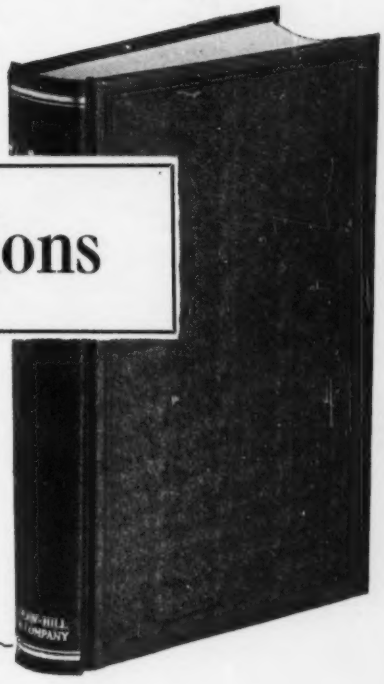

Chemical Calculations

By H. V. ANDERSON

Professor of Chemistry, Lehigh University

Sixth Edition, 299 pages, 27 tables, 11 figures, $4.75

THIS valuable book provides you with a sound review and analysis of calculations common to chemical research and practice—serves as a helpful guide spotlighting the "common-sense" method of approach in solving everyday problems. It includes scores of illustrative examples dealing with equation writing, thermometric calculations, gas-volume relations, oxidation reduction, gram-equivalent, molar and normal concentration, principle of equivalency, thermochemical reactions, electrochemistry, chemical equilibrium, solubility-product principle, and so on.

This revised Sixth Edition is packed with useful explanations and data for the practicing chemist. The step-by-step presentation in solving illustrative examples in logical sequence leads to a better, more thorough understanding of the solution. The use of dimensional units as an aid in solving various problems is stressed, and the use of significant figures is emphasized.

Revised material includes data on exponents and significant figures, gram-atom and gram-mole relations, fundamental gas laws, subject of percentage concentration, and so on. Emphasis is placed on chemical equation writing. You'll find this book a reliable guide in making a wide variety of common calculations.

Here's some of the information packed into 27 helpful tables:

—Conversion Table for Pressure
—Vapor Pressure of Water in Millimeters of Mercury
—Common Radicals with Names, Formulas and Valence
—Boiling-point and Freezing-point Constants for Various Solvents
—Calorific Power of Some Substances
—Heats of Formation of Some Oxides
—Calorific Power of Some Gases and Liquids
—Conversion Factors for Weights and Measures
—Density of Gases
—Percentage of Effective Ionization of Electrolytes at 18°C

Keep this handy reference on common calculations at your fingertips—to help you solve a wide variety of chemical problems

CONTENTS

1. Measures and Weights
2. Density
3. The Language of Chemistry
4. Gram-Atom and Gram-Mole
5. The Measurement of Temperature
6. Effects of Changes in Pressure and Temperature on the Volume of Gases
7. Mole-weight—Gas-volume Relations
8. Derivation of Chemical Formulas
9. Chemical Equations. Nonredox Type
10. Oxidation-reduction
11. Gram-equivalent
12. Molar and Normal Concentration
13. Principle of Equivalency
14. Combination of Gases
15. Thermochemical Reactions
16. Electrochemistry
17. Chemical Equilibrium; Reversible Reactions
18. Solubility-Product Principle

THE ELECTROCHEMICAL SOCIETY, INC.
216 West 102nd Street
New York 25, New York

Please send me _____ copies of the 6th edition of Anderson's "Chemical Calculations":

Name_____

Street_____

City, State_____

Price: $4.75 plus postage

We've found that "KARBATE" equipment cuts costs wherever corrosion is a factor!

WHY SHOULD YOU USE

KARBATE

BRAND

IMPERVIOUS GRAPHITE PROCESS EQUIPMENT?

ANSWER: Because *only* "Karbate" products combine:

- **Corrosion resistance**
- **Immunity to thermal shock**
- **Freedom from metallic contamination**
- **High thermal conductivity**
- **Low first cost *and* low maintenance**
- **Workability — readily fabricated and serviced in the field**
- **Sturdy, durable constructions**
- **Standard stock units**
- **Complete technical service**

Manufactured Only By National Carbon Company

"Karbate" impervious graphite is a "must" in many highly corrosive services. But these applications only begin to measure the possibility of savings offered by "Karbate" products in a wide range of process locations. Wherever corrosion, contamination or thermal shock must be eliminated, "Karbate" products save time and money all the way down the process line.

WRITE FOR LITERATURE!

The term "Karbate" is a registered trade-mark of Union Carbide and Carbon Corporation

NATIONAL CARBON COMPANY

A Division of Union Carbide and Carbon Corporation
30 East 42nd Street, New York 17, N. Y.

Sales Offices: Atlanta, Chicago, Dallas, Kansas City, Los Angeles, New York, Pittsburgh, San Francisco

IN CANADA: Union Carbide Canada Limited, Toronto

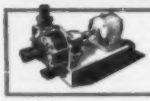

Pumps — Catalog Section S-7250

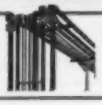

Pipe and Fittings — Catalog Section S-7000

Heat Exchangers — Catalog Sections S-6740 and S-6840

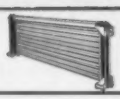

Cascade Coolers — Catalog Section S-6820

HCl Absorbers — Catalog Section S-7460

DEPENDABILITY

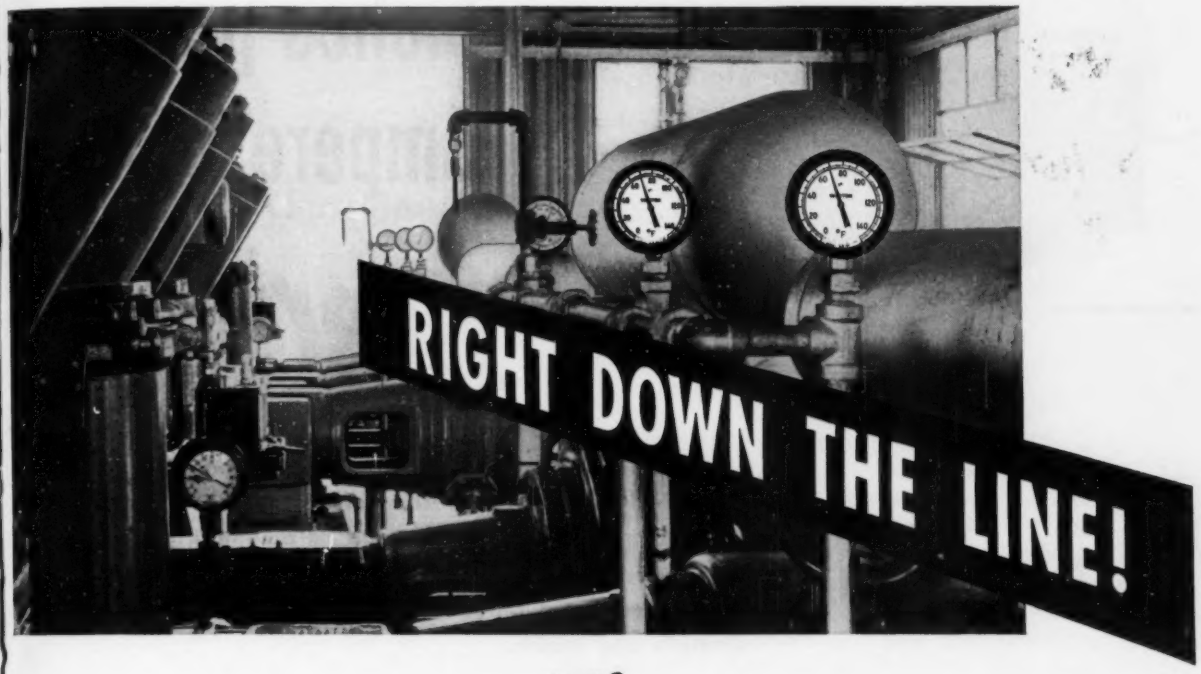

Weston thermometers with Multiple bimetal helix

The reasons why WESTON all-metal industrial thermometers excel in dependability and long life . . . enjoy such outstanding preference throughout industry . . . stem in large part from Weston's exclusive design and manufacturing methods. The critical *sensing elements* are all Weston-made in the shorter *multiple helix* form to insure rugged, *nonsagging* units. They are then *cycle-seasoned,* over broad temperature ranges, to insure *consistently precise indications* over far longer periods. Thus they serve better, longer, at far lower over-all costs. Bulletin containing sizes, ranges and prices, available on request. WESTON Electrical Instrument Corporation, 614 Frelinghuysen Ave., Newark 5, N. J.

WESTON

Thermometers

AVAILABLE THROUGH LEADING DISTRIBUTORS

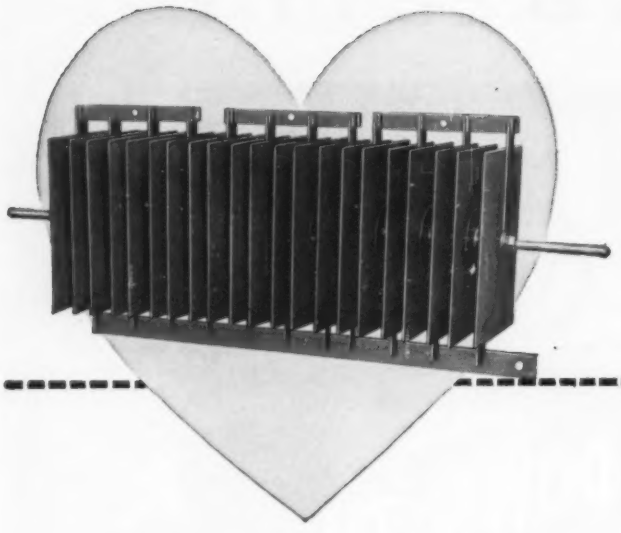

Six Square Inches per Ampere* of "Heart"!

The selenium stack is the heart of any selenium rectifier. For it is the quality of the stack and its accompanying circuitry that determines the effectiveness of a rectifier, just as the state of the heart and blood vessels of a human determine his strength and health.

IT'S A PROVEN FACT, RAPID RECTIFIER STACKS STAND UP LONGER IN HARD SERVICE. HERE'S WHY:

1) Rapid allows 6 square inches per ampere of plate surface in full wave bridge circuits. For years we have maintained this standard (somewhat higher than other makes), since we feel allowing this much area results in maximum life expectancy.
2) The plates in Rapid stacks use triple purified Selenium.
3) They are carefully tested and balanced for even current distribution.
4) They are coated with an exclusive material rendering them absolutely impervious to the corrosive conditions existing in plating rooms.
5) The plates are spaced an average of ½ inch, diminishing the possibility of dust, dirt and corrosive material becoming lodged between plates, thus allowing heat to dissipate readily.

Rapid designs its stacks to much higher standards than most other manufacturers.**

For example:

In tests performed at ambient temperatures of over 30°C, a recognized electrical manufacturers' group standard allows a temperature rise in the stack of 60°C; and, a rise of 40°C at the same ambient temperature for 1000 hours is permitted without derating.

Rapid standards permit a maximum stack temperature rise of only 22°C above the ambient. This low rise is made possible only because of the large area used per ampere, the plate spacing, high purity of Selenium used, the advanced circuitry and the engineering skill which designs the complete rectifier unit for the specific job.

So, when you buy a rectifier, check its heart. Make sure the one you buy offers the most advanced design for longest life . . . In other words, make sure you get a Rapid Rectifier.

*In forced air cooled, three phase, full wave bridge circuit units.
**All three phase rectifiers are designed with a full wave circuit.

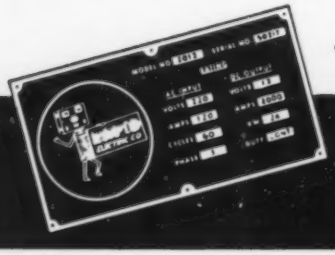

THE NAMEPLATE THAT MEANS *"More Power to You!"*

RAPID ELECTRIC COMPANY

2881 Middletown Road • New York 61, N. Y. • Phone: Talmadge 8-2200

Editorial

Sustaining Members Aid Publication

ALL TECHNICAL SOCIETIES face the increasingly difficult problem of publishing the growing volume of technical papers at a time when publishing costs continue to rise. The most eloquent evidence of the rate of increase of the technical literature is to be seen in the record of *Chemical Abstracts* which in 1954 abstracted 67,606 papers and 11,083 patents—an increase of 9 per cent over the previous year. The 50 new journals of chemical interest established during the year will doubtless enlarge the abstracting and publishing task still further.

It has been said that the editors of journals can do considerably more than their printers in reducing costs. The Technical Editor of this JOURNAL and his staff insist upon the elimination of unessential verbiage, tables, and graphs. They reject or divert to other publications a sizeable proportion of the manuscripts that are offered. As a result of the fourfold multiplication of papers presented before the national meetings it has become possible to increase the quality level of acceptability for publication. The growing popularity of the JOURNAL may reflect appreciation of this improvement; approximately 40 per cent of its subscribers are nonmembers of the Society.

An increase in the budget for this year will permit the publication of a somewhat larger number of manuscripts and thus aid in reducing the backlog of accepted papers and shorten the period between receipt of manuscripts and publication. Looking further ahead it seems certain that measures must be taken to cut publication costs which at present are higher than for some other journals.

It is a pleasure to acknowledge here the industrial sources that now provide a major proportion of the funds required for the publication of this JOURNAL. These are advertising and sustaining membership subscriptions. Mr. Bain has been able to demonstrate to many of the country's leading manufacturers that the JOURNAL is an effective advertising medium. The continuing support of 81 sustaining members who carry a total of 102 sustaining subscriptions provides indispensable financial assistance and evidence of good will for which the Society is most grateful. Elsewhere in this issue will be found an article entitled "The Alcoa Story." This is the first of a series of brief feature articles on the Society's sustaining members.

—RMB

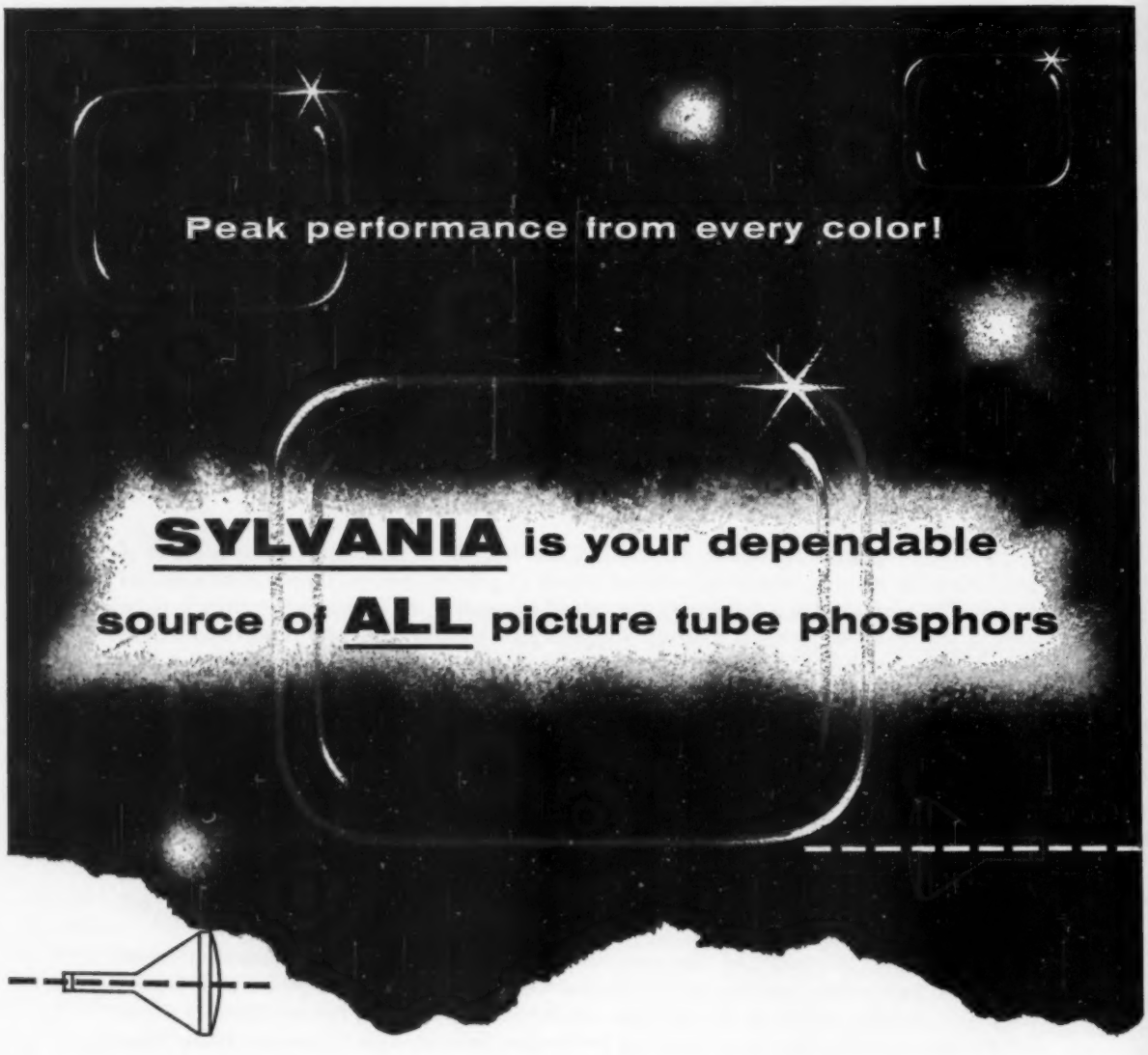

Whether you need phosphors for black-and-white or color picture tubes, Sylvania's long experience, highly developed production facilities and exacting quality control add up to *dependability*.

All Sylvania tube phosphors are rigidly inspected for purity, particle size, brightness and uniformity of color. There is a full range of phosphor formulations available to meet your requirements, including special blends for maximum cross-burn resistance. All Sylvania phosphors can be supplied in 1500-lb. lots to eliminate color-matching problems.

To help you secure long-lasting screen brightness and good color, Sylvania also manufactures high-purity *potassium silicate*. Exact control of potassium-to-silica ratio assures maximum wet-screen strength.

For complete information about high-performance Sylvania phosphors and TV Picture Tube components, write to:

SYLVANIA ELECTRIC PRODUCTS INC.,
1740 Broadway, New York 19, N. Y.
In Canada:
Sylvania Electric (Canada) Ltd.,
University Tower Bldg., St. Catherine St.,
Montreal, P. Q.

SYLVANIA

Lighting • Radio • Electronics • Television • Atomic Energy

Review of Articles on Luminescence for 1953–1954[1]

Gorton R. Fonda[2]

New Phosphors

A phosphor was "made to order" by Prener, Hanson, and Williams by dehydrating hormotome, a zeolite, and heating at 400°C in mercury vapor to form centers of free mercury atoms, emitting a broad band with a peak at 3700 Å under excitation by 2537 Å (1). Prener has also prepared a magnesium oxide phosphor activated with Mn^{IV}; when fired with lithium, its red fluorescence comprises a number of bands (2).

Among the sulfides, Gobrecht and Hahn have prepared polysulfides of the alkaline earths, similar to those of the alkalies, fluorescing yellow to orange-red under 3650 Å (3). By firing in pure H_2S above 1020°C and in absence of chloride, Froelich obtained a zinc sulfide high in copper which emitted yellow and red bands under u.v. and cathode rays and in electroluminescence. The copper retained was 0.05–0.15%. Active centers were ascribed to neutral copper atoms or Cu_2S. An orange colored luminescence appeared under stimulation by 0.8–1.1 μ (4). Under excitation by a tungsten lamp with suitable filters, Garlick and Dumbleton were able to obtain *IR* emission at 90°K and 290°K in the range of 1–3 μ from specially prepared sulfides and selenides of zinc, cadmium, lead, and mercury (5).

There are several new phosphates. Henderson and Ranby prepared one of barium and titanium which emitted a whitish blue, close in spectral emission to magnesium tungstate; maximum brightness under 2537 Å was given by the composition $2Ba_2P_2O_7 \cdot TiO_2$ (6). Smith has extended the luminescence of his $\beta Zn_3(PO_4)_2$:Mn by addition of cadmium phosphate. The effect is to reduce the efficiency under cathode rays (c.r.) but to modify the emission, shifting the peak to about 6500 Å at 60 mole % $Cd_3(PO_4)_2$; this is further in the red than given by either of the single phosphates (7). Butler has studied the emission under 2537 Å of $Ca_3(PO_4)_2$ activated with tin and manganese and prepared in a reducing atmosphere. With 0.005 Sn, $\alpha Ca_3(PO_4)_2$ is formed; its blue emission is shifted to shorter wave lengths by partial substitution of barium. With 0.04 Sn, $\beta Ca_3(PO_4)_2$ results, emitting a 6300 Å band as well as a 4950 Å; partial substitution of strontium suppresses the 4950 Å band and shifts the 6300 Å to 6150 Å; in the presence of manganese as well, only one band appears at 6500 Å, and this is shifted to 6350 Å by strontium (8). Zalm and Klasens formed a modification of manganese-activated zinc silicate by incorporating the phosphate radical at 820°C. A new band appeared at 6100 Å in addition to the normal green (9).

There are several new halide phosphors. Both Klasens, Zalm, and Huysman (10) and Smith (11) have studied manganese-activated ABF_3 compounds of perovskite structure, where *A* is an alkaline metal and *B* a metal of the second Periodic column. Substitutions produced extensive variations in the spectral positions of the emission bands under c.r., ranging from 4950 Å to 6000 Å. In explanation, Smith generalizes by relating the predominantly orange bands to manganese in 6 coordination and the greenish bands to 8 coordination. Klasens and coworkers came to a more specific conclusion by detailed measurements of the changes in structural dimensions produced by the substitutions; they found shifts to shorter wave length to accompany increases in the spacing of Mn-*F* ions. They believe that this relation is in accord with the conclusion that an increase in the space available for the activator ion allows a greater approach to the state of the free ion. Guenther has found a unique red emission under 3650 Å for $5Al_2O_3 \cdot CaF_2$:Mn, fired at 1250°–1400°C; refiring in hydrogen kills the red and brings out a yellow under 2537 Å (12). Swindells has rendered LaOCl luminescent under c.r. by activating it with the trivalent metals bismuth, antimony, samarium, praseodymium, and niobium, all of such ionic size that they are capable of substitution for lanthanum; the emission lies in the blue, green, and red (13). Gobrecht and Becker have found that chlorides, bromides, and iodides of thallium and lead become luminescent at 93°K on absorbing traces of water, emitting at 4500–6000 Å under excitation by 2537 Å and 3650 Å (14).

A fresh attempt, this time by Botden, van Doorn, and Haven, has proven that *F*-centers in alkaline halide crystals are also luminescence centers under irradiation in the *F*-band below 100°K, emitting very weakly at 1.0–1.5 μ. The crystals were colored additively by heating in metallic vapor or by electrolyzing (15).

Phosphor Characteristics under U.V. Excitation

Both Ward (16) and Ranby and Rice (17) have discussed the chemistry of phosphors. The former suggests possible coordinations between the activator and the host crystal; the latter deals with applications and practical features of their preparation. Jerome has calculated the quantum efficiency of lamp phosphors from lamp measurements (18).

In a study of red emitting phosphors having a high quenching temperature under excitation by 3650 Å, Klasens discloses how the introduction of lithium raises this temperature for magnesium arsenate from 250° to 330°C and lowers the susceptibility of Mn^{IV} to reduction (19). In the related field of sensitized luminescence, Ginther describes manganese-activated calcium fluoride sensitized by two types of cerium ions, singlets and aggregates. In both cases energy may be transferred directly from sensitizer to activator ions over 30–80 lattice sites, but no transfer is possible between sensitizer ions (20).

Various borates and aluminates activated by lead or thallium have been found by Ranby and Henderson to de-

[1] This review, written in January 1955, covers those articles published in scientific journals and written in English, German, and French that have come to the writer's attention since writing the previous review, published in the June 1953 JOURNAL, **100**, 155*C*.

[2] Consultant, General Electric Co., 1028 Parkwood Blvd., Schenectady, N. Y.

velop maximum luminescence only under cascade excitation. As an example, $5CaO \cdot 3Al_2O_3$:Tl emitted a bright yellow luminescence with 3650 Å after radiation with 2537 Å or with 45 v x-rays; the brightness was not lowered by heating to 100°C or by the lapse of a week after the 2537 Å radiation (21).

Several studies pertain to the character of absorption and emission bands, particularly at low temperatures. Tests by Klick on cadmium sulfide crystals show that photoconductivity is generated by radiation at the absorption edges and that the energy gap between the absorption edge and the onset of emission is too great for the acceptance of resonance radiation as the cause of the emission (22). Klick has also measured the change in width with temperature of absorption and emission bands of potassium halides, zinc and cadmium sulfides, and zinc tungstate; at low temperature they all approach a constant value which is still appreciable at 4°K (23). The absorption band in KCl:Tl corresponding to the transition $^1S_0$—$^3P_1{}^0$ was found by Johnson and Williams to be shifted 4 Å to longer wave length at 2000 atm pressure, in agreement with theory (24).

Studer and Fonda (25) and Schulman, Ginther, and Claffy (26) remain in disagreement, despite further measurements, as to whether differences in optical characteristics of $CaSiO_3$:Pb are due to changes in structure or to changes in lead content.

From calorimetric measurements on manganese-activated zinc silicates containing variable amounts of iron, Bodó concluded that the loss in quantum efficiency due to the presence of iron arises from an internal conversion into thermal energy rather than from a release of infrared radiation (27).

Phosphor Characteristics under CR Excitation

Tests made at 20 kv on the irradiated side of heavy phosphor layers by Bril and Klasens show intrinsic efficiencies ranging from 23% for ZnS:Al:Ag to about 8% for Zn_2SiO_4:Mn and $\beta Zn_3(PO_4)_2$:Mn and 7% for the green emitting zinc oxide (28). The same authors have also reviewed and retested the characteristics of various flying spot phosphors and deem $2CaO \cdot Al_2O_3 \cdot SiO_2$:Ce to be the best; its blue emission has an intrinsic efficiency of 4% and a decay time of about 10^{-6} sec (29). Larach has measured the spectral emission and relative peak intensity of zinc selenide with various activators and coactivators (30). Stout has studied the relation between electron emission and luminescence characteristics of barium oxide (31). Kaisel and coworkers have found that luminescence could be excited from ZnO:Zn by 3-v electrons; they discuss the significance of this on the distribution of energy levels (32).

Among various studies on screen characteristics, Ehrenberg and Franks have measured the penetration and scattering of a beam of 10–40 kv electrons in single crystals of thallium-activated iodides and in calcium and cadmium tungstates by means of photomicrographs. The depth distribution of penetration follows a parabola rather than the Thomson-Whiddington curve (33). Koller describes a method for obtaining a thinner and brighter screen with 10–30% voids by coating zinc sulfide particles with silicone, compressing on a water surface, and transferring to the screen (34). In tests dealing mainly with zinc silicate, Dowling and Sewell found a linear relationship between brightness and voltage except for distortion at low voltage due to dead layers on the crystal surfaces. Loss in energy with beam penetration was exponential (35). The same authors found a reduction in secondary emission ratio due to surface contamination with organic vapors and relate it to x-burn formation (36). Hazel and Schnable have made further studies on the adherence of screens prepared with Kasil binder and discuss the polymerization of silica (37).

Broser and Reichardt relate the loss in luminescence of sulfide phosphors during grinding to the loss that accompanies bombardment with alpha particles. As a sequence to earlier work, they ascribe both to the formation of discrete metastable states resulting from lattice dislocations and serving as media for radiationless transitions (38). Hanle and Rau have measured the rate of disintegration of ZnS:Cu, Zn_2SiO_4:Mn, and $MgWO_4$ under bombardment by positive ions of the inert gases and find it to increase with the atomic weight of the gas and to decrease for the three phosphors in the order named. They ascribe this also to the formation of lattice defects (39). Rottgardt applies the same explanation to the loss in luminescence under electron bombardment, the raster burn of TV tubes. For zinc fluoride the loss was 50% at a time when the blackening was only 1–2%. The rate of loss for various phosphors tested at 4 kv increased in the order Zn_2SiO_4:Mn, ZnS:Ag, and CdS:Cu. The lattice dislocations are ascribed to ionization which accompanies electron impact (40).

Electroluminescence

Several phosphors have been described which exhibit electroluminescence (e.l.). In addition to those noted above (4), Froelich has studied the formation of sulfides in H_2S at 1100°C with trivalent coactivators, primarily ZnS:Al:Cu. With increasing activator concentration, the emission, under 3650 Å but not in e.l., shifted from green to orange, with bands at 5150 Å, 5550 Å, and 5900 Å, blended together. The solubility of Cu_2S was higher than in ZnS:Cu. When fired with oxide additions, such as moisture, the phosphors developed strong e.l. in the green, ascribed to oxide barriers (41). He has also described sensitization of ZnS:Mn for yellow e.l. by addition of one part of copper to twenty of manganese and firing in H_2S at 1100°C (42). Phosphors of ZnS:Cu with lead as an essential ingredient have been described by Waymouth and by Homer, Rulon, and Butler. Green luminescence resulted with $4(10)^{-4}$–$1.5(10)^{-3}$ g atoms of copper and blue with 3–$6(10)^{-4}$ Cu and a minimum of chloride. Yellow and orange emission resulted on addition of manganese. The role of lead may be to promote a surface layer of Cu_2S (43). Halstead and Koller have studied changes in the light emission of ZnS:Mn for temperatures of 77°K to 200°C and at 20–5000 cps (44).

The characteristics of e.l. cells have received much attention. From a general review, Curie concludes that the three essentials for bright e.l. are well-developed crystals, creation of donor levels on the surface of grains, and reduction in the number of traps (45). A particularly helpful review is given by Zalm, Diemer, and Klasens as part of a description of their original work. They consider a copper rich layer on the surface of grains to be the essential feature for e.l. Their green emitting phosphor is ZnS:Cl:Cu with $6(10)^{-4}$ Cu, and their blue is ZnS:Al:Cu with 10^{-3} Cu and $8(10)^{-4}$ Al, both fired at 1200°C. From electrical and optical measurements and examination under the microscope, they find that e.l. is emitted from the surface of grains on the cathode side; they ascribe secondary peaks at zero voltage of the a-c wave to the presence of traps. They arrive at the same explanation for e.l. as did Piper and Williams in 1952 (46). An interesting zinc oxide cell with a rod electrode is described by Fischer; it emits e.l. at a low voltage only when the rod is cathode (47).

Gobrecht, Hahn, and Gumlich describe cells of ZnO, ZnS, and CdS rendered e.l. by partial oxidation and warn against spurious e.l. resulting from glow discharges in released vapor. They describe also the occurrence of electrothermoluminescence which arises on warming cells from 170°K, a release of luminescence at temperatures corresponding closely to the peaks of glow curves (48). Destriau's equation for the voltage dependence of e.l. has been revised by Howard, Ivey, and Lehmann on the basis of their tests with cells of ZnS:Ag, ZnS:Cu, and ZnO:Zn (49). Nudelman and Matossi have studied the character of the emission waves produced from ZnS:Cu:Pb by the application of nonsinusoidal fields and conclude that excitation is due to collision processes of accelerated electrons (50).

Tests have also been made on luminescent characteristics of individual phosphor grains as illustrative of the mechanism of e.l. Burns has reviewed all cases of e.l. on record with the aim of presenting a consistent interpretation (51). Waymouth and Bitter have studied the localized characteristics as seen under the microscope and derived conclusions from their observations (52). Roberts has measured the variations of the dielectric constant under simultaneous illumination (53).

In a life test of ZnS:Cu:Pb in e.l. cells carried up to 13,000 hr, Jerome and Gungle noted that the major light loss occurred in the first 1000 hr, followed by a static condition after about 2000 hr. They found evidence that the decrease in light output is due to an increase in the power loss in the dielectric rather than to depreciation of the phosphor (54).

Schoen has reviewed tests on light emitted by carborundum crystals under passage of a current; he offers an explanation for them on the basis of electron transitions between various types of energy states (55). From measurements of the e.l. spectrum of silicon carbide crystals and its dependence on temperature, as well as from the electrical characteristics, Szigeti concludes that its e.l. is produced by accelerated carriers within the barrier layer. He derives an energy diagram to conform to a free carbon content as the luminescence center (56).

Radioluminescence

Three studies have been made on the optical properties of alkaline halides activated with silver. Mandeville and Albrecht find different types of decay for the two bands in the phosphorescence of NaCl:Ag that follows excitation by u.v. or alpha particles (57). The buildup of the 2500 Å and 4000 Å emission bands in NaCl:Ag was found by Hanle and Hinrichs to be extremely fast under electron excitation and slower under x-ray, varying with the silver content; decay time decreased with increase in silver. Irradiation with light after decay produced radio-photoluminescence and stimulation (58). Etzel and Schulman studied the emission, excitation, and absorption spectra of silver-activated chlorides and bromides. Under x-radiation five new absorption bands were noted, excitation within three of which produced luminescence. The nature of these centers is discussed (59).

The phosphorescence of several thallium-activated halides was measured at various temperatures by Neuert and Retz-Schmidt after excitation by gamma rays. Results show that there may be a disturbing effect due to phosphorescence in the measurement of weak beta or gamma rays by the scintillation method (60). Measurements by Emigh and Megill on the long-time decay of NaI:Tl excited by Co-60 indicate that different trap levels give rise to independent, monomolecular processes (61). Bose and Sharma have also studied the different decay rates of thallium-activated as well as of pure alkaline halides at liquid oxygen and at room temperature (62).

Phosphorescence and Thermoluminescence

A novel method for measuring short decay after u.v. excitation has been devised by Bril, Klasens, and Zalm. A quartz window is mounted on a TV tube and coated internally with an u.v. emitting phosphor having a rapid decay. Its u.v. emission under a c.r. beam pulse is used to excite the experimental phosphor placed externally (63).

In a test on fifty phosphors, Gobrecht, Hahn, and Koesel confirm expectation by finding that those with bimolecular decay exhibit good photoconductivity, and those with exponential decay a poor one (64). The self-activated alkali metal polysulfides, as well as uranyl salts, show only exponential decay in tests by Gobrecht, Hahn, and Gretzinger, with no evidence of thermoluminescence. With increase in the atomic weight of the metal of the sulfide and also with decrease in temperature, emission shifts to longer wave length and the decay constant decreases. This is taken to denote stronger coupling within the molecule, with consequent lower probability for radiationless transitions (65).

Multiple emission bands of manganese sometimes overlap so closely that they cannot be resolved, as with cadmium borate. Dziergwa has demonstrated their presence in this phosphor by finding different rates of decay in different spectral regions, two exponential and one bimolecular (66).

From diverse tests, Bube concludes that trapping centers in sulfide and silicate phosphors are associated with crystal defects (67). That the introduction of gallium is a means of augmenting these defects is a conclusion of Bube and Larach from its effect in lowering the emission and intensifying high temperature glows in zinc and magnesium silicates and zinc germanate (68). In tests on KCl:Tl, Johnson and Williams found that the addition of calcium, strontium, and barium failed to affect the glow curve and concluded, therefore, that lattice vacancies are not the source of traps. The effect of cadmium in introducing new emission bands and in modifying the glow curve is ascribed to interactions between thallium and cadmium ions (69). For cubic ZnS:Cu, Gillson finds that different glow curves result under excitation by u.v. of different wave length, denoting four groups of traps which vary in speed and extent of filling with the type of excitation employed (70). From decay measurements on ZnS:Cu and CaS:Bi, Curie calculates a distribution of traps whose depths coincide with those shown by glow curves (71). From a review of long-time decay, Honig shows how the distribution of activation energies among the filled traps may be computed from the observed curves (72).

Mechanism of Luminescence

Williams has completed a study of the KCl:Tl system, aimed at a calculation of the factors responsible for the character of absorption and emission bands. The agreement with experiment denotes that the basic theory is essentially complete (73). Considerations are given by Johnson for the construction of its configuration coordinate model (74). A similar model has been employed by Hameka and Vlam for calculation of the change with temperature of the spectral location and band width in the emission of calcium tungstate (75).

Two papers deal with the dependence of luminescence efficiency upon activator concentration. On the basis of previous considerations and new data on calcium oxide phosphors prepared with various activators and physical treatments,

Ewles and Lee endeavor to strengthen their previous conclusion that a luminescence center represents an association between an activator ion and a large but definite number of host crystal ions. They consider this view fundamental to the 1950 theory of Johnson and Williams which led to a similar expression on the postulate that a center is an activator ion which has no other activator ion within a specified number of lattice positions (76). Dexter and Schulman propose a theory for the migration of excitation energy from one activator center to another until eventually it is lost at a lattice imperfection (77). This conception of quenching is similar to that proposed by Broser (38).

Dexter has extended the earlier studies of Schulman and Botden on the transfer of excitation energy to include a range of 1000 lattice sites surrounding each sensitizer atom (78).

Several papers deal with energy transitions in zinc sulfide. According to Klasens, the energy level introduced by a monovalent activator is not a discrete state of the activator, but results from a disturbance of the adjoining sulfur ion under the change in the electrostatic field acting upon it. Similarly, traps are to be considered as disturbed zinc ions (79). This approach had been suggested earlier by Kroeger. It has been developed in more detail by Hoogenstraaten, who assigns values to the trap depths associated with the various coactivators (80); it is also discussed by Kroeger and Vink (81). As a specific case, Hoogenstraaten and Klasens describe the transitions in a band model proposed to explain the properties of ZnS:Cu:Co (82). Bube reviews the transitions that may account for the luminescence of the various zinc sulfide phosphors (83).

REFERENCES

1. J. S. Prener, R. E. Hanson, and F. E. Williams, *J. Chem. Phys.*, **21**, 759 (1953).
2. J. S. Prener, *ibid.*, **21**, 160 (1953).
3. H. Gobrecht and D. Hahn, *Z. Physik*, **135**, 523 (1953).
4. H. C. Froelich, *J. Opt. Soc. Amer.*, **42**, 982 (1952); *This Journal*, **100**, 280 (1953).
5. G. F. J. Garlick and M. J. Dumbleton, *Proc. Phys. Soc. B*, **67**, 442 (1954).
6. S. T. Henderson and P. W. Ranby, *This Journal*, **98**, 479 (1951).
7. A. L. Smith, *ibid.*, **101**, 244 (1954).
8. K. H. Butler, *ibid.*, **100**, 250 (1953).
9. P. Zalm and H. A. Klasens, *Philips Research Repts.*, **8**, 386 (1953).
10. H. A. Klasens, P. Zalm, and F. O. Huysman, *ibid.*, **8**, 441 (1953).
11. A. L. Smith, *This Journal*, **101**, 189 (1954).
12. G. Guenther, *Proc. Intern. Sym. Reactivity of Solids*, Gothenburg, Part I, 143 (1954).
13. F. E. Swindells, *This Journal*, **101**, 415 (1954).
15. T. P. J. Botden, C. Z. van Doorn, and Y. Haven, *Philips Research Repts.*, **9**, 469 (1954).
14. H. Gobrecht and F. Becker, *Z. Physik*, **135**, 553 (1953).
16. R. Ward, *J. Phys. Chem.*, **57**, 773 (1953).
17. P. W. Ranby and A. P. Rice, *Ind. Chemist*, **28**, 545 (1952).
18. C. W. Jerome, *This Journal*, **100**, 586 (1953).
19. H. A. Klasens, *Philips Research Repts.*, **9**, 377 (1954).
20. R. J. Gunther, *This Journal*, **101**, 248 (1954).
21. P. W. Ranby and S. T. Henderson, *Proc. Phys. Soc. B*, **67**, 496 (1954).
22. C. C. Klick, *Phys. Rev.*, **89**, 274 (1953).
23. C. C. Klick, *J. Phys. Chem.*, **57**, 776 (1953).
24. P. D. Johnson and F. E. Williams, *Phys. Rev.*, **95**, 69 (1954).
25. F. J. Studer and G. R. Fonda, *J. Opt. Soc. Amer.*, **42**, 360 (1952).
26. J. H. Schulman, R. J. Ginther, and E. W. Claffy, *ibid.*, **43**, 318 (1953).
27. Z. Bodó, *Acta Physica*, **3**, 23 (1953).
28. A. Bril and H. A. Klasens, *Philips Research Repts.*, **7**, 401 (1952); *Philips Tech. Rev.*, **15**, 63 (1953).
29. A. Bril and H. A. Klasens, *ibid.*, **7**, 421 (1952).
30. S. Larach, *J. Chem. Phys.*, **21**, 756 (1953).
31. V. L. Stout, *Phys. Rev.*, **89**, 310 (1953).
32. S. F. Kaisel and C. B. Clark, *J. Opt. Soc. Amer.*, **44**, 134 (1954); R. E. Shrader and S. F. Kaisel, *ibid.*, **44**, 135 (1954).
33. W. Ehrenberg and J. Franks, *Proc. Phys. Soc. B*, **66**, 1057 (1953).
34. L. R. Koller, *J. Opt. Soc. Amer.*, **43**, 620 (1953).
35. P. H. Dowling and J. R. Sewell, *This Journal*, **100**, 22 (1953).
36. P. H. Dowling and J. R. Sewell, *J. Appl. Phys.*, **25**, 228 (1954).
37. J. F. Hazel and G. L. Schnable, *This Journal*, **100**, 65 (1953); *J. Phys. Chem.*, **58**, 812 (1954).
38. I. Broser and W. Reichardt, *Z. Physik*, **134**, 222 (1952).
39. W. Hanle and K. H. Rau, *ibid.*, **133**, 297 (1952).
40. K. H. Juergen Rottgardt, *Naturwissenschaften*, **40**, 315 (1953); *Z. angew. Phys.*, **6**, 160 (1954).
41. H. C. Froelich, *This Journal*, **100**, 496 (1953).
42. H. C. Froelich, *J. Opt. Soc. Amer.*, **43**, 320 (1953).
43. J. F. Waymouth, *This Journal*, **100**, 81 (1953); H. H. Homer, R. N. Rulon, and K. H. Butler, *ibid.*, **100**, 566 (1953).
44. R. E. Halstead and L. R. Koller, *Phys. Rev.*, **93**, 349 (1954).
45. D. Curie, *J. Phys. radium*, **14**, 672 (1953).
46. P. Zalm, G. Diemer, and H. A. Klasens, *Philips Research Repts.*, **9**, 81 (1954).
47. A. Fischer, *Z. Naturforsch.*, **8a**, 756 (1953).
48. H. Gobrecht, D. Hahn, and H. E. Gumlich, *Z. Physik*, **136**, 612, 623 (1954).
49. B. T. Howard, H. F. Ivey, and W. Lehmann, *Phys. Rev.*, **96**, 799 (1954).
50. S. Nudelman and F. Matossi, *This Journal*, **101**, 546 (1954).
51. L. Burns, *ibid.*, **100**, 572 (1953).
52. J. F. Waymouth and F. Bitter, *Phys. Rev.*, **95**, 941 (1954).
53. S. Roberts, *J. Opt. Soc. Amer.*, **43**, 590 (1953).
54. C. W. Jerome and W. C. Gungle, *This Journal*, **100**, 34 (1953).
55. M. Schoen, *Z. Naturforsch.*, **8a**, 442 (1953).
56. G. Szigeti, *Acta Physica*, **4**, 65 (1954).
57. C. E. Mandeville and H. O. Albrecht, *Phys. Rev.*, **90**, 25 (1953).
58. W. Hanle and H. Hinrichs, *Z. angew. Physik*, **6**, 201 (1954).
59. H. W. Etzel and J. H. Schulman, *J. Chem. Phys.*, **22**, 1549 (1954).
60. H. Neuert and T. Retz-Schmidt, *Z. Physik*, **134**, 163 (1953).
61. C. R. Emigh and L. R. Megill, *Phys. Rev.*, **93**, 1190 (1954).
62. H. N. Bose and J. Sharma, *Proc. Phys. Soc.*, **66B**, 371 (1953).
63. A. Bril, H. A. Klasens, and P. Zalm, *Philips Research Repts.*, **8**, 393 (1953).
64. H. Gobrecht, D. Hahn, and H. J. Koesel, *Z. Physik*, **136**, 57 (1953).
65. H. Gobrecht, D. Hahn, and B. Gretzinger, *ibid.*, **139**, 309 (1954).
66. H. Dziergwa, *ibid.*, **135**, 283 (1953).
67. R. H. Bube, *J. Phys. Chem.*, **57**, 785 (1953).
68. R. H. Bube and S. Larach, *J. Chem. Phys.*, **21**, 5 (1953).
69. P. D. Johnson and F. E. Williams, *ibid.*, **21**, 125 (1953).
70. J. L. Gillson, Jr., *J. Opt. Soc. Amer.*, **44**, 341 (1954).
71. D. Curie, *Phys. Rev.*, **90**, 154 (1953).
72. J. M. Honig, *J. Chem. Phys.*, **22**, 1689 (1954).

73. F. E. Williams, *J. Phys. Chem.*, **57**, 780 (1953).
74. P. D. Johnson, *J. Chem. Phys.*, **22**, 1143 (1954).
75. H. F. Hameka and C. C. Vlam, *Physica*, **19**, 943 (1953).
76. J. Ewles and N. Lee, *This Journal*, **100**, 392 (1953).
77. D. L. Dexter and J. H. Schulman, *J. Chem. Phys.*, **22**, 1063 (1954).
78. D. L. Dexter, *ibid.*, **21**, 836 (1953).
79. H. A. Klasens, *This Journal*, **100**, 72 (1953).
80. W. Hoogenstraaten, *ibid.*, **100**, 356 (1953).
81. F. A. Kroeger and H. J. Vink, *J. Chem. Phys.*, **22**, 250 (1954).
82. W. Hoogenstraaten and H. A. Klasens, *This Journal*, **100**, 366 (1953).
83. R. H. Bube, *Phys. Rev.*, **90**, 70 (1953).

Current Affairs

Alcoa—ECS Sustaining Member

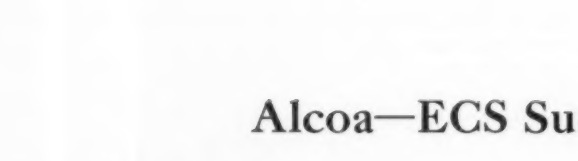

©Aluminum Co. of America

View of a potline in which aluminum is smelted at Alcoa's Rockdale, Texas, Works.

The aluminum industry was founded upon the discovery of Charles Martin Hall, an Oberlin College graduate, that aluminum oxide could be dissolved in molten cryolite and there reduced electrolytically to metallic aluminum without decomposition of the cryolite. This discovery, made in 1886, led to the formation two years later of the Pittsburgh Reduction Company in Pittsburgh, Pa. In 1907 this became the Aluminum Company of America, or Alcoa, as it is popularly known.

From the first small Pittsburgh plant with a production of 50 pounds per day, Alcoa now makes aluminum at seven smelting plants located at Alcoa, Tenn., Badin, N. C., Massena, N. Y., Point Comfort and Rockdale, Texas, and at Vancouver and Wenatchee, Wash. Including rolling and fabricating plants, Alcoa now operates on a nationwide basis with more than 40 plants.

Hall's basic invention of electrolytically reducing alumina dissolved in cryolite is still the process by which the world's supply of aluminum is produced. In the current, improved process, smelting takes place continuously in a row of many electrolytic cells. These are connected electrically in series and are called pot lines. The pots are deep rectangular steel shells lined with carbon to serve as the cathode, or negative pole, to which the electric current flows. Eventually, when a layer of metallic aluminum covers the carbon bottom, this aluminum serves as the cathode. Current is introduced through anodes in the form of a set of carbon blocks suspended in each pot; in some smelting plants a self-baking type of continuous carbon anodes is used instead. It is essential that these anodes be of high purity in order to avoid contamination of the aluminum. Today, pot lines are operating with currents of 50,000 to 60,000 amp.

The growth of the aluminum industry is reflected in the reduction of price of the light metal. In 1888 aluminum cost $8.00 a pound; today the price is $0.21 a pound. Alcoa, through its research, engineering development, and manufacturing enterprise, has been the foremost contributor to the growth of the aluminum industry.

Gordon Research Conferences, July 1955

The 1955 Gordon Research Conference on Corrosion will be held from July 18 through July 22. The Conference on the Chemistry and Physics of Metals will be held from July 25 through July 29.

The Gordon Research Conferences, sponsored by the American Association for the Advancement of Science, were established to stimulate research in universities, research foundations, and industrial laboratories. This purpose is achieved by an informal type of meeting consisting of the scheduled lectures and free discussion groups. Sufficient time is available to stimulate informal discussions among the members of a Conference. Meetings are held in the morning and in the evening, Monday through Friday, with the exception of Friday evening. Afternoons are available for recreation, reading, resting, or participation in discussion groups as the individual desires.

This type of meeting is a valuable means of disseminating information and ideas which otherwise would not be realized through the normal channels of publication and scientific meetings. In addition, scientists in related fields become acquainted and valuable associations are formed which result in collaboration and cooperative effort between different laboratories.

It is hoped that each Conference will extend the frontiers of science by fostering a free and informal exchange of ideas between persons actively interested in the subjects under discussion The purpose of the program is not to review the known fields of chemistry, but primarily to bring experts up to date as to the latest developments, analyze the significance of these developments, and to provoke suggestions as to underlying theories and profitable methods of approach for making new progress. In order to protect individual rights and to promote discussion, it is an established rule of each Conference that all information presented is not to be used without specific authorization of the individual making the contribution, whether in formal presentation or in discussion. No publications are prepared as emanating from the Conferences.

The morning sessions, Monday through Friday, are scheduled from 9:00 A.M. to 12:00 Noon, Eastern Daylight Saving Time. The second session of each day is held in the evening from 7:30 to 10:00 P.M., Monday through Thursday. There are no Friday evening meetings.

Accommodations are available for a limited number of women to attend each Conference, also for wives who wish to accompany their husbands. All such requests should be made at the time of the request for attendance because these limited accommodations will be assigned in the order that specific requests are received.

Individuals interested in attending the Conferences are requested to send in their applications to the Director. Each applicant must state the institution or company with which he is connected and the type of work in which he is most interested. Attendance at each Conference is limited to 100.

Requests for attendance at the Conferences, or for any additional information, should be addressed to W. George Parks, Director, Department of Chemistry, University of Rhode Island, Kingston, R. I. From June 10 to September 2, 1955, mail should be addressed to Colby Junior College, New London, N. H.

Shown below are the programs for the 1955 Conference on corrosion and the Conference on the Chemistry and Physics of Metals.

Corrosion

E. A. Gulbransen, *Chairman*
J. J. Harwood, *Vice Chairman*

Fundamental Studies in Oxidation and Corrosion

Monday, July 18

Theory and Nature of Surfaces

A. Gwathmey, *Chairman*

R. D. Heidenreich—Application of Electron Instrumental Methods to the Study of Metal Surfaces.
J. S. Koehler—Structural Defects Produced by Cold Work and Their Possible Influence on Chemical Reactions.
N. Cabrera—The Nature of a Metal Surface as Suggested by Theories of Crystal Growth.
Open Discussion—The Nature of a Metal Surface on an Atomic Scale.

Tuesday, July 19

Substructure in Oxidation and Corrosion

J. J. Harwood, *Chairman*

E. Machlin—Recent Concepts and Observations of the Structure of Grain Boundaries and Subboundaries.
R. Bakish—The Chemistry of Grains and Grain Boundaries.
M. Metzger—Recent Investigations in the Field of Nucleation During the Oxidation of Pure Metals.
M. Simnad—Influence of Substructure upon Electrochemical Exchange, Electrodeposition, and Oxidation of Metals.
W. Harris—Oxide Substructure Formed on Single Metal Crystals.

Wednesday, July 20

Nature and Composition of Oxide Films

T. Rhodin, *Chairman*

F. Wormwell—Recent English Research on Films and Surface Layers on Metals.
T. Rhodin—Oxygen Adsorption on Stainless Steel.
W. Smeltzer—Kinetics of Oxide Film Formation on Aluminum-Magnesium Alloys.
T. Rhodin, *Organizer*. T. Gray, *Chairman*—Electrical Properties of Oxides.
F. Morin—Electron Transfer in Bulk Oxides of the Transition Metals.
D. Vermilyea—Electrical Properties of Oxide Films on Metals.

Thursday, July 21

Studies on Oxidation of Metals

W. J. Moore, *Chairman*

N. Cabrera—Recent Developments in the Theory of Oxidation.
W. Moore—Diffusional Mechanisms in Oxidation of Copper and Zinc.
J. Benard—Structural Aspects in the Selective Oxidation of Some Binary Alloys.
E. Birchenall—Studies on the Oxidation and Sulfidation of Iron.
J. Waber—Experimental Observations on the Cubic Law of Oxidation.

Friday, July 22

Corrosion of Zirconium and Other Metals

D. Thomas, *Chairman*

R. Misch—Electrical Properties of Oxide Films on Zirconium.
G. Cartledge—Inhibition of Corrosion by the Pertechnatate Ion.
G. Adams, Jr.—Subject to be announced.

Chemistry and Physics of Metals
Atom Movements

L. S. Darken, *Chairman*
R. Smoluchowski, *Vice-Chairman*

Monday, July 25

R. E. Hoffman—Self-diffusion in Dilute Binary Solid Solutions.
R. W. Balluffi—The Kirkendall Effect.
N. H. Nachtrieb—Self-diffusion in Crystalline Solids and in Liquids.
D. Lazarus—Diffusion in Noble Metals.
C. E. Birchenall—The Effect of Dissolved Carbon on the Self-diffusion of Iron in Gamma-Iron.

Tuesday, July 26

R. E. Ogilvie—Analysis of Diffusion Couples by X-ray Absorption.
A. S. Nowick—Study of Atomic Mobility by Anelastic Methods.
B. Schoeck—Interaction of Dislocations and Interstitials.
D. Turnbull—Role of Dislocations and Grain Boundaries in Precipitation Phenomena.
J. H. Koehler—The Quenching-in of Vacancies in Pure Gold.

Wednesday, July 27

E. S. Machlin—On the Driving Force for Atom Movements during Recrystallization.
W. C. Winegard—Segregation of Solute to Metal Surfaces.
Round Table—Phenomenology of Irreversible Processes. Howard Reiss, *Chairman*.

Thursday, July 28

Bruce Chalmers—Crystal Growth from the Melt.
K. A. Jackson—Solid Liquid Equilibria in Two Component Systems.
W. G. Pfann—Transport of Solutes by Zone Melting.
N. Cabrera—Recent Developments in Crystal Growth.
Amos Shaler—Sintering.
M. T. Simnad—Self-diffusion and Vapor Nucleation.

Friday, July 29

H. Reiss—The Influence of Holes and Electrons on the Heterogeneous Equilibria and Motions of Impurities in Semiconductors.
G. J. Dienes and G. H. Vineyard—Kinetics of Order-Disorder Transformations.

SECTION NEWS

Chicago Section

On March 4, R. Scott Modjeska, of the Scientific Control Laboratory, addressed the members of the Chicago Section on Electrodeposition on Nonconductors.

The basic problem in plating nonconducting materials is to obtain adherence of the plate to the base material. Sometimes organic materials are coated with paraffin or lacquer prior to applying the metallic coating. Preliminary conducting coatings can be put on nonconducting material by applying copper powder in gum-free cellulose and dissolving out the organic material, by putting on a thin film of silver by chemical reduction, by metal vaporizing, or by using a reducible metal spray. Normal electroplating can then be done over this initial conducting coating. Even with the best techniques, however, the initial coating typically does not have really good adherence to the plastic or other nonconductor.

If the plating is applied for decorative purposes, it is usually desirable to have a high gloss surface. This type of surface is typically much more difficult to acquire on plastics than on metals, since the latter can be buffed smooth prior to plating, and the plastics are difficult to buff. The processes are inherently more expensive than plating on metals both because of the techniques required and the greater care in handling and operations. Cleanliness is of extreme importance in all phases of the operation. Rinsing must be done with high quality distilled water throughout. Even with the most careful operational procedures rejects run high, so that the total cost of such plated objects is high.

For functional plating, the problems in obtaining good adhesion are the same as in decorative plating. If the piece is such that it can be enveloped with the plate, it usually wears fairly well since cohesion in the plate itself tends to hold it on. Sometimes plates appear to have better adhesion than they really do due to low coherence between grains in the plating itself. There are some special cases in which mechanical locking of the plate in surface roughness has helped considerably. In general, better intercrystalline locking is obtained from complex copper plating solutions than from the simple copper sulfate solution.

The market for decorative platings generally runs to small plastic objects which are more attractive when they have a shiny metallic plate on them. For functional plating, the printed circuits are a relatively new and fast growing market. Plated wave guides are in some demand.

J. E. Draley, *Secretary*

Niagara Falls Section

Expanding applications of the germanium power rectifier were reviewed by Mr. George F. Farnsworth, General Electric engineer, at the March meeting of the Niagara Falls Section.

The construction of the germanium power rectifier was shown. Emphasis was placed on its simplicity, relatively small size, and its efficient operation below 250 v.

The fact that aging does not exist with germanium rectifiers was proven in a life test of over three years. Its high performance in the 5800 kw of germanium power supplies thus far installed was mentioned.

The fact that the germanium power rectifier industry was rapidly expanding was highlighted by the fact that 6100 additional kilowatts will be installed and operating by the middle of this year.

High interest in this subject was evidenced by the number of questions asked during the discussion period.

L. A. Stoyell, *Secretary*

Washington-Baltimore Section

The thirty-first technical meeting of the Section was held on March 17 at the National Bureau of Standards. The speaker was Dr. Sidney M. Selis of the Diamond Ordnance Fuze Laboratories, whose topic was High Temperature Electrochemistry.

Dr. Selis described some of the experimental intricacies of high temperature investigations. The electrolytes commonly used in such work, eutectic mixtures of salts, must be prepared in as pure a state as possible, and removing the last traces of water presents difficulties. In the work described, chlorides of magnesium, nickel, and lithium were of particular interest with and without additions of silica and chromates. Reference electrodes for use in molten salt electrochemical work are now available and the designs of the silver, silver chloride and lead, lead chloride, and chlorine electrodes were briefly described.

Dr. Selis showed several proposed cell reactions that are supported by electrochemical measurements. For example, the emf, temperature relation for magnesium and nickel electrodes in the potassium-lithium chloride eutectic have been measured. The same cell has been studied with chromate and silicate additions and with additions of excess metal ion to the electrolyte. The proposed cell reactions are further supported by the identification of the several oxides and salts by x-ray diffraction, and by time-potential diagrams.

The discussion period was followed by a coffee hour.

Jeanne Burbank,
Secretary-Treasurer

PERSONALS

Herbert Bandes has been appointed Manager of the Chemistry Laboratory of Sylvania Electric Products Inc. The

Herbert Bandes

Chemistry Laboratory was formerly a part of the company's Physics Laboratory but Sylvania research in chemistry has expanded to the point at which it is advisable to administer the Chemistry Laboratory as a separate organizational unit under Dr. Bandes. Since joining Sylvania as a senior engineer in 1944,

1948 Corrosion Handbook

Members of the Society who wish to purchase copies of "Corrosion Handbook," H. H. Uhlig, Editor, 1948 edition, should send their orders for the book to Society Headquarters, 216 West 102nd St., New York 25, N. Y., in order to receive the 33⅓% discount given ECS members by John Wiley & Sons, Inc. The book costs $15.00. Members will, of course, pay postage; New York City residents will be billed for the city sales tax in addition.

Dr. Bandes has been interested in the fields of electroplating, radiochemistry, luminescence, inorganic semiconductors, and solid state physics. He is Vice-Chairman (Luminescence Group) of the Electronics Division of the Society and is a past chairman of its New York Metropolitan Section.

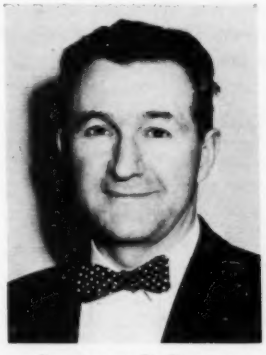

SHERWOOD B. SEELEY

SHERWOOD B. SEELEY, Technical Director of the Joseph Dixon Crucible Co. of Jersey City, N. J., was awarded a Certificate of Distinction by the New York University College of Engineering during the Midwinter Convocation at its Centennial Celebration. The citation reads in part ". . . New York University College of Engineering 1954–1955 hereby confers on Sherwood Bassett Seeley, valued alumnus of the College, whose professional achievements and services to the common good in our judgment are of distinct credit to himself and to this Institution in which he received part of his education, this Certificate of Distinction. . . ."

LOUIS KOENIG, Associate Director of Southwest Research Institute, was recently appointed Vice-President of the San Antonio research institute. Dr. Koenig, as Vice-President, will direct Southwest Research Institute's expanded chemistry, chemical engineering, minerals, metals, high energy, and applied biology divisions. He has been with Southwest Research Institute since 1951. Previously he served as assistant director of research at Stanford Research Institute and chairman of Armour Research Foundation's chemistry and chemical engineering department.

T. P. HOAR, English metallurgist, addressed Pittsburgh business and industry representatives at Carnegie Tech's Research Conference 15 on April 22. The Conference dealt with "Electrochemistry in Metallurgy" and Dr. Hoar spoke on selected topics in this field. Now a professor of metallurgy at Cambridge University, Dr. Hoar received international recognition when his thesis research became a classic on the corrosion of metals. It was the last quantitative proof of the electrochemical nature of corrosion in aqueous solutions. Other speakers were Dr. LING YANG and Dr. M. SIMNAD, both of Carnegie Tech. The research conferences are part of the school's plan to serve industry with new basic knowledge through cross-fertilization of scientific ideas.

CHARLES B. SANBORN

CHARLES B. SANBORN has joined the Electroplating Section of the Development and Research Division of The International Nickel Co., Inc., New York, N. Y. The Electroplating Section is principally concerned with the technical aspects of the applications and uses of nickel coatings. Mr. Sanborn was formerly associated with Graham Crowley & Associates, Inc., Chicago; Sherwin-Williams Co., Cleveland; and American Steel & Wire Co., Cleveland, where he was Senior Research Chemist at the company's research laboratories. He is a past chairman of the Cleveland Section of the Society.

FREDERICK WILLIAM DODSON

Fred Dodson, a long-time and active member of The Electrochemical Society, died at his home in Madison, N. J., on February 19, 1955. Mr. Dodson was born in Washington, D. C., on May 4, 1895. After graduation from high school in 1913, he left Washington for the course in electrochemistry at the Massachusetts Institute of Technology, where he obtained the B.S. degree. He ranked well scholastically and was a member of Beta Theta Pi social fraternity and of Pi Delta Epsilon, the journalism honorary fraternity.

After graduating in 1917, Fred joined the Bureau of Standards as a research chemist working on problems supplied by the International Association of Electrotypes. He soon realized that he would gain greater satisfaction in work allowing him to combine his technical ability with his gift for expression in writing. As a first step in this direction, he joined the U.S. Patent Office on January 1, 1918 as an assistant examiner. While with the Patent Office, he studied law at George Washington University, receiving his L.L.B. in 1922. During this period, he was on leave from May 1918 to July 1919 as an officer in the U. S. Navy. Most of his service was in the Atlantic and Mediterranean areas.

Shortly after receiving his law degree, Fred accepted a position as Patent Attorney with the Boston law firm of Heard, Smith and Tennant. He spent two years in active practice with this firm and then in 1924 transferred to the New York offices of Prindle, Bean and Mann. In 1931, the Bakelite Corporation, who were establishing a corporation patent department at the time, recognized Fred as a most promising young attorney and added him to their staff. Subsequently, when Bakelite joined Union Carbide and Carbon Corporation in 1940, Fred and the other Bakelite attorneys moved into the Patent Department of the parent company. He was a highly valued attorney for Carbide from this time on and rapidly reached the rank of senior patent attorney.

Fred was a member of the New York Patent Law Association, a member of the Massachusetts, New York, and District of Columbia Bars, and had been admitted to practice before the U. S. Supreme Court, the U. S. and Canadian Patent Offices, and the State and Federal Courts of Massachusetts, New York, and the District of Columbia. He was Chairman of the Patent Committee of The Electrochemical Society at the time of his death and had held this job since 1936. One of his greatest interests was the JOURNAL of The Electrochemical Society for which he prepared summaries of those patents of electrochemical interest.

Professionally, Fred was a man with a wide range of knowledge and abilities. His patent experience was primarily connected with the fields of resins, fungicides, insecticides, silicon chemistry, and electrochemistry. His employers recognized his versatility, however, and never hesitated to

assign him difficult, complex cases in many other fields.

At work or at home, Fred was a delightful companion, a courteous gentleman, and a helpful and wise adviser. Many of his friends remember with pleasure fishing trips to Barnegat Bay. Probably fishing was Fred's greatest hobby, although he also took a great interest in his garden and in travel.

He leaves behind him his wife, Hester Irene Dodson of Madison, N. J.; his children, Fred M. Dodson of Acworth, N.H., and Dorothy Belle Dodson of Madison; his mother, Marie Gertrude Dodson of Washington, D. C., and his sister, Mrs. Robert S. Gordon of Scarsdale, N. Y.

FRANK AUSTIN LIDBURY

Frank Austin Lidbury, distinguished scientist and industrialist, died at his home in Niagara Falls, N. Y., on September 17, 1954, at the age of 75.

Mr. Lidbury was born in Middlewich, England, on March 14, 1879. He graduated with honors in chemistry from Owen College, Manchester, England, and worked on a graduate fellowship at the University of London from 1898 to 1900 and at the University of Leipzig from 1900 to 1901.

He came to the United States in 1903, joining the staff of the Oldbury Electro-Chemical Co. He was vice-president of the company until 1923 when he became President, continuing in this capacity until his retirement in 1927.

Mr. Lidbury was a Past President of The Electrochemical Society, which he joined in 1903.

He was a Schoellkopf medalist of the Western New York Section of the American Chemical Society. He also was past district governor of Rotary and a member of the Niagara Club, the Buffalo Club, the Engineers Club of New York, and the Savage Club of London, England.

He is survived by his wife, Bessie Dixon Lidbury, and a brother, Sir Charles Lidbury of England.

NEW MEMBERS

In April 1955 the following were approved for membership in The Electrochemical Society by the Admissions Committee:

Active Members

William G. Burgers, Delft, Technical University, Laboratory of Physical Chemistry, 136, Julianalaan, Delft, Netherlands (Corrosion, Electrodeposition, Theoretical Electrochemistry)

Olin B. Cecil, Organic Chemicals Div., Monsanto Chemical Co.; Mail add: 921 N. Harrison, Kirkwood 22, Mo. (Theoretical Electrochemistry)

Augustus M. Chreitzberg, Jr., Naval Ordnance Lab.; Mail add: 8517 Eleventh Ave., Silver Spring, Md. (Battery)

Arthur H. Dierker, A. H. Dierker & Assoc., 939 King Ave., Columbus 12, Ohio (Electrothermics & Metallurgy)

Rupert L. Duffner, Hudson Wire Co., Ossining, N. Y. (Electrodeposition)

Thomas G. Edgeworth, Aluminum Co. of Canada, Shawinigan Falls, Que., Canada (Industrial Electrolytic)

Guy R. B. Elliott, Diamond Ordnance Fuze Labs.; Mail add: 4850 Bayard Blvd., Washington 16, D. C. (Theoretical Electrochemistry)

Robert W. Fritts, Milwaukee Gas Specialty Co., P. O. Box 461, Milwaukee 1, Wis. (Electronics)

Terry S. Gamble, National Carbon Co., 805 Davenport Rd., Toronto, Ont., Canada (Electrothermics & Metallurgy)

Tim W. Heilala, Penn Salt Manu-

ECS Membership Statistics

The following two tables give breakdown of membership as of April 1, 1955. The Secretary's Office feels that a regular accounting of membership will be very stimulating to membership committee activities. In Table I it should be noted that the totals appearing in the right-hand column are *not* the sums of the figures in that line since members belong to more than one Division and, also, because Sustaining Members are not assigned to Divisions. But the totals listed are the total membership in each Section. In Table I, Sustaining Members have been credited to the various Sections. Therefore, the total appearing for January 1, 1955 is 2141 as compared with the total of 2041 reported in the February Journal the difference being the 100 Sustaining Members that we had on record January 1, 1955.

TABLE I. *ECS Membership by Sections and Divisions*

Section	Division												
	Battery	Corrosion	Electric Insulation	Electrodeposition	Electronics	Electro-Organic	Electrothermics & Met.	Industrial Electrolytics	Theoretical	No Division	Totals as of 4/1/55	Totals as of 1/1/55	Net Change
Chicago	10	30	3	46	12	8	10	11	18	15	107	107	+5
Cleveland	42	36	4	46	33	8	18	27	41	15	165	157	+15
Detroit	5	17	6	33	5	7	5	4	21	21	75	77	+8
India	5	1	2	9	3	3	3	9	6	4	24	23	+1
Midland	6	13	0	5	1	2	6	14	6	4	37	37	+1
New York	61	100	19	132	62	26	45	51	76	75	415	375	+41
Niagara Falls	6	19	0	15	2	6	44	44	11	24	126	116	+21
Pacific Northwest	4	12	0	7	1	2	3	12	12	5	36	30	+7
Philadelphia	20	26	5	38	39	18	17	13	46	30	160	151	+16
Pittsburgh	3	27	4	21	7	5	19	14	24	13	79	74	+10
San Francisco	7	9	1	13	6	3	7	18	10	3	40	38	+2
Washington-Baltimore	33	37	11	32	18	3	12	11	26	9	109	104	+5
Ontario-Quebec	7	11	0	13	0	2	19	21	5	13	53	45	+10
U.S. Nonsection	66	149	22	157	85	50	92	93	134	104	617	609	+36
Foreign Nonsection	29	38	6	48	17	24	28	51	50	58	178	178	+2
Total as of 4/1/55	304	525	83	615	291	167	328	393	486	393	2221		
Total as of 1/1/55	281	516	81	590	276	169	309	374	460	306		2141	
Net Change	+23	+9	+2	+25	+15	−2	+19	+19	+26	+87			

TABLE II. *ECS Membership by Grade*

	Total as of 4/1/55	Total as of 1/1/55	Net Change
Active	1961	1889	+72
Life	14	14	0
Emeritus	37	39	−2
Associate	60	63	−3
Student	41	31	+10
Honorary	5	5	0
Sustaining	103	100	+3
Total	2221	2141	+80

facturing Co., Calvert City, Ky. (Industrial Electrolytic)

TAKESHI KETA, Nihon Sekiso Dry Battery Laboratory Ltd., Co.; Mail add: 278 Shimura Motohasunumacho, Itabashi-ku, Tokyo, Japan (Battery)

ARTHUR M. KILLIN, Electro Metallurgical Co.; Mail add: 4803 Lewiston Rd., Niagara Falls, N. Y. (Electrothermics & Metallurgy)

RALPH W. KULLMANN, National Carbon Co.; Mail add: 1360 Roselle Ave., Niagara Falls, N. Y. (Industrial Electrolytic)

NORMAN E. LAYCRAFT, Dept. of Public Works, Development Engineering Br.; Mail add: Box 882, Ottawa, Ont., Canada (Corrosion)

PETER R. MARSH, Driver Harris Co., Ltd.; Mail add: 101 Gates Ave., Montclair, N. J. (Electrothermics & Metallurgy)

JOHN T. MCCORMACK, Reynolds Metals Co., 4th and Canal, Richmond 9, Va. (Industrial Electrolytic)

WILLIAM L. MINARIK, General Mills Research Labs., 2010 E. Hennepin, Minneapolis 13, Minn. (Electronics)

MARTIN A. PRIETO, Western Electrochemical Co., 9036 Culver Blvd., Culver City, Calif. (Battery Industrial Electrolytic, Theoretical Electrochemistry)

MOISES G. SANCHEZ, Davison Chemical Co., Div. of W. R. Grace & Co., Baltimore 3, Md. (Industrial Electrolytic, Theoretical Electrochemistry)

THOMAS P. G. SHAW, Shawinigan Chemicals Ltd., Shawinigan Falls, Que., Canada (Electro-Organic)

GEORGE R. SHERWOOD, Wayne University; Mail add: 4841 Cass Ave., Detroit 1, Mich. (Electrodeposition)

Associate Member

IAN MACSWAN, Titanium Alloy Mfg. Div., National Lead Co.; Mail add: R. D. #2, Lewiston, N. Y. (Electrothermics & Metallurgy)

Student Associate Member

ARTHUR COHEN, McGill University; Mail add: 5859 Hutchison St., Montreal 8, Que., Canada (Electrodeposition, Electrothermics & Metallurgy, Industrial Electrolytic, Theoretical Electrochemistry)

Transfers to Active Membership

ARTHUR J. KERBECEK, JR., Food Machinery & Chemical Corp.; Mail add: 318 Highland Ave , Apt. 2, South Charleston, W. Va. (Electrodeposition)

DOUGLAS PERRY, Humble Oil and Refining Co., Houston Research Center, P. O. Box 2180, Houston, Texas (Corrosion)

Student Associate Memberships, Awarded by Cleveland Section for 1955

EUGENE P. SCHWARTZ, Western Reserve University; Mail add: 11205 Bellflower Rd., Cleveland 6, Ohio

HAROLD ROBERT GERBERICH, JR., College of Wooster; Mail add: 2536 Christmas Run Blvd., Wooster, Ohio (Theoretical Electrochemistry)

TITO T. SERAFINI, Case Institute of Technology; Mail add: 9318 Harvard Ave., Cleveland 5, Ohio (Electro-Organic)

JACK C. VOGT, Fenn College; Mail add: 5340 Knollwood Dr., Parma 29, Ohio (Theoretical Electrochemistry)

LETTERS TO THE EDITOR

Dear Sir:

I have studied the interesting work "Correlation of Limiting Currents under Free Convection Conditions" by C. R. Wilke, M. Eisenberg, and C. W. Tobias in the November 1953 issue of the JOURNAL and would like to make the following comments.

Measurements which were made within the scope of work done with the Laboratory of Physical Chemistry of the Swiss Federal Institute of Technology[1] showed that, for example, with current densities which are about a third of the limiting current density, the former is practically constant over the whole height of the cathode, provided the cathode covers the entire end of the cell.[2] If the cathode does not completely fill the cross section of the cell, a heavier deposition on the edges takes place. Therefore, I am wondering whether the current density distribution below the height of 1 cm, as plotted in Fig. 9 of the authors' paper and observed during their tests, might not by chance be due to so-called edge effects, i.e., to the cell geometry and not to natural convection. I am also wondering whether the asymmetry in the current density distribution is not in connection with the asymmetry of the geometrical arrangement in this way so that the cathode top edge nearly reaches the liquid level, whereas the lower cathode edge is at a greater distance from the bottom of the cell. In case of a prolonged electrolysis, development of layers of different density may also lead to asymmetry of the current density distribution.

W. RÜEGG
Laboratory
Injecta Limited
Teufenthal/AG, Switzerland

Dear Sir:

I wish to make the following remarks concerning the comments made above by Dr. Rüegg.

In the experiment represented in Fig. 9 of the above-mentioned paper, we were particularly careful to obtain a uniform primary current distribution. To accomplish this a 7.6 cm high electrode was used, whose lower edge began about 1 cm from the bottom of the Lucite cell. To avoid the effect of such an edge, a 1 cm Lucite plate was placed on the bottom of the cell so that effectively the electrode started from an insulator wall. The cell was filled only slightly (1–2 mm) above the upper edge of the cathode. In this manner (since the air acted as much as an insulator as the Lucite) a practically perfect geometry was obtained.[3]

Furthermore, to ascertain that the primary current distribution would be uniform for this geometry under conditions of uniform forced convection, an experiment with strong stirring was carried out in the same cell. In this control experiment, because of the uniformity of the rates of mass transfer practically over the entire electrode, the primary uniform current density distribution was not upset and this was verified by stripping sections and weighing.

As a matter of fact, if edge effect would be of any far-reaching significance we would have obtained a stronger edge effect at the top of the electrode than at the bottom, because the distance from the level at the top (2 mm) was no doubt larger than the possible clearance of the lower edge from the inserted Lucite plate.

Dr. Rüegg states that "in case of prolonged electrolysis, development of different layers of density may also lead to asymmetry in the current

[1] *Helv. Chim. Acta*, **36**, 1624 (1953).

[2] *See* also J. B. MOHLER, *Metal Ind. (London)*, **83**, No. 11, 219 (1953); J. STEINER, *Z. physik. Chem.*, **196**, 243 (1950).

[3] C. KASPER, *Trans. Electrochem. Soc.*, **77**, 353 (1945).

density distribution." As he is no doubt aware, it is precisely these density gradients that account for the bouyancy force developed in the cell which gives rise to the laminar type flow produced by the natural convection.[4]

We have found, in our work, that the time to establish natural convection in a cell is relatively short. Although dependent on both bulk electrolyte concentration and the magnitude of applied current, we have found under ordinary conditions that within a few minutes such a boundary layer is well developed and it does not take any prolonged period to obtain this secondary nonuniformity in the current distribution.

I wish, furthermore, to point out that an examination of the experimental curve in Fig. 9 shows that the relationship of the dependence of the local current density on the $-\frac{1}{4}$ power of the distance from lower edge (x) is well borne out by the experiment. This agreement is quite satisfactory within the experimental precision of the method of stripping and sectioning the deposited metal layer.

Strictly speaking, variation of the local current density depends not only on the distance of the lower edge (x) but also on other variables such as kinematic viscosity, diffusion coefficient, and the difference in concentration between the bulk of the electrolyte and the interface. Of these, the concentration gradient is the most important one since it enters with the 1.25 power. At the present time, insufficient experimental and theoretical evidence is available as to the variations of the concentration on the interface ($y = 0$), so that it is hard to give quantitative predictions for the variation of ΔC in the x direction. However, it is possible that this variation is significant enough and should not be ignored in the study of the distribution of the current along the electrode.

Morris Eisenberg
Stanford Research Institute
Stanford, Calif.

Dear Sir:

I am very interested in the thorough study of natural convection presented in the paper by C. R. Wilke, M. Eisenberg, and C. W. Tobias in the November 1953 issue because we are working on the same field in our laboratory. I have measured recently (by an impedance bridge method) the current density at which Cu-powder starts to be formed, when Cu is deposited from a $CuSO_4$ bath.[5] This current should correspond to the limiting current density.[6] It was found that at a vertical electrode of 4 mm height, under natural convection conditions, the current density at which Cu-powder starts to be formed was proportional to $C_o^{1.25}$ within a concentration range of $CuSO_4$ $0.01M$ to $CuSO_4$ $1M$.[5] These results are in very good agreement with those obtained by the authors.

On the other hand, Laitinen and Kolthoff[7] and, more recently, Skobets, Berenblyum, and Atamanenko[8] have found that the limiting current density under natural convection conditions is proportional to C_o (and not to $C_o^{1.25}$). Concentrations used by these authors ($2 \times 10^{-4}M$ to $5 \times 10^{-3}M$) were, however, much smaller than in the experiments where proportionality between the limiting current and $C_o^{1.25}$ was observed.

We are now engaged in our laboratory in an interferometric study of cathode films at vertical electrodes and the results obtained so far seem to show that the diffusion layer thickness increases with decreasing current density as long as the current density is high enough, but that the diffusion layer thickness remains more or less constant when the current density is smaller than about 2 ma/cm². A marked departure from the theoretical behavior has also been observed by Wilke, Eisenberg, and Tobias at low current densities, as may be seem from Fig. 7 of their paper.

It is true that the above experiments are not strictly comparable with each other (in the interferometric measurements the current was smaller than the limiting current density; in the experiments of Laitinen and Kolthoff wire electrodes were used). It is still interesting that all of them seem to indicate that the theoretical relationship between limiting current and concentration (or between diffusion layer thickness and current density) in general no longer holds when the current density and, therefore, the difference between the density of the solution at the electrode surface and in the bulk electrolyte is too small. I wonder if this behavior may be explained sufficiently by the circumstance that α and other properties are not strictly independent of concentration. There is also a possibility that some basic assumption made in the theory no longer holds when the current density becomes too small. The boundary layer equations of Prandtl, for instance, are approximations, which are valid only at high Reynolds numbers. It should be noted, however, that in the experiments of Wilke, Eisenberg, and Tobias, as shown in Fig. 7 of their paper, the departure from the theoretical behavior was greater with the higher electrodes than with the small ones. We are now making further interferometric measurements at small current densities. In case the authors have made experiments at smaller concentrations and, therefore, smaller current densities than those indicated in Fig. 7, we would appreciate it if they would let us know their results.

N. Ibl
Dept. of Physical Chemistry
and Electrochemistry
Swiss Federal Institute of Technology
Zurich, Switzerland

Dear Sir:

We were pleased to learn that Dr. Ibl and co-workers have, in addition to ourselves, confirmed the dependence of the limiting current density under conditions of natural convection on the 1.25 power of the bulk concentration as predicted in the theoretical development.[9]

The fact that Laitinen and Kolthoff as well as Skobets and co-workers have found the dependence only on the 1.00 power of the concentration can be explained, at least partially, by their use of dilute solutions up to $5 \times 10^{-3}M$.

Dr. Ibl rightly suggests that α might not be constant in the low concentration region. Indeed, as already indicated by us on p. 520 of our paper and will be demonstrated in a future publication,[10] in the dilute region (below about $10^{-2}M$) α is proportional to

[4] C. R. Wilke, C. W. Tobias, and M. Eisenberg, *Chem. Eng. Progr.*, **49**, 663 (1953); G. H. Keulegan, *J. Research Nat. Bur. Standards*, **47**, 156 (1951).

[5] To be published in *Helv. Chim. Acta*.

[6] N. Ibl and G. Trümpler, *Helv. Chim. Acta*, **35**, 363 (1952).

[7] H. A. Laitinen and I. M. Kolthoff, *J. Phys. Chem.*, **45**, 1061 (1941).

[8] E. M. Skobets, L. S. Berenblyum, and N. N. Atamanenko, *Zavodskaya Lab.*, **14**, 131 (1948).

[9] C. R. Wilke, C. W. Tobias, and M. Eisenberg, *Chem. Eng. Progr.*, **49**, 663 (1953).

[10] M. Eisenberg, C. R. Wilke, and C. W. Tobias, To be published.

$C_o^{-1/2}$. Substitution into equation (XXI) would then result in a prediction that the limiting current would depend on $C_o^{1.12}$. I believe that it would take experiments of very high precision to distinguish, for instance, between the power 1.00 and 1.12 when dilute solutions with resulting small I_L-values are employed. Any additional convection due to incidental temperature gradients or to vibrations could also obscure the results in the low current density region.

On the other hand it is pertinent to observe that Laitinen and Kolthoff employed thin wire electrodes. For such a small radius of curvature the hydrodynamic equations developed for a flat plate can apply only to a limited extent.

We believe that the points stressed above explain the deviation from the theoretical concentration dependence of I_L for dilute solutions. We do not see any reason why the theory should not hold for low concentrations (i.e., low currents). The laminar flow produced at the cathode under conditions of natural convection involves very small velocities and would correspond to very low Reynolds numbers—if such numbers can be defined for the case of free convection at a flat vertical plate. At high velocities a turbulent free convection flow would form. For such a case equation (XXI) does not apply and a different theoretical analysis would be required. In case of very tall electrodes it is indeed possible to observe (with a suitable beam of ordinary light) how the laminar convective flow at the lower end of the electrode gradually increases upward and becomes turbulent near the upper edge.[11] For the turbulent free convection case the boundary layer thickness can be expected to be uniform and therefore I_L to vary only with the 1.00 power of the bulk concentration.

M. Eisenberg
Stanford Research Institute
Stanford, Calif.

[11] Compare Fig. 2 of paper in footnote 9 p. 140C.

NEWS ITEMS

NSF Science Awards

The National Science Foundation, Washington, D. C., has announced the award of 715 predoctoral graduate fellowships in the natural sciences for the academic year 1955–1956. Successful fellows were selected from 2931 applicants from all parts of the continental United States, Alaska, Hawaii, and Puerto Rico. Honorable mention was accorded 1409 applicants. In addition to the predoctoral fellowships awarded, the Foundation also announced the names of 70 winners of postdoctoral fellowships. All awards were approved by the National Science Board upon the recommendation of Alan T. Waterman, Director of the Foundation.

The largest group of predoctoral fellowships, 167, was awarded in chemistry. In other fields the number of awards were: physics 151, engineering sciences 107, mathematical sciences 52, biochemistry 35, zoology 50, earth sciences 30, microbiology 20, psychology 27, biophysics 8, botany 16, agriculture 14, medical sciences 11, astronomy 9, genetics 10, anthropology 5, general biology 3.

Of the postdoctoral awards, 26 were made in the life sciences, 15 in chemistry, 15 in physics and astronomy, 11 in the mathematical sciences, 1 in the earth sciences, and 2 in the engineering sciences.

The fellows may attend any accredited nonprofit educational institution of higher learning in the United States or abroad.

Predoctoral fellowships carry stipends of $1400 for first year, $1600 for intermediate years, and $1800 for the terminal year of graduate study. Postdoctoral fellowships carry a stipend of $3400. All fellowships include additional allowances for dependents, tuition, and other normal expenses.

An announcement of the National Science Foundation predoctoral and postdoctoral fellowship programs for 1955–1956 will be made about October 1. Application forms will not be available until that time.

EJC Elects Constituent and Associate Societies

Engineers Joint Council has announced the election of The American Society of Refrigerating Engineers as a constituent society and the election of the American Institute of Industrial Engineers as an associate, the first organization to become an EJC associate. EJC now has nine constituent societies with a total membership of more than 196,000.

Objectives of EJC are the advancement of the general welfare of mankind through the available resources and creative ability of the engineering profession; cooperation among the branches of the profession; advancement of the science and profession of engineering; development of sound public policies in national and international affairs wherein the profession can be helpful through the services of members of the profession.

EJC has been taking steps toward increasing the unity of the engineering profession. A total membership of at least 5000 is required of a national organization to qualify for constituent membership. The American Society of Refrigerating Engineers, which has headquarters in New York City, has more than 6200 members. A recent constitutional amendment permits EJC to admit as Associates national organizations of less than 5000 members. The American Institute of Industrial Engineers, Columbus, Ohio, has some 3000 members.

Ozone Measuring Instrument

For the first time in scientific annals, a photoelectric instrument has been developed for the automatic, around-the-clock measurement of ozone—the poisonous, smelly gas suspected of being the major cause of smog in the Los Angeles atmosphere.

Announcement of the device, nearly a year in the making, was made by Dr. Lauren B. Hitchcock, president and managing director of the Air Pollution Foundation, who called the new ozone yardstick "an historic chapter in the battle against smog."

The first of these devices—conceived, developed, and built by the Foundation—has been placed in operation in North Hollywood. The design of the new instrument has been made available to the County Air Pollution Control District and the District has ordered that three additional devices be constructed.

Soon it will be known accurately how much poisonous ozone exists in Los Angeles' smoggy air and where most of the concentrations occur. With this information, the remaining problems—what causes ozone and how to remove it—will be well on the way to solution.

First Synthetic Mica Product

The first commercially manufactured synthetic mica component—a radio tube element spacer—was displayed at the 1955 Radio Engineering Show

held March 21–24 at Kingsbridge Armory, New York City.

The development of the new process by the Synthetic Mica Corporation, a wholly owned subsidiary of Mycalex Corporation of America, Clifton, N. J., provides America with a domestic source of this strategic material. More than 90% of the high-grade mica used in this country is being imported from India.

The synthetic mica radio tube element spacer exhibited actually improves vacuum tube reliability due to the fact that the synthetic material can be made chemically pure and free of the out-gassing components of natural mica at high temperatures. Production of the element spacers requires no specialized machinery; they are punched by conventional manufacturing methods from a sheet of synthetic mica.

The world's first synthetic mica plant, built by the Synthetic Mica Corporation at Caldwell Township, N. J., was scheduled to begin production in May.

New discovery solves acid copper plating problems...cuts plating costs

NEW ANACONDA

"PLUS-4" ANODES

(PHOSPHORIZED COPPER)

WHY PLATING WITH "PLUS-4" ANODES COSTS LESS!

+1 no anode sludge

+2 no copper "build-up" in solution

+3 smooth, heavy cathode deposits (no "bagging" or diaphragms required)

+4 up to 15% more cathode deposit per anode

ANACONDA "Plus-4" Anodes are the result of a revolutionary research discovery which disclosed that controlled additions of phosphorus and certain other elements to electrolytic tough pitch copper produced an anode for acid copper plating with which sludging off of copper particles was completely suppressed. This phenomenon eliminated copper sludge, copper "build-up" in the electrolyte, and migration of copper particles to the cathode causing nodular roughness. It was also discovered that anodes of phosphorized copper corroded much more uniformly, leaving a small, compact "fish" – providing an additional saving in scrap loss. ANACONDA "Plus-4" Anodes are made in all standard sizes and shapes . . . cost no more than ordinary rolled anodes.

SPECIAL TRIAL ORDER –

For details on how you can get a test supply of "Plus-4" Anodes sufficient to fill one tank, write to *The American Brass Company, Waterbury 20, Conn.* In Canada: *Anaconda American Brass Ltd., New Toronto, Ont.*

*For use under Patent No. 2,689,216

55145

"PLUS-4" ANODES AN ANACONDA® PRODUCT made by The American Brass Company

High-Purity Graphite

A new process developed by the Stackpole Carbon Company, St. Marys, Pa., permits the purification of graphite in diameters up to 2¾ in., and up to 43 in. in length, to almost the levels of purity previously achieved only in small-diameter, high-purity, spectrographic rods.

The four new high-purity grades all have a total ash content of 0.003% or less. Purification is carried out as a separate process on completely finished items to eliminate all possible contamination from machining or excessive handling.

The improved machining characteristics and larger sizes of the new grades open up many new fields for the economical use of this exceptionally pure material. Several of the Stackpole high-purity grades have been used successfully as crucibles and boats in the final purification of germanium. As heating elements in electric furnaces, they have shown materially longer life at very high temperatures. Other tests indicate improved tube performance when the new graphite is used as anodes in evacuated electron tubes.

Details on the physical and electrical properties of all new grades of new Stackpole High-Purity Graphite are available on request to the manufacturer.

Yardney Silvercels Power Latest Guided Missile

The contribution being made to U.S. defense by pint-size silver-zinc storage batteries—now revealed to be powering the nation's newest and "most important" guided missile, the USAF's Hughes Falcon—was outlined in April for a group of the nation's top aeronautical and electronic engineers.

Dr. Paul L. Howard, technical director of the Yardney Electric Corp., N. Y., which pioneered the development of silver-zinc batteries, discussed the operation and performance of Yardney Silvercels before the American Institute of Electrical Engineers, Dallas chapter meeting. The revolutionary, superpowerful storage cells now are coming into wide use in advanced secret aircraft, missiles, torpedoes, and various electronic and instrument applications.

Dr. Howard, former consultant to the Atomic Energy Commission and chief of the Navy's battery development division, noted that the "several" Yardney Silvercels used to power the rockets and electronic-guidance system

of the Falcon are smaller than ordinary cigarette packs and weigh only about three ounces each. They are rated at three ampere-hours, but are capable of much higher rates of discharge.

The 6-ft long, 100-lb Falcon, the nation's smallest guided missile, was made possible through the miniaturization of such components.

MEETINGS OF OTHER ORGANIZATIONS

American Society for Engineering Education, Annual Meeting, Pennsylvania State University, State College, Pa., June 20–24. The meeting will feature over 75 conferences dealing with all areas of engineering education, physics, mathematics, international relations, research, and others bearing upon the broad subject of engineering education. All sessions will be open to foreign guests who wish to attend. For further information write to the Secretary of the ASEE, Northwestern University, Evanston, Ill. For information regarding housing accommodations write to Professor Kenneth Holderman, Pennsylvania State University, State College, Pa.

American Electroplaters' Society, 42nd Annual AES Convention and 4th Industrial Finishing Exposition, Cleveland, Ohio, June 20–25.

American Physical Society, Toronto, Canada, June 22–24. Further information from: Karl K. Darrow, Columbia University, New York 27, N.Y.

ASTM, 58th Annual Meeting, Chalfonte-Haddon Hall, Atlantic City, N.J., June 26–July 1.

AIEE, Committee on Technical Operations, Summer General Meeting, New Ocean House, Swampscott, Mass., June 27–July 1.

Chemical Institute of Canada, Physical Chemistry Division Conference, Montreal, Canada, Sept. 8–9. Topic: Nuclear Chemistry.

American Chemical Society, National Meeting, Minneapolis, Minn., Sept. 11–16. Further information from: A. T. Winstead, 1155 Sixteenth St., N.W., Washington 6, D.C.

Illuminating Engineering Society, National Technical Conference, Cleveland, Ohio, Sept. 12–16. Further information from: A. D. Hinckley, Executive Secretary, 1860 Broadway, New York 23, N. Y.

Instrument Society of America, 10th Annual Conference and Exhibit, Shrine Exposition Hall and Auditorium, Los Angeles, Calif., Sept. 12–16. The theme will be "Instrumentation Paces Automation." Further information from: William H. Kushnick, 1319 Allegheny Ave., Pittsburgh 33, Pa.

American Institute of Mining and Metallurgical Engineers, Industrial Minerals Division, Asheville, N. C., Sept. 19–22. Further information from: H. N. Appleton, Assistant Secretary, 29 W. 39th St., New York 18, N. Y.

American Institute of Chemical Engineers, Regional Meeting, Lake Placid Club, Lake Placid, N. Y., Sept. 25–28. Further information from: Stephen L. Tyler, Executive Secretary, 25 W. 45th St., New York 36, N. Y.

BOOK REVIEW

Chromium Plating by P. Morisset, J. W. Oswald, C. R. Draper, and R. Pinner. Published by Robert Draper Ltd., 83/85 Udney Park Road, Teddington, Middlesex, England, 1954. 586 pages, 78/— net.

This is an excellent reference book on chromium plating, covering both European and American developments up to the end of 1953.

Although it is essentially based on "Chromage," published in French by Mr. Morisset, it has had the benefit of translation and additions by the English co-authors. It is a very complete work covering the uses and testing of chromium deposits as well as the theoretical and practical aspects of deposition and associated or, as the authors prefer to call them, "ancillary" processes.

The division of the subject is practical even though it results in some repetition, and if the section on "Theoretical Aspects" is briefer than one would like

MANUSCRIPTS AND ABSTRACTS FOR FALL MEETING

Papers are now being solicited for the Fall Meeting of the Society, to be held at the William Penn Hotel in Pittsburgh, October 9, 10, 11, 12, and 13, 1955. Subjects to be covered at the technical sessions will be Batteries, Corrosion, Electrodeposition, Electro-Organics, and Electrothermics and Metallurgy.

To be considered for this meeting, triplicate copies of abstracts (not to exceed 75 words in length) must be received at Society headquarters, 216 West 102nd Street, New York 25, N. Y., *not later than June 15, 1955*. Complete manuscripts should be sent in triplicate to the Managing Editor of the Journal at the same address.

this is due only to the dearth of material in this field. The authors have done a commendable job in standardizing the units of measurement used in the numerous graphs. One must still, however, realize that the British gallon is not equivalent to the American.

The section on hard chromium plating is quite complete, covering everything from the selection of the basis metal to treatment after hard chrome plating.

In the section devoted to properties of chromium deposits the authors have attempted, with reasonable success, to correlate the available data. This section covers hardness, wear resistance, friction, corrosion resistance, structure, and numerous other properties and is followed by a section on industrial applications.

Decorative chromium plating is quite fully covered, including the preparation and preplating of most commonly used basis metal. The book concludes with a section on miscellaneous associated material such as control, health hazards, and waste disposal.

In all it is a very satisfactory compendium, quite replete with graphs and illustrations and, except for an occasional use of the expression "theoretical speed of deposition" where "average speed of deposition" would be more correct, it is carefully written. The bibliography, which was selected from world-wide sources, seems quite complete and lists 425 references.

R. A. EHRHARDT

RECENT PATENTS

Selected from the Official Gazette.

March 1, 1955

Alexander, R. E., 2,703,311, Cadmium fluoborate electroplating solution

Clough, P. J., and Godley, P., 2,703,334, Coating

Andrus, O. E., 2,703,335, Sealed thermopiles

Lucas, G. B., 2,703,336, Electrical accumulator and separator

March 8, 1955

Baty, J. A., and Crowther, M. P., 2,703,432, Apparatus for manufacture of battery plate separators

Ransburg, E. M., 2,703,549, Apparatus for the electrostatic spray coating of articles

Hesch, F. H., 2,703,781, Anodic treatment of aluminum surfaces

Fields, E. K., 2,703,784, Corrosion inhibitors and compositions containing the same

Anderson, M. L., 2,703,790, Electron emissive materials

Prosser, E. A., 2,703,819, Electrolyte level indicator

Engelhardt, R., and Arledter, H., 2,703,857, Capacitor

March 15, 1955

Pantchechnikoff, J. I., 2,703,917, Manufacture of transistors

Robinson, P., and Peck, D. E., 2,704,105, Dielectric materials

Marriott, R. A., and Labbe, A. L., 2,704,135, Electrode suspension means for electrostatic precipitators

Ishler, H. K., and Grabiec, J. J., 2,704,169, Electronic tube

Pike, R. D., 2,704,239, Production of sodium bicarbonate and soda ash from trona

Avery, H. S., 2,704,240, Process of preparing tungstic oxide from sintered masses containing tungsten carbide

Gannon, C. E., 2,704,241, Device for dispensing alkali and water

Payson, P., 2,704,250, High temperature high strength alloys

Vordahl, M. B., 2,704,251, Titanium-base manganese alloy

Comeforo, J. E., 2,704,261, Machinable ceramic and process of manufacture

Michel, J. M., and Hager, K. F., 2,704,264, Process of protecting surfaces of metals against corrosion

Lyon, D. A., 2,704,265, Electrically conducting films on cast plastics

Yoshida, T., 2,704,273, Process for chromium electrodeposition

March 22, 1955

Hewitt, L. C., and Paul, A. J., 2,704,419, Glass furnace

Ohliger, L. P., 2,704,420, Process for making composite glass articles

Alexander, W. F., 2,704,512, Metal printing plate and method of producing same

Galloway, C. D., 2,704,593, Apparatus for assembling storage battery elements

Welker, H., 2,704,708, Method for the preparation of germanium

Markoski, J. A., 2,704,726, Method for producing a fluorescent screen and product

Pawlyk, P., 2,704,727, Method of deposition of nonconductive copper coatings from vapor phase

Electrochemist or Electrochemical Engineer

Major Electrochemical producer needs experienced man for project leader of experimental phase of development program on fused salt electrolysis. Should have several years experience in laboratory or plant development of fused salt cells. Minimum of BS degree in chemistry, chemical engineering, electrochemical engineering or related field is required. *Submit full details of your qualifications, including college transcript, to:*

ETHYL CORPORATION
c/o R. S. Asbury
Box 341
Baton Rouge, Louisiana

Pawlyk, P., 2,704,728, Gas plating metal objects with copper acetylacetonate

Deprez, C., 2,704,743, Mercury cathode electrolysis apparatus

McFarland, A. M., 2,704,780, Leakproof dry cell

Mautner, R. S., and Rosenberg, S., 2,704,781, Storage batteries

March 29, 1955

Schell, J. W., 2,704,992, Gas plating apparatus

Jumer, J. F., 2,705,191, Method and solution for treating aluminum

Faust, J. W., Jr., and Wynne, R., Jr., 2,705,192, Etching solutions and process for etching members therewith

Shen, T. E., and Plessner, K., 2,705,204, Ceramic dielectric materials

Heiskell, T. W., and Farmer, A., 2,705,219, Process of removing nitrogen trichloride from chlorine gas

Arthur, E. P., 2,705,220, Electrochemical apparatus

Ellis, G. B., 2,705,249, Primary alkaline cell

Kirkman, F. J., 2,705,250-251-252-253, Primary cell and battery

Middleton, R. G., 2,705,254, Battery and electrical conductor bracket therefor

Berlinger, F. J., 2,705,279, Portable self-contained flashlight and switch device therefor

April 5, 1955

Deer, L. L., 2,705,500, Cleaning aluminum

Laymon, K. T., 2,705,736, Voltage divider post for an electric battery

Daily, A. M., and Cocanower, G. M., 2,705,749, Variable electrical resistor and method of manufacture

LITERATURE FROM INDUSTRY

"The Electron Microscope." Illustrated brochure is available on the electron microscope. Included is complete information on two new RCA models, the EMU-3 and EML-1. Also listed are typical electron microscope applications. Radio Corp. of America. P-298

Oscillographic Recorder. Brochure describes a new oscillographic recorder which has a response up to 900 cycles, an unusual feature for direct writing oscillographs. Oscillograms are traced on blackened 35 mm acetate film by styli directly actuated by small excursions of galvanometer type movements. The magnified image of the film is directly projected on a built-in screen for studying or monitoring the progress of the recording. Eight recording channels provided, plus a ninth for use as timing or reference marking. Technology Instrument Corp. P-299

Control Catalogue. New 68-page catalogue of general purpose control devices, including a special section correlating by horsepower components for each type of motor control application, has been announced. The 2-color publication contains photos, book prices, wiring diagrams, and dimensions on motor starters, contactors, relays, solenoids, switches, push buttons, and pilot devices. Also included is information comparing applications and merits of manual and magnetic control, and across-the-line and reduced-voltage control. General Electric Co. P-300

Santolene® C, "single treatment" rust and corrosion inhibitor for petroleum products, is the subject of a recently published booklet. An ashless organic liquid, the material prevents rust and corrosion problems in clean petroleum products at concentrations of from 10 to 40 parts per million, depending on the corrosiveness of the product. It is compatible with the antioxidants, scavengers, dyes, and other additives used in gasolines. Because it is completely soluble in petroleum products it can be blended by injection or simple mixing. Monsanto Chemical Co. P-301

Motor Buying Information. 28-page catalogue of buying information on a-c motors is available. A special section on the selection of integral horsepower motors covers horsepower requirements, enclosures, starting current limitations, speeds, motor types, and selection of fuses and circuit breakers. Descriptions and specifications include single-phase, polyphase, totally enclosed fan cooled, and gear-type integral horsepower motors. Information on all motors includes photos, ratings, book prices, dimensions, weights, frame numbers, and standard modifications. General Electric Co. P-302

Thermocouple and Pyrometer Supplies. New edition of bulletin on thermocouples and pyrometer accessories has been published. Contains extensive engineering data on the selection and installation of the proper types of thermocouples, wells, head assemblies, and other pyrometer accessories, as well as recommended thermocouples for specific installations in the chemical, metal-working, iron and steel, ceramic, petroleum, food, and glass industries, and many others. The Bristol Co. P-303

Electrometer. Bulletin is offered on the Cary Model 30 Vibrating Reed Electrometer, which is used for radioactivity measurements, C^{14}, H^3, S^{35} determinations, mass spectrometry, electrical property measurements, and similar applications where very small currents, charges, and voltages are measured. Information is included on performance, operating principle, specifications, and modifications and accessories. Applied Physics Corp. P-304

Measurement and Control. Catalogue illustrates and describes the Weston Inductronic® System for Measurement and Control. It gives technical information, as well as application data, on the basic Weston Inductronic D-C Amplifying unit as well as on its companion models such as multirange d-c amplifiers, sensitizing amplifiers, integrating fluxmeters, limit and knife-edge control units, and product resolvers. Weston Electrical Instrument Corp. P-305

Hermetic Seals. Data sheet available on ADVAC Hermetic Seals, for temperatures to 1400°F, for pressures to 2000 psi. The ADVAC metallizing process makes it possible to produce hermetic seals capable of withstanding higher temperatures and severe thermal shock. These super-rugged seals are the result of the integration of the metal coating into the ceramic (aluminum oxide) itself. "Wedding" the two materials furnishes a bond for the soldering or brazing of metal parts. Advanced Vacuum Products, Inc. P-306

Rotameter Kits. 8-page bulletin includes pictures of all models, design and construction details, capacity charts, etc., on the complete and integrated system of rotameter kits for research laboratory, pilot plant, and field testing. Guaranteed interchangeability feature of the Brooks® Tru-Taper precision bore Rotameter tube, details regarding better than 20–1 flow ranges provided by dual-float principle with Accura-Density metering floats, and other important technical information is graphically presented. Brooks Rotameter Co. P-307

NEW PRODUCTS

PIPE THREAD SEALING COMPOUND. Gilbreth 18, new thread sealing compound of Teflon (duPont Trademark) has been announced. It is chemically inert, biologically inert, and can be used continuously from −150°F to 500°F. Seals threads completely without cementing. Equipment can be readily dismantled after intensive use. Recommended for pipes carrying volatile acids, alkalies, and solvents. The Gilbreth Co. N-168

HIGH TEMPERATURE MICROSCOPE. Newly developed, high temperature microscope provides a practical and efficient means for both visual examination and the photographic recording of specimens during their molten state in a microfurnace. Intended for refractories and ceramic research. Easy to adjust and operate. Over-all dimensions of the instrument are: 30 in. in length, 12 in. in height, 4⅛ in. in width. American Optical Co. N-169

FILTERING SPECIAL CORROSIVE SOLUTIONS. Certain solutions, that must be filtered, present a special corrosion problem. For example, the following plating solutions cannot be filtered without causing corrosion of stainless steel equipment: high chloride solutions, high chromic acid solutions, fluoboric acid solutions containing chlorides, high acid sulfate solutions. However, they can be filtered successfully by using special alloys and plastic materials. Sethco Filter Pumps VHI-5 and VHI-10, rated at 50 and 100 gal/hr, respectively, are equipped with Hastelloy C pumps, fittings, rigid unplasticized polyvinylchloride filter assemblies, and meet these exacting requirements. Hastelloy C Alloy is a nickel, molybdenum, chromium, tungsten, iron alloy. It is the most universally corrosion-resistant alloy available. The rigid P.V.C. filter assembly offers complete resistance to any type of plating or electropolishing solution. The Sethco LHI series, rated at 50 and 100 gal/hr, is identical to the VHI series, except that the filter assemblies are fabricated of high temperature Lucite. The LHI series can be used for filtering all the above-mentioned plating solutions, except the chromium plating solutions. Sethco Mfg. Co. N-170

To receive further information on any New Product or Literature from Industry listed above, send inquiry, with key number, to JOURNAL of The Electrochemical Society, 216 West 102nd Street, New York 25, N. Y.

Please print your name and address plainly.

FREQUENCY CHANGER. Answering the need for a compact supply to furnish constant 420 cycles, with output frequency as invariable as the input, a new unit has been developed. Motor is synchronous type, direct coupled in a compact unitary combination with a "Nobrush" 420 cycle generator. Resulting combination is free of brushes, exciter, slip rings, etc. Without any regulator or delicate auxiliary of any kind, the unit will maintain output voltage to better than 2% for a given load. Gerator Corp. N-171

A-C CLAMP VOLT-AMMETER. A lightweight, pocket-size Clamp Volt-Ammeter, with a single, easily read scale for all ranges and functions, and employing a special shock-mounted instrument movement, has been introduced. It incorporates the well-known Weston CORMAG® self-shielded mechanism with spring-backed jewels. Instrument furnished in a sturdy, scuff-proof case with convenient compartment for voltage test leads. Contains 6 current ranges of 300/150/60/30/15/6 amp, and 3 voltage ranges of 600/300/150 v. Weston Electrical Instrument Corp. N-172

TEFLON® COATINGS. A wide variety of problems are being solved by the use of Teflon coatings bonded directly to equipment and machine parts which are handling materials which are sticky or tend to leave undesirable deposits or scale. Teflon dispersion coatings may be bonded to any metal having a melting point over 750°F, except copper, by means of special primers and process developed by E. I. du Pont de Nemours & Co., Inc. The primer and finish coats are fused at a temperature of approximately 700°F after having been applied by spray. Although Teflon itself is unaffected by practically all common chemicals at temperatures up to 500°F, the coatings are not recommended for protecting metals against the attack of severely corrosive chemicals, since the coatings have a certain inherent film porosity which cannot be overcome by multiple coats. The fact that Teflon is chemically inert, however, broadens the scope of application. Information and literature available. Electro Chemical Engineering & Manufacturing Co. N-173

MAGNISTORS. A new rival to transistors and magnetic cores has been announced. These basic circuit elements, called Magnistors, have all the advantages of transistors and magnetic cores without the attendant disadvantages. In addition, they can be used in many places where electronic tubes are used with an enormous increase in dependability which is characteristic of magnetic circuits. The Magnistors will be sold as components as well as in complete packaged systems. They are classified into two specific groups. One, amplifiers in which extremely small electrical signals can control other circuits having several thousand times the power. The other, a "two state" or bistable storage device which can be turned "on" and "off" by small electrical pulses. Potter Instrument Co. N-174

TWO-FOOT FURNITURE UNIT. Newest unit in the Fisher Unitized Furniture line, a drawer-cupboard unit only 2 ft wide, fits easily into the left-over space at the end of bench assemblies or any other "tight" installation, can be squeezed in to take up nonutilized slack. Height of the unit is universal 36 in.; thus it forms a continuous working surface with the other "standing height" units in the laboratory. The unit is made of heavy-gauge steel; bonderized to make the finish adhere and for rust-proofing; with *three* baked-on coats of enamel for high resistance to chemical, mechanical wear. All units have kiln-dried birch reagent shelf with acid-proof finish. Fisher Scientific Co. N-175

ADVERTISERS' INDEX

American Brass Company..... 142C
Enthone, Incorporated..... Cover 4
Great Lakes Carbon Corporation..... Cover 2
McGraw-Hill Book Company, Inc..... 123C
National Carbon Company..... 124C
Rapid Electric Company..... 126C
Sylvania Electric Products Inc... 128C
Weston Electrical Instrument Corporation..... 125C

1955

EX

142C
ver 4

ver 2

123C
124C
126C
128C

125C

ation.
lable.
Manu-
N-173

ansis-
been
nents,
dvan-
cores
tages.
many
used
epend-
mag-
vill be
com-
are
. One,
ll elec-
ircuits
s the
te" or
an be
l elec-
Co.
N-174

Newest
rniture
ly 2 ft
space
or any
an be
l slack.
36 in.;
vorking
anding
y. The
steel;
adhere
baked-
ance to
l units
shelf
ientific
N-175

h
p
th
fr

st
ra
L
ce
If
in
ca
ce

fo
h
ef
m
tv
th
p

p
d
st
I
si

o

p
3

Resistance Studies on Various Types of Dry Cells[1]

RICHARD GLICKSMAN AND C. K. MOREHOUSE

RCA Laboratories, Radio Corporation of America, Princeton, New Jersey

ABSTRACT

A direct current method has been devised for measuring the internal resistance of dry cells. Data are presented which show that the internal resistance of a Leclanché type of dry cell is greater when measured at low current drains than at high current drains. This difference is believed to be due to a film formation on the zinc anode. It is also shown that during discharge the drop in terminal voltage of a dry cell owing to an increase in internal resistance is small. It is believed that *p*H changes of the electrolyte at the electrode surfaces and the change in the composition of the surface of the manganese dioxide electrode account for most of the potential drop when a Leclanché cell is discharged.

Studies made on magnesium-manganese dioxide cells show that these cells undergo greater instantaneous voltage fluctuation than the conventional Leclanché cells. This voltage fluctuation is due to a high resistance coating on the magnesium anode. The direct current method for measuring internal resistances of dry cells described in this paper could be useful in the study of film formation on the surface of magnesium electrodes.

INTRODUCTION

Resistance of cell components and departure of half-cell potentials from their reversible electrode potentials are some of the factors which determine the rate at which electrical energy can be withdrawn from any electrochemical cell.

The mercuric oxide-zinc type of dry cell has a constant voltage curve when discharged over a wide range of current drains, whereas the voltage of the Leclanché (manganese dioxide-zinc) type of cell decreases with time, especially at high discharge rates. It has been the opinion of many that the increase in internal resistance is an appreciable factor in causing this drop in terminal voltage of the Leclanché cell during discharge.

Several alternating and direct current methods for measuring the internal resistance of batteries have been proposed (1–4). It is essential that the effect of electrode polarization be eliminated when making resistance measurements by either of these two methods. Direct current measurements, unless they are made in short time intervals, include some polarization effects.

A direct current method has been devised, whereby pulses of current on the order of $\frac{1}{5}$th of a second duration are withdrawn from the cell and the instantaneous *IR* drop measured. This instantaneous *IR* drop represents the voltage drop due to the resistance of cell components.

Measurements have been made on several types of dry cells using this method to determine the change of resistance as the cells are discharged and the effect of resistance on cell performance.

[1] Manuscript received August 20, 1954. This paper was prepared for delivery before the Boston Meeting, October 3 to 7, 1954.

EXPERIMENTAL APPARATUS

The apparatus designed for making the resistance measurements consists of (*a*) an RCA WO-27A D-C oscilloscope with a P-7 screen that retains the image for a few seconds; (*b*) a discharge circuit containing a variable resistance and a booster battery for maintaining a constant current; and (*c*) a potentiometer circuit to balance out the voltage of the cell under test allowing potential changes to be read on the oscilloscope.

A circuit diagram of the apparatus is shown in Fig. 1. A and C designate the anode and cathode of the cell being tested, and T is a reference saturated calomel electrode used for single electrode studies. Cell electrodes are connected to the oscilloscope and potentiometer circuit by means of two switches. Switches S_1 and S_2 in the position shown connect the anode and cathode to the oscilloscope. If S_1 is moved to position T, the half-cell readings of either electrode can be made depending on the position of switch S_2. Current drawn from the test cell by the oscilloscope and potentiometer circuit is negligible, being less than 1 μa.

The discharge circuit consists of a series of microswitches, S_3, S_4, S_5, and S_6, for opening and closing the discharge circuit at controlled time intervals, a milliameter, MA, a variable resistance, R_L, and a booster battery, B_2, connected in series with the test cell A-C.

The potentiometer circuit consists of a variable resistance, R_p and a battery, B_1. The voltage of the

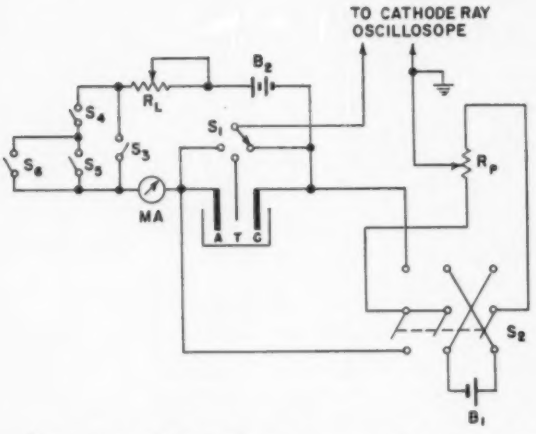

FIG. 1. Schematic diagram of apparatus used for d.c. resistance measurements of galvanic cells.

potentiometer circuit is adjusted to equal and oppose that of the test cell when on open circuit.

Two procedures, (*a*) the potential-decay, and (*b*) the potential-recovery, for measuring the resistances of cells have been used in this work.

Potential-decay method.—If switch S_3 is left open, switches S_4 and S_5 must be closed in order to draw current from the cell. Switches S_4 and S_5 are operated by cams mounted on slow speed shafts driven by fractional horsepower motors. They continually make and break the circuit, S_4, once every second and S_5 once every nine seconds; therefore, current flows through the experimental cell every ninth second when both S_4 and S_5 are closed. The time interval of any one discharge is one-fifth of a second. This setup was included so as not to discharge the cell at too fast a rate while making measurements. However, if switch S_6 is closed, the current that flows through the experimental cell is controlled by S_4 alone, and the cell will be discharged for one-fifth of a second every second.

In this method, the cell is on open circuit and a pulse of current is withdrawn from it. There is an instantaneous drop in potential, which manifests itself as a vertical drop on the oscilloscope, followed by a more gradual drop in potential due to polarization of cell electrodes. Resistance can then be calculated from a measurement of the instantaneous *IR* drop and the current flowing. This is termed the potential-decay method of measuring the resistance.

Potential-recovery method.—An alternate method of measuring resistance is to measure the instantaneous *IR* recovery when the load is taken off the cell. This measurement can be controlled simply by closing and opening switch S_3, and thereby causing the battery to go from a closed circuit to an open circuit condition, with the accompanying increase in voltage.

Measurements by these two methods are made 10^{-3}–10^{-4} sec after the current has been switched on or off. This would preclude any change in potential due to polarization effects which are negligible during this short time interval.

VARIATION OF INTERNAL RESISTANCE WITH CURRENT DRAIN IN DRY CELLS

Experimental

Resistances of various size Leclanché and alkaline RM-1 cells were measured at various current drains by the potential-decay method. Short pulses (1/5 sec duration) of current ranging from 5 to 800 ma were withdrawn from the cell and the resistance computed from the instantaneous *IR* drop as measured on the oscilloscope.

Results obtained are shown in Fig. 2; each point represents the average of 2–4 measurements.

It should be noted from these data that the resistance of the Leclanché cell decreases as the current drain is increased, whereas the resistance of the RM-1 alkaline cells was nearly constant over the discharge current range of 5–200 ma.

Additional Leclanché cells were tested by the same potential-decay method as used above, only the cells were discharged 10–20 times at pulses of 1/5th sec duration before the actual *IR* drop was measured. Data as presented in Table I show that under these conditions the measured resistance is more nearly constant as the current drain is increased from 25 ma to 400 ma.

A third set of results was gathered on D size Leclanché cells, using the potential-recovery method previously described. The cells were discharged continuously for 5 min after which the current was interrupted and the instantaneous increase in potential was measured on the oscilloscope. Results presented

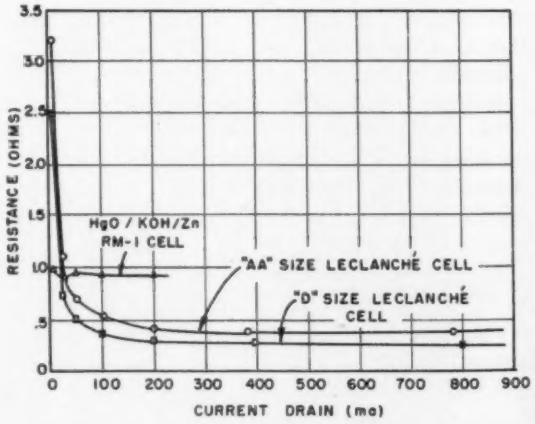

FIG. 2 Effect of current drain on the internal resistance of dry cells.

TABLE I. *Internal resistance (ohms) of size D Leclanché dry cells measured at various current drains*

Current drain (ma)	Potential-decay method			Potential-recovery method	
	No. 5	No. 6	No. 7	No. 8	No. 9
25	0.28	0.28	0.33	0.22	0.19
50	0.25	0.31	0.30	0.22	0.19
100	0.23	0.28	0.27	0.22	0.18
200	0.22	0.21	0.23	0.20	0.18
400	0.20	0.23	—	—	—

in Table I are in agreement with those obtained by the second procedure, but are not in agreement, at low current drains, with data gathered by the first technique.

In order to determine which electrode of the Leclanché cell was causing a variation of resistance with current drain, a cell was constructed in a beaker using the same size electrodes as found in the conventional D size Leclanché type dry cell. A saturated calomel reference electrode was used to measure the change of potential at the two respective electrodes as the current drain was varied. It was found qualitatively that the resistance between the manganese dioxide and the reference electrode was constant by the potential-decay method over the current drain range 25–200 ma. The resistance between the reference electrode and the zinc electrode, however, decreased as the current drain was increased in the manner shown in Fig. 2. These data, while qualitative, show that the zinc electrode is the electrode which causes a variation in resistance when measured under certain conditions.

Discussion

Vinal (1) has pointed out that, as far back as 1885, Preece found that the resistance of a cell was greater when measured at high current drains than when measured at low current drains. This has been observed by several subsequent experimenters (1, 2), and appears to be true for primary and secondary batteries.

Since resistances of the electrolyte, electrodes, and separator are definite physical quantities independent of the current flowing through the cell, there must be another resistance factor which varies with current drain. Chaney (5) investigated the performance of dry cells and concluded that there is a contact resistance in dry cells due to the formation of a hydrogen layer or film on the zinc as a product of the zinc corrosion reaction. It is Chaney's opinion that this film is considerably altered as the current drain is varied, being removed at high current densities.

Data presented in this paper support Chaney's findings, namely, that the resistance of a dry cell is less when the current drain is greater. The variation of resistance is believed to be due to a film formed over the surface of the zinc electrode, the nature of which varies as the cell is subjected to varying current drains. The present experiments have not identified the existence or the nature of the film, but it is believed that a film does exist and that this film is either a hydrogen layer or an oxide type of coating. Constant resistance values can be obtained providing the cell is discharged a sufficient amount to remove the film.

Effect of Discharge on the Internal Resistance of Dry Cells

The Leclanché and the alkaline RM type cells differ in their discharge characteristics, especially at high discharge rates. The RM cell has a constant voltage discharge curve, whereas the voltage of the Leclanché cell decreases gradually with time. Many observers believed that this difference is due to a large extent to an increase in the internal resistance of the Leclanché cell, caused by the formation of high resistant products such as $Mn_2O_3 \cdot H_2O$, $ZnO \cdot Mn_2O_3$, $Zn(NH_3)_2Cl_2$, or $ZnCl_2 \cdot 4Zn(OH)_2$, whereas a more conductive discharge product, metallic mercury, is formed in the alkaline mercuric oxide cell.

Leclanché and RM dry cells were discharged continuously at 200, 100, and 50 ma constant current drains and the internal resistance measured by interrupting the flow of current at various time intervals of discharge. The instantaneous increase in potential was measured on the oscilloscope and the resistance calculated.

The change in cell voltage with time for a D size Leclanché cell discharged continuously at 200 ma constant current is presented in Fig. 3. Also included is a curve showing the potential (IR) drop with time

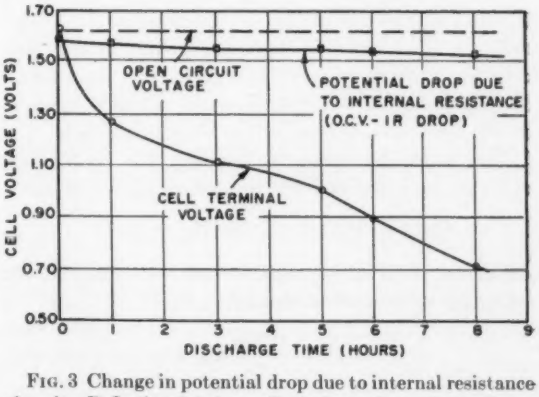

FIG. 3 Change in potential drop due to internal resistance of a size D Leclanché dry cell discharged continuously at 200 ma constant current drain.

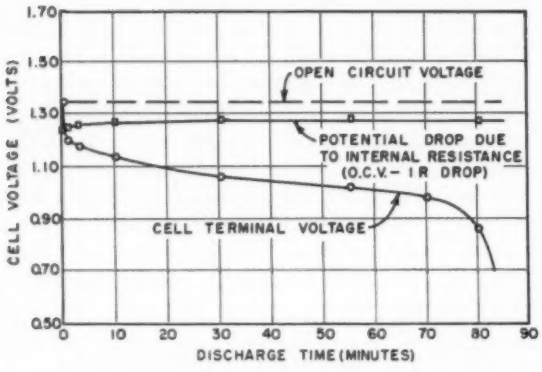

FIG. 4 Change in potential drop due to internal resistance of an alkaline-mercuric oxide RM-1 dry cell discharged continuously at 100 ma constant current drain.

as a result of the change in resistance as the cell is discharged. The potential loss due to internal resistance is small, varying from approximately 0.04 to 0.08 during cell discharge. This corresponds to an increase in resistance from 0.20 to 0.41 ohm as the cell voltage decreases from 1.62 to 0.72. Even when the cell is discharged for 24 hr to a voltage of 0.07, the resistance increases only to 0.74 ohm. These data show that the voltage drop owing to a change in internal resistance is negligible compared to the total drop in cell voltage.

Comparable results obtained on mercuric oxide RM-1 cells are shown in Fig. 4.

These data show that the internal resistance of the mercuric oxide cell does decrease slightly, but this change is a minor factor in causing a change in cell voltage as the cell is discharged.

Discussion

It has been shown by others that the manganese dioxide is the limiting electrode of a Leclanché dry cell. This paper shows that the potential decrease or increase due to a change of internal resistance is small as the Leclanché or the alkaline RM type cells are discharged. A more important factor than resistance which probably contributes to the gradual drop in potential is a change of *p*H of the electrolyte at the electrode surface due to the cell reaction.

The cathodic reaction for the Ruben-Mallory cell can be expressed by the following equation:

$$HgO + H_2O + 2e^- = Hg + 2OH^-$$

Applying the Nernst equation to the reaction, the following expression is obtained:

$$E = E^0 - \frac{0.059}{2} \log a^2_{OH^-}$$

Since E^0 is a constant, the potential E of the half-cell reaction is dependent on the concentration of the hydroxide ion, i.e., it is a function of *p*H. Since the electrolyte in this cell is strongly basic (35–40% KOH), it would be expected that formation of hydroxyl ions during discharge would have little or no effect on the *p*H of the electrolyte and, therefore, the electrode potential. The fact that the system has a fairly constant discharge potential is probably due to the direct reduction of mercuric oxide to mercury without intermediate products, along with a constant *p*H during discharge.

The cathodic reaction for the Leclanché cell can be written:

$$2MnO_2 + 2H^+ + 2e^- = Mn_2O_3 \cdot H_2O$$

and applying the Nernst equation, it is seen that this electrode is *p*H dependent:

$$E = E^0 - 0.059\ pH$$

Cahoon (6) and McMurdie, Craig, and Vinal (7) investigated the effect of *p*H on the manganese dioxide potential. The latter showed that in acid solutions the change in potential of the manganese dioxide electrode is 0.12 v per unit change of *p*H, while in basic solution the change in potential is 0.06 v per unit of *p*H. Cahoon and Heise (8) reported that as a D size Leclanché cell is discharged through a 4 ohm resistance, the *p*H of the paste layer changes from 4.7 to 3.8, while the innermost portion of the manganese dioxide cathode mix changes from 5.8 to 10.1. On the basis of these data, change in *p*H can account for approximately 30% of the total potential drop from a 1.50 voltage level to the 0.75 v end point. It has also been shown by Herbert (9) that the manganese dioxide electrode polarizes to an appreciable extent when discharged in a strongly alkaline solution. Thus, while the effect of *p*H on the manganese dioxide electrode is a factor in causing the Leclanché cell to polarize on discharge, there must be other factors which play a major role.

Ferrell and Vosburgh (10) assumed that a solid solution is formed between the manganese dioxide and a lower oxide of manganese, and that the oxidation potential is dependent on the composition of the solid solution. Johnson and Vosburgh (11) found that electrodes made with mixtures of precipitated manganese dioxide and manganese oxyhydroxide have potentials varying linearly with the logarithm of the ratio of the two oxides.

It is concluded from a survey of the literature and data presented in this paper that polarization of the manganese dioxide electrode is due to a change in *p*H of the electrolyte and electrode composition at the electrode surface, which results in a lower electrode potential. It is also recognized that, depending on the rate of discharge, a variation in

electrode potential can be caused by diffusion effects at the electrode surface. This is shown by the difference in performance of a Leclanché cell when it is discharged at high and low current drains and on continuous and intermittent types of tests. Change in internal resistance accounts for only a small percentage of the total voltage drop as the cell is discharged.

Application of Present Methods to a Study of Magnesium-Manganese Dioxide Type Dry Cells

Magnesium-manganese dioxide dry cells of the type described by Kirk, Fry, and George (12, 13) were studied with the apparatus shown in Fig. 1. The cells were of the conventional construction and contained magnesium alloys, AZ10A and AZ31A, as anodes, an African manganese dioxide cathode blended with acetylene black and barium chromate, an absorbent paper separator, and a magnesium bromide electrolyte. Data obtained on magnesium and zinc-manganese dioxide AA size dry cells discharged intermittently at current drains of either 10 or 50 ma are plotted in Fig. 5. The discharge cycle as shown is approximately $\frac{1}{5}$ sec duration followed by 1 sec open circuit.

The data presented show changes in terminal voltage of the cell after the discharge cycle had been repeated approximately five to ten times.

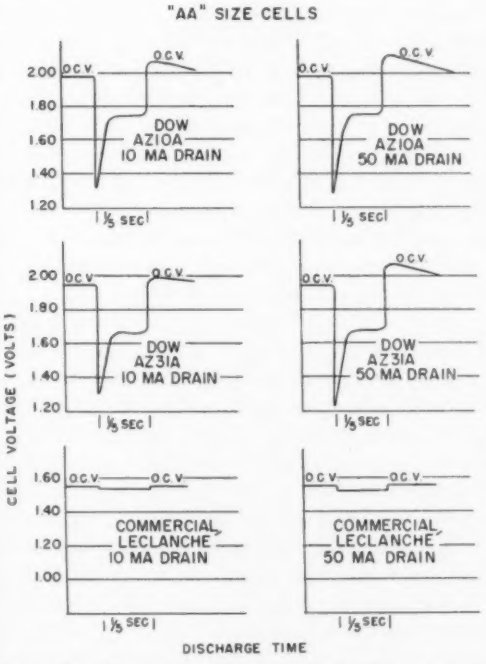

Fig. 5 Oscillographic measurements of change in voltage of AA size magnesium and zinc Leclanché type cells, subjected to 10 and 50 ma constant current drains.

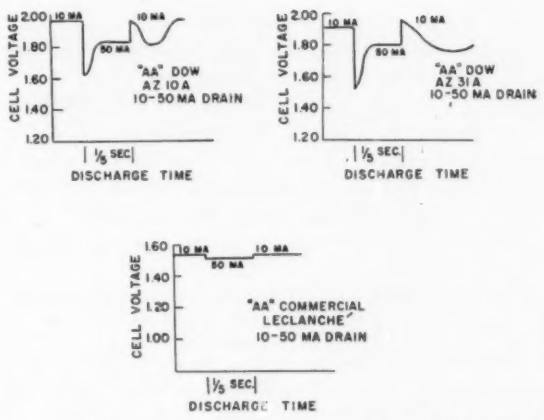
CELL VOLTAGE
10 MA
50 MA
"AA" DOW AZ 10 A 10-50 MA DRAIN
"AA" DOW AZ 31 A 10-50 MA DRAIN
"AA" COMMERCIAL LECLANCHE 10-50 MA DRAIN
1/5 SEC
DISCHARGE TIME

Fig. 6 Oscillographic measurements of change in voltage of AA size magnesium and zinc Leclanché type cells when subjected to a change in constant current drains from 10 to 50 ma.

The large initial drop is due to the resistance of the oxide or chromate type film on the magnesium, the voltage rising as the oxide layer is removed reaching a more steady state. When the circuit is opened the cell voltage rises above the original open circuit value and then gradually returns to its original value. This is primarily due to the reformation of the oxide coating on the surface of the magnesium.

The apparatus shown in Fig. 1 was modified to measure voltage fluctuations of cells discharged intermittently for 1 sec on a 10 ma drain followed by a $\frac{1}{5}$ sec discharge at a 50 ma drain. This represents a condition which might be encountered in a transistor-operated radio receiver utilizing a class B amplifier circuit. Results obtained on AA size magnesium and zinc-type cells are shown in Fig. 6. It is seen that the magnesium cells, while operating at a higher voltage level than the Leclanché cell, have a larger potential drop as the load is changed from 10–50 ma. This is because of the existence of a high resistance film on the magnesium anode.

Data presented in this section show that, because of the coating on the magnesium anode, the voltage of the magnesium dry cell undergoes greater fluctuation than the Leclanché cell. This method of study is suggested as a means of studying the "delayed action" as encountered in magnesium dry cells.

Acknowledgment

The authors wish to express their appreciation to Dr. Ross E. Shrader for assistance in designing and constructing the equipment for making the d-c resistance measurements.

Any discussion of this paper will appear in a Discussion Section to be published in the December 1955 Journal.

REFERENCES

1. G. W. VINAL, "Storage Batteries," 3rd ed., Chap. VII, John Wiley & Sons, Inc., New York (1940).
2. E. F. NORTHRUP, "Methods of Measuring Electrical Resistance," Chap. XI, McGraw-Hill Book Co., New York (1912).
3. N. C. CAHOON, *Trans. Electrochem. Soc.*, **92**, 159 (1947).
4. W. HEUBNER, *Elektrotech. Z.*, **61**, 149 (1940).
5. N. K. CHANEY, *Trans. Am. Electrochem. Soc.*, **29**, 183 (1916).
6. N. C. CAHOON, *Trans. Electrochem. Soc.*, **68**, 177 (1935).
7. H. F. MCMURDIE, D. N. CRAIG, AND G. W. VINAL, *ibid.*, **90**, 509 (1946).
8. N. C. CAHOON AND G. W. HEISE, *J.* (*and Trans.*) *Electrochem. Soc.*, **94**, 214 (1948).
9. W. S. HERBERT, *This Journal*, **99**, 190*C* (1952).
10. D. T. FERRELL, JR., AND W. C. VOSBURGH, *ibid.*, **98**, 334 (1951).
11. R. S. JOHNSON AND W. C. VOSBURGH, *ibid.*, **100**, 471 (1953).
12. R. C. KIRK AND A. B. FRY, *J.* (*and Trans.*) *Electrochem. Soc.*, **94**, 277 (1948).
13. R. C. KIRK, P. F. GEORGE, AND A. B. FRY, *This Journal*, **99**, 323 (1952).

Investigation of Storage Battery Failure by a Method of Plastic Impregnation[1]

A. C. Simon and E. L. Jones

Naval Research Laboratory, Washington, D. C.

ABSTRACT

Electrolytic cells may be prepared for microscopic examination by replacement of the electrolyte with liquid epoxy resin, which later hardens. The cell containing the hardened plastic may then be cut into sections and the cell elements examined in detail after suitable grinding and polishing. Growth and buckling of plates may be observed and measured and the rate of corrosion determined from the area of the remaining metal in the grid cross section if the area of the original is known. Modified chemical microscopy, spot testing, and physical measurements offer possibilities for identification of products of reaction and corrosion.

Introduction

In any post-mortem examination of the lead-acid storage battery, the fragile condition of the remaining grid structure and the tendency of the active materials to shed makes the task more difficult. The plates tend to disintegrate after disassembly of the elements so that the original physical relationship of the various parts becomes uncertain and the cause of failure may evade detection.

Just as metallography has immeasurably increased the knowledge of the structure of metals so likewise do well-prepared cross sections of battery elements offer equal possibilities for increased knowledge of battery processes. An attempt to prepare such specimens was first reported by Buckle and Hanemann (1), who impregnated individual battery plates with carnauba wax and subjected them to microscopic examination after suitable polishing. Sections of plates have also been imbedded in the thermoplastic resins used for mounting metallurgical specimens. These methods are not suitable for the impregnation of an entire cell and, in addition, require the use of heat or pressure that may produce changes in the active material.

The present description is based on the use of an epoxy resin that may be introduced into the cell as a liquid and then left to harden by catalytic action. The solid cell may then be sectioned, polished, and the resulting cross section of the battery element studied for both macro- and microstructure (Fig. 1).

Although the method herein described offers no microscopic technique that could be considered new, the application of an impregnating and sectioning technique to the study of cell processes appears to offer unusual possibilities for investigation. In this paper the authors have attempted to give examples of possible applications rather than a report on a specific use. The method, however, has been applied with considerable success to a study of the mechanism of grid corrosion, the results of which will be subsequently reported. The procedure described is by no means perfected, but produces results encouraging enough to justify further investigation.

Experimental Procedure

The procedure outlined below has been applied to many types of batteries without difficulty. Experience has shown, however, that a plastic suitable for impregnating a storage battery cell should possess the following characteristics: (*a*) the plastic or any contained solvents should not react with any cell unit such as case, separators, or active material; (*b*) the plastic in the liquid condition should possess a low viscosity; (*c*) the period of setting should be long enough to allow penetration of the plastic to all parts of the cell and into the various porous portions; (*d*) the plastic should have good adherence to all cell constituents; (*e*) the plastic should not shrink to any great extent in the solidification process; (*f*) the solidification process should take place without the liberation of excessive heat.

A plastic that completely meets these requirements has not as yet been found. Of all the plastics tried, an epoxy resin has been used most extensively.[2, 3]

The described method is based upon the use of the epoxy in the impregnation of the cell as a unit. The

[1] Manuscript received October 14, 1954. This paper was prepared for delivery before the Boston Meeting, October 3 to 7, 1954.

[2] The specific material used was Coil Seal No. 11, National Engineering Products, Inc., Washington, D. C.

[3] Another material used successfully was Scotch Cast No. 3, Minnesota Mining and Manufacturing Company, Minneapolis, Minn. It has a low viscosity and long pot life so that penetration is excellent; it has the further advantage that little heat is generated in setting.

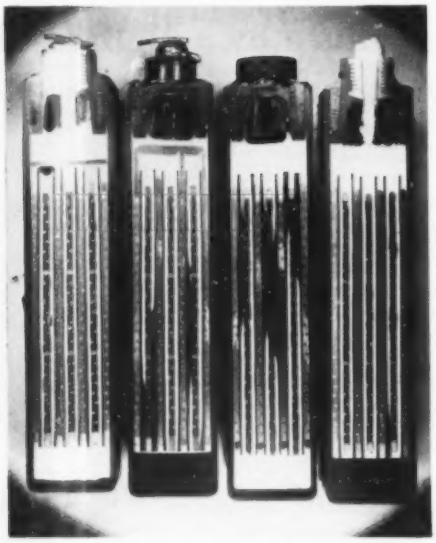

FIG. 1. Cross sections of storage battery cell after impregnation with plastic. ½ actual size before reduction for publication.

same method, modified to individual requirements, can be used with other plastics and for mounting or impregnating individual cell constituents or other substances of a porous nature.

Impregnation of the Cell

For satisfactory impregnation with plastic the cell must be washed free of acid and dried. The acid is not emptied by inverting the cell. Instead, a small hole is made at the bottom while a stream of water is run in at the top. In this way the acid may be slowly replaced by water without unduly heating the electrolyte or plates and with minimum disturbance to sediment and loose corrosion products. The washing is continued until the water gives no acid test.

After washing, the cell is drained and dried by passing a stream of warm air through it. After drying, the cell is evacuated of air and any residual water vapor. A length of tubing is extended from the cell to a position outside of the vacuum system, and the plastic mix is forced into the cell by atmospheric pressure. After the plastic has been introduced, atmospheric pressure is restored on the cell and the plastic is allowed to harden.

Caution is required in the use of this plastic in lead-lead acid batteries. It is important that no more than 400 ml of the plastic be mixed and used at one time and, if more than this amount is required, that each batch harden before adding the next. The solidification reaction is exothermic and is accelerated by heat. So much heat can be generated in large masses of the plastic that an almost explosive reaction takes place with the lead oxides of the plates. In addition, heating accelerates the hardening process and causes difficulty in proper impregnation even if the reaction with the lead oxides is not initiated. Large cells can be filled with successive portions of the plastic mix, and hardening and cooling of each mix will occur without any sign of the successive layers being visible in the section.

Cutting, Grinding, and Polishing the Section

The abrasive action of the lead oxides has been found to be destructive to cutting tools. A narrow-bladed skip-tooth band saw is used for the preliminary sectioning. Excessive friction at the cutting edge may cause ignition of the section, so a sharp saw, a slow saw speed, and a light feed should be employed. Use of a water coolant is advisable, but an alkali soap type of coolant should be avoided since it will corrode the specimen.

After sectioning, the sample is brought to a smooth condition by hand grinding under a stream of water. Garnet Number 80 waterproof paper is used for rough grinding the specimen to a flat surface and silicon carbide waterproof papers, grades 240 and 400 mesh, are used for intermediate grinding. Fine grinding is accomplished with grade 600 griteloth.[4] When this technique is used, grinding is rapid, the paper does not become clogged by lead particles, and no hazard is caused by the fine lead and lead oxide dust produced in polishing.

A final hand polishing is given the specimen on a wet, tightly stretched surface of airplane wing fabric. A paste of polishing powder type A-5175[5] is used as the polishing agent.

APPLICATIONS

Since the plastic is an excellent insulating material, a current path is furnished only by those conducting portions of the section that were in actual contact before impregnation took place. The section may thus be tested with a good ohmmeter or similar device for such conditions as shorts between positive and negative plates, separation of active material from the grid, and broken grid sections. By progressive sectioning and testing, the source of such conditions may be located and subjected to microscopic examination (Fig. 2).

Growth of plates, distortion of grids, breakage of separators, and "treeing" can be detected in the macro section. The universal measuring microscope can be used to measure distortion and growth in the section with a high degree of precision. A contour-measuring projector can also be used for direct visual

[4] Bay State Abrasive Products Company, Westboro, Mass.

[5] Linde Air Products Company, New York, N. Y.

FIG. 2. Short circuit, between positive plate (center) and negative plate connecting strap (top), located by electrical conductance test and progressive sectioning. Short occurred because of growth of positive plate and "treeing" from negative plate connecting strap. 4× before reduction for publication.

comparison of sections from newly assembled and used cells.

Higher magnification reveals the structure of the active material and its relation to the products of grid corrosion. The harder parts of the corrosion product, portions of the positive active material, sponge lead, lead sulfate crystals, the metal of the grid, and the plastic material used for impregnation are capable of a high polish, and the section can be observed by bright-field vertical illumination (Fig. 3). By this means the boundaries between metal, corrosion product, and active material are usually sharply defined, but much detail is lacking. A better idea of the actual appearance and colors of the various constituents can be obtained through the use of dark-field illumination. With at least one type of illuminator[6] the over-all appearance of the specimen can be much improved if observed by dark-field illumination through a cover glass attached to the surface by immersion oil (Fig. 4).

Careful polishing reveals the microstructure of the metal as well as that of the corrosion product, but with dark-field illumination the brightness of the metal is relatively so much greater than that of the corrosion product that the detail in both, visible to the eye, is difficult to reproduce in a single photographic print.

[6] Trivert illuminator, Bausch and Lomb Optical Company, New York, N. Y.

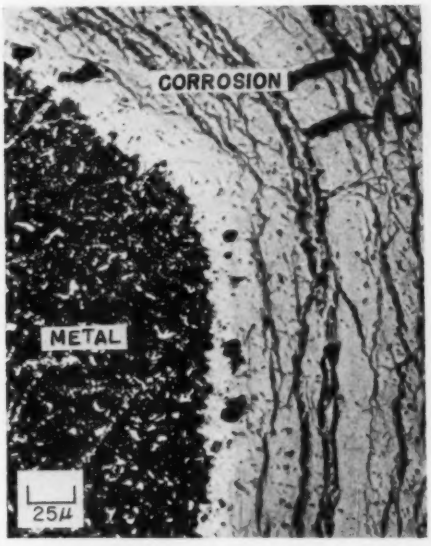

FIG. 3. Positive plate photographed under bright-field illumination. Portion of grid member appears at left and a portion of the corrosion ring at right. Section has been rubbed with dry polishing powder to subdue reflectivity of the lead. The bright particles in the grid member are segregated antimony. 400× before reduction for publication.

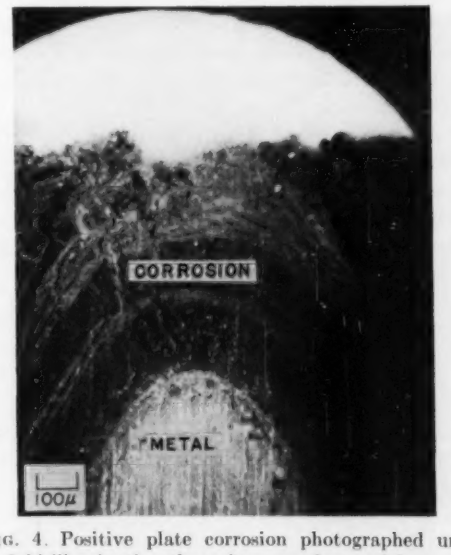

FIG. 4. Positive plate corrosion photographed under dark-field illumination through cover glass and immersion oil. Section was ground on number 600 griteloth but not polished. Direction of grinding is indicated by metal smear across dark corrosion product. Such smears and surface dirt can be removed with Scotch tape. 100× before reduction for publication.

The high reflectivity of the various polished surfaces is misleading, and the use of polarized light has been found helpful in differentiating polished crystal surfaces from metal surfaces. This is particu-

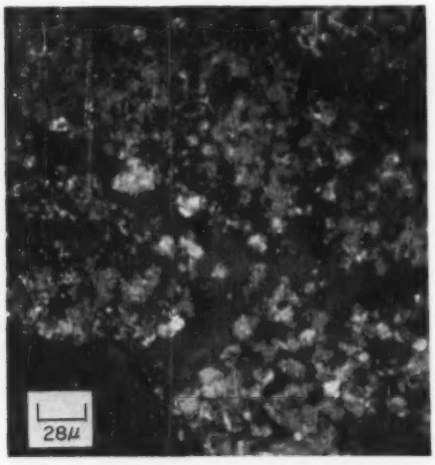

FIG. 5. Section of negative plate photographed under bright-field illumination. The bright areas of apparent metal are revealed as sulfate crystals when examined under polarized light (Fig. 6). 350× before reduction for publication.

larly useful in the examination of the negative plate (Fig. 5 and 6).

A planimeter or a grid laid out on transparent material may be used to measure the relative areas of corrosion product and the remaining grid metal either indirectly from a photographic negative or directly from a projected image of the corroded grid member. Comparison of the remaining metal with that present before corrosion began gives the corrosion rate. However, as a result of variable casting conditions, the actual grid sections of a new grid vary in shape and area to a considerable extent. For this reason it is necessary to use the average of a number of observations to obtain a reliable figure. In a study of the corrosion of 25 different batteries, for example, twelve individual measurements were taken at random positions on a cross section of each battery. The area of both remaining grid metal and corrosion product was recorded and the results averaged. When the planimeter was used, individual measurements at any one position were found reproducible with an accuracy of 1% or better. However, the deviation, or the amount that single independent measurements at different positions on the section differed from the most probable value, was as high as 10%. This figure represents the reliability of a single measurement. The average deviation, which is a measure of the reliability of the average value (twelve measurements), did not exceed 3% in any section and in the majority of sections was less than 1%. Variations in grid cross section introduced greater uncertainty than the method of measurement or variations in corrosion penetration. The area of corrosion product, in general, was remarkably uniform throughout the section and independent of the original grid area.

Under varied operating conditions differences in the active material, corrosion product, and metal are easily detected. For example, the appearance of the negative active material is quite different before and after cycling. The dendritic lead structure of the newly formed negative plate changes gradually to a mass of crystals, presumably lead sulfate (Fig. 6).

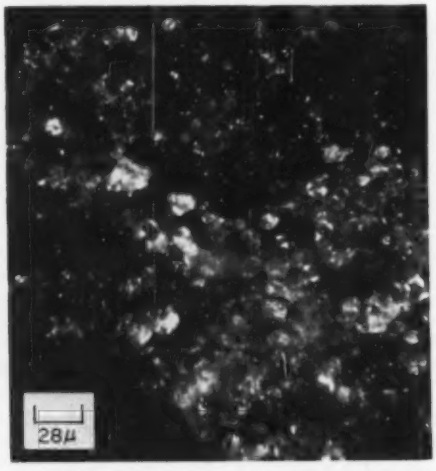

FIG. 6. Section of negative grid (same area as in Fig. 5) photographed by polarized light. 350× before reduction for publication.

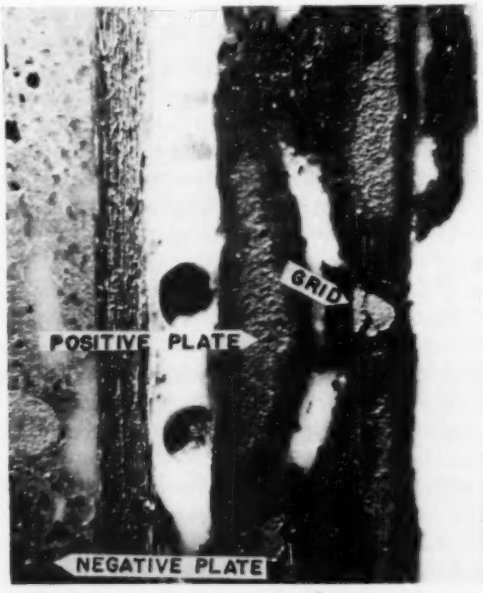

FIG. 7. Positive plate in cross section, showing manner in which splitting of the active material (dislodgment of pellets) takes place along the center line of the plate. Grainy appearance of surface was caused by incomplete impregnation with plastic. 5× before reduction for publication.

The positive plate in cross section appears to be split down the center after a few charge cycles (Fig. 7). This might be attributed to the pressure set up by the change from lead to oxides or sulfates of greater volume during corrosion. Apparently other factors are at work, however, since under different operating conditions the corrosion layer can become quite thick without causing any splitting of the active material.

It may be possible to determine the constituents of the active material and the chemical composition of the various layers in the corrosion product that surrounds the grid members. There are, first of all, definite color differences among the various products, and these show up beautifully in color photography. The hardness, as determined with the Eberbach micro hardness tester, varies considerably and consistently among the various constituents that are otherwise distinguishable. The various parts of the section also show some differences under polarized light. These purely physical differences may be supplemented by chemical tests. As in the case of metal surfaces, various parts of the section react differently to chemical reagents, and the plastic impregnating material usually remains inert. The resulting reaction products often remain as crystals of different shape and color. Comparison of such reactions for unknown corrosion products and known lead oxides or sulfates may offer a definite clue to identity.

As an example, a solution of ammonium acetate applied to the surface of the section changes the corrosion ring next to the metal surface of the positive grid from black to white (Fig. 8) without producing any effect on other parts of the corrosion product. Tests on various lead oxides show that ammonium acetate produces this effect with lead oxide (PbO), which indicates that the layer next to the metal surface may be lead oxide.

Results of such tests must be confirmed by other means, however, since the possibility of an electrochemical reaction must also be considered. Ammonium acetate or acetic acid, for example, shows a rapid and pronounced attack on the metal of the positive grid, but has an inappreciable effect on the metal of the negative. No such attack is observed on cross sections of the same positive grid, however, when the active material and corrosion products have been scraped off. This indicates that the corrosion by ammonium acetate had an electrochemical origin. Thus, a determination of weight loss by stripping the corrosion product with ammonium acetate would produce a serious error due to metal corrosion, although tests on bare metal with the same solution would indicate that attack on the grid metal was negligible.

In order to use chemical tests as a means of identification, it is advisable to use known oxides in making up artificial sections that contain the same electrochemical couples as those suspected and then compare chemical reactions against these known standards.

FIG. 8. White ring formed in positive grid corrosion product adjoining metal surface by the use of an ammonium acetate etch. Compare this with Fig. 3, a similar section prior to etching. 250× before reduction for publication.

There is also the possibility that microdrilling (2) or sampling methods can be used to remove portions of the material on a selective basis so that x-ray or electron diffraction studies can be made.

Discussion and Conclusions

The ideal method of investigating battery processes from the standpoint of microscopic inspection would be one by which the actual processes could be watched as they occur. Although this may eventually be possible, present methods of attaining this goal leave much to be desired.

By microscopic examination of impregnated sections removed from a series of cells that have operated under various conditions, an approximation can be made of the changes that occur. The permanent nature of the specimens makes possible a large number of manipulations and measurements and a direct comparison of different characteristics at any future time.

Unfortunately, the plastic cannot be added to the operating cell to seal it at once against any further change. The necessary washing and drying operations undoubtedly produce some changes from operating conditions. The sponge lead of the negative will be oxidized to some extent, some lead sulfate and oxide will be dissolved, sediment may be washed out or

disturbed, wood separators may split, and so forth. The entrance of the plastic may also cause a slight washing action at exposed surfaces, and displacement of material and the heat evolved in setting up of the plastic may also cause some changes.

Fortunately, these effects do not appear to have a large order of magnitude. Lead sulfate and the lead oxides have a low solubility in water and solution is slight during washing. Reprecipitation of lead salt crystals also appears to occur only slightly during the drying process. The oxidation of sponge lead is a surface effect and, since examination is made of the cross section, it can be discounted. As far as comparison is possible, little difference is observed in microstructure or appearance between cross sections obtained from impregnated cells and sections examined immediately after removal from the electrolyte.

Although physical changes do occur, they may be considered to have a low order of magnitude. Cells of similar construction and operated in the same manner show reproducibly the same microstructure in the impregnated section even though this microstructure may not be exactly that which would be observed in the operating cell immediately before impregnation. If the separate cells of a similar series, therefore, are operated under different conditions and variations are found in the observed microstructure of the individual cells after impregnation, then these differences in observed microstructure may be attributed safely to differences in cell operation and so evaluated.

Any discussion of this paper will appear in a Discussion Section to be published in the December 1955 JOURNAL.

REFERENCES

1. H. BUCKLE AND H. HANEMANN, *Z. Metallkunde*, **32**, 120 (1940).
2. F. R. BRYAN AND C. H. NEVEU, *Metal Progr.* **64**, No. 6, 83 (1953).

The Effect of Cobalt on the High Temperature Oxidation of Nickel[1]

S. F. Frederick[2] and I. Cornet

University of California, Berkeley, California

ABSTRACT

Nickel-cobalt alloys of high purity, in sheet form, were oxidized in air at temperatures ranging from 800° to 1400°C. The oxidation rate of high purity carbonyl nickel was found to be lower than previously reported in the literature. The oxidation rate increased with increasing cobalt content, but the effect was small until over 11% cobalt had been added. The activation energy for oxidation decreased with increasing cobalt content from a value of 51 kcal/mole for pure nickel to about 28.8 kcal/mole for pure cobalt.

Introduction

Nickel and cobalt are frequently used as basis metals or as alloying constituents for oxidation resistant alloys for relatively high temperature applications. There have been many studies of the oxidation behavior of pure nickel (1–3) and of pure cobalt (1, 4, 5), generally because of their intrinsic importance, but relatively little information is available on the effect of cobalt on the rate of oxidation of nickel (1, 6).

While determining the heat of formation of nickel oxide, Kelley and Humphrey (7) reported that high purity nickel could be ignited only with difficulty, and when ignited did not react completely. Addition of a small amount of cobalt, however, promoted ignition and assured a complete reaction. This experimental report seemed sufficient reason for re-examining the effect of cobalt on the oxidation of nickel.

Experimental

Materials

High purity carbonyl nickel powder was graciously supplied by the International Nickel Company. Spectrographically pure cobalt sponge was purchased from Johnson, Matthey and Company, Ltd. All test samples were prepared from these two materials, for which analyses are presented in Tables I and II.

Approximately 10 g of sample of the desired composition was melted in a crucible in a hydrogen atmosphere using an induction heated carbon block as the heat source. Pure cobalt was melted in a ZrO_2 crucible (Norton sintered ZrO_2, no binder). Pure nickel and all nickel-cobalt alloys were melted in MgO crucibles.

The melting procedure was to place the crucible with the charge in the carbon block in the induction furnace and evacuate the chamber to a pressure of less than 5×10^{-3} mm mercury with a Welch Duo Seal vacuum pump. With an Ajax-Northrup 40 kw high frequency converter, the temperature was raised in about 10 min to 1100°–1200°C, as measured with an optical pyrometer. Hydrogen was introduced. The charge was then melted and heated to the range 1550°–1600°C. The system was evacuated again and a fresh supply of hydrogen introduced. After one minute the system was again evacuated and the metal allowed to freeze and cool under vacuum. The metal charge was in the molten state for approximately 5–7 min.

Except for the 78% cobalt alloy and the pure cobalt, samples were prepared as follows. Ingots were cold rolled in multiple passes, with no intermediate anneals, to sheet about 0.3 mm thick. Rectangular specimens of 2–10 cm^2 total area, including edges, were cut from the sheets. Specimens were drilled, and then polished with 3/0 emery paper. Dimensions were measured with a micrometer stage on a metallurgical microscope to the nearest 0.1 mm. Specimens were then washed with soap and water and rinsed in alcohol, dried, and weighed with an analytical balance to the nearest 0.1 mg. They were then either tested immediately or placed in a desiccator until testing.

An attempt was made to cold roll the 78% cobalt alloy and the pure cobalt, but they proved to be too brittle. Therefore, small chips were broken from the ingots; each chip was placed in an ordinary metallurgical mounting press, heated to 240°C, and pressure applied. With the small chip size used, specimens were thus hot forged with pressures, based on chip

[1] Manuscript received August 27, 1954. From a thesis submitted by S. F. Frederick to the Graduate School of the University of California in partial fulfillment of the requirements for the degree of Master of Science.

[2] Present address: Douglas Aircraft Company, Santa Monica, California.

TABLE I. *Analysis of carbonyl nickel*

Element	Spectrographic estimate of quantity present
	%
Silicon	Trace (0.001)
Iron	0.003
Copper	0.0005
Magnesium	0.0001
Chromium	Less than 0.001
Manganese	N.D.—less than 0.002

Other elements were not detected.

Spectrographic analysis provided through the courtesy of G. M. Gordon.

TABLE II. *Analysis of cobalt sponge*

Element	Spectrographic estimate of quantity present
	%
Silicon	0.002 (average value)
Magnesium	0.0005
Aluminum	0.0002
Manganese	0.0001
Calcium	—

The following elements were only detected by the total combustion method: iron, less than 0.001%; nickel, 0.0005%.

No lines of the following elements were observed: Ag, As, Au, Be, Bi, Cd, Cr, K, Li, Mo, Na, Pb, Rb, Sb, Sn, Ti, V, W, Zn, Zr.

Analysis furnished by Johnson, Matthey and Company, Limited.

area, of approximately 200,000 psi. Instead of trying to cut these specimens into shapes convenient for measuring, thereby reducing the already small areas, the areas of these specimens were measured by making contact prints of them. The prints were cut out, weighed, and compared with a weighed and measured area of print. Subsequent surface preparation was the same as for the other alloy specimens.

Testing Procedure

The specimen was suspended by a platinum wire in a Burrell vertical tube Glo-bar furnace. The 1 in. diameter tube was vented at the top and bottom, allowing an air flow due to convection currents through the furnace, thus preventing any oxygen depletion during the test. Preliminary tests with specimens of different areas also showed that oxygen depletion was not a factor. Temperatures in the test zone were maintained within ±5°C by a Leeds & Northrup Micromax temperature controller. The original plan was to weigh the specimen continuously during the testing period, and an automatic recording balance of the type developed by the National Bureau of Standards was constructed for that purpose (8). Unfortunately, the convection currents in the furnace tube prevented establishing the initial zero point with any precision, and the weight-time records could not be considered reliable enough to detect deviations from the parabolic rate. Therefore, a parabolic rate was *assumed* for all tests and independent measurements of the weight change together with the total time were used to calculate the *parabolic rate constant* K_p by the relation

$$K_p = \frac{(W_f - W_o)^2}{A^2 t}$$

where W_o is the initial weight of the specimen, W_f is the final weight of the specimen, A is the total surface area of the specimen (including the edges), and t is the total time of testing.

Tests varied in duration from a minimum of 13 min for 100% cobalt at 1405°C to a maximum of 1638 min for 100% nickel at 806°C. For a given alloy, however, the test duration varied widely, 84–1638 min for pure nickel, 13–1464 min for pure cobalt, for example. Despite the wide variation in duration of tests, results were quite self-consistent. Thus, for pure nickel at 1405°C, for times of 84, 88, and 558 minutes, K_p values were 5.82, 6.17, and 5.79×10^{-9}, respectively.

Results

In Fig. 1, the logarithm of the parabolic rate constant for each alloy is plotted as a function of the reciprocal of the absolute temperature. From the

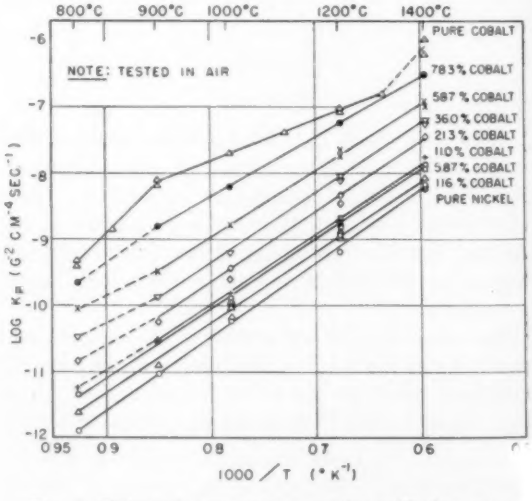

FIG. 1. Effect of temperature on the oxidation rate of nickel-cobalt alloys. K_p = oxidation rate assuming a parabolic law of oxidation is followed.

curves in Fig. 1, the activation energy E for oxidation was calculated using the relation

$$E = -R\left\{\frac{\ln K_p}{1/T}\right\} = -2.3Rs$$

where R is the gas constant and s is the slope of the curve. In Fig. 2, the activation energy for oxidation is shown as a function of cobalt content. Fig. 3–8 show rate constants for the indicated temperatures as a function of cobalt content. In drawing these curves, Fig. 1 was arbitrarily selected as the primary curve and the curves on Fig. 3 through 8 were drawn to be consistent with Fig. 1. Fig. 9 shows photomicrographs of the cross section of some of the oxidized samples.

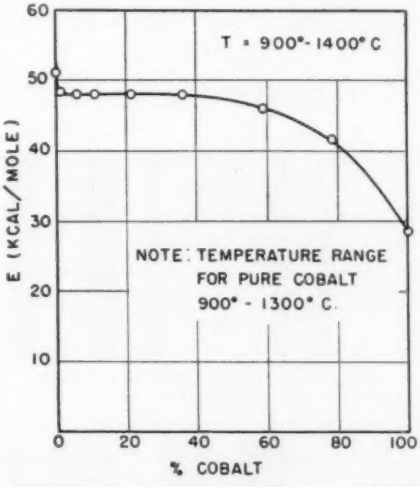

FIG. 2. Activation energy for oxidation of nickel-cobalt alloys.

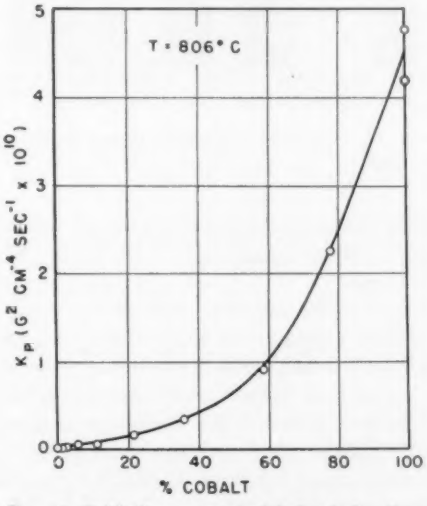

FIG. 3. Oxidation rate of nickel-cobalt alloys

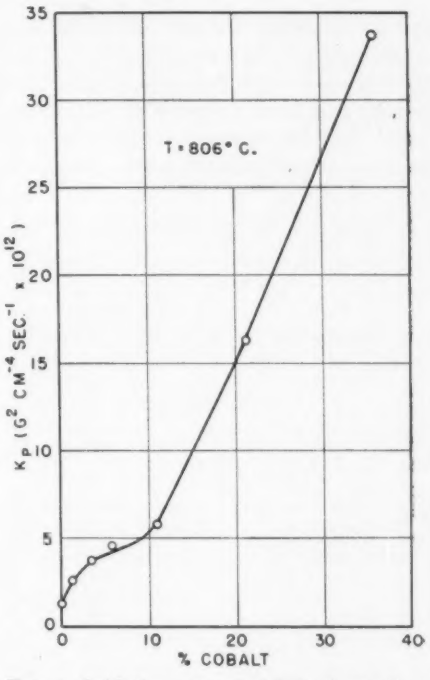

FIG. 4. Oxidation rate of nickel-cobalt alloys

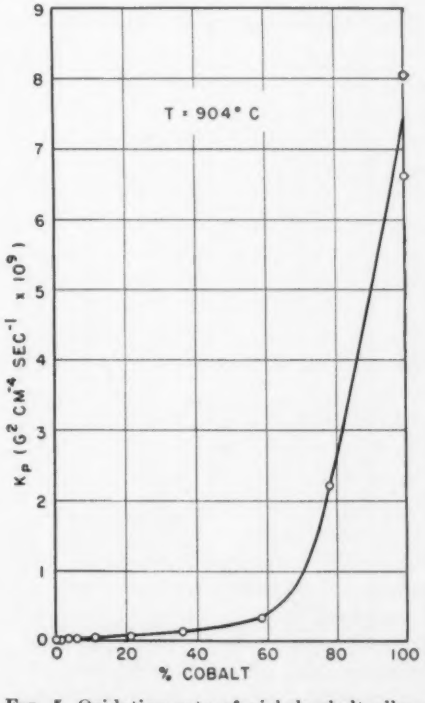

FIG. 5. Oxidation rate of nickel-cobalt alloys

Data are reported for 80 individual tests, for nickel alloys containing (nominally) 0, 1, 3, 6, 11, 21, 36, 59, 78% cobalt, and for 100% cobalt. Many duplicate tests at a given temperature for a given alloy gave rate constants so close that the points coincide on the scale of presentation used. Thus in Fig. 7, at 1205°C there are coincident experimental points for nickel alloys containing 0, 1.16, 3.42, 5.87, and 11.0% cobalt.

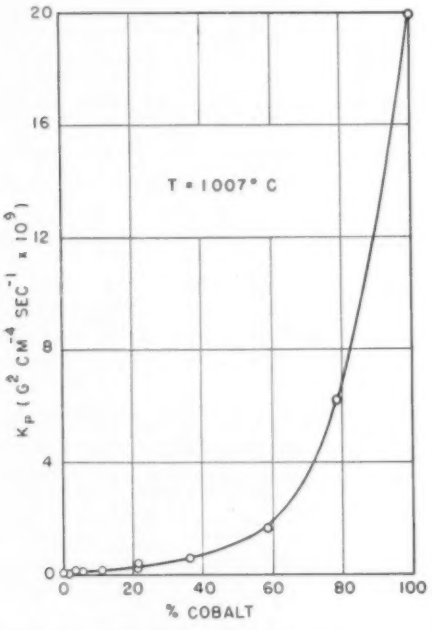

FIG. 6. Oxidation rate of nickel-cobalt alloys

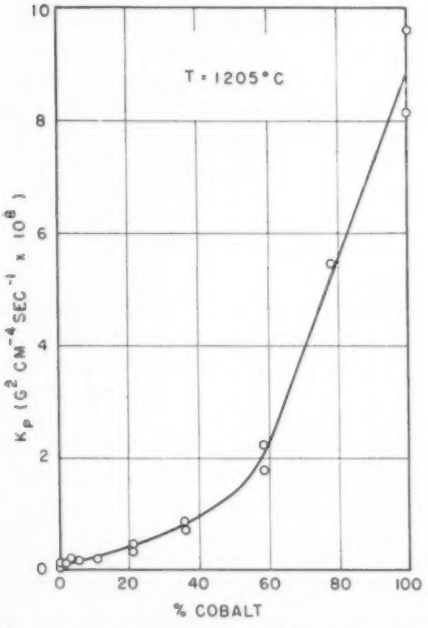

FIG. 7. Oxidation rate of nickel-cobalt alloys

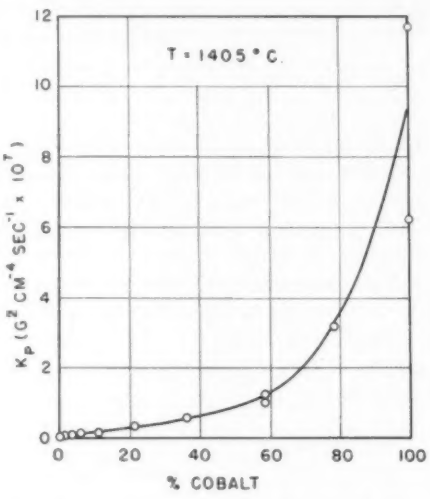

FIG. 8. Oxidation rate of nickel-cobalt alloys

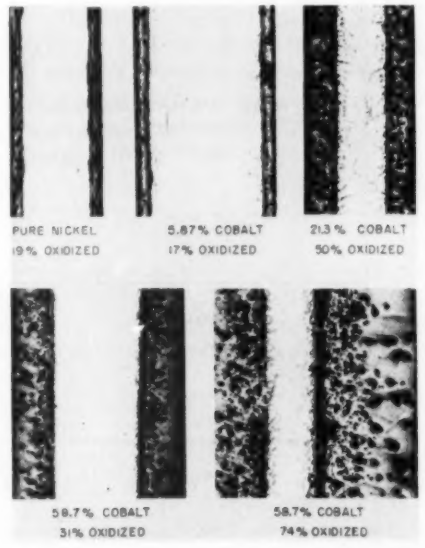

FIG. 9. Cross sections of samples tested at 1205°C. Unetched. 150X

Besides the 80 tests reported above, some data were obtained initially for alloys containing 0.1, 0.2, 0.4, and 0.6% cobalt, since it was thought that a very small amount of cobalt might greatly affect the oxidation rate of nickel. For these concentrations of 0.1–0.6% cobalt, rates were the same as for 1.16% cobalt alloy. Data for these 0.1–0.6% cobalt alloys, therefore, were not shown.

Discussion

Oxidation of Pure Nickel

Nickel oxide is a *p*-type semiconductor. From the observations that NiO has a NaCl type structure with an excess of oxygen compared to the stoichiometric composition (9), and from the variations of electrical conductivity when ions of higher or lower valency are added, a model of the oxide film has been proposed (1) as shown in Fig. 10. In this model there are occasional vacancies in place of nickel ions. Concentration of vacancies is highest at the oxide-atmosphere interface and lowest at the oxide-metal interface. There are also trivalent nickel ions or "electron holes" to maintain electrical neutrality. Oxidation of nickel proceeds predominantly by diffusion of nickel ions and electrons through the oxide film to the oxide-atmosphere interface where the reaction $Ni^{++} + 2e^- + \frac{1}{2}O_2 = NiO$ occurs. Diffusion of nickel ions is the rate-controlling process.

Over a wide range of temperatures nickel obeys the parabolic law of oxidation (1), derived experimentally by Tammann (10) and by Pilling and Bedworth (11), and derived on the basis of electrochemical theory by Wagner (1, 12). As with other kinetic processes the rate of oxidation is temperature dependent and follows Arrhenius' equation

$$K_p = A \exp^{-E/RT}$$

where K_p is the parabolic rate constant, A is a constant, E is the activation energy for oxidation, R is the universal gas constant, and T is the absolute temperature.

Qualitatively, therefore, the oxidation of nickel is well understood. Quantitatively, however, some problems remain. The theoretical determination of the oxidation rate of nickel, based on semiconductor theory, is hampered by the fact that measurements of the electrical conductivity of nickel oxide have

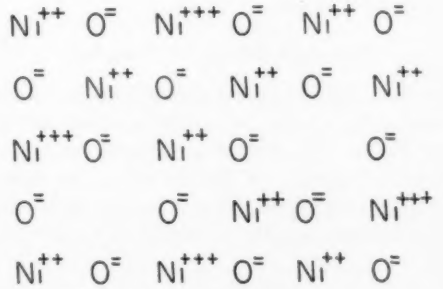

Fig. 10. Model of nickel-oxide film showing cation vacancies and corresponding trivalent nickel ions or "electron holes."

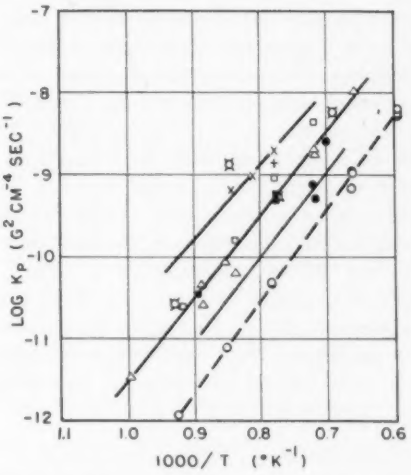

Fig. 11. Oxidation rate of nickel of different purities [cf. Kubaschewsky and Hopkins (1)]. ×, Nickel 'A', 98.88% Ni, 0.48% Fe, 0.18% Mn, 0.17% Si; □, electrolytic nickel, 99.67% Ni, 0.25% Fe, 0.03% C, 0.04% Si, trace Mn; ⌑, carbonyl nickel, 0.04% C, 0.12% Fe, 0.09% O, nil S; +, nickel, 0.5–1.0% Mn, some Fe, nil Mg; △, 'Rein-nickel,' 0.07% Si, 0.07% Cu, 0.27% Fe, 0.20% Co, 0.01% Cr, 0.01% Al, nil Mn; ▲, electrolytic nickel remelted in vacuo; ●, carbonyl nickel remelted in vacuo; ○ — — — ○, present investigation.

been made on samples of highly impure or incompletely stated composition (2).

There are problems also in the experimental determination of the oxidation of nickel. Rates are particularly influenced, even by a factor of tenfold, by small quantities of impurities in the metal (1) (cf. Fig. 11). It is difficult to compare results of various investigations because of differences in metal composition, specimen preparation, method of measurement-thickness of film or weight gain, oxidizing atmosphere, and other variables. However, the results of the present investigation are in good agreement with rate constants previously reported (Fig. 11), although E is 51,000 cal/mole as compared to 45,000 cal/mole, and rate constants are somewhat lower than previously reported by Kubaschewski and Hopkins (1).

Moore and Lee (2, 4), using a nickel foil of purity comparable to the present material, reported a slightly lower rate constant, $(1.71 \pm 0.30) \times 10^{-12}$ (g^2/cm^4sec) at 900°C, and $(5.86 \pm 0.20) \times 10^{-13}$ (g^2/cm^4sec) at 800°C; but they found $E = 38.4$ kcal/mole. However, the study of Moore and Lee was performed at 10 cm pressure of oxygen and based on measurements of film thickness rather than weight gain. The effect of oxygen pressure may not be important, since it has been reported that there is no change in the oxidation rate of pure

nickel for pressures of 1 atm to 500 psi (13). However, data of Wagner and Grunewald at 1000°C have indicated that the rate constant varied as $P_{O_2}^{1/5.3}$ (2), and other data have shown the conductivity of nickel oxide to vary as $P_{O_2}^{1/4}$ above 350°C (2).

Data of Gulbransen and Andrew (3) on the oxidation of high purity nickel yield a heat of activation of 41.2 kcal/mole compared to 51.0 kcal/mole for the present study. Data of Gulbransen and Andrew (3) on extrapolation to 1000°C yield parabolic rate constants similar to those obtained in the present study. However, Gulbransen and Andrew performed their experiments in oxygen at 0.1 atm, and limited oxidation to relatively thin films.

Oxidation of Nickel-Cobalt Alloys

Small additions of many metals have been shown to increase the oxidation rate of nickel (1). This may be explained by considering the effect of adding chromium. Since chromium forms a trivalent ion, two chromium ions and a vacancy are equal to three nickel ions. Therefore, addition of chromium to nickel should increase the concentration of vacancies in the oxide film, thereby increasing the diffusion rate of nickel ions, giving a higher oxidation rate. Experiments confirm this picture; the oxidation rate of nickel-chromium alloys increases up to about 6% chromium, then the rate decreases to a minimum at 40% chromium, the decrease being attributed to the formation of the spinel $NiO \cdot Cr_2O_3$.

Nickel and cobalt form a continuous solid solution (14) and there is evidence that their oxides are mutually soluble. Unlike nickel, which forms only the one stable oxide NiO, cobalt may form Co_3O_4 and CoO below 900°C, but only CoO is stable above that temperature. At temperatures where an appreciable quantity of trivalent cobalt ions are formed, cobalt would be expected to affect oxidation rates much as does chromium. However, at higher temperatures, where cobalt forms stable divalent ions only, it should not greatly accelerate formation of nickel oxide. NiO and CoO have the same crystal structure and almost the same lattice parameter (4.17 Å for NiO and 4.25 Å for CoO). The activation energy for oxidation of cobalt at high temperature is reported to be only slightly lower than E for nickel, but cobalt oxidizes about 25 times faster than nickel (1). In nickel alloys containing small concentrations of cobalt, formation of CoO in the oxide layer may be expected, with a corresponding increase in oxidation rate, assuming that no double oxide is formed.

Experimental results obtained are quite consistent with the foregoing theory. Additions of up to 11% cobalt have only small effect on the oxidation rate of nickel. This would indicate that probably nickel oxide is formed with cobalt present substitutionally. The external appearance of the oxide film tends to support this view. The color of the oxide changes from the green of nickel oxide to the blue-black of cobalt oxide by the time the cobalt content has reached 11%. The oxide on the 3% alloy is almost as dark as on the 11% alloy, while oxide on the 1% alloy is still quite green. As the cobalt content is increased over 11% (Fig. 4), there is a rapid increase in the oxidation rate, with an even more rapid increase over about 60%, possibly indicating that cobalt oxide is becoming the predominant constituent of the oxide film.

Although there is a fair amount of scatter in the data, particularly at the higher temperatures, the photomicrographs of Fig. 9 show that this may be expected as internal oxidation is present. Internal oxidation would indicate that there are some deviations from the parabolic rate law.

Preece and Lucas (6) have reported on the oxidation of nickel, cobalt, and cobalt + 40% Ni in the temperature range 800°–1200°C. Their results are not directly comparable with data of the present investigation because they used materials of commercial purity and specimens cut from vacuum melted ingot without further treatment. Furthermore, they appear to have used a 24 hr oxidation test, regardless of temperature, and they did observe some internal oxidation above 1000°C.

Oxidation of Pure Cobalt

The hot-press-forged cobalt sheet used in this investigation had some edge fissures, introducing an uncertainty in the determination of surface area and possibly introducing some deviations from parabolic oxidation rates. Oxidation rates of pure cobalt in the range 800°–1200°C given by Preece and Lucas (6) are greater than rates of the present investigation by factors up to tenfold; this would be expected because Preece and Lucas used material of commercial purity.

Activation Energy for Oxidation

The rate data obtained permit determination of the activation energy for oxidation of nickel-cobalt alloys. For pure nickel, E is approximately 51,000 cal/mole. E drops to 48,000 cal/mole with the addition of small quantities of cobalt; beyond 40% Co, E decreases rapidly to 28,800 cal/mole for pure cobalt.

Conclusions

With the assumption that nickel-cobalt alloys oxidize according to the parabolic rate law, it was

found that additions of up to 11% cobalt had only a small effect on the oxidation rate of nickel. More than 11% cobalt caused a rapid increase in the rate of oxidation, while more than 60% cobalt caused an even more rapid increase in the rate. The absolute value of the oxidation rate of pure nickel was found to be below the values previously reported in the literature for the temperatures investigated.

The activation energy for oxidation of pure nickel in the temperature range 800°–1400°C was found to be 51,000 cal/mole compared to 45,000 cal/mole reported in the literature. The activation energy for the oxidation of pure cobalt was found to vary; a value of 28,800 cal/mole was found for the temperature range 900°–1300°C. The activation energy for oxidation of nickel-cobalt alloys was found to decrease with increasing cobalt content in the temperature range 900°–1400°C.

Acknowledgments

The authors express their appreciation of the assistance of T. Hazlett and Paul Langstrom in preparing the high purity alloys.

Any discussion of this paper will appear in a Discussion Section to be published in the December 1955 Journal.

References

1. O. Kubaschewski and B. E. Hopkins, "Oxidation of Metals and Alloys," pp. 31–32, 44, 68–69, 120–125, 162–163, 176–177, 197–199, Academic Press, Inc., New York (1953).
2. W. J. Moore and J. K. Lee, *Trans. Faraday Soc.*, **48**, 916 (1952).
3. E. A. Gulbransen and K. F. Andrew, *This Journal*, **101**, 128 (1954).
4. W. J. Moore and J. K. Lee, *J. Chem. Phys.*, **19**, 255 (1951).
5. C. R. Johns and W. M. Baldwin, *J. Metals*, **1**, 720 (1949).
6. A. Preece and G. Lucas, *J. Inst. Metals*, **20**, 219 (1952).
7. K. K. Kelley and G. L. Humphrey, Private communication.
8. Anon., *Natl. Bur. Standards Tech. News Bull.*, **37**, 86 (1953).
9. J. S. Anderson, *Ann. Repts. Progr. Chem.* (*Chem. Soc. London*), **43**, 104 (1946).
10. G. Tammann, *Z. anorg. Chem.*, **111**, 78 (1920).
11. N. B. Pilling and R. E. Bedworth, *J. Inst. Metals*, **29**, 529 (1923).
12. C. Wagner, "Diffusion and High Temperature Oxidation of Metals," in "Atom Movements," pp. 153–173, American Society for Metals, Cleveland (1951).
13. W. M. Fassell, Jr., R. C. Peterson, D. W. Bridges, and J. P. Bauer, "The High Pressure Oxidation of Metals," paper presented by W. M. Fassell, Jr., at AIME Pacific Northwest Metals and Minerals Conference (May 1, 1954).
14. C. E. Lacy, "Metals Handbook," p. 1192, American Society for Metals, Cleveland (1948).

Reaction of Nitrogen with Uranium[1]

M. W. Mallett and A. F. Gerds

Battelle Memorial Institute, Columbus, Ohio

ABSTRACT

Rates of reaction of nitrogen with uranium were determined by volumetric measurements in the temperature range 550°–900°C at atmospheric pressure. The reactions were found to follow a parabolic rate law with some deviations initially and also after the period of parabolic reaction. Surface reaction products formed in the temperature range 550°–750°C were identified by x-ray diffraction studies to consist principally of UN_2 with slight evidence of U_2N_3 in some cases. Between 775° and 900°C the three nitrides UN, U_2N_3, and UN_2 were found in the surface reaction product. The parabolic rate constant for the reaction between 550° and 750°C was found to be $k = 202 \exp(-25{,}500/RT)$ $(ml/cm^2)^2/sec$. The activation energy, 25,500 cal/mole, has a probable error of ±1800 cal/mole. Between 775° and 900°C the parabolic rate constant is $k = 3.95 \exp(-15{,}100/RT)$ $(ml/cm^2)^2/sec$, where 15,100 ±2000 cal/mole is the energy of activation. It has not been determined if the change in rate constant near the temperature of the beta to gamma transformation in uranium has any special significance.

Introduction

This investigation was made to obtain fundamental information on the kinetics of reaction of nitrogen with uranium. Surface reactions of massive uranium with nitrogen were studied in the temperature range 550°–900°C at a pressure of 1 atm. No information concerning this subject was found in the literature.

Three nitrides of uranium are reported in the literature (1, 2). The mononitride, UN, has a face-centered cubic structure, $a_o = 4.880$ Å, and has 4 molecules in a unit cell. The sesquinitride, U_2N_3, has a body-centered cubic structure of the Mn_2O_3 type with 16 molecules per unit cell and lattice constant of 10.678 Å. The dinitride, UN_2, has a face-centered cubic, fluorite-type structure with 4 molecules per unit cell and $a_o = 5.31$ Å. The dinitride is reported to form only at high nitrogen pressures.

Materials

The uranium rod used in this study was fabricated from a 1⅛-in. square bar sawed from an ingot of good purity. After heating to 600°C in a helium atmosphere, the square section was rolled to 1 1/16-in. round rod. The surface of the rod was vapor blasted to remove contamination, reheated to 600°C in helium, and rolled to 7/16-in. round rod. After again vapor blasting and pickling, the rod was cold swaged to approximately ⅜-in. diameter. Test specimens, each about 1½-in. long and 1 1/32-in. diameter, were machined from the rod.

The uranium was analyzed for impurities by means of chemical, spectrographic, and vacuum-fusion methods. The total of all measured impurities in the metal was only about 400 ppm and each detected impurity was present in a concentration of less than 100 ppm. The following elements were detected as impurities: aluminum, calcium, carbon, chromium, copper, iron, magnesium, manganese, molybdenum, nickel, nitrogen, oxygen, silicon, and vanadium.

Nitrogen used in this study was prepared by passing Matheson prepurified tank nitrogen over zirconium turnings heated at 850°C. The gas was dried by passing through a dry ice-acetone cold trap. A sample of the purified gas was analyzed by means of a mass spectrometer and found to contain 99.8 vol % nitrogen and 0.2 vol % argon.

Procedure

Apparatus and sample preparation.—The reaction rate of nitrogen with uranium was determined by volumetric measurement of the rate of gas consumption by the metal specimen at elevated temperatures. A Sieverts-type apparatus, slightly modified from that described (3, 4) previously, was used. In this work, the uranium specimen was supported on a Vycor stool within the Vycor reaction tube. A platinum-platinum + 10% rhodium thermocouple was spot welded to the top of the specimen. The thermocouple was calibrated (3) against a standardized optical pyrometer. A Vycor tube sealed at both ends was used to reduce the dead volume of the reaction system. Specimens were heated by induction, power being supplied by a 4-kw tungsten-gap-type converter. Temperatures were maintained to ±10°C.

Uranium specimens were abraded through 600-grit silicon carbide papers soaked in kerosene. Specimens were then rinsed with naphtha, ethyl

[1] Manuscript received September 23, 1954. Work performed under AEC Contract W-7405-eng-92.

ether, and cp acetone. After determining the dimensions of the specimen with a micrometer, the thermocouple was attached. The specimen, together with the thermocouple, reaction tube, and dead volume reducer, was placed in a dry-box which was flushed with argon for 1 hr to displace the air. The dry-box also contained trays of magnesium perchlorate desiccant to remove moisture from the argon. The specimen was lightly abraded in the dry-box with dry 600-grit silicon carbide paper to remove surface oxidation, after which it was mounted in the reaction tube inside the dry-box. A rubber stopper was placed in the ground glass joint by which the reaction tube was attached to the Sieverts apparatus. The assembled tube was then removed from the dry-box, attached to the Sieverts apparatus, and immediately evacuated. Because of the rapid surface oxidation of uranium, the final dry abrading of the uranium specimens in the argon atmosphere was deemed necessary. The customary rinse in an organic solvent was avoided since no solvent was found which did not accelerate atmospheric oxidation or otherwise contaminate the uranium surface.

Degassing.—Since uranium exists in three allotropic forms, it was desirable to degas specimens in the modification in which the reaction was to be studied to avoid changing the grain size of the metal. Specimens were degassed at a pressure of less than 10^{-4} mm mercury according to the following schedule: (*a*) for reaction rate studies in the alpha phase (below 665°C) specimens were heated for 1 hr at 650°C; (*b*) for reactions in the beta, specimens were heated for 1 hr at 750°C; (*c*) for reactions in the gamma, specimens were held for 1 hr at the operating temperatures prior to reacting.

Reaction rate studies.—Nitrogen was added in measured quantities from a 50-ml gas buret to the reaction system containing the uranium specimen heated to the desired temperature. Progress of the reaction was followed by observing pressure changes in the closed system with an open-end mercury manometer. Measured amounts of nitrogen were added from time to time to maintain the pressure between ¾ and 1 atm. The system was evacuated and the specimen was cooled to room temperature in the evacuated system after the reaction had proceeded for the desired period of time.

Individual points in a reaction rate experiment were determined by calculating the amount of gas remaining in the gas phase at any time and subtracting this amount from the total gas addition. The difference (measured to 0.04 ml STP) is a measure of the nitrogen consumed by the uranium specimen. The quantity of gas reacted per unit area was computed by using the original dimensions of the specimens.

Results and Discussion

Quality of uranium metal.—It is customary to express surface reaction rates in terms of the gas consumed per unit of surface area based on geometric measurements, even though the true surface area is known to be greater than these measurements indicate. The roughness factor of carefully polished specimens is around 2 to 2½. If the method of abrasion is kept uniform from specimen to specimen, the roughness factor will be very nearly the same for all specimens.

During the early stages of this study, it was difficult to obtain uranium rod free of cracks and other surface defects. Because of this, the ratio of true area to geometric area varied erratically and this was reflected in the calculated reaction rates. Later the uranium was carefully selected from the best available metal. Occasionally even this metal contained some surface defects.

Fig. 1 shows the microstructure at the surface of the cross section of a uranium specimen reacted with nitrogen for 3 hr at 800°C. This specimen was etched electrolytically in a 10% citric acid solution at a potential of 10 v d.c. on the open circuit to remove the worked surface of the metal. Presence of the nitride reaction product at the surface of the metal is evident. Nitrogen also appears to have penetrated into the uranium and reacted with the metal to form nitride at the site of a defect in the metal surface. All specimens used in reaction rate studies were sectioned and examined metallographically after reaction to determine if they were free of surface defects. Data obtained on specimens showing defects were discarded.

Surface-reaction product.—The rate of surface reaction of nitrogen with massive uranium was studied in the temperature range 550°–900°C at atmospheric pressure. Specimens reacted with nitrogen between 775° and 900°C produced a tightly

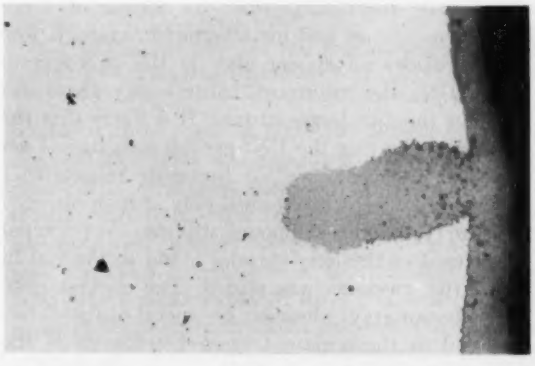

Fig. 1. Uranium reacted with nitrogen at 800°C for 3 hr. Note nitride at site of defect. Citric acid etch. 100× before reduction for publication.

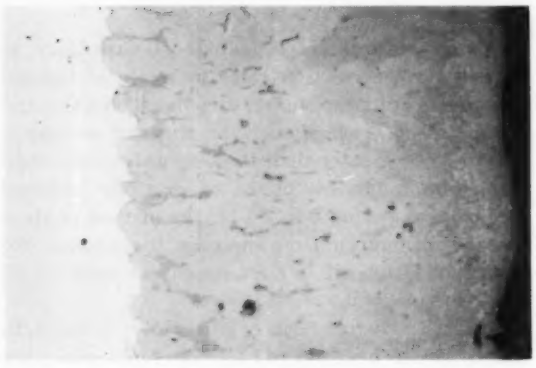

FIG. 2. Uranium reacted with nitrogen at 900°C for 4½ hr. Citric acid etch. 500× before reduction for publication.

FIG. 3. Uranium reacted with nitrogen at 600°C for 5 hr. Citric acid etch. 500× before reduction for publication.

adherent surface film which appeared roughened at the surface exposed to nitrogen. This roughened surface tended to powder off slightly on exposure to the atmosphere at room temperature. The microstructure at the surface of the cross section of a uranium specimen reacted with nitrogen at 900°C for 4½ hr is shown in Fig. 2. Three nitrides were identified in the surface reaction product by means of x-ray diffraction studies and metallographic examination. These nitrides all appear gray in the photomicrograph. UN_2, the outermost, lightest gray phase was found at the nitride-gas surface. It is likely that the compound showing the UN_2 crystal structure is deficient in nitrogen since the literature reports that stoichiometric UN_2 is obtained only at high nitrogen pressure (1, 2). This compound was also the principal constituent of the loose powder found in the vial in which the specimen was stored. The darkest gray (actually tan-gray) phase, at the metal-nitride interface and in the apparent grain boundaries of the thick, intermediate-gray U_2N_3,[2] was identified as

[2] X-ray diffraction studies of the surface reaction products showed a phase having a hexagonal structure isomorphous with Th_2N_3. This new uranium nitride is assumed to be U_2N_3 on the basis of its structure. No evidence of the body-centered cubic U_2N_3 (1) was found in the present study.

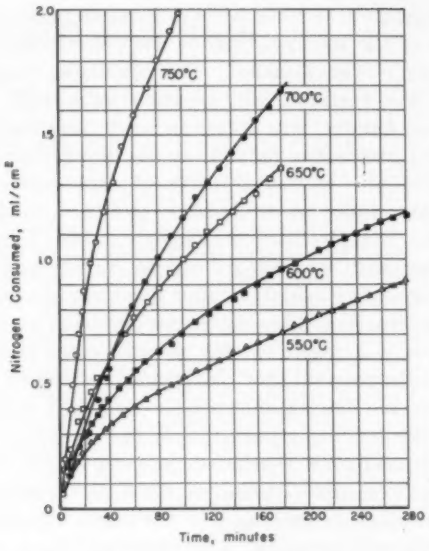

FIG. 4. Uranium-nitrogen reaction at 550°–750°C

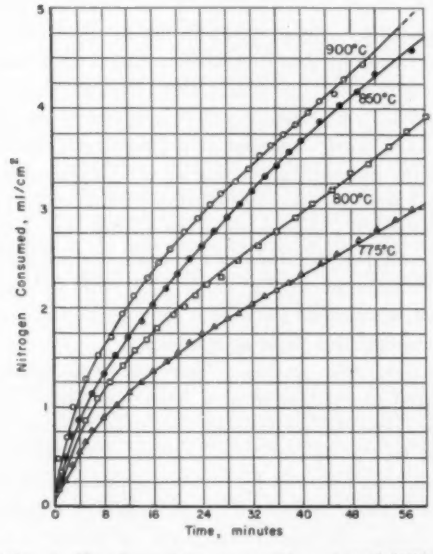

FIG. 5. Uranium-nitrogen reaction at 775°–900°C

UN. U_2N_3 which lies between the UN and UN_2 was the phase present in greatest quantity in the surface reaction product.

Specimens reacted with nitrogen between 550° and 750°C also produced tightly adherent surface films, but these films were much less rough on the exposed surface than those produced at higher temperatures. The microstructure at the surface of a specimen

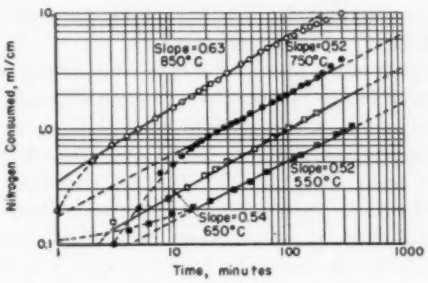

FIG. 6. Typical log-log plots for uranium-nitrogen reaction in the range 550°–850°C.

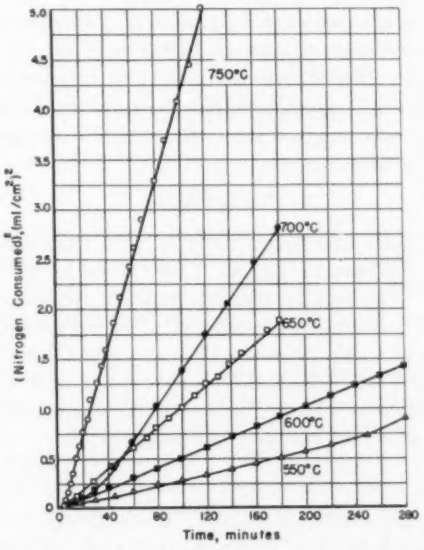

FIG. 7. Uranium-nitrogen reaction at 550°–750°C

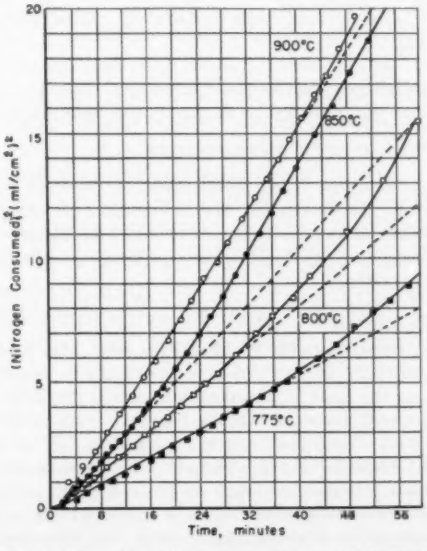

FIG. 8. Uranium-nitrogen reaction at 775°–900°C

TABLE I. *Rate constants, k, determined at various temperatures for the reaction of nitrogen with uranium*

Temp, °C	$k \times 10^4$, $(ml/cm^2)^2/sec$	Slope of log-log plot
550	0.463	0.52
600	0.542	0.54
600	0.855	0.52
650	1.76	0.54
700	2.90	0.62
750	7.06	0.52
750	9.70	0.55
775	23.6	0.58
800	34.9	0.57
800	40.0	0.57
850	43.5	0.63
900	54.7	0.60
900	65.5	0.53

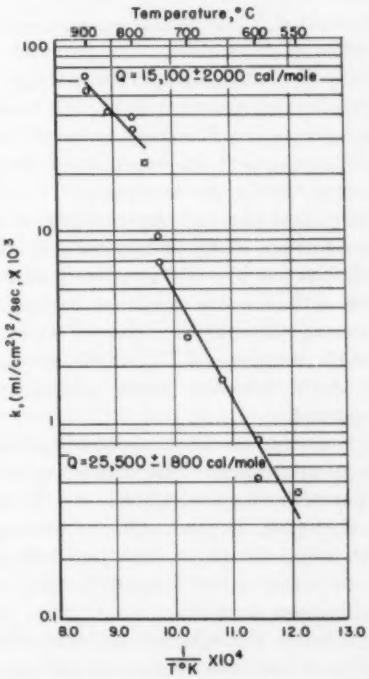

FIG. 9. Uranium-nitrogen reaction; variation of parabolic rate constant with temperature.

reacted with nitrogen at 600°C for 5 hr is shown in Fig. 3. The surface film appears to contain only one phase. The outermost surface reaction product on these specimens powdered off on storing. This powder was identified as face-centered-cubic UN_2. UN_2 also was the chief constituent in the adherent surface films where some evidence for U_2N_3 was found in some of the x-ray diffraction patterns. No UN was found in any of the surface films of specimens reacted with nitrogen below 750°C.

Hardness traverses of specimen cross sections revealed no evidence of solution of nitrogen in the

metal. This is what one would expect since the solubility of nitrogen in uranium is very low (<100 ppm) over the entire range 550°–900°C.

Reaction rates.—The reaction of nitrogen with uranium was found to follow a parabolic rate law over the entire range of temperatures 550°–900°C. Reactions were continued for times up to 6 hr. Reactions showed initial induction periods ranging from about 1 min to as long as 15 min. Since uranium metal oxidizes readily in air at room temperature, it is likely that during these induction periods, the reaction of nitrogen is hindered by a thin oxide film already on the uranium. However, after the initial nitride film has formed, further reaction (film thickening) proceeds in a parabolic manner.

Some deviations from parabolic behavior also were noted after a considerable amount of nitrogen had been reacted. These deviations generally were in the direction of rates faster than parabolic and occurred over the entire temperature range studied. Deviations became apparent in shorter times at the higher temperatures. This may indicate that these deviations are caused by cracking of the surface films at some limiting thicknesses.

Several typical plots of the amounts of gas consumed vs. time are shown in Fig. 4 and 5. The crossing of some of the lines in the vicinity of the origin is evidence of the varying lengths of the initial induction periods of nonparabolic behavior. Only the first 60 min of the reactions at 775°–900°C are plotted in Fig. 5 since the behavior became extremely erratic after this period.

If the logarithm of the amount of nitrogen consumed is plotted against the logarithm of time, a straight line with a slope of 0.5 results if the parabolic rate law is obeyed. Typical plots, as seen in Fig. 6, show both initial deviations from parabolic behavior and also deviations after a considerable amount of nitrogen has been reacted.

In Fig. 7 and 8, the square of the amount of nitrogen consumed per unit surface is plotted against time. These plots show the periods of time over which parabolic behavior was observed. The induction period for the reaction at 700°C is especially noticeable. The break from parabolic behavior to a faster rate for the reaction at 550°C also is evident.

The dashed line extensions of the straight line portions of the curves of Fig. 8 show the extent of the deviations from the initial period of parabolic reaction. All of the reactions in this temperature range have very short, almost negligible, induction periods and show deviations to faster rates following the period of parabolic reaction. Parabolic rate constants were calculated for each reaction by determining the slope of the straight line portions of the curves in Fig. 7 and 8. Rate constants calculated in this manner and slopes of the log-log plots are listed in Table I.

An Arrhenius plot of the rate constants is shown in Fig. 9. It can be seen that the experimental points appear to fall on two straight lines, the one covering the range from 550° to 750°C and the other, the range from 775° to 900°C. The Arrhenius-type equation, $k = A \exp(-\Delta H/RT)$, was determined for each line by the method of least squares. At 550°–750°C the parabolic rate constant is $k = 202 \exp(-25{,}500/RT)$ $(\text{ml/cm}^2)^2/\text{sec}$ where $25{,}500 \pm 1800$ cal/mole is the activation energy and the probable error[3] in a calculated k is $\pm 20\%$. At higher temperatures, 775°–900°C, the parabolic rate constant is $k = 3.95 \exp(-15{,}100/RT)$ $(\text{ml/cm}^2)^2/\text{sec}$. The activation energy is $15{,}100 \pm 2000$ cal/mole and the probable error in k is $\pm 10\%$. It is not known whether it is significant that the apparent change in activation energy occurs at about the beta to gamma transformation in uranium (770°C).

Conclusions

Nitrogen was found to react with uranium in a parabolic manner in the temperature range 550°–900°C. The surface reaction product formed below 750°C consisted principally of UN_2 with some evidence of U_2N_3. Between 775° and 900°C, the compounds UN, U_2N_3, and UN_2 were found in the films. An apparent change in activation energy for the reaction occurs between 750° and 775°C.

Acknowledgments

The experimental reaction rate experiments were performed by Mr. B. G. Koehl. X-ray diffraction studies of the surface reaction products were carried out by Mr. D. A. Vaughan. Specimens were prepared for metallographic examination by Miss Betty J. Hannahs.

Any discussion of this paper will appear in a Discussion Section to be published in the December 1955 JOURNAL.

REFERENCES

1. R. E. RUNDLE, N. C. BAENZIGER, A. S. WILSON, AND R. A. MCDONALD, *J. Am. Chem. Soc.*, **70,** 99 (1948).
2. J. J. KATZ AND E. RABINOWITCH, "The Chemistry of Uranium," p. 235, McGraw-Hill Book Co., Inc., New York (1951).
3. M. W. MALLETT, J. BELLE, AND B. B. CLELAND, *This Journal*, **101,** 1, (1954).
4. A. F. GERDS AND M. W. MALLETT, *ibid.*, **101,** 4, (1954).

[3] From the least square calculation, the probable error in k can be calculated by the equation $k = A \exp(-\Delta H/RT) \exp \pm PE_k$. The probable error in log k is $PE_k = 0.6745 \sqrt{\Sigma d^2/n^2}$ where Σd^2 is the summation of the squares of the differences between the least square calculated values of log k and the experimental values of k, and n is the number of experimental values of log k used. For this work the approximation is used that $\exp \pm PE_k = 1 \pm PE_k$.

Kinetics of Surface Reactions of Metals

I. Iron[1]

DONALD M. SOWARDS AND NORMAN HACKERMAN

Department of Chemistry, The University of Texas, Austin, Texas

ABSTRACT

The reaction of iron with dilute, aqueous acetic acid was studied in a closed system with a nitrogen atmosphere at 34°C. The solution was sprayed on the metal continuously for periods up to 24 hr. The extent of reaction, determined gravimetrically, was found to be directly proportional to exposure time. The reaction rate was a function of acidity, flow rate, gaseous atmosphere composition, temperature, and nature of the adherent reaction products. Total activity and type of local activity changed with exposure conditions. This can be explained in terms of the defect structure of the film on the metal. Identity and properties of the films check with those described by others. It was concluded that ferrous acetate, ferrous carbonate, monobasic ferric acetate, and dibasic ferric acetate protect the underlying metal when formed as adherent, continuous films on the surface.

INTRODUCTION

Corrosion studies are usually classed in one or two categories: dry oxidation of metals by gases, and wet corrosion of metals by liquids. However, in terms of the role of the solid reaction products, the two may be quite similar.

Experimental dry oxidation rate curves which can be described by linear, parabolic, cubic, logarithmic, or asymptotic equations are quite common. Satisfactory theoretical expressions for rate constants for the second, third, and fifth type have been derived (1, 2). Theory requires a defect lattice and a sustained electric field in which ions without excessive kinetic energy may migrate. In these polyphase systems, a potential gradient and an electrical double layer contribute to the electric field in varying amounts according to scale thickness; thus, theoretical applications are restricted to specific cases of film thickness where field strengths are calculable. There is little doubt of the conceptual correctness of the theory because of successful verifications in several cases (3).

Evans (4) suggests a direct connection between dry oxidation and wet corrosion wherein metal ions, emerging from thin oxide film on the metal, are incorporated in the film on reacting with oxide ions at the film-solution interface. Oxide ions are presumed to form from environmental oxygen and electrons from the metal by way of the film. Thus, with poor circulation, the oxygen supply is insufficient for good oxide coverage, and metal ions escape into solution, thereby increasing the corrosion rate. This is found, for example, with iron or zinc in distilled water, showing the importance of films in wet corrosion. These films may form in several ways.

Atmospheric oxygen is consumed rapidly by iron (5), producing an oxide film that is difficult to remove, even by exposure to hydrogen at elevated temperatures (6, 7). When iron is immersed in dilute acid, the initial dissolution rate decreases rapidly during the first few minutes (8, 9). The initially high rate is attributable to exposure of metal either by cathodic reduction of oxide film in the cell, Fe/electrolyte/oxide/Fe (10, 11), or by film rupture (12). Decrease in reaction rate under these conditions involves only inorganic substances, and as Hoar (12) and Hackerman (13) indicate, may be attributable to film formation or repair. Although there is insufficient evidence for determining which of these predominates (12), strict repair should be limited to continuation of the existing lattice, thus limiting the number of metal oxides to those of a structure compatible with that of the protecting oxides.

The expected behavior of iron oxide in wet corrosion reactions has been determined (14, 15), and recently an experimental system yielding results which are expressible in terms of the laws of film growth was described (16). It was believed that investigation of corrosion in such a system would provide information about the initial conditions of film formation and subsequent behavior in a corrosive medium. In view of the earlier work (16), the present effort was arrived at determining: (*a*) rate and mechanism of the reaction of iron

[1] Manuscript received August 26, 1954. This paper was prepared for delivery before the Wrightsville Beach Meeting, September 13 to 16, 1953, and is based in part on a dissertation by Donald M. Sowards, submitted to the faculty of the Graduate School of the University of Texas in partial fulfillment of the requirements of the degree of Doctor of Philosophy.

coupons exposed in a weak acid spray system; (*b*) dependence of reaction rate on solution composition, conditions of exposure, and physical nature of the products; (*c*) identification of the solid, adherent reaction products; (*d*) temperature coefficient of the reaction.

Materials and Procedure

Iron coupons[2] (2 × 5 × 0.15 cm) were polished on No. 2 emery, No. 2/0 emery, and ferric oxide on worn No. 2/0 emery. This gave a mirror-bright surface visually free from scratches and pits.

Fig. 1. Spray chamber showing spray unit, coupon, and coupon holder.

They were reduced and annealed in hydrogen (950°C for 2 hr), cooled slowly, and pumped for 8 hr at 0.05 mm Hg.

Deaerated distilled water was used for solution preparation and for cleaning the system.

C. P. Bakers Analyzed grade acetic acid in sealed, ¼-lb bottles was used.

Reagent grade acetone was dried over anhydrous potassium carbonate for five months (17) and distilled in an all-glass still, the fraction distilling at 56.2 ± 0.1°C and 756 mm Hg (18) being collected for wash liquid.

Water-pumped nitrogen was scrubbed in an acidic solution of vanadyl sulfate over lightly amalgamated zinc (19), then concentrated sodium hydroxide, saturated lead nitrate, and finally moist glass wool. The flow rate was less than 500 ml/min.

Tank hydrogen was passed through a palladium catalytic deoxifier and a 15-in. column of anhydrous magnesium perchlorate.

The spray chamber with coupon and holder is shown in Fig. 1. All parts were Pyrex glass except the top and bottom which were neoprene. The spray unit was of one-piece construction and required 5 l/min gas flow with a 150 mm Hg pressure drop across the unit for normal operation. Pressure fluctuation in the chamber was less than 10 mm Hg. The Y-shape coupon holders were of Pyrex glass.

The entire system was made of Pyrex and Tygon housed in an air thermostat. Details of the system are available elsewhere (20). Before a run, the system was rinsed with six 7–14 l portions of water and flushed with nitrogen; the solution and gas were then circulated at thermostated temperature for 8 hr while 90 l of nitrogen swept through the system.

On removal, coupons were rinsed with acetone, vacuum dried, and weighed. Next, they were descaled for 5 min in 10% sulfuric acid containing 150 ppm inhibitor[3] while cathodically protected (3 v, 0.6 amp). The final weight was then taken.

Most runs were made at 34 ± 0.1°C, but some were also made at 20.0° and 41°C in order to obtain the temperature coefficient of the reaction.

Iron coupons were continuously sprayed with dilute acetic acid in a closed system for periods up to 24 hr. They were placed about 4 cm directly below the spray nozzle.

Nitrogen, pure or containing 1% or less of air, was circulated at a constant velocity of about 5 l/min in each of the spray units.

The acetic acid volume was 10–14 l, and the concentration 0–1000 ppm. Acidity changed with time, observations being made over the range *p*H 3.4–7.0. The ratio of solution volume to metal surface varied because of the necessity of removing coupons during the run; therefore, *p*H vs. time relations were not amenable to quantitative interpretation.

The liquid circulation rate varied from coupon to coupon, but was usually constant for a single coupon. In cases of variation, the weighted average rate was used. Flow rates are expressed in terms of the number of drops per minute leaving the coupon.

[2] All cut from the same sheet of Armco Ingot iron and certified by the supplier, Armco Steel Company, Middletown, Ohio, to contain: 0.010% C, 0.010% Mn, 0.005% P, 0.012% S, 0.002% Si, and 0.040% Cu.

[3] Rodine No. 77, American Paint Company.

The volume of a drop was determined to be reproducibly 0.13 ml.

There were two distinct flow regions on all coupons; an active region directly below the spray nozzle and a stagnant region on other parts. The flow rate in the stagnant region was about one-tenth of that in the active region. The coupons were located so that active and stagnant regions were about equal in area.

Results

Initial film formation.—When coupons were first exposed to the spray, they remained bright for about five minutes if air was absent, but for only a few seconds if air was present. In either case a very thin, black, transparent film then appeared, covering the entire surface within 3–5 sec; it remained for about 10 sec, then, within 1–2 sec, it disappeared in the region of active flow. The re-exposed surface was as bright as the initial surface; in fact, if there was a pre-exposure film, the surface was now mirror bright.

In the stagnant region, the black film thickened rapidly and became opaque. After about 30 min with traces of air or 2–3 hr in its absence, a faint tan film formed in patches over the black film. There was always black scale between the tan film and metal unless at least one volume per cent of air was present, in which case tan rust appeared everywhere. Several attempts to identify the black film material by x-ray analysis failed.

Post-exposure observations.—Scale characteristics were also affected by flow rate and acidity. In nitrogen with flow rates of 5–100 drops/min, up to 1 mg/day of adherent scale was formed on each coupon if the initial *p*H was greater than 4; 5–15 mg/day formed at lower initial *p*H. At other flow rates or with air present, more scale was formed, about 20–30 mg/day under optimum scaling conditions.

The descaled coupon was abraded on No. 2 emery, and relative metal loss from different regions was determined by the amount of abrasion required to remove the etch marks. Under certain exposure conditions more metal was lost in the stagnant region; under different ones, more metal was lost in the active region. There were still other exposure conditions such that the metal was lost uniformly from the entire surface. The region of metal loss was a function of relative flow rate and was independent of the absolute flow rate.

With initial *p*H less than 4, major metal loss was in the stagnant region. The region of active flow remained smooth except for microgrooves parallel to the direction of flow. These were very shallow, ranging up to 2 cm in length. They increased in number and were closer together with decreasing initial *p*H. Below *p*H 3.5, the region of active flow was uniformly etched, but greater attack was noted underneath the scale.

More metal was lost from the active flow region if the initial *p*H exceeded 4.5. The stagnant region scale, although limited in quantity, was more adherent, and the metal remained smooth except for an occasional rough spot. In the intermediate range, *p*H 4.0–4.5, the metal was lost uniformly from the entire coupon surface, although scattered etched patches under the scale sometimes occurred in the stagnant region.

Reaction rate.—Results of runs in solutions with an initial *p*H of 4.4–3.5 are shown in Fig. 2. The zero time and weight loss point has been chosen as common to all curves, although there was an initially rapid, irregular reaction. However, the errors are no

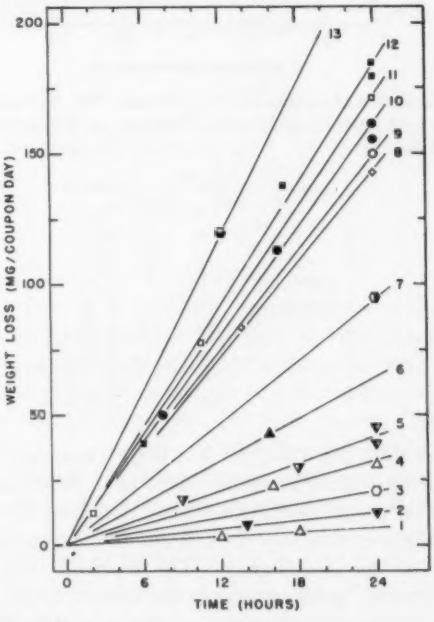

Fig. 2. Weight loss of iron coupons in acetic acid at comparable solution flow rates as a function of time.

Curve	*Conc (ppm)*	*Slope*
1	15	0.29
2	25	0.52
3	—	0.87
4	95	1.35
5	140	1.75
6	150	2.70
7	200	3.92
8	285	6.00
9	385	6.25
10	600	6.75
11	1000	7.17
12	375 (41°C)	7.62_5
13	385	10.3
	(Approx. 1% air)	

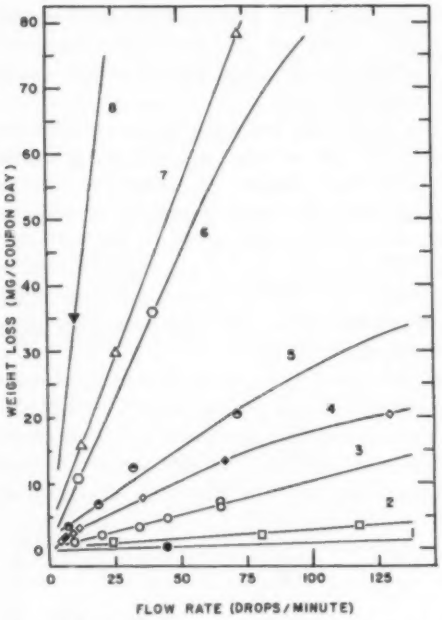

FIG. 3. Weight loss of iron coupons for one-day exposures in dilute acetic acid solutions as a function of liquid flow rate.

Curve	HAc conc (ppm)	Initial pH
1	0	7.0
2	0	5.0
3	0	4.6
4 (open pts.)	0	4.4_5
4 (solid pts.)	15	4.4_5
5	25	4.3
6	0	4.0
7	95	3.9
8	150	3.8

greater than 5% after the first hour. Duplicate time points were taken at the end of 24 hr to illustrate the effect on weight loss obtained by doubling the flow rate. Some curves have been drawn to conform to the trend of the entire group. The reaction rates are given in the figure caption as the slopes. Aside from curve 13, determined with air present, and curve 12, representing a run at 41°C, solution acidity was essentially the only variable in these experiments.

The effect of flow rate on weight loss is illustrated in Fig. 3. These curves all approach a maximum weight loss value, although this is not evident in the figure. An approach to a constant value also appears in the *p*H vs. time curves in Fig. 4. (The high degree of reproducibility is apparent.) This value is between *p*H 4.9–5.0 and is also reached by solutions with an initial *p*H greater than 5 (not shown). This is approximately the *p*H of a solution saturated with ferric hydroxide.

Electrical conductivities.—Specific conductivities

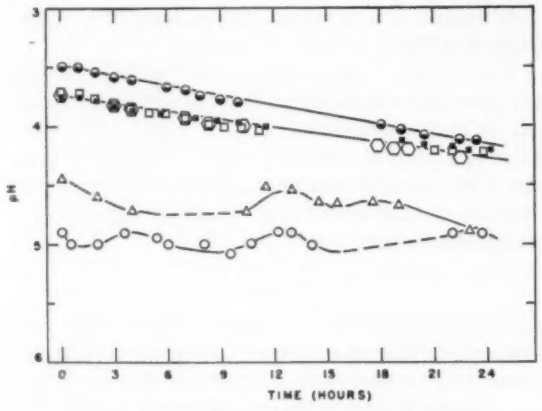

FIG. 4. Solution *p*H as a function of time

of several powdered salts prepared in the course of this work were measured but are good only to an order of magnitude.

Ferrous carbonate	(2) × 10^{-9} (ohm-cm)$^{-1}$	at 26°C
Ferrous acetate	(5) × 10^{-7}	25°C
Monobasic ferric acetate	(1) × 10^{-7}	25°C
Dibasic ferric acetate	(2) × 10^{-7}	25°C

Coefficients are given only for comparative purposes. Compounds show an increase in conductivity with increasing temperature at about room temperature. All of them are considered to be electronic conductors (21).

DISCUSSION

The reproducible behavior observed during initial film formation and in curves of Fig. 4 are indicative of the reliability of the experimental method employed in these experiments.

The electrochemical nature of the reaction under study has been well established, and although no potential measurements were made in the course of this study,[4] results are interpreted in terms of current corrosion theory. (All potentials refer to the standard hydrogen potential.) When the potential of iron in an acid solution increases to about −0.3 v (i.e., changes from more negative values), a black, nonprotecting film appears and hydrogen evolution decreases. Further increase in potential is accompanied by a transformation of this film to a brown film, the change apparently originating at the region of highest current density. At still more positive

[4] Separate studies in this laboratory showed that while forming similar films fully immersed in 2500 ppm acetic acid, the open circuit potential of these same coupons is about −0.3 v. The polarization curves are linear, at least at low current densities, with a potential of −0.2 v at 4 ma/cm² applied anodic current, and −0.5 v at 4 ma/cm² applied cathodic current.

potentials, the brown film disappears, leaving a bright metallic surface (21, 22).

Identification of the films was based on reports of similar films (14, 15, 21, 22). The black film was magnetite and is nonprotective on the basis of previous reports and observation here of its behavior in the descaling process. This is implied also by linearity of the rate curves. The thin, flaky brown film was ferric oxide as reported for other air-free systems [(15); see also (14, 21, 22)]; it may form a protective film when deposited in direct contact with the surface.

When the coupons were first exposed in the present system the active metal underwent anodic polarization. The time required for appearance of the magnetite film corresponded to that required for the potential to reach about −0.3 v. Film formation reduced the cathodic reaction rate either by lengthening the diffusion path or by altering the over-all diffusion mechanism. The cathodic process was either hydrogen evolution or oxygen reduction depending on exposure conditions. The initial rapid reaction depended on cathodic depolarization by oxygen adsorbed when coupons were weighed.

Nitrogen-air atmosphere.—Only a few runs were made with traces of air present. These were made in order to determine the effect of oxygen on the appearance of the scale and the reaction rate in general so that, in the absence of a direct test for the presence of oxygen, its presence might be suspected. The abundance of red ferric oxide formed under these conditions, along with traces of green magnetite, was considered to be evidence of the presence of traces of air in the system; otherwise, it was considered to be absent. The reaction rate was greater with oxygen present (compare curves 9 and 12 of Fig. 2); however, the linear law was followed for only about 20 hr when the rate began to decrease rapidly because of the type of film formed.

Nitrogen atmosphere.—With film formation, the differential flow regions began to affect subsequent behavior. Because of the higher solution replenishment rate, the active flow region became the place of major cathodic activity. The potential in this region became more positive, and the magnetite film disappeared. Location of the anodic site as indicated by the region of metal loss depended on acidity and, to some extent, on the relative flow rate. The sensitivity of anodic activity to changes in acidity and flow rate is shown in Fig. 5.

Above *p*H 5, the anodic region was restricted to the region of active flow because of low electrical conductivity of the solution and low degree of cathodic activity elsewhere, i.e., low rate of replenishment of hydrogen ion for the cathodic reaction. There appears to be a semiprotective, invisible film present in this *p*H range[5] because of the dependence of reaction rate on flow rate and because the *p*H changes to a constant value of 5, suggesting a buffered system. The nonprotective nature of this film is shown by the fact that on starting at *p*H 7, the slowest reaction condition in this work, the rate curve was linear for at least 48 hr. During this time the *p*H changed to 5 in 26 hr and was constant thereafter.

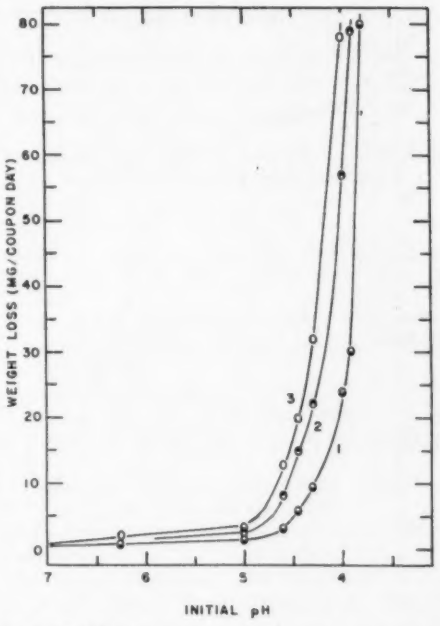

FIG. 5. Weight loss of iron coupons for one-day exposures in dilute acetic acid solutions at constant flow rates as a function of initial solution *p*H.

Curve	*Flow rate (drops/min)*
1	25
2	75
3	125

Below *p*H 4, the anodic region was the region of stagnant flow, but there was an increasing amount of anodic activity in the active flow region as the acidity increased. This was indicated by the microgrooves. In this *p*H range, the reaction rate was under anodic control. As *p*H decreased and the rate of hydrogen evolution increased, there was an increasing amount of anodic activity in the active flow (cathodic) region because the high degree of anodic polarization forced an expansion of the anodic area

[5] Above *p*H 6, the initial film is gray rather than black, but this is probably due to the small amount of film material formed.

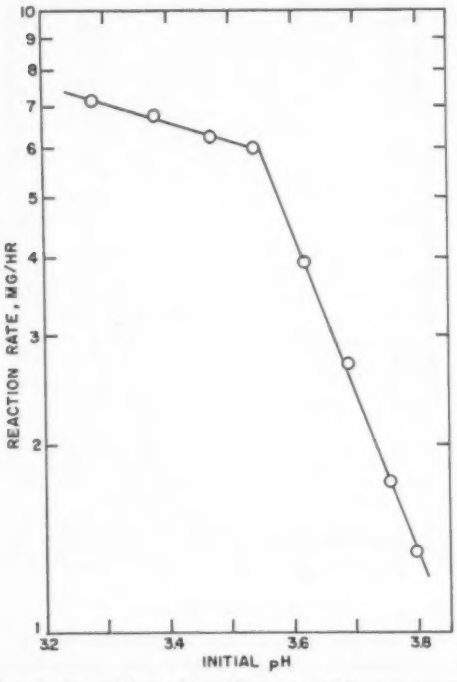

FIG. 6. Logarithm of reaction rate of iron coupons for one-day exposures at comparable flow rates as a function of initial solution *p*H.

from the stagnant into the active flow region. It should be noted that this movement of anodic into cathodic area had a twofold effect in keeping the total anodic and cathodic activity in balance; it simultaneously increased total anodic activity and lowered total cathodic activity. This is graphically illustrated in Fig. 6 and 7 where it may be seen that there was an abrupt decrease in reaction rate at *p*H 3.5 with increasing *p*H. As previously mentioned, the active flow region was uniformly etched with microgrooves below *p*H 3.5. The fact that most of the metal loss occurred in the stagnant flow region under these conditions suggests that the major effect of microgroove formation was to lessen total cathodic activity, i.e., reduce the total effective cathodic area.

It is interesting to note the similarity of Fig. 7 with previously reported results for mild steel immersed in oxygen-containing solutions of varying *p*H (23). The present work shows that the *p*H at which the film dissolves, as indicated by an abrupt increase in reaction rate with decreasing *p*H, is a function of other exposure conditions as well as of the specific acid present (see Fig. 5 also), and that this behavior is not restricted to systems containing oxygen.

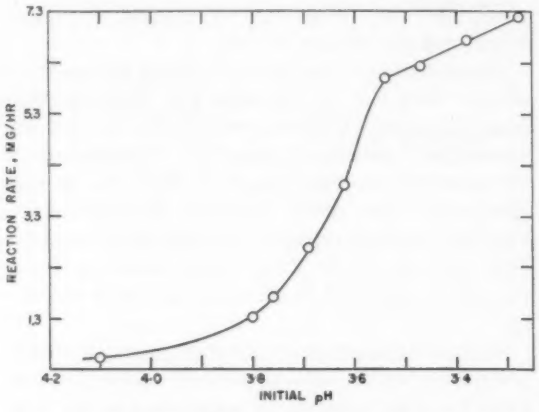

FIG. 7. Reaction rates of iron coupons for one-day exposures at comparable flow rates as a function of initial solution *p*H.

In the intermediate range, *p*H 4–5, the reaction was under mixed control in view of the uniform loss of metal from the entire surface regardless of relative flow rate. There was probably a nearly homogeneous distribution of physically small active sites which became polarized and were forced to migrate, thereby covering the entire surface during the time of measurement.

The source of the films formed in these experiments is not known. In the high *p*H range, the buffering agent was probably ferric hydroxide because of the approach to *p*H 5. Also, the time required for this *p*H to be reached was in keeping with the time necessary for the reaction to generate the appropriate amount of iron as ferric ion. Its semiprotecting properties were in keeping with those expected for a slightly insufficient amount of film material. The abrupt increase in reaction rate in Fig. 5 was at the *p*H expected for film solubility. This could also have been the cause of the linear reaction rate observed for both changing and constant *p*H in the runs with initial *p*H 7. The *p*H at the coupon should be the same and constant after the first minutes of the reaction, thus affording a constant supply of hydrogen ion to the cathode. It is possible that the half-cell reaction $Fe/Fe(OH)_3$, with a potential[6] just -0.25 v vs. a hydrogen electrode in a solution of the same *p*H and a partial pressure of hydrogen

[6] Using a *p*H-independent potential difference of -0.3, as this implies, a value of 1000 ohms/cm (for approximately 350 ppm acid), and 0.6 ma (calculated from rate curve and area), an active distance between local anodes and cathodes of 2 cm may be calculated from Ohm's law. This is the maximum distance for interaction of local elements, and is sufficient to allow the cathodic active flow region to stimulate the stagnant anodic region.

$= 10^{-7}$ (21) could have been the source. Likewise, Fe/Fe_3O_4 may have a potential of -0.3 v with the same conditions of reference (21), thus indicating a source for this material also. The high degree of anodic polarization which has been suggested for this system makes these possibilities even more attractive. The thin flaky, brown ferric oxide overlying the magnetite was probably produced electrically by the conversion of magnetite, as noted above, at electrical leaks with high current flow through the nonprotecting magnetite. They should be more adherent and less restricted in location if deposited from solution.

Reaction rates indicated by the slopes of curves 9 and 12, Fig. 2, were used to calculate a temperature coefficient for reactions under these supposedly similar conditions. A value of 5 kcal/°C/g atom was found. Similar conditions for curve 13 and a run at 20°C (not shown) with about 1% air present gave a value of 3 kcal/°C/g atom. Both of these values indicated diffusion control in the rate-determining step of the reactions. It is not prudent, however, to attach too much significance to these values.

The linear relation of log hydrogen ion activity to time which is found in Fig. 4 is suggestive of a first order dependence of rate on hydrogen ion activity.

The slope of that portion of the curve between *p*H 3.5 and 3.8 in Fig. 6 is -0.4 which is in exact agreement with the value predicted for an air-free system by Gatty and Spooner (24). It is postulated here that the break in the curve at *p*H 3.5 is a function of relative and absolute flow rates, as well as of the ratio of stagnant flow to active flow region. These factors probably affect the comparison of the different curves of Fig. 2–6, since this comparison should be made with these factors held constant. This has been considered with the present results when possible.

From the resistivities and nature of the current carriers in the solids prepared for resistance measurements in this work, it is concluded that they would protect the underlying metal if they formed adherent, continuous films on the surface.

ACKNOWLEDGMENT

Financial support of this project by the Office of Ordnance Research under Contract DA-23-072-ORD-216 is gratefully acknowledged.

Any discussion of this paper will appear in a Discussion Section to be published in the December 1955 JOURNAL.

REFERENCES

1. C. WAGNER, *Z. physik. Chem.*, **21B**, 25 (1933).
2. N. CABRERA AND N. F. MOTT, *Repts. Progr. Phys.*, **12**, 163 (1948).
3. O. KUBASCHEWSKI AND B. E. HOPKINS, "Oxidation of Metals and Alloys," pp. 119–142, Academic Press Inc., New York (1953).
4. U. R. EVANS, *Nature*, **168**, 853 (1951).
5. H. H. UHLIG, *This Journal*, **97**, 215*C* (1950).
6. E. J. CAULE AND M. COHEN, *Can. J. Chem.*, **31**, 237 (1953).
7. F. C. TOMPKINS, *Z. Elektrochem.*, **56**, 360 (1952).
8. R. V. COMEAUX, *Corrosion*, **8**, 305 (1952).
9. V. D. YAKHONTOV, *J. Appl. Chem. (U.S.S.R.)*, **19**, 761 (1946).
10. W. SCHWARZ, *Z. Elektrochem.*, **55**, 170 (1951).
11. U. R. EVANS AND I. D. G. BERWICK, *J. Chem. Soc. (London)*, **1952**, 3432.
12. T. P. HOAR, *Trans. Faraday Soc.*, **45**, 683 (1949).
13. N. HACKERMAN, *Corrosion*, **4**, 45 (1948).
14. H. O. FORREST, B. E. ROETHELI, AND R. H. BROWN, *Ind. Eng. Chem.*, **23**, 650 (1931); G. L. COX AND B. E. ROETHELI, *ibid.*, **23**, 1015 (1931).
15. M. G. FONTANA AND W. A. LUCE, *Corrosion*, **5**, 189 (1949).
16. E. E. GLENN AND N. HACKERMAN, *This Journal*, **100**, 339 (1953).
17. C. F. H. ALLEN, Editor, "Organic Syntheses," **20**, p. 7, John Wiley and Sons, Inc., New York (1950).
18. J. TIMMERMANS, "Physico-Chemical Constants of Pure Organic Compounds," p. 354, Elsevier Publishing Co., Inc., New York (1950).
19. L. MEITES AND T. MEITES, *Anal. Chem.*, **20**, 984 (1948).
20. D. M. SOWARDS AND N. HACKERMAN, Technical Report, Office of Ordnance Research Contract No. DA-23-072-ORD-216, University of Texas, February 10, 1953; *ibid.*, July 1, 1953.
21. M. POURBAIX, *Corrosion*, **5**, 121 (1949).
22. J. H. BARTLETT AND L. STEPHENSON, *This Journal*, **99**, 504 (1952).
23. H. H. UHLIG, Editor, "The Corrosion Handbook," pp. 128, 129, John Wiley & Sons, Inc., New York (1948).
24. O. GATTY AND E. C. R. SPOONER, "The Electrode Potential Behavior of Corroding Metals in Aqueous Solutions," p. 279, The Clarendon Press, Oxford (1938).

The Difference Effect on Aluminum Dissolving in Hydrofluoric and Hydrochloric Acids[1]

M. E. Straumanis and Y. N. Wang

Department of Metallurgy, University of Missouri School of Mines and Metallurgy, Rolla, Missouri

ABSTRACT

The positive difference effect was observed during dissolution of high purity aluminum coupled with platinum in 0.05, 0.1, 0.25, 0.5, 0.75, 1.0, and 2.0 hydrofluoric acid at 25°C. The effect was directly proportional to the galvanic current up to 60 ma/cm², being nearly independent of the concentration of the acid. The proportionality constant, K, was 5.34, corresponding to a polarizability of 77% for the aluminum in hydrofluoric acid.

Positive as well as negative difference effects were observed under the same conditions while aluminum was dissolving in 0.1, 0.25, 0.5, 0.75, 1, and 2N hydrochloric acid. Points for the positive effect at low current densities, as well as those for the negative effect at higher current densities up to 200 ma/cm², lay along a downward exponential curve. The effect was independent of the concentration of the acid.

The positive effect is explained by the anodic polarization of aluminum by the additional current, and the negative one, which actually represents an overlapping of both effects, by the breakdown of the surface film because of the same current. A theoretical treatment of both effects is given. The term "polarizability" in per cent (P %) is introduced. The dissolution of aluminum in hydrofluoric acid is an electrochemical process.

Introduction

Even purest aluminum dissolves readily in hydrofluoric acid, and at a much higher rate than in hydrochloric acid. So it was important to know whether one of the symptoms of the electrochemical mechanism of reaction (1), the difference effect, still occurs while aluminum is dissolving in hydrofluoric acid. On the other hand, it was also important to study the effect on the same metal dissolving with a much slower rate in hydrochloric acid, because the comparison of both effects might give some clue to the mechanism of dissolution and the surface condition of aluminum in the two acids.

The difference effect is established by comparing the rate, V_1, of hydrogen evolution of a metal dissolving in an acid or base, with that, V_2, observed during anodic polarization of the metal at a current density, I. Usually these two rates are not equal, and the difference Δ, known as "difference effect" (2) is

$$V_1 - V_2 = \Delta \qquad (I)$$

If $V_2 < V_1$ the effect is "positive" and shows how much has to be added to the lower rate, V_2, to restore the previous rate, V_1. This effect has been studied on: aluminum in sodium hydroxide (2, 3); zinc in sulfuric acid (2, 4); and titanium in hydrofluoric acid (1). If $V_2 > V_1$, the effect is "negative" because Δ has to be subtracted from V_2, to get V_1. This type of effect was observed on magnesium corroding in sodium chloride (5), and on aluminum dissolving in hydrochloric acid (5). However, only one concentration of the acid was used in the latter case.

Experimental Procedure and Materials Used

The experimental procedure was the same as described previously (1). Some improvements were made by using glass tubes and joints, wherever possible, to reduce the loss of hydrogen by diffusion through the rubber parts. Potential measurements of the dissolving metal were not made during these experiments, but were made separately.

The dissolving electrode (anode) with a surface of one cm² exposed to the acid was made of an aluminum sheet.[2] It was cold rolled to a final thickness of 1 mm. The analysis supplied with this material claimed the following impurities: Si, 0.0015; Fe, 0.0007; Cu, 0.0004; and Mg, 0.0007% by weight. It showed a much higher dissolution rate in 2N hydrochloric acid than the 99.998% French aluminum[3] used in previous experiments (7). From the point of view of local cells the aluminum of this investigation was of lower purity. The acids used were of the highest purity commercially obtainable.

[1] This paper was prepared for delivery before the Boston Meeting, October 3 to 7, 1954 and is based on a thesis submitted by Y. N. Wang in partial fulfillment of the requirements for the Ph.D. degree to the Graduate School of the University of Missouri.

[2] Obtained from The Aluminum Company of America, designated H-18 temper.

[3] Compagnie Alais, Froges et Camargue, France.

The method of calculation of the results was the same as pointed out previously (1). The difference effect [Equation (I)] expressed in $mm^3cm^{-2}min^{-1}$ was calculated by the equation:

$$\Delta = V_1 + 6.97I - V_t \qquad \text{(II)}$$

where V_t is the total rate of hydrogen evolution from the anode and platinum cathode while the current I was flowing through the circuit. The factor 6.97 converts the milliamperes passing the cathode for one minute into mm^3 of hydrogen.

Results

Aluminum in hydrofluoric acid.—The velocity of dissolution of this aluminum is comparable to that of titanium in 0.02 to 10*N* hydrofluoric acid (6), although aluminum shows a lower rate, especially at concentrations of 4 to 8*N*. The dissolution reaction is

$$Al + 3H^+ \rightarrow Al^{3+} + 1\tfrac{1}{2}\ H_2 \qquad \text{(III)}$$

and AlF_3 is formed which does not completely dissolve in the acid. In a porous state it partially sticks to the dissolving plate, especially in the corners. However, this salt does not have the property of some oxide layers or protective films which adhere firmly to the surface of the metal, inactivating the local cathodes, and stopping the dissolution reaction. Aluminum fluoride specks on the aluminum surface do not prevent dissolution of the metal but they slow down the rate of reaction, as could be concluded from special experiments.

The difference effect was determined in seven concentrations of hydrofluoric acid at 25°C: 0.05, 0.1, 0.25, 0.5, 0.75, 1, and 2*N*. All measurements showed that a positive effect results [equation (I)], as shown in Table I. The approximate constancy of the *K* value [equation (IV)] in the last column of the table indicates that the difference effect is proportional to the anodic current passing the aluminum surface, as found by other investigators (1–6). The empirical equation (II)

$$\Delta = KI \qquad \text{(IV)}$$

combined with equation (II), gives an expression for *K*:

$$K = 6.97 + \frac{V_1 - V_t}{I} \qquad \text{(V)}$$

In the positive effect V_t must be larger than V_1 so *K* is always smaller than 6.97. However, sometimes larger values are found, e.g., 8.55 in Table I. It is believed that this comes from experimental difficulties and inaccuracies, from a breakdown of part of a protective scale possibly present on the surface, or from a sudden increase in the rate of self-dissolution V_1 of the metal. A reverse effect, producing too low *K*-values, would originate from a sudden decrease of V_1.

The constants *K* obtained in all concentrations of

TABLE I. *Positive difference effect on* Al *in 2N* HF, *25°C. Hydrogen volumes reduced to normal conditions*

Time	V_1	I	$6.97I$	V_t	Δ	K
min	mm^3/cm^2 *min*	ma/cm^2	mm^3/cm^2 *min*	mm^3/cm^2 *min*	mm^3/cm^2 *min*	mm^3/ma *min*
0	0	—	—	—	—	—
5	262.6	0		—	0	—
10	377.5	0		—	0	—
15	443.2[1]	0		—	0	—
20	492.2[2]	0		—	0	—
25	—	5.1	35.5	525.4	23.0	4.51
30	—	5.1		525.4		
35	558.0[3]	0				
40	—	10.2	71.1	541.8	87.3	8.55
45	—	10.2		541.8		
50	558.0	0				
55	—	15.0	104.6	525.4	104.4	6.95
60	—	15.0		591.0		
65	558.0	0				
70	—	20.0	139.4	558.2	139.2	6.96
75	—	20.0		558.2		
80	558.2[4]	0				
85	—	35.0	254.4	607.4	188.7	5.17
90	—	38.0		723.8		
95	541.6[5]	0				
100	—	58.0	390.3	689.6	267.1	4.77
105	—	54.0		689.4		
110	591.0[6]	0				
115	—	58.0	404.3	623.8	314.0	5.41
120	—	58.0		771.6		
125	623.8[7]	0				

Average values for V_1: [1], [2], and [3]: 512.9; [4] and [5]: 549.9; [5] and [6]: 566.3; [6] and [7]: 607.4.

TABLE II. *Slope constant K of the positive difference effect, equation (IV), obtained with* Al *in various concentrations of* HF *at different current densities I.*

I	Concentration of HF in *N*							*K* avg
	0.05	0.1	0.25	0.5	0.75	1.0	2.0	
ma/cm^2								$mm^3/ma \cdot min$
2.5	5.35	5.29	5.31	—	—	—	—	5.32
3.6	5.83	—	—	—	—	—	—	5.83
5.1	—	2.96	6.96	2.88	2.63	9.07	4.51	4.84
7.0	—	3.80	6.41	—	—	—	—	5.11
10.2	—	—	5.73	6.53	6.58	7.81	8.55	7.04
15.0	—	—	4.03	5.86	5.91	6.69	6.95	5.89
20.0	—	—	—	—	—	6.18	6.96	6.57
28.0	—	—	—	—	5.49	—	—	5.49
30.0	—	—	—	—	5.04	—	—	5.04
33.5	—	—	—	—	—	3.70	—	3.70
36.5	—	—	—	—	—	2.88	5.17	4.03
56.0	—	—	—	—	—	—	4.77	4.77
58.0	—	—	—	—	—	—	5.41	5.41
K avg	5.59	4.01	5.69	5.09	5.13	6.06	6.05	5.34

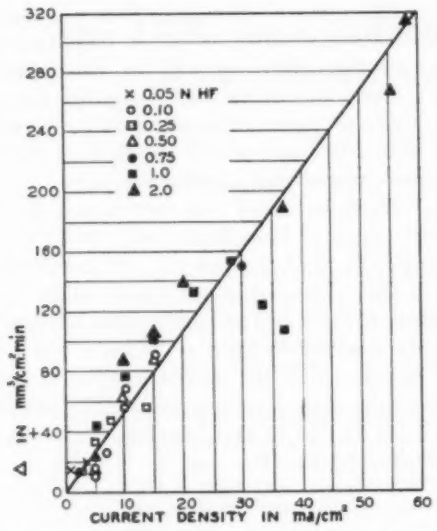

FIG. 1. Positive difference effect on aluminum in 7 hydrofluoric acid concentrations vs. current density. The ordinate shows the rate of hydrogen evolution to be added to the rate observed under current to obtain the initial rate V_i.

hydrofluoric acid at different current densities are summarized in Table II.

The scattering of the K values is the consequence of the difficulty of reproduction of Δ-measurements, as already pointed out. The scattering can be even better seen from the difference effect current density plot (Fig. 1). Nevertheless, a straight line can be drawn through the accumulation of the experimental points with a slope constant $K = 5.34$. However, it seems that at lower acid concentrations straight lines with a slightly larger K can be drawn through experimental points. Inserting the value 5.34 for K in equation (V) gives

$$V_i - V_1 = (6.97 - 5.34)I = 1.63I \quad \text{(VI)}$$

This means that instead of 6.97 mm³ of hydrogen as a total result only 1.63 mm³/ma/cm² of anodic surface are developed by the couple. Approximately 77% of the current went to overcome the difference effect and only 23% of it contributed to the increase of the rate of dissolution of the anodically polarized aluminum.

Potential of aluminum in hydrofluoric acid.—For the explanation of the difference effect some knowledge of the electrochemical behavior of aluminum in hydrofluoric acid is necessary. No published potential measurements of aluminum in hydrofluoric acid were found. The potential difference of the chain

$$\text{Al//HF}\,|\,\text{KCl sat.}\,|\,1N\ \text{KCl},\ \text{Hg}_2\text{Cl}_2\text{//Hg}$$

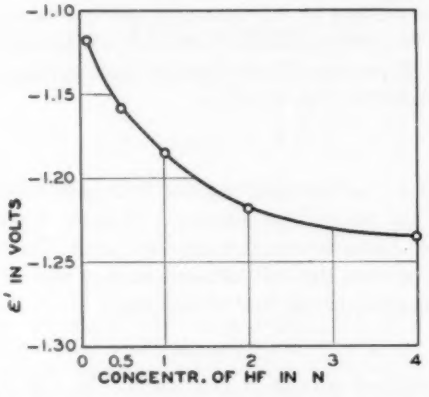

FIG. 2. Dissolution potential ϵ' of Al in HF vs. concentration of the acid. Hydrogen scale.

was measured, and the values obtained were reduced to the potential of the normal hydrogen electrode. As the metal dissolved in the acid, the measured potentials were dissolution potentials ϵ'. The tip of a Luggin capillary was pressed against the clean surface of the aluminum electrode under the acid.

After immersion of the electrode in the acid, the potential drops suddenly, then it becomes slowly less negative, and after a few hours a fairly steady potential is established. This potential is plotted against the concentration of the acid in Fig. 2, which clearly shows that the potential of aluminum decreases with the concentration, reaching values as low as −1.23 v in 4N acid. This very negative potential exceeds that of −1.209 v measured on amalgamated aluminum in 0.1N hydrochloric acid (9), and approaches that of −1.38 to −1.4 v obtained in a 1N sodium hydroxide solution (8). The equilibrium potential of aluminum calculated from the thermal data of the dissolution reaction is −1.69 v (10).

For potential measurements under anodic current, the aluminum electrode of the aforementioned chain was connected with a platinum electrode 1 cm away from the aluminum. Both electrodes had an area of 2 x 2 cm exposed to the electrolyte, and their construction has been described previously (11). By means of a rheostat and a milliampmeter in the aluminum-platinum chain, a given current density could be obtained.

Results are shown in Fig. 3. It follows from this figure that in each case the increase of current density is associated with the shifting of the potential of the dissolving aluminum toward more positive values, as it was also found in the cases of titanium, zinc, and other metals (1, 12–17). The irregularity of the curves in Fig. 3 is explained by the fact that the rate of self-dissolution of the aluminum

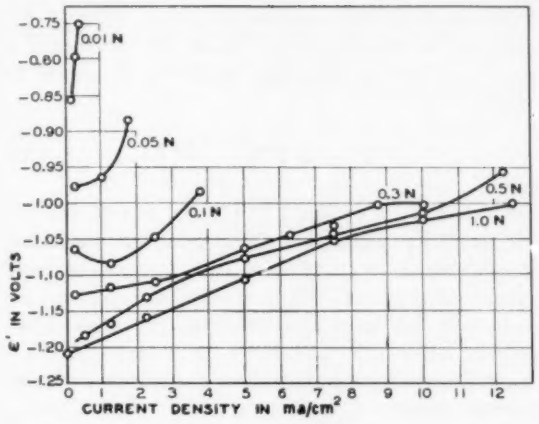

FIG. 3. Electrode potential ϵ' of Al vs. current density in various concentrations of HF.

electrode was not included in the current density given. This rate may influence the potential of the metal (12).

Aluminum in hydrochloric acid.—The fairly noble potential of −0.577 for aluminum in 1*N* hydrochloric acid (18), as compared with that in hydrofluoric acid, shows that surface conditions of the dissolving metal are quite different in both cases. The less negative potential indicates that there is a film or a scale on aluminum in hydrochloric acid, which probably is less porous, less soluble in the acid, and which sticks better to the metal than that at equilibrium on aluminum in hydrofluoric acid. Hence, another kind of difference effect was to be expected on aluminum in hydrochloric acid. Measurements, carried out in one concentration of the acid by other workers, showed that the effect was negative (5).

The experiments were repeated here using the following acid concentrations: 0.1, 0.25, 0.5, 0.75, 1, and 2*N*. The experimental procedure and the calculation [equation (II)] were the same as already demonstrated in the case of the positive effect. An example of the negative effect is shown in Table III obtained in 1*N* hydrochloric acid. The table shows two features that were not observed previously: (*a*) at small current densities the difference effect is positive, which turned out to be true also with other concentrations of the acid; and (*b*) *K* values show that experimental points do not lie on a straight line, but on an irregular curve. However, if all the experimental points obtained in the other concentrations of the hydrochloric acid are plotted against the current density, a quite regular curve can be drawn through the accumulations of the points, as shown in Fig. 4. Thus, the couple Al/HCl/Pt develops more hydrogen than expected from the initial rate of dissolution of aluminum and the current produced by the cell.

TABLE III. *Negative difference effect on* Al *dissolving in 1N* HCl, *25°C; hydrogen volumes reduced to normal conditions*

Time	V_1	I	$6.97I$	V_t	Δ	K
min	mm^3/cm^2 *min*	ma/cm^2	mm^3/cm^2 *min*	mm^3/cm^2 *min*	mm^3/cm^2 *min*	mm^3/ma *min*
0	0	0	—	—	—	—
20	0	0	—	—	—	—
30	—	5	34.9	24.7	+14.2	+2.84
40	—	5		33.1		
50	16.5	0	—	—		
60	—	10	69.7	74.3	+7.8	+0.78
70	—	10		82.6		
80	16.6[1]	0	—	—		
90	—	15.5	105.2	132.1	−10.4	−0.68
100	—	14.9		140.4		
110	24.8[2]	0	—	—		
120	—	20.0	136.6	173.4	−16.2	−0.82
130	—	19.2		173.5		
140	16.5[3]	0	—	—		
150	—	30.0	202.1	247.8	−29.2	−1.00
160	—	28.0		247.8		
170	16.5	0	—	—		
180	—	48.0	345.0	363.4	−35.0	−0.71
190	—	51.0		429.5		
200	16.5	0	—	—		
210	—	81.0	568.1	716.6	−117.5	−1.44
220	—	82.0		685.6		
230	16.5[4]	0	—	—		
240	—	116.0	717.9	908.5	−79.1	−0.77
250	—	90.0		710.3		
260	8.3[5]	0	—	—		

Average values for V_1: [1] and [2]: 20.7; [2] and [3]: 20.65; [4] and [5]: 12.4.

THEORY OF THE DIFFERENCE EFFECT

The fact that the negative difference effect also shows as a positive one at low current densities (Fig. 4) can be explained by the assumption that every difference effect appears as the result of an overlapping of both positive and negative effects. Hence, the correct expression for the difference effect observed should be:

$$\Delta = V_1 - (V_2 + V_4) \qquad \text{(VII)}$$

V_4 is the increase of hydrogen evolution due to the negative difference effect, which is also a function of anodic current density. Thus, under conditions where there is no appreciable film on the metallic surface, for instance aluminum in hydrofluoric acid, or amalgamated aluminum in hydrochloric acid (14), the term V_4 can be neglected, and a pure positive effect results. But if there is a film on the surface of the metal (aluminum in hydrochloric acid), the breakdown of the film as a result of applied or self-generated anodic current (see below), causes the additional rate V_4. It is clear then that at low current

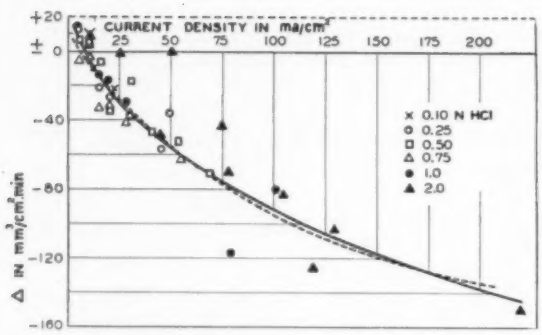

FIG. 4. Solid curve: difference effect on Al in HCl: positive at small current densities, negative at larger ones. The negative effect shows the rate of hydrogen evolution that has to be subtracted from the one observed under current to obtain the initial rate V_1. Dashed line: theoretical curve.

densities $V_1 > (V_2 + V_4)$, and the positive effect is still observed. With increasing current density $V_2 + V_4$ may become equal to V_1, and no effect appears, $\Delta = 0$ (see Fig. 4). Finally, at still higher current densities, V_1 is overbalanced by $V_2 + V_4$, and the negative effect shows up.

Attempts have never been made to derive the curve for the negative difference effect theoretically, although the positive one was successfully explained by Straumanis (1, 4, 13). In the following an expression for both effects is derived on the basis of equation (VII) and using the concept of local currents in a form proposed by Straumanis (4, 19).

The rate V_1 is given by

$$V_1 = \frac{\Delta v}{\Delta t . A} = k_1 z' \frac{\eta - \epsilon'}{r} \qquad \text{(VIII)}$$

where Δv is the volume of hydrogen evolved in the time Δt on the surface area A, η is the hydrogen overpotential of the local cathodes (its value is negative), z' the number of active local cathodes (cells) per unit area, ϵ' the dissolution potential of the base metal, and r the average resistance of a local cell. k_1 is a constant converting the current into volume units of hydrogen (20).

Polarizing the same metal surface anodically with a current density I, ϵ' changes to a more noble value (ϵ'_2). But the values of the variables η and r cannot change appreciably: the first because the local cathodes are polarized to a maximum according to the logarithmic Tafel's rule, and small changes in the local current, due to $\epsilon' \rightarrow \epsilon'_2$, do not alter η; the second because the resistance of the electrolyte in the interface, around the local cathodes, does not change much with the polarizing current. Therefore, the expression for V_2 is

$$V_2 = k_1 z' \left(\frac{\eta - \epsilon'_2}{r} \right) \qquad \text{(IX)}$$

Simultaneously the polarizing current breaks down one part of the protective film on the metal, and a number of new active local cathodes, z'', starts to work

$$V_4 = k_1 z'' \left(\frac{\eta - \epsilon'_2}{r} \right) \qquad \text{(X)}$$

Substituting in equation (VII) the values for V_1, V_2, and V_4 [equations (VIII), (IX), (X)] and simplifying

$$\Delta = \frac{k_1}{r} [z'(\eta - \epsilon') - (z' + z'')(\eta - \epsilon'_2)] \qquad \text{(XI)}$$

Now, the question is, how does z'' increase with the current density. According to Evans (14), Kroenig and Uspenskaja (5), and the authors' observations, parts of a film are stripped down from the surface of aluminum if the metal immersed in hydrochloric acid is touched by a platinum wire under the acid. Simultaneously the rate of hydrogen evolution increases on the surface of the aluminum. Evidently the discharge of electrons on the platinum surface forces Al^{3+} to leave the compact metal. But as it is covered largely by a dense protective film, the latter partially breaks down upon the impact of the Al^{3+} leaving the metal. The breakdown uncovers a number of new local cathodes (z'') which immediately start to act. The situation is then as shown in Fig. 5. It is quite clear that the film will not adhere equally to the whole surface of the metal. The weakest spots of the film will break down at first, then with increasing current density those which adhere slightly better follow, and so on. It can be assumed that the breakdown of parts of the film, or the uncovering of new active cathodes, z''_1, with

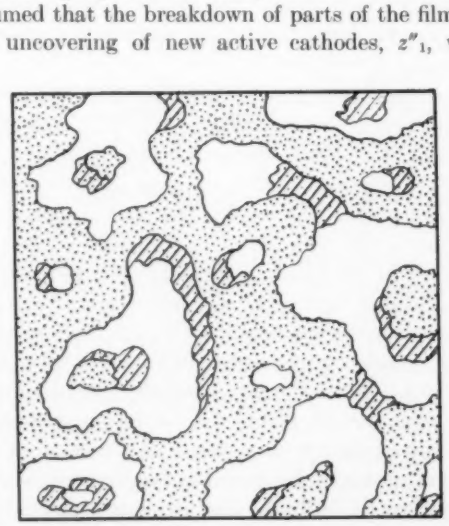

FIG. 5. Increase of z'' with current I. White areas: protective film per surface area unit. Dotted: areas producing the rate V_1 and V_2 (after anodic polarization); number of local cathodes z'. Striped and dotted: areas with the film broken down while current I is flowing, producing the rate V_4, number of local cathodes z''.

increasing current density i is proportional to the number of cathodes still under the protective film:

$$\frac{dz_1''}{di} = k_3[(z - z') - z_1'']$$

or

$$\int_0^I di = \frac{1}{k_3}\int_0^{z''} \frac{dz_1''}{D - z_1''} \qquad \text{(XII)}$$

where z is the total number of local cathodes on the dissolving metal surface, while z' is the number of active cathodes present in the pores before passing the current I. Therefore, z''_1 can increase according to (XII) from 0 to z''; $z - z' = D$. The solution of this well-known type of equation (XII) gives for I:

$$I = \frac{1}{k_3}\ln\frac{D}{D - z''},$$

and for z'':

$$z'' = D(1 - e^{-k_3 I}) \qquad \text{(XIII)}$$

Substituting (XIII) for z'' in equation (XI) and rearranging:

$$\Delta = \frac{k_1}{r}[z'(\epsilon_2' - \epsilon') - D(\eta - \epsilon_2')(1 - e^{-k_3 I})] \qquad \text{(XIV)}$$

This is the general equation for the difference effect, the positive as well as the negative.

For aluminum dissolving in hydrofluoric acid or in strong bases, the formation of new local cathodes z'', due to the film stripping effect by the polarizing current, can be neglected as already mentioned. Thus, z'' becomes zero if k_3 of equation (XIII) is zero. Substituting 0 for k_3 in equation (XIV), the second term of this equation vanishes. ϵ'_2 in the rest of the equation can be replaced by

$$\epsilon'_2 = \epsilon' + k_2 I \qquad \text{(XV)}$$

because the potential ϵ' of an anodically polarized metal, also of aluminum in hydrofluoric acid (Fig. 3), frequently increases linearly with current density (12, 14–17). k_2 is the slope constant. Under such conditions equation (XIV) converts into

$$\Delta = \frac{k_1 k_2 z' I}{r} = KI \qquad \text{(XVI)}$$

as all the four constants can be joined into a new one K, if the effect is observed in one concentration of the acid. However, if the concentration of the acid is changed, e.g., decreased, then, as shown by Fig. 3, the constant k_2 increases. Simultaneously, the average resistance, r, of a local cell increases also. Hence, the effect of changed concentrations of the acid may nearly cancel out. Equation (XVI) for the positive difference effect reveals that the effect is proportional to the current density, I, is independent of the nature of the dissolving metal, and may be nearly independent of the concentration of the corrosive agent used. This is shown by difference effect measurements on titanium (1) and aluminum (Fig. 1) in hydrofluoric acid.

To derive the curve for the negative effect one has to assume that the values of ϵ'_2 and η [equation (XIV)] are independent of the current density because: (*a*) with increase of current a part of the film breaks down and the actual current density, at least in the beginning of the process, remains approximately the same (21); and (*b*) if it is assumed that ϵ'_2 changes according to equation (XV) also during the breakdown of the film, the curve obtained goes through a minimum in contradiction to experimental results (Fig. 4). The constancy of η has already been discussed. Under such conditions a curve is calculated, the course of which agrees quite well with experiment (Fig. 4).

The discussion of this chapter shows that both effects, the positive and the negative one, can be well explained quantitatively using the concept of local currents.

Conclusion

The appearance of the difference effect and its theoretical treatment confirms again the assumption previously made by other authors (14) that the presence of the negative effect is a consequence of tight protective films on a metal which dissolves in a certain corrosive electrolyte. For instance, because there are no such films on aluminum dissolving in strong bases (3, 22), or in hydrofluoric acid, the positive effect appears, but, since there are films on this metal dissolving in hydrochloric acid, the negative effect shows up. The presence of a film is indicated by the comparatively noble potential of the metal, or its absence by a very negative potential.

The positive difference effect gives information about the polarizability of a metal. It is well known that metals are not equally polarized by an anodic current of the same strength. Some show slight potential shifts toward more positive values, and others larger shifts under the same conditions. However, potential measurements on working electrodes are not always reliable. The positive difference effect, according to the theory developed, is caused by the shift just mentioned and is independent of potential measurements. Constant K of equation (IV) shows directly the mm³ of hydrogen by which

TABLE IV. *Polarizability of some metals in per cent*

Metal	K	Electrolyte	$P\%$
Zn	2.5	H_2SO_4	36
Al	5.34	HF	77
Ti	5.7	HF	84

the rate of dissolution (per cm² and minute) of a common metal is decreased per each milliampere of the current discharged through the platinum cathode. Furthermore, it was shown that the maximum value for K is 6.97, meaning there is no hydrogen evolution on the dissolving metal when connected to a platinum anode (1). Therefore, the anodic metal is totally polarized (100%) as the hydrogen produced by the current is completely subdued by the difference effect. On the other hand, if $K = 0$, there is no difference effect at all, and no anodic polarization (0%). In between are the K values for different metals, and their polarizability in per cent (P%) can be expressed as follows:

$$P\% = \frac{100K}{6.97} = 14.35K \qquad \text{(XVII)}$$

Table IV shows the polarizability of some elements, for which K was determined in the units used above.

This shows that titanium and aluminum are polarized much more strongly than zinc by the same current density. The polarizability of a metal exhibits its ability to deliver electrons for the local cathodes and to expel anions into the respective corrosive agent; if the rate of both processes is high, the polarizability is low and vice versa.

Acknowledgments

Sincere thanks are given to Dr. J. A. Nock, Jr., Assistant Chief of the Physical Metallurgy Division, Aluminum Research Laboratories, Aluminum Company of America, for the donation of the aluminum sheet used for this investigation, and to Dr. C. B. Gill for the correction of the English of the manuscript.

Any discussion of this paper will appear in a Discussion Section to be published in the December 1955 JOURNAL.

References

1. M. E. Straumanis and P. C. Chen, *This Journal*, **98**, 351 (1951).
2. A. Thiel and J. Eckell, *Z. Elektrochem.*, **33**, 370 (1927).
3. M. A. Streicher, *J.* (*and Trans.*) *Electrochem. Soc.*, **93**, 304 (1948).
4. M. Straumanis, *Z. physik. Chem. A*, **148**, 349 (1930).
5. W. O. Kroenig and V. N. Uspenskaja, *Korrosion u. Metallschutz*, **11**, 10 (1935); **12**, 123 (1936).
6. M. E. Straumanis and P. C. Chen, *This Journal*, **98**, 234 (1951).
7. M. Straumanis, *Korrosion u. Metallschutz*, **14**, 1 (1938).
8. L. Kahlenberg and J. A. Montgomery, *Trans. Am. Electrochem. Soc.*, **36**, 285 (1919).
9. J. Heyrovský, *J. Chem. Soc.*, **117**, 32 (1920).
10. W. M. Latimer and B. S. Greensfelder, *J. Am. Chem. Soc.*, **50**, 2202 (1928).
11. M. E. Straumanis and P. C. Chen, *Corrosion*, **7**, 229 (1951).
12. M. Straumanis, *Z. physik. Chem. A*, **147**, 161 (1930).
13. M. Straumanis, *Korrosion u. Metallschutz*, **14**, 67 (1938).
14. U. R. Evans, "Metallic Corrosion, Passivity and Protection," p. 34, difference effect p. 220, Longmans, Green & Co., New York (1948); *see* also U. R. Evans and T. P. Hoar, *Proc. Roy. Soc.* (*A*), **137**, 343 (1932).
15. R. B. Mears, *J.* (*and Trans.*) *Electrochem. Soc.*, **95**, 1 (1949); R. B. Mears and R. H. Brown, *This Journal*, **97**, 75 (1950).
16. R. H. Brown, G. C. English, and R. D. Williams, *Corrosion*, **6**, 186 (1950).
17. M. A. Streicher, *J.* (*and Trans.*) *Electrochem. Soc.*, **96**, 170 (1949).
18. C. J. de Gruyter, *Rec. trav. chim.*, **44**, 960 (1925).
19. M. Straumanis, *Korrosion u. Metallschutz*, **9**, 1, 29 (1933).
20. M. E. Straumanis and C. B. Gill, *This Journal*, **101**, 10 (1954).
21. U. R. Evans and T. P. Hoar, *Trans. Faraday Soc.*, **30**, 424 (1934).
22. M. E. Straumanis and N. Brakšs, *J.* (*and Trans.*) *Electrochem. Soc.*, **95**, 98 (1949); **96**, 21 (1949); **96**, 310 (1949).

Recent Innovations in the Control and Operation of Zirconium Reduction Furnaces[1]

F. E. Block and A. D. Abraham

U. S. Department of the Interior, Bureau of Mines, Albany, Oregon

ABSTRACT

A general outline of the Kroll process for production of zirconium sponge is presented. Recent trends in automatic furnace control and instrumentation are reported. Modification of furnace operations to streamline production are discussed in terms of sponge quality.

Introduction

The Kroll process for producing zirconium by magnesium reduction of zirconium chloride under a helium atmosphere is the primary method for its manufacture today. Development of this process has been the subject of several articles (1–5). Although much effort has been devoted to developing a continuous process, no successful approach is evident. The most noteworthy accomplishments to date have been directed toward increasing efficiency through better utilization of existing plant equipment and by streamlining production operations. This paper covers recent experimental studies made in an effort to develop an automatically controlled reduction furnace and methods for increasing production quality and efficiency.

The Kroll process in its earliest form consisted of a purification step in which crude zirconium chloride was sublimed in a hydrogen atmosphere and condensed on water-cooled coils suspended from a cover that floated in a molten lead-alloy seal. The solid block of dense chloride that resulted was free from contaminating oxides and iron. In the reduction step that followed, the chloride was resublimed in a helium atmosphere and reduced in a crucible containing molten magnesium. The reaction product consisted of fine zirconium crystals surrounded by magnesium and covered by a layer of magnesium chloride. The mixture was subjected to vacuum distillation to remove magnesium and magnesium chloride and resulted in a sponge-like product of sintered zirconium crystals.

Recently it has been demonstrated that the purification step can be eliminated by allowing crude zirconium chloride to outgas at reduced pressure below 331°C, the sublimation temperature of the chloride (5, 7). Since this combined purification-reduction step is carried out in a single furnace, a considerable reduction in the amount of equipment and handling was realized.

During the reduction step careful furnace control is necessary to maintain the reaction rate in balance with the rate of zirconium chloride sublimation. Efforts to control the furnace automatically require regulation of temperature, pressure, and gas phase composition.

The bulk of the volume of the reduction crucible is actually employed to contain the by-product magnesium chloride, and only a relatively small amount of zirconium sponge remains after this salt is removed by distillation; therefore, a means for tapping the salt from the crucible and adding more magnesium in order to continue the reaction is desirable (6, 7). Another approach toward better utilization of distillation furnace capacity is the use inside the reduction crucible of expendable liners which can be stripped from the reaction products after the reduction, allowing two or more metallic reguli to be combined for a single distillation.

Experimental

Automatic furnace control.—A conventional zirconium reduction furnace was used in this work (Fig. 1). It consisted of a stainless steel retort 28 in. in diameter and 72 in. deep, heated in a Nichrome wound pit furnace. An annular trough attached to the upper edge of the retort contained molten lead-antimony alloy which served to seal the retort from the atmosphere while allowing the retort top to rise or descend as the gas volume changed. Suspended from the top were steel coils through which air or water was passed to cool the retort atmosphere or condense excess zirconium chloride. Gas valves were incorporated in the top to bleed vapors or add helium to the retort. A chromium iron reaction crucible was placed in the bottom of the crucible and an Inconel charge vessel above it. Independently controlled heating zones were employed for the

[1] Manuscript received July 30, 1954. This paper was prepared for delivery before the Chicago Meeting, May 2 to 6, 1954.

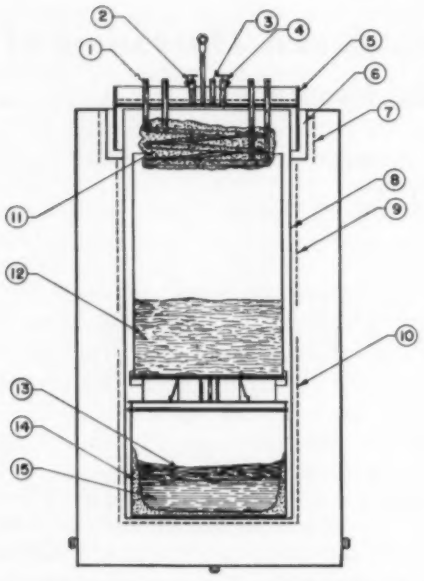

FIG. 1. Zirconium reduction furnace. 1, Condensing coils; 2, retort bleeder valve; 3, evacuation tube; 4, gas inlet valve; 5, floating retort top; 6, lead alloy seal; 7, lead seal heating element; 8, retort shell; 9, chloride zone heating element; 10, reduction zone heating element; 11, condensed zirconium chloride; 12, zirconium chloride charge; 13, unreacted magnesium; 14, zirconium; 15, magnesium chloride.

reaction crucible, charge can, retort top, and lead seal.

The rate at which zirconium chloride reacted was measured by suspending the charge vessel from the retort top. By measuring the pressure required to float the entire assembly at various time intervals, the rate of sublimation, hence the rate of reaction, could be calculated. Reaction rates varying from 4 to 80 lb zirconium chloride per hour were found to be common during an efficient reduction run. During the first 5–7 hr of the reaction, the rate was found to fluctuate rapidly, and it was during this period of increased activity that maximum rates were observed. Although it is difficult to determine the composition of gases in the retort with any degree of accuracy, a composition corresponding to approximately 30% helium and 70% zirconium chloride at the start of the reaction was found to result in a maximum reaction rate of 80 lb/hr. By following a rigid schedule for adding helium or bleeding gases from the system, this composition could be maintained and the reaction made to progress at a predetermined rate. Having established these conditions, the process could be started and stopped on a time schedule and controlled by some form of instrumentation.

During manual operation the floating retort top functions to prevent rapid pressure changes within the retort and allows an opportunity to correct for changes in reaction rate. By maintaining an immobilized top, pressure fluctuations could be used as a means for compensating automatically for the changing reaction rate. Although various devices were tested for measuring the retort pressure, best results were obtained when using a diaphragm type of element operating from a remote position. In order to prevent condensation of zirconium chloride in the pressure sensing line, a helium purge flow of 0.1–0.2 ft^3/hr was employed.

Automatic control was achieved by modifying a Forboro Model 40 Hyper-Reset controller to operate a pneumatic proportioning valve and six electrical relays within the pressure range 0–2.5 psi gauge. In operation the control cycle was as follows: when the retort pressure was in the range 0.5–1.3 psi the furnace operated satisfactorily and no control action occurred in this neutral range. If the reaction rate fell below the chloride sublimation rate and the pressure began to rise, compressed air was metered to the retort condensing coils through the pressure controlled proportioning valve. If the pressure could not be controlled by condensation of zirconium chloride alone, a relay actuated a pneumatically operated valve which bled gases from the retort and reduced the pressure to the neutral range. An audible alarm was employed as a warning in the event of an excessive pressure rise due to mechanical failures. If, instead, the reaction rate exceeded the chloride sublimation rate and the pressure began to decrease, additional heat was applied to that section of the retort containing the charge, and zirconium chloride was sublimed at an increased rate. If the pressure continued to fall because of an excessive reaction rate, a second pneumatically operated valve admitted helium to the retort to return the pressure to the neutral range. Addition of helium also tended to moderate the reaction by reducing the concentration of gaseous zirconium chloride in the retort. This entire sequence of operations was carried out at pressures above atmospheric to prevent air contamination through minor leaks in the apparatus. It was necessary to freeze the retort top into the lead-alloy seal during these tests in order to maintain the retort at a constant volume and allow the pressure to reflect changes in reaction rate.

Previous experience with retort bleeder valves has demonstrated that they must operate above 331°C to prevent fouling by condensation of zirconium chloride between the moving parts. Because of the corrosive nature of the gases being handled, auxiliary electric heaters have not been successful. A valve, consisting of a stem machined to a taper at its lower portion and ground to fit into a tapered seat in the retort top, was used for this work. The stem was moved in and out of its seat by a diaphragm air motor

TABLE I. *Average analytical values for zirconium sponge produced during plant operation and by various operational modifications*

Analysis No.	Description	Analysis, ppm				
		O_2	Al	Pb	Fe	Si
1	Average for plant production	980	37	41	444	56
2	Automatically controlled reduction furnace	833	39	15	568	83
3	Drain crucible tests	992	69	59	530	45
4	Two crucible tests	836	30	29	616	78
5	Lined crucible tests	740	22	26	278	55

linked to the stem through a lever arm. By insulating the valve to reduce heat losses it was heated sufficiently through conduction from the retort.

The valve employed to admit helium to the retort was similar in design except that its stem was sealed from the atmosphere with high temperature packing.

Table I, analysis No. 2, is an average analysis for sponge produced during an automatically controlled reduction cycle, and analysis No. 1 is an average for normal production quality sponge produced during the same operating period. Because the retort was sealed and operated at a slight positive pressure throughout the cycle, air contamination was completely eliminated. This probably accounts for the reduction of approximately 150 ppm in the oxygen content of sponge produced in these tests.

Oxygen determinations reported were made by the hydrogen chloride method (8). Metallic elements were determined by quantitative spectrographic analyses.

Operational innovations.—Early attempts to tap molten salt from the reduction crucible before adding more magnesium demonstrated that back reaction occurred between the zirconium chloride vapors and the exposed zirconium metal (7). Since the lower chlorides were pyrophoric and were not reduced during the subsequent reaction, metal losses often resulted. To minimize this effect experiments were performed in which a sufficient depth of salt was maintained in the crucible to cover the reduced zirconium, while excess salt was drained continuously. A furnace modified to hold a retort almost twice the normal length and having a third independently controlled heating zone was used (Fig. 2). The furnace was loaded with 1000 lb zirconium chloride positioned in the upper heating zone. The middle heating zone was occupied by a normal size crucible fitted with a centrally located overflow drain pipe and charged with 220 lb magnesium. A cowl-like cover surrounded the drain pipe to within 2 in. from the bottom. Occupying the lowest heating zone and supporting the crucible was a steel container of sufficient volume to receive the material drained

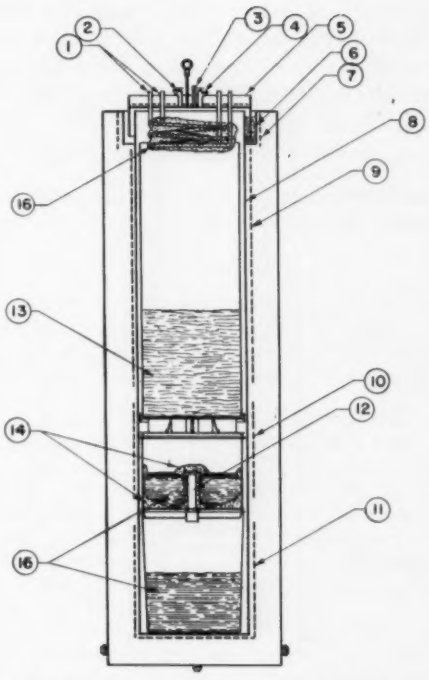

FIG. 2. Drain crucible retort. 1, Condensing coils; 2, retort bleeder valve; 3, evacuation tube; 4, gas inlet valve; 5, floating retort top; 6, lead alloy seal; 7, lead seal heating element; 8, retort shell; 9, chloride zone heating element; 10, reduction zone heating element; 11, lower zone heating element; 12, drain pipe assembly; 13, zirconium chloride charge; 14, zirconium; 15, magnesium chloride; 16, condensed zirconium chloride.

from the crucible. After the chloride charge had been heat conditioned at reduced pressure, the crucible was heated to melt the magnesium and promote the reaction in the usual manner. As the reaction progressed, metallic zirconium formed in the bottom of the crucible while a layer of magnesium chloride formed beneath the molten magnesium. When the liquid level reached the height of the drain pipe, molten salt was drained from the crucible as rapidly as it was formed. A small amount of magnesium was inadvertently trapped in the annular space between the drain pipe and its cover and was drained from the crucible. This amount was small, however, since the magnesium layer rose above the lower lip of the drain pipe cover rapidly and prevented further entrance of magnesium.

Single batches of zirconium containing up to 350 lb, twice the normal amount, could be made in this apparatus in approximately 70% of the time required to produce an equivalent amount in a conventional furnace. Analysis No. 3 in Table I is an average analysis for zirconium sponge produced in these tests. Neither the quality of the sponge nor the efficiency of the reaction had suffered; however, separation of

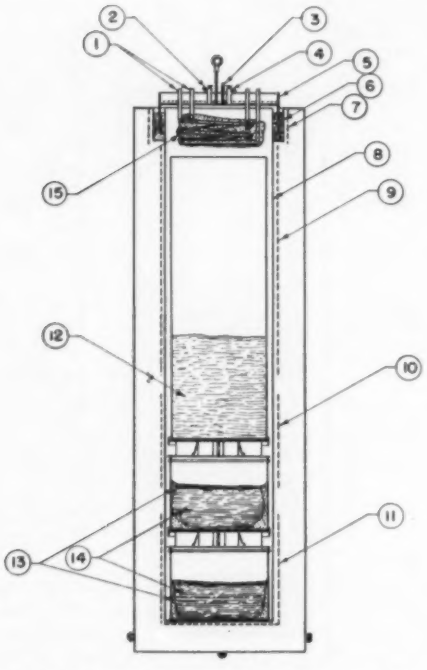

FIG. 3. Two crucible retort. 1, Condensing coils; 2, retort bleeder valve; 3, evacuation tube; 4, gas inlet valve; 5, floating retort top; 6, lead alloy seal; 7, lead seal heating element; 8, retort shell; 9, chloride zone heating element; 10, upper reduction zone heating element; 11, lower reduction zone heating element; 12, zirconium chloride charge; 13, zirconium; 14, magnesium chloride; 15, condensed zirconium chloride.

the sponge from the crucible and its components was more difficult.

The above equipment was modified to allow use of two conventional crucibles as depicted in Fig. 3. In these experiments the furnace was charged with 1000 lb zirconium chloride and 120 lb magnesium in each crucible. After the reaction had been initiated in the upper crucible and was approximately one-fifth completed, the magnesium in the lower crucible was melted and the reaction was initiated in this crucible. A yield of approximately 165 lb zirconium sponge, which is equal to the amount produced in a conventional reactor, was obtained in each of the crucibles. In terms of production capacity, only 75% of the normal furnace time was required to produce an equivalent amount of sponge. Analytical data for the sponge produced in these tests are tabulated in Table I, analysis No. 4. No significant variation in the impurity content from the normal production sponge was observed. Because the automatic furnace controller described previously was employed in these tests, a reduction in the level of oxygen contamination was achieved. A comparison of sponge quality between the upper and lower crucibles did not indicate a significant difference.

This same apparatus was tested using a single crucible twice the depth of a conventional type in order that double the amount of sponge could be formed in it. Because only half as much of the liquid surface was exposed to the retort atmosphere, a slightly higher yield of recoverable metal was obtained.

Operations involving the lined reduction crucible were performed in the conventional reduction furnaces illustrated in Fig. 1. Liners were fabricated from 0.025-in. type AISI 1095 carbon steel sheet by autogenous oxyacetylene welding. No deviation from the normal furnace operation was made during the reduction step. After reduction, the liner and its contents were removed from the reduction crucible by inverting it. The liner subsequently was handled in a low-humidity room maintained at a dew point of −15°C. After the liner was cut down one side, it could be peeled from the reduction mass with little difficulty. After removal of the liner, approximately 90% of the magnesium chloride could be split away from the metallic regulus by separating the layers with a chisel.

The regulus, which normally weighs 190–200 lb and is formed in the shape of a ring, was chucked in a lathe and the outer surface on both the sides and the bottom was scalped to a depth of approximately ¼ in. The material removed represented approximately

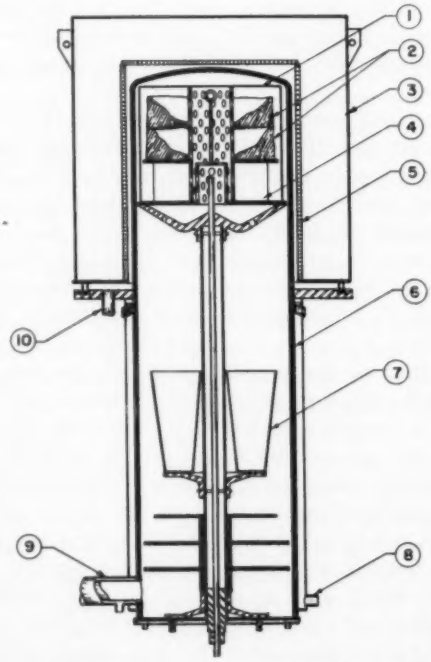

FIG. 4. Distillation retort. 1, Distillation crucible; 2, zirconium sponge; 3, furnace; 4, baffle; 5, heating element; 6, retort shell; 7, salt collector; 8, cooling water inlet; 9, retort evacuation tube; 10, furnace evacuation tube.

10 lb or 5% of the original weight of metal. Two or three reguli were combined in a single crucible and distilled in the apparatus shown in Fig. 4. The metal was distilled by heating for 24 hr at a temperature setting of 1000°C and at an absolute pressure below one micron. After distillation the metallic sponge could be removed from the crucible easily for crushing and blending.

Table I, analysis No. 5, lists the average analysis for sponge produced by the lined crucible technique. A general reduction in each of the metallic impurities is apparent because the portion of the sponge previously in contact with the reduction crucible liner had been removed prior to distillation. The most significant benefit, however, is the decrease in oxygen contamination of over 200 ppm. This reduction may be due to the presence of 2–3 times the normal amount of zirconium sponge in the distillation retort, resulting in a correspondingly lower degree of contamination per unit sponge weight during the high temperature distillation. A reduction in manpower normally required to break the pyrophoric sponge from the crucible by hand methods is also achieved.

Acknowledgments

This investigation was conducted under a project sponsored jointly by the U. S. Bureau of Mines and the Navy, Bureau of Ships, under AEC contract No. At–(11–1–140). The authors wish to acknowledge the leadership and guidance offered by S. M. Shelton, A. H. Roberson, and H. L. Gilbert and the cooperation extended by the staff of the Zirconium Production plant in which this investigation was made.

Any discussion of this paper will appear in a Discussion Section to be published in the December 1955 Journal.

REFERENCES

1. W. J. Kroll, A. W. Schlechten, and L. A. Yerkes, *Trans. Electrochem. Soc.*, **89**, 263 (1946).
2. W. J. Kroll, A. W. Schlechten, W. R. Carmody, L. A. Yerkes, H. P. Holmes, and H. L. Gilbert, *ibid.*, **92**, 99 (1947).
3. W. J. Kroll, C. T. Anderson, H. P. Holmes, L. A. Yerkes, and H. L. Gilbert, *ibid.*, **94**, 1 (1948).
4. W. J. Kroll, W. W. Stephens, and H. P. Holmes, *Trans. Am. Inst. Mining Met. Engrs.*, **188**, 1445 (1950).
5. S. M. Shelton and E. D. Dilling, "The Production of Zirconium Sponge," chapter in "Zirconium and Zirconium Alloys", p. 82, ASM, Cleveland (1953).
6. W. J. Kroll, W. F. Hergert, and L. A. Yerkes, *This Journal*, **97**, 305 (1950).
7. H. L. Gilbert and C. Q. Morrison, "Variations and Modifications of the Kroll Process for the Production of Zirconium," a paper presented before the Washington, D.C., meeting of the A. I. Ch. E., March 1954.
8. E. B. Read and L. P. Zopatti, "Determination of Oxygen in Zirconium Metal," U. S. Atomic Energy Commission AECD-2798, declassified February 14, 1950.

A Metallurgical Evaluation of Iodide Chromium[1]

D. J. Maykuth, W. D. Klopp, R. I. Jaffee, and H. B. Goodwin

Battelle Memorial Institute, Columbus, Ohio

ABSTRACT

Both the physical condition and the purity of chromium are important factors in its ductility. By proper fabrication techniques, iodide chromium sheet having an average ductile-to-brittle bend-transition temperature below 0°C has been obtained. Small quantities of oxygen, nitrogen, iron, molybdenum, tungsten, and silicon have little effect on the bend ductility of chromium. However, nickel, carbon, or sulfur adversely affect both the hot and cold ductility.

Introduction

While chromium finds widespread use in electroplated form and as an alloying addition to other metals, the cold brittleness of commercially available grades of the metal has thus far precluded any direct applications of it in massive form. Recent work at various laboratories, however, has furnished strong evidence that pure chromium is actually a ductile metal.

The first report of any ductility in chromium was that given by Kroll (1). By utilizing various reduction processes, he obtained chromium granules of "better than 99 per cent purity" which, although brittle when cold, could withstand deformation by forging when red hot. In later work (2), Kroll and his associates prepared chromium powder which analyzed 99.9% pure by the reduction of chromic chloride with magnesium and subsequent deoxidation with pure, dry hydrogen. Sheet prepared from this product by powder metallurgical processes was ductile at temperatures above 500°C but brittle at temperatures below 500°C.

At about this same time, Greiner (3) showed that chromium could be deformed in compression at room temperature. Additional evidence of the ductility of chromium in cold compression was obtained in exploratory work at Battelle (4).

In 1952, Hayes (5) and Gilbert (6) reported that arc melting of hydrogen-treated chromium had been accomplished and that successful forging, rolling, and swaging of this material had been carried out. A representative analysis (7) of the hydrogen-reduced arc-melted chromium showed that 0.001% iron, 0.05% silicon, 0.003% oxygen, 0.002% nitrogen, and 0.005% hydrogen were present. In regard to all other metallic impurities, the metal was described as pure as the best spectrographic standards available. The workability of this chromium was shown by the ability to drill, saw, grind, tap, turn, and file in the cold state, and to spot weld chromium to either chromium or iron. The metal could not be bent cold, but did withstand a free bend at 325°C.

Recently, Sully and coworkers (8), using sintered compacts of hydrogen-reduced electrolytic chromium, showed that chromium undergoes a sharp transition in bend tests from brittleness to appreciable ductility over the range of a few degrees of temperature. The lowest temperature at which he found substantial ductility in bend tests was 50°C. In a study of the influence of impurities on this transition temperature, Sully observed that oxygen in the range 0.001–0.9% has hardly any influence on the transition temperature. He stated that elements in solid solution show a marked effect in raising the transition temperature, the extent being roughly proportional to the amount of solid solution hardening. Thus, the addition of 1% nickel raised the transition temperature to over 400°C. Copper and aluminum were also reported to have similar effects. In short-time, elevated temperature tensile tests, none of the sintered chromium samples showed any significant ductility at temperatures up through 900°C.

The present research was carried out to further identify the compositional factors that affect the ductility of chromium. This problem was approached by preparing chromium of the highest purity possible and by studying the effects of deliberate additions of various impurity elements on the properties of this chromium.

Experimental Methods

Materials

Information available at the time this research was started indicated that, among the various contaminants normally present, oxygen was particularly deleterious to the ductility of chromium. Since one of the chief virtues of the "iodide" process is the removal of nonmetallic contaminant elements, it was selected as being most likely to yield pure chromium metal. A detailed description of the work leading to the successful adaptation of the iodide purification

[1] Manuscript received September 9, 1954. This paper was prepared for delivery before the Chicago Meeting, May 2 to 6, 1954.

process for chromium is beyond the scope of this paper. For this reason, only a brief description of the processes and equipment used is given at this time.

Dehydrogenated, electrolytic chromium was used as the primary chromium source for all of the material prepared in this work. After iodination, the thermal decomposition of the chromous iodide was effected by either of two deposition units especially evolved for this work. The first of these, hereafter referred to as the "metal" unit, consisted of a molybdenum-lined Hastelloy B reaction bulb in which deposition of the chromium occurred on an electrically-heated filament wire. The other deposition unit, hereafter called the "Vycor" unit, resembled the conventional Van Arkel-de Boer deposition chamber, excepting that a heated, re-entrant Vycor tube was used for the deposition surface in place of a metal filament.

Representative analyses for iodide chromium and the electrolytic chromium from which it was produced are given in Table I. Both the metal and Vycor units were capable of producing chromium of this quality. However, since both of these operations are batch processes, compositions of the various chromium lots produced by both methods were subject to significant departures from the values listed in Table I.

Chromium prepared in the metal unit suffered one major disadvantage in that metallic contamination was necessarily introduced, during arc melting, from the filament material. For this purpose, tungsten and molybdenum wires of a 3-mil diameter were the only satisfactory materials available. Attempts were made to remove as much of the filament as possible by breaking the chromium crystals free and physically separating the dissimilar metals. Despite these efforts, a tungsten or molybdenum pickup in amounts from 0.03 to 0.56% was incurred during arc melting of the crushed, metal-unit chromium.

In order to isolate the effects of the various major contaminant elements on the structure and properties of iodide chromium, alloys containing deliberate binary additions of oxygen, nitrogen, carbon, sulfur, nickel, iron, silicon, and tungsten were prepared using the following materials:

Element	Material form
Oxygen	cp Cr_2O_3
Nitrogen	gaseous, tank nitrogen
Carbon	spectrographic rod
Sulfur	99% pure Cr_2S_3
Nickel	cp shot
Iron	cp powder
Silicon	97.6% pure lump
Tungsten	99 + % pure wire

For alloying purposes, master alloys for oxygen, carbon, nickel, iron, and silicon were prepared by encapsulating the alloy additions in a small, unalloyed, iodide chromium ingot and arc melting. A nitrogen master alloy was made by arc melting iodide chromium under a nitrogen atmosphere. Alloys with tungsten and sulfur were made by direct melting charges of iodide chromium with tungsten wire and Cr_2S_3, respectively.

TABLE I. *Representative analyses for feed chromium and as-deposited chromium from which it was prepared*

Element	Composition, wt %	
	Electrolytic feed material	As-deposited†
O	0.38	0.0044
N	0.006	0.0013
H	0.0056‡	0.00008
C	0.004	0.002
S	0.019	0.011
Al	0.005	ND*
Ca	0.001	0.005
Cu	0.002	<0.001
Fe	ND	0.003
Mg	0.002	0.002
Mn	ND	—
Mo	0.01	0.005
Ni	0.003	ND*
Si	0.01	<0.005

* ND designates not detected.
† Prepared in Vycor unit.
‡ After degassing.

Procedures

Analyses.—Two methods of chemical analysis for the oxygen content of chromium have been mentioned in the literature. These are the method of Adcock (9) and the use of vacuum fusion (10). Sully (11) has shown that both methods are in good agreement at oxygen levels down to about 0.02%, although, as Sully points out, special treatment must be given to chromium analyzed using Adcock's method in order to prevent the loss of some oxide. However, the use of Adcock's method at lower oxygen concentrations than 0.02% is not so reliable since no means is provided for separating other impurities from the oxide. These and other limitations of Adcock's procedure have been adequately described elsewhere (2, 5, 6).

In the present work, the vacuum-fusion method of oxygen analyses was used. Basically, this consists of using carbon to reduce the chromium oxide to form carbon monoxide, which is then collected, analyzed, and converted to a weight percentage of oxygen. Examination of the thermodynamics of the reaction indicated that a temperature of 1500°–1600°C would be sufficient to insure complete reduction of the oxide by carbon. Experimental work showed that no significant gettering of the carbon monoxide occurred by the chromium during the reaction. An important

factor in the technique is to add the chromium to the iron bath at a rather low temperature, such as 1200°C. When this procedure was used, the vacuum-fusion method gave reproducible results for oxygen content with an accuracy of about ±4 ppm. The nitrogen and hydrogen contents of the chromium samples were determined concurrently during the vacuum-fusion analysis for oxygen.

Carbon and sulfur analyses were carried out by using ignition methods in a Leco Carbon Determinator and Leco Sulfur Determinator, respectively. In the adaptation of these processes to chromium, it was found essential to use a finely divided sample and to provide suitable fluxes so that complete oxidation of the sample would occur. For fluxing, an iron-lead bath in the carbon determination and an iron-tin bath in the sulfur determination were found to be satisfactory.

Metallic impurities in chromium were determined by the spectrographic method. In the early part of the work, analyses were carried out by direct metal arcing on a 10-mg sample. Later, two other modifications of the spectrographic method were tried in order to increase the sensitivity of the method. These modifications may be briefly described as follows.

(*A*) $CrSO_4$ solution method. Both standards and the samples are dissolved in sulfuric acid and dried by baking at 500°C. The sample and standard are arced separately, and their spectra recorded on the same film. A densitometer is employed to determine the relative intensities of the spectrum lines, and the analysis is calculated from the densitometer readings.

(*B*) Concentration method. The sample is dissolved in hydrochloric acid and then perchloric acid is added. Chromium is evaporated off as chromyl chloride, concentrating the impurities in the residue which is redissolved in a hydrochloric-nitric acid solution. Standards are also prepared by dissolving chromium containing known amounts of impurities in the hydrochloric-nitric acid mixture. The spectra of the sample and standards are photographed on the same film.

Use of the concentration method significantly lowered the detection limits for metallic elements. However, both the $CrSO_4$ solution and concentration methods were in excellent agreement down to the lower limits of the direct-metal-arc method. The accuracy of the direct-metal-arc method is believed to be about ±25 relative %, and that of the concentration method is somewhat better.

Melting.—All of the evaluation work was carried out with 8-g ingots prepared from individual runs of iodide chromium by arc melting under an atmosphere of argon gas of 99.95% purity on a water-cooled copper hearth. A description of the furnace used has been given previously in the literature (12).

Prior to melting, two charges of iodide chromium and one titanium gettering ingot were placed in three shallow receptacles provided on the copper hearth. Melting was conducted by directing the arc first to the titanium getter button and then, in succession, to each of the chromium charges. In order to insure homogeneity, each ingot was given a minimum of three melts, with the ingot being inverted prior to each succeeding melt.

Bend testing.—The principal means of evaluating the ductility of chromium was the determination of the bend-transition temperature of sheet samples. For this purpose, a small stainless steel jig was constructed. This consisted of a female die, containing a 75° V-notch, enclosed in a perforated sleeve. This assembly was inserted either into a furnace or a refrigerating bath, depending on the test temperature desired. The male die consisted simply of a stainless steel plunger whose lower end was finished with 1/16-in. round radius.

In operation, a sample was placed across the notch in the female die and the plunger lowered through a guide block onto the center of the sample. In all cases, the bending stress was applied at a constant deflection rate of 0.05 in./min by lowering the crosshead of a tensile testing machine onto the top of the plunger. Vertical travel of the plunger was followed by means of a dial gauge in contact with the crosshead.

All bend-test samples were cut to approximately 0.4 in. long by 0.2 in. wide, using a water-cooled, abrasive, cut-off wheel. Except where otherwise indicated, the sample direction was oriented so that its longitudinal axis was parallel to the rolling direction of the sheet from which it was prepared. Prior to testing, all samples were finish ground by hand along both the edges and the flat surfaces, using 600X abrasive paper. Here, the final direction of polishing was oriented parallel to the longitudinal sample axis, to minimize any notch effects. The final thickness of all samples tested ranged between 0.015 and 0.030 in.

Two types of bend test were carried out using this equipment. In one type, called the "one-shot" method, a sample was bent through the total allowable vertical deflection (approximately 0.120 in.) of the jig at a single test temperature. Mating a 0.030-in. specimen to a 1/16-in. radius corresponds to 20% elongation in the outer fibers.[2] Because the amount of sample material from some runs of iodide chro-

[2] Calculated from the expression:

$$\text{Elongation, \%} = \frac{t/2}{R + t/2} \times 100$$

where t is the thickness of the specimens and R is the bend-die radius.

mium was limited, use was also made of a second test method, called the "progressive" bend-test method. In this procedure, each sample was subjected to a vertical deflection of only 30 mils at a given test temperature. If the sample withstood this bending, the temperature was reduced and an additional deflection increment of 30 mils was applied. The temperature and also the deflection at which fracture occurred were noted. Subsequent examination of a large number of samples broken in the progressive bend test showed that, in every instance where fracture occurred at 25 mils or greater, some permanent set (i.e., plastic deformation) had occurred. Samples which failed at a total deflection of less than 25 mils generally showed no evidence of ductile behavior.

As shown in Fig. 1, a fairly good correlation was obtained between the two test methods on wrought samples taken from the same piece of chromium sheet. Both types of test indicated an average ductile-to-brittle transition range of −20° to 0°C for this material. As indicated in the figure, many of the samples tested by the one-shot method showed varying degrees of ductility (greater deflection than 25 mils), even though they fractured before taking a complete bend. For the purpose of determining the transition temperature, these samples were labeled "ductile." Although many of the one-shot samples tested above the transition range took the full bend, none of the one-shot samples tested below the transition range showed evidence of ductility.

However, it was later found that annealed samples were subject to rheotropic recovery, i.e., bending above the transition temperature enabled ductility to be retained below the transition temperature. Thus, the correlation between one-shot and partial bend methods does not hold for annealed samples. Consequently, bend-transition temperatures for annealed chromium sheet were determined by one-shot bend tests.

For the purposes of comparison and discussion, bend data on individual samples from each chromium sheet were summarized and are reported in the two following categories:

(*A*) *Transition range.*—This was defined as the range extending from the highest temperature at which any of the individual bend-test samples was brittle (i.e., broke at a deflection of less than 25 mils with no permanent set) to the lowest temperature at which any of the individual samples was ductile (i.e., withstood a deflection greater than 25 mils and showed evidence of plastic deformation).

(*B*) *Average bend-transition temperature.*—This was taken for each chromium sheet as a statistical average based on the number of individual samples

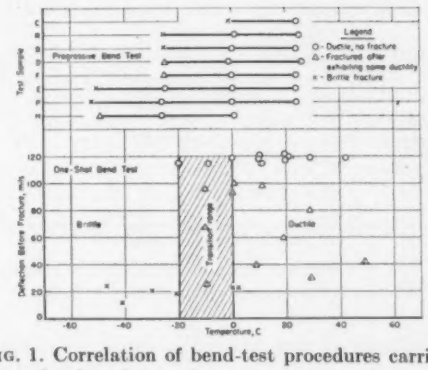

FIG. 1. Correlation of bend-test procedures carried out on wrought chromium strip.

tested and the lowest test temperature at which bend ductility was observed in each sample.

Tensile testing.—Tensile-test samples were prepared by clamping the chromium sheets between mild steel plates and grinding in a reduced section ¼-in. wide over a 1-in. gauge length. During the first attempt at edge grinding two chromium sheets, both samples failed as a result of cracks that developed at several points on each sample. This brittle behavior was apparently caused by the development of fine surface cracks as a result of heat checking or fatigue. Before grinding the balance of the tensile samples, the jig containing the blanks was dipped into a room-temperature-setting plastic to eliminate sample vibration within the jig during grinding. All of these samples were edge ground successfully.

Tensile testing was carried out with a Baldwin Southwark tensile-testing machine, at a constant strain rate of 0.01 in./min. Elastic extensions of the samples during testing were measured by means of an SR-4 resistance-type strain gauge glued to one side of the reduced section of the samples.

Experimental Results with Unalloyed Iodide Chromium

Melting

Despite the use of a titanium gettering melt, the unalloyed chromium ingots picked up an average of about 25 ppm of oxygen during arc melting. Neither the nitrogen nor hydrogen content, both of which were usually less than 10 ppm, was altered significantly during melting. Spectrographic analysis showed that no significant metallic contamination occurred from either the copper hearth or the tungsten electrode.

After triple-inversion arc melting, the hardness of the iodide chromium prepared in the Vycor unit increased from an average of 136 VHN in the as-deposited condition to an average value of 141 VHN, an increase of only 5 VHN. Although the average as-deposited hardness of chromium prepared in

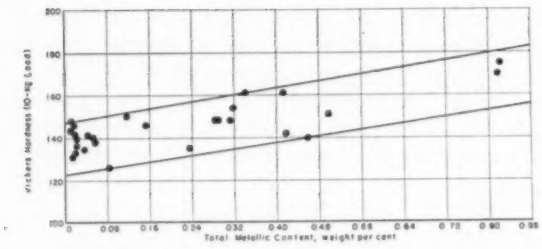

FIG. 2. Correlation of metallic contaminant elements in arc-melted iodide chromium with as-cast hardness.

metal apparatus was somewhat lower than that of chromium prepared in the Vycor unit (128 VHN, as compared with 136 VHN), ingots made from metal-unit chromium had an average increase of 17 VHN points after triple arc melting. The slightly greater hardness increase occurring in these ingots during melting was attributed to solid-solution hardening from the residual molybdenum or tungsten filament wires contained in the chromium made in the metal unit.

Comparison of cast hardnesses with compositions of various chromium samples did not show that any one contaminant element had a greater hardening effect than any of the others, although several samples contained from 0.1 to 0.5% of either nickel, iron, and/or molybdenum or tunsgten. As shown in Fig. 2, a rather broad correlation was found when the cast hardnesses were plotted against the total metallic-impurity content. This would indicate that metallic contaminants, at the levels encountered, have only a small, equivalent, additive effect on the hardness. No correlation of the quantity of carbon or sulfur with cast hardness was possible with the data available. Also, rather wide variations of total oxygen content (from 70 to 160 ppm) and total nitrogen content (from 10 to 50 ppm) appeared to have no effect on hardness.

Fabrication

Hot rolling.—Hot rolling of the unprotected ingots in air proved to be the most expedient method of fabrication. Experiments with a large number of ingots from different lots of iodide chromium indicated that the optimum preheating temperature was in the range of 700°–800°C. Increasing the temperature to 850° or 900°C resulted in a high incidence of failure as a result of hot shortness.

Straight rolling of the ingots to 30-mil sheet at 600°C produced sheet with severe edge cracks as a result of excessive hot-cold work. However, it was shown that iodide chromium can be rolled to satisfactory sheet at temperatures as low as 500°C, so long as appropriate annealing treatments are provided.

In this work, 700°C was used as the rolling temperature for most of the material evaluated. Direct rolling of the ingots to sheet at 700°C elongates, but does not otherwise refine, the large, as-cast grain structure. Also, sheet prepared in this manner tended to show a spread in hardness. For these reasons, an intermediate annealing treatment of 1 hr in argon at 1000°C was incorporated as part of the standard fabrication procedure. After annealing, rolling was resumed at 700°C and continued to a final reduction of 80%.

Vacuum-fusion analyses showed that an oxygen pickup of from 10 to 35 ppm occurred during fabrication when the procedure outlined above was used. Some slight increase in the nitrogen and hydrogen contents of some of the chromium ingots also occurred as a result of working in air at 700°C. Generally, however, concentrations of nitrogen and hydrogen in the fabricated iodide chromium sheets rarely exceeded 30 and 3 ppm, respectively.

Forging and swaging.—Attempts were made to forge several good-quality ingots by directing hammer blows to the edges of the ingots in a direction transverse to the columnar grain structure. Forging was tried using preheating temperatures of both 700° and 800°C, but in neither case could cracking be avoided. Although the ingot worked at 800°C seemed more amenable to plastic deformation, fine transcrystalline cracks developed on the ingot surface, despite the facts that (*a*) forging was carried out using light hammer blows, and (*b*) the ingot was reheated frequently between forging operations. These findings are consistent with early work on arc-melted chromium done at the Bureau of Mines (6).

On the other hand, working in a direction perpendicular to the usual rolling direction was accomplished by encasing an ingot in an iron sheath and swaging at 700°C. A chromium rod approximately 0.05 in. in diameter by 6 in. long was prepared by using this procedure.

Effect of contaminant elements on fabricability.—A small number of ingots from some of the first lots[3] of the iodide chromium prepared cracked up during attempted rolling by the standard procedure. Fabrication data for these lots are given in Table II along with similar data for material which fabricated satisfactorily.

Most of the ingots that failed to fabricate contained nickel in quantities of 0.27% or greater. This

[3] Most of these were prepared in a Hastelloy B reaction bulb and contained appreciable quantities of nickel that had transferred to the chromium from the Hastelloy B during deposition. This transfer of nickel was subsequently eliminated by inserting a molybdenum-sheet liner in the reaction chamber.

TABLE II. *Fabrication data for representative arc-melted unalloyed iodide chromium ingots rolled in air at 700°C*

Ingot	Composition, wt %						Vickers hardness		Final reduction, %	Quality of sheet
	O	N	C	S	Ni	Total Metallics	As-cast	As-fab.		
R27-1	0.0013*	0.0004*	0.002*	0.005*	0.1	0.460	140	236	80	Good
R28-1	0.0090	<0.0030	—	—	0.2	0.819	170	308	88	Poor
R29-1	—	—	—	—	0.3	<0.318*	154	—	15	No good
R30-1	—	—	—	—	0.3	<0.340*	161	—	18	No good
R31-1	—	—	—	—	0.27	<0.286*	148	—	19	No good
R33-1	—	—	—	—	0.4	<0.412*	139	—	35	No good
R34-1	—	—	—	—	0.09	0.512	123	226	80	Good
R39-1	—	—	—	—	0.33	0.419	142	—	25	No good
R42-1	—	—	0.004	—	0.001*	<0.014*	131	—	37	No good
R44-1	—	—	0.002	0.013	0.008*	<0.082*	126	—	37	No good
R45-1	—	—	0.005	0.011	0.003*	0.153*	146	—	47	No good
R46-1	—	—	0.007	0.009*	0.003	0.036	134	223	80	Good
R35-1	0.0160	0.0050	—	—	<0.001	0.044	141	218	80	Good
R36-1	0.0042*	0.0013*	0.002*	0.011*	0.0005	0.118	150	218	80	Good
R37-1	0.0042*	0.0005*	—	—	0.005	0.059	138	221	80	Good
R38-1	0.0190*	<0.0050*	0.002*	0.015*	ND*,†	0.010*	143	210	80	Good
R40-1	0.0100	0.0030	0.001	—	ND*,†	0.020*	133	213	80	Good
R41-1	0.0074	<0.0007	0.007	—	ND*,†	0.021*	140	205	80	Good
R43-1	0.0140*	<0.0003*	—	—	ND*,†	0.011*	148	211	80	Good
R49-1	0.0073	0.0010	0.002*	0.002*	0.001	0.020	141	215	80	Good
R50-1	0.0120*	0.0012*	0.002*	0.017*	0.0005*	0.017*	161	—	80	Poor

* Analysis on the as-deposited form of the metal.
† ND means "not detected."

indicates that the fabricability tolerance for nickel is slightly less than 0.2%. On the other hand, several ingots (R27-1 and R34-1) containing 0.3 and 0.4% molybdenum and one other containing 0.2% tungsten rolled to satisfactory strip. The highest contaminant levels encountered for iron and silicon were 0.1 and 0.016%, respectively, and ingots containing these amounts of either element also fabricated successfully. The data also indicate that oxygen in amounts up to 0.019% does not affect the fabricability of chromium adversely.

Other work, described in a later section of this paper, showed that the presence of either carbon or sulfur in relatively small quantities is definitely deleterious to the ductility of chromium. Thus, chromium containing above 0.016% carbon or about 0.02% sulfur cannot be fabricated to sound sheet. Since several ingots, listed in Table II, made from chromium containing up to 150 ppm of sulfur rolled to good sheet, the tolerance for sulfur is probably at least this great. However, it seems possible that the poor fabricability of Ingot R50-1 (made from chromium low in all impurities except oxygen and sulfur) can be attributed to its sulfur content, which was determined by analysis to be 170 ppm. This suggests that an increase in the sulfur content from 150 ppm to 170 ppm produces a sharp decrease in the fabricability of chromium.

Although complete analytical data were not obtained on all of the material tested, the data available for Ingots R44-1, R45-1, R46-1, R36-1, R38-1, R49-1, and R50-1 suggest that the ductility of chromium is closely related to the total amounts of carbon, sulfur, and metallic-impurity elements, as well. The limited data for these alloys in Table II indicate that, if the total amount of carbon and sulfur exceeds 150 ppm and the total metallic content exceeds about 500 ppm, the chromium is not amenable to rolling at 700°C.

Recrystallization Behavior

Softening curves were determined on 30-mil chromium sheet prepared by straight rolling at 600°, 700°, and 900°C. These data, given in Fig. 3, show that the hardness started to drop after 1 hr at 800°C. After 1 hr at temperatures above 900°C, the hardness is reduced to about the same level as for the as-cast condition.

Metallographic examination of the samples used to construct Fig. 3 showed that recrystallization be-

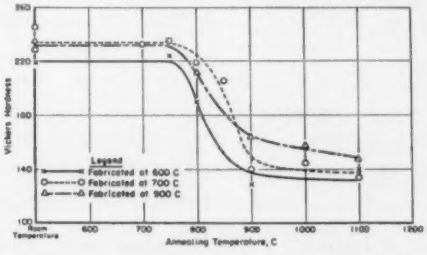

FIG. 3. Softening curves for iodide-chromium sheet fabricated at various temperatures after 1-hr annealing treatments.

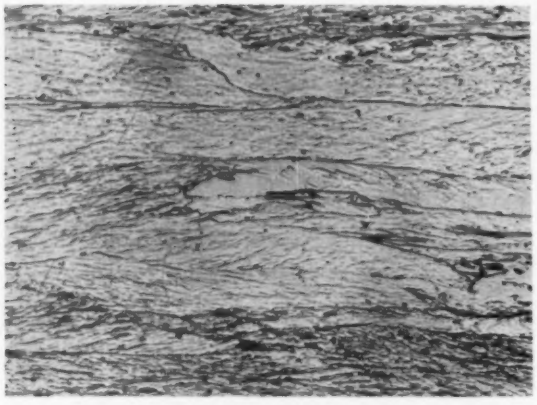

FIG. 4. Longitudinal fibered grain structure of iodide-chromium sheet rolled at 700°C. Oxygen content of 0.0093%; electrolytic etch in 10% oxalic acid. 250×.

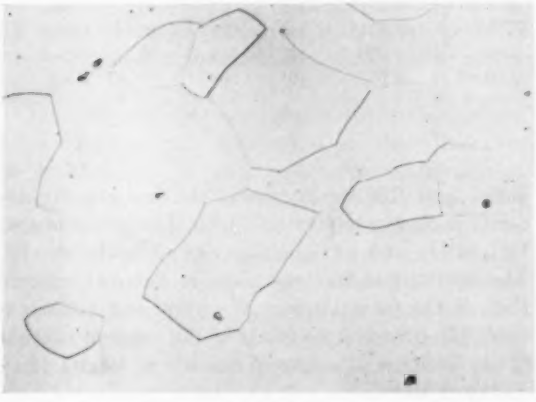

FIG. 5. Recrystallized grain structure of iodide-chromium sheet fabricated at 700°C and annealed 1 hr at 1000°C. Oxygen content of 0.0074%; note the rounded, gray, oxide inclusions; electrolytic etch in 10% oxalic acid. 500×.

FIG. 6. Equiaxed iodide-chromium sheet containing 0.001% carbon. Note the round, light-colored carbide particles in the lower part of the photograph; electrolytic etch in 10% oxalic acid. 500×.

gan on all samples after 1 hr at 800°C. Sheet fabricated at 600°C was completely recrystallized after 1 hr at 900°C, whereas complete recrystallization in sheet fabricated at 700° and 900°C required 1 hr at 1000°C. Fig. 4 and 5, respectively, illustrate typical wrought and recrystallized structures observed in these samples. The grain size in the crystallized samples usually ranged between 0.03-mm and 0.05-mm average grain diameter. No gross differences in grain growth for any of these samples were noticed over the time and temperature intervals investigated.

Metallography

All of the annealed sheet samples examined contained varying amounts of Cr_2O_3. At the oxygen contents normally encountered (i.e., less than 200 ppm), the oxides generally appeared as small, rounded, gray inclusions, illustrated in Fig. 5, randomly distributed in the grain structure. Only a very few oxide particles were observed in a sample from R40-2, which had the lowest analyzed oxygen content (60 ppm). Since so few oxide particles were noted in this specimen, the solubility limit of chromium for oxygen is probably only slightly below 60 ppm. Other work on chromium-carbon alloys described in a later section of this paper indicated that, in the presence of excess carbide, the oxygen-solubility limit actually was located between 20 and 40 ppm.

It was observed later that sulfur in chromium also forms a compound very similar in appearance to the oxide. Available data indicate that sulfur, in the quantities normally observed (i.e., less than 0.015%), is soluble in chromium. Nevertheless, since the sulfur content was not determined on most of the chromium samples, it is possible that, in some instances, small quantities of the sulfide phase coexisted with the oxide phase.

Similarly, most of the annealed-sheet samples also contained a few small, light-colored, rounded particles tentatively identified as a carbide of chromium. Since none of these samples contained an appreciable number of carbides, visible detection and identification of this phase in the unalloyed iodide chromium was sometimes difficult. However, as shown in Fig. 6, a few widely scattered carbides were observed in chromium samples which had analyzed carbon contents of 0.001 and 0.002%, respectively. These data, therefore, suggest that the solid solubility of carbon in chromium is very low.

Bend Ductility

Effects of fabrication variables and annealing treatments.—In an evaluation of the hot malleability of iodide chromium, several ingots were initially rolled to a 50% reduction at 700°C, annealed, then rolled

at progressively lowering finishing temperatures of 600°, 550°, and 500°C, respectively. Bend data from these sheets, given in Table III, show that variations in rolling temperature between 500° and 700°C have little effect on the ductile-to-brittle bend transition range of the as-fabricated chromium sheet.

In another experiment, five ingots prepared from the same lot of iodide chromium were used to study the effects of increasing amounts of hot-cold work on the bend ductility. All five ingots were fabricated first to varying thicknesses by rolling at 700°C and annealed for 1 hr at 1000°C. These billets were then rolled to the same final thickness of 30 mils at 700°C, and tested for bend ductility in the as-fabricated condition. The reductions given during the final rolling operations ranged from 25 to 90%.

As shown in Fig. 7, the hardness of the as-fabricated sheets increased from 200 to 222 VHN as the final reduction was increased from 25 to 90%. Fig. 7 also shows that all of the bend samples from each of these sheets had a brittle-to-ductile transition temperature of about 0°C. This shows that variations from 25 to 90% in the final reduction after intermediate annealing have no significant effect on the bend-transition temperature. On the other hand, recrystallized samples from these same chromium sheets showed significantly higher average transition temperatures, ranging from 65° to 150°C. These data are also shown in Fig. 7. It is apparent from these data that optimum bend ductility in the iodide chromium sheet is associated with a fibered grain structure.

The effect of stress-relief annealing treatments in the recovery range on the bend ductility of as-fabricated chromium sheet was investigated. This work indicated that 1-hr stress-relief anneals at 500° and 600°C increase the transition temperature by about 60°C, whereas treatment at 700°C apparently has no effect.

Rheotropic recovery of annealed chromium.—Early in this research, considerable scatter in the bend ductility of annealed, recrystallized chromium was noticed when the progressive bend test was used. The scatter was found to be the result of rheotropic recovery. This phenomenon appears in metals crystallizing in other than the face-centered-cubic lattice that show a sharp ductile-to-brittle transition (13). By prestraining annealed samples of a metal which exhibits this behavior at a temperature above the transition temperature, ductility can be retained at temperatures considerably below the transition temperature. This ductility is termed "rheotropic recovery," since rheotropy is related to flow or strain.

Since chromium is subject to this phenomenon, the progressive bend test is invalid for determining

TABLE III. *Effect of variations in rolling temperature on the bend ductility of iodide chromium sheet*

Ingot	Fabrication-temp range, °C		Vickers hardness	Bend ductility		
				Transition range, °C		Transition temp, °C
	Start	Finish		Highest brittle	Lowest ductile	
R41-1	700*	700*	205	−25	−25	−25
R41-5	700	600	219	0	−25	0
R41-4	700	550	224	25	0	25
R41-2	700	500	228	0	−25	0

* Standard fabrication procedure.

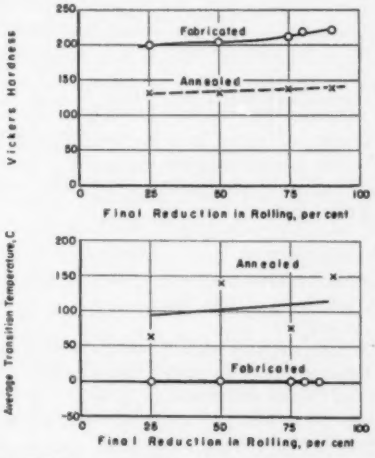

FIG. 7. Effect of reduction in rolling on the hardness and bend-transition temperature of iodide-chromium sheet.

the transition temperature of annealed bend-test samples. Partial bending above the transition temperature strains the sample enough to allow it to be bent below this temperature. By reappraisal of progressive bend data for annealed samples, a sharp, well-defined transition temperature was obtained when only the results of the first bending temperature were considered. Fig. 8 illustrates a typical bend-transition temperature curve obtained on recrystallized chromium sheet.

There is no evidence of rheotropic recovery in wrought samples, evidently because they are already highly strained from the hot-cold work resulting from rolling at 700°C.

Bend anisotropy.—In a study of the anisotropy of wrought chromium sheet, two groups of bend-test samples were prepared from a single sheet. One group was cut so the longitudinal axes of the samples were parallel to the rolling direction; this was the procedure normally used for all bend samples. The other bend-test samples were cut with their longitudinal axes perpendicular to the rolling direction. Bend-transition temperatures were determined on

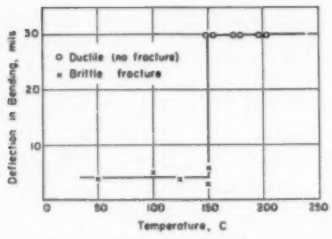

FIG. 8. A typical bend-transition temperature curve for recrystallized iodide-chromium sheet.

TABLE IV. *Effect of machining on the bend ductility of iodide chromium sheet fabricated using the standard procedure at 700°C*

Ingot	Method of finishing to size	Vickers hardness	Bend ductility		
			Transition range, °C		Avg transition-temp, °C
			Highest brittle	Lowest ductile	
R38-2	Abrasive cut-off wheel*	218	−25	−25	0
	Edge ground, transverse to rolling direction	220	50	0	15
	Edge milled, transverse to rolling direction	216	50	25	30
R41-1	Abrasive cut-off wheel*	205	−25	−25	−25
	Edge ground, parallel to rolling direction	205	100	75	85

* Standard procedure.

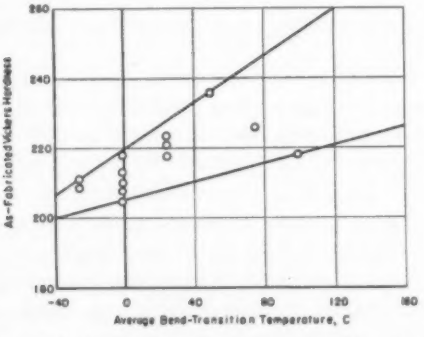

FIG. 9. Relationship between as-fabricated hardness and average bend-transition temperature for iodide-chromium sheet, made using the standard fabrication procedure. Each point represents a separate lot of iodide chromium.

samples from the two groups, both in the as-fabricated condition and after a recrystallizing anneal.

Transition temperatures of samples cut parallel to the rolling direction from the wrought sheet were the lowest (about 75°C) of any for the four test conditions. Conversely, transition temperatures for transverse samples from the wrought sheet were the highest (about 300°C). After a recrystallizing anneal, average transition temperatures of both longitudinal and transverse bend-test samples were about the same, the values being intermediate to those obtained in the wrought longitudinal and transverse specimens. Thus, recrystallization tends to overcome the bend anisotropy shown by the as-fabricated sheet, but at the expense of the excellent longitudinal-bend-transition temperature of the wrought material.

Effect of machining on bend ductility.—As a result of the ill effects experienced in the grinding of sheet chromium (described in an earlier paragraph of this paper), it was decided to investigate the effect of machining on the bend-transition temperature. Three groups of samples were prepared from the same sheet after hand grinding the surface with 600X abrasive paper. One group was edge ground (transverse to the rolling direction) to size, another was edge milled (transverse to the rolling direction) to size, and the third group was cut to size using a cut-off wheel. One out of seven samples failed during milling, and two out of seven failed during grinding. Bend data on the balance of these samples, given in Table IV, indicated transition temperatures of about 15° and 30°C, respectively, for ground and milled samples, as compared with 0°C for samples prepared using the cut-off wheel.

Additional bend samples were made from a second sheet of chromium. One group was edge ground parallel to the rolling direction, and a control group was made using the cut-off wheel. Again, as shown in Table IV, machine-ground samples showed a much higher average bend-transition temperature.

This work shows that machining by grinding or milling is definitely detrimental to the bend ductility of chromium. This would appear to be associated with a notch effect caused by these machining operations. If macronotches were the reason for the apparent brittle behavior, one should expect that orienting the scratches parallel to the rolling direction would minimize this effect. However, the bend-test data do not support this point of view. It seems plausible that, if neither machine grinding nor milling generates either micro- or macrocracks directly, these operations actually may work harden a thin surface layer of the metal to a point where further action of the fiber stress in bending accelerates fracture of the surface layer. This would lead to an early fracture in bend testing. Whatever the true mechanism responsible for the deleterious effects of machining on bend ductility may be, this is further evidence that the ductility of chromium is very sensitive to surface effects.

Correlation of Bend Ductility and Hardness

A plot of the as-fabricated hardnesses vs. average bend-transition temperatures shown for a number of lots of unalloyed iodide chromium is shown in Fig. 9.

This plot shows that a rough correlation between these properties exists. Thus, those chromium sheets which had higher as-fabricated hardnesses generally showed higher transition temperatures. The wide spread in fabricated hardness is probably the result of compositional differences within these samples, which caused differences in the rate of strain hardening.

The bend-ductility data for each lot of unalloyed iodide chromium were also compared with its composition. Results of this work are more conveniently discussed in the following section of this paper.

Tensile Properties

Several sheet tensile-test samples were prepared from lots of iodide chromium that had shown ductile-to-brittle transitions in bending at temperatures well below room temperature. All samples were tensile tested at room temperature in the as-fabricated condition. After grinding to shape, each sample was hand polished on both the flat surfaces and edges with 600X abrasive paper, taking care to polish in a direction parallel to the longitudinal axis of the specimen.

Despite the precautions taken in their preparation, all of the tensile samples failed by brittle fractures in the reduced sections at stresses between 15,000 psi and 62,000 psi. None of the samples showed any measurable permanent elongation or reduction in area. The best values obtained for the tensile properties of wrought iodide chromium sheet are:

Proportional limit, psi	33,000
0.1% offset yield strength, psi	58,000
Maximum load, psi	62,000
Modulus of elasticity, psi	45,000,000
Per cent elongation in 1 in.	0

Examination of broken samples indicated that fracture was initiated by formation of fine cracks which developed along the edges of the sheets during application of the load. Bend tests on samples prepared from both stressed and unstressed tensile samples showed consistently higher transition temperatures than did samples taken from other portions of the original wrought sheets. This and the fact that several bend-ductile chromium sheets failed in grinding suggests that the tensile ductility as well as the bend ductility of chromium is extremely sensitive to surface effects.

Evaluation of Effects of Impurity Elements in Chromium

Hardness and Fabricability of Chromium-Impurity Alloys

Compositions, hardnesses, and fabrication data for all alloys investigated are listed in Table V, which also includes data for the unalloyed iodide chromium lots from which the majority of these alloys were prepared.

Oxygen (up through 0.18%), iron (up through 0.25%), silicon (up through 0.15%), and tungsten (nominally up through 0.2%) have no deleterious effects on the fabrication of chromium by rolling at 700°C. Similarly, none of these alloy additions showed any significant effect on the hardness of the chromium from which they were prepared. Master alloy data, also given in Table V, show that increasing the quantity of oxygen up through 0.57% or iron up through 1% (nominal) still has no significant effect on the hardness.

Nickel, carbon, and sulfur, on the other hand, are definitely detrimental to the fabricability of chromium. Thus, chromium which contains nickel in excess of 0.2%, or carbon and/or sulfur above about 0.015%, cannot be fabricated to sound strip by rolling at 700°C. Neither nickel nor carbon in quantities up through 0.2% has any effect on the cast hardness of the chromium used as a base. However, increasing the quantity of either of these elements to about 1% results in a hardness increase of about 100 Vickers points. The addition of 0.2% sulfur appears to increase the hardness only slightly.

Because of insufficient material, no attempts were made to fabricate the only two nitrogen alloys prepared. Hardness data on these alloys showed that additions of up to 0.124% nitrogen have relatively little effect on the hardness of chromium.

Metallography

Oxygen-addition alloys.—As mentioned in an earlier paragraph, most of the unalloyed chromium samples examined contained varying amounts of small, rounded, gray inclusions of chromium oxide. Fig. 5 and 10 illustrate typical structures at increasing levels of oxygen content.

Actually, the lowest oxygen contents of all the arc-melted metal examined were obtained in the carbon alloys. This is understandable, since carbon, in the quantities added, acts as a deoxidizer. Examination of the two lowest oxygen-content carbon alloys showed that only a very few, small, scattered oxides were present at 0.004% oxygen. No oxides were observed in the carbon alloy containing 0.002% oxygen. On the other hand, two unalloyed ingots prepared from the same lot of chromium contained a significantly larger number of oxide particles in proportion to their analyzed oxygen contents of 0.006 and 0.010%, respectively. These data indicate, therefore, that the solubility limit of oxygen in chromium is slightly below 0.004%.

Carbon-addition alloys.—Work on unalloyed chromium samples showed that the solubility limit of

TABLE V. *Compositions, hardnesses, and fabrication data for contaminant alloys in an iodide chromium base*

Ingot	Analyzed composition, wt %								Quality of sheet as-rolled at 700°C	Vickers Hardness		
	O	N	C	S	Ni	Fe	Si	W		As-cast	As-fabricated	As-annealed at 1000°C
Unalloyed controls												
R40-2	0.0060	<0.0020	—	—	<0.001	0.002	0.015	—	Good	139	213	138
R40-1	0.0100	0.0030	0.001	—	<0.001	0.002	0.01	—	Good	133	209	134
R38-3	0.0190*	<0.0050*	0.002*	0.015*	ND*	0.001*	0.003*	—	Good	142	222	140
R43-1	0.0140*	<0.0003*	—	—	ND*	0.002*	<0.005*	—	Good	148	211	—
Oxygen alloys												
R40-X1	0.012	0.002	0.007	—	<0.001	0.008	0.007	—	Good	146	204	147
C3	0.015	<0.002	—	—	—	—	—	—	—	150	—	141
R40-X2	0.051	<0.002	—	—	—	—	—	—	Good	141	210	152
R40-X3	0.075	<0.002	—	—	—	—	—	—	Good	138	207	154
C4	0.096	<0.002	—	—	—	—	—	—	—	155	—	161
R40-X4	0.180	<0.003	0.005	—	0.002	0.015	0.007	—	Good	145	212	156
R43-M4	0.57	<0.01	—	—	—	—	—	—	—	148	—	—
Nitrogen alloys												
C5	0.052	0.069	—	—	—	—	—	—	—	154	—	147
C6	0.059	0.124	—	—	—	—	—	—	—	174	—	158
Carbon alloys												
R40-C5	0.0040	0.002	0.011	—	—	—	—	—	Good	147	214	—
R40-C1	0.0020	<0.002	0.016	—	—	—	—	—	Poor	140	232	161
C1	0.049	<0.004	0.04	—	—	—	—	—	—	159	—	154
R40-C2	—	—	0.052	—	—	—	—	—	Did not roll	138	—	—
C2	0.008	—	0.09	—	—	—	—	—	—	146	—	144
R40-C3	—	—	0.1†	—	—	—	—	—	Did not roll	144	—	—
R40-C4	—	—	0.2†	—	—	—	—	—	Did not roll	160	—	—
R43-M5	—	—	1.0†	—	—	—	—	—	—	228	—	—
Sulfur alloys												
R38-S1	—	—	—	0.02†	0.007	0.003	0.005	—	Did not roll	136	—	—
R38-S2	—	—	0.010	0.22†	0.007	0.003	0.002	—	Did not roll	161	—	—
Nickel alloys												
R40-N1	—	—	—	—	0.01†	—	—	—	Good	138	214	—
R40-N2	—	—	—	—	0.055	0.002	0.01	—	Good	126	222	127
R40-N3	—	—	—	—	0.101	0.003	0.01	—	Good	128	224	129
R40-N4	—	—	—	—	0.199	0.005	0.005	—	Poor	140	241	151
R43-M2	—	—	—	—	1.0†	—	—	—	—	230	—	—
Iron alloys												
R40-F1	—	—	—	—	<0.001	0.016	0.01	—	Good	139	216	138
R40-F2	—	—	—	—	<0.001	0.058	0.01	—	Good	135	204	131
R40-F3	—	—	—	—	0.001	0.117	0.003	—	Good	132	214	132
R40-F4	—	—	—	—	0.001	0.246	0.003	—	Good	130	219	133
R43-M1	—	—	—	—	—	1.0†	—	—	—	151	—	—
Silicon alloys												
R40-S1	—	—	—	—	<0.001	0.002	0.03	—	Good	144	206	144
R40-S2	—	—	—	—	<0.001	0.003	0.07	—	Good	142	217	141
R40-S3	—	—	—	—	<0.001	0.005	0.07	—	Good	136	217	144
R40-S4	—	—	—	—	<0.001	0.01	0.15	—	Good	133	243	145
R43-M3	—	—	—	—	—	—	1.0†	—	—	166	—	—
Tungsten alloys												
R38-W1	—	—	—	—	—	—	—	0.05 †	Good	141	224	156
R38-W2	—	—	—	—	—	—	—	0.2†	Good	145	217	148

* From analysis on as-deposited chromium used for this ingot.
† Nominal composition.
ND means "not detected."

carbon in chromium is less than 0.001%. As illustrated in Fig. 6 and 11, increasing the quantity of carbon from 0.001 to 0.016% results in an increasing amount of the carbide, which, in the annealed samples, generally assumes the form of spheroids. Examination of a cast 0.04% carbon alloy showed that, in this condition, some carbides also assumed the form of rods or platelets. This would indicate that

some carbide precipitated from the chromium during cooling, and suggests that the terminal solid solution of chromium shows a decreasing solubility for carbon with decreasing temperature. At levels of 0.09% carbon and above, the carbide phase also occurs, in the cast structures, in an interdendritic filler pattern as an almost continuous phase. Examination of the nominal 0.2% carbon alloy, after attempted fabrication and annealing, showed that many of the interdendritic carbide patches contained fine particles of another microconstituent, which was identified tentatively as eutectic particles of carbon-rich chromium.

These observations are consistent with the partial chromium-carbon equilibrium diagram given on page 1181 in the 1948 Edition of the *ASM Metals Handbook*. This diagram shows that chromium containing "probably less than 0.1 per cent" carbon undergoes a eutectic reaction at 1475°C with a carbon-rich phase containing about 5% carbon. This same source lists the eutectic composition at 4.5% carbon and identifies the carbon-rich phase as Cr_4C or $Cr_{23}C_6$, which has a cubic structure having an a_0 value of 10.64kx units.

Nitrogen-addition alloys.—The structure of the cast 0.069% nitrogen alloy contained many short rods or plates of a Widmanstätten-type precipitate, similar in color to the chromium matrix. As in the case of the chromium-carbon alloys, the Widmanstätten form indicates that the nitrogen-rich phase shows a decreasing solubility in the chromium terminal solid solution with decreasing temperature. This is illustrated more clearly in the 0.124% nitrogen alloy structure shown in Fig. 12. Here, the nitrogen-rich phase occurs in appreciably larger plates and also at the grain boundaries. A heat treatment of 24 hr at 1000°C followed by water quenching had no significant effect on either the quantity or the mode of occurrence of these Widmanstätten structures. This suggests that there is relatively little change in the solubility of this phase in chromium at temperatures up to 1000°C.

Aside from these two alloys, none of the arc-melted chromium samples examined contained any recognizable quantity of the nitrogen-rich phase. The highest analyzed nitrogen content in any sample to which nitrogen was not added deliberately was 0.032% (for an arc-melted sample of as-received electrolytic chromium). On this basis, the solubility limit of nitrogen in chromium was placed tentatively between 0.032 and 0.069%.

Sulfur addition alloys.—Of the two sulfur-addition alloys prepared, the one containing nominally 0.022% sulfur did not contain any second phase which could be associated with sulfur. However, the nominal 0.22% sulfur alloy definitely contained an

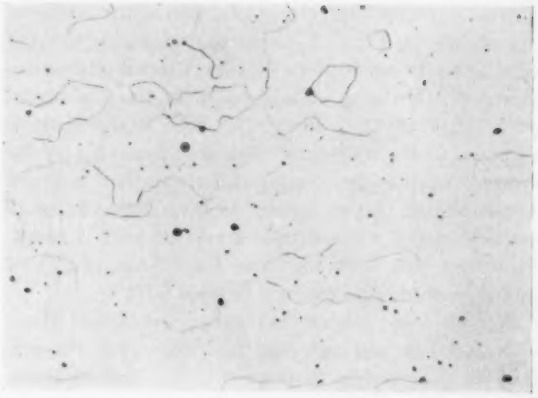

FIG. 10. Oxide inclusions in chromium containing 0.051% oxygen; electrolytic etch in 10% oxalic acid. 500×.

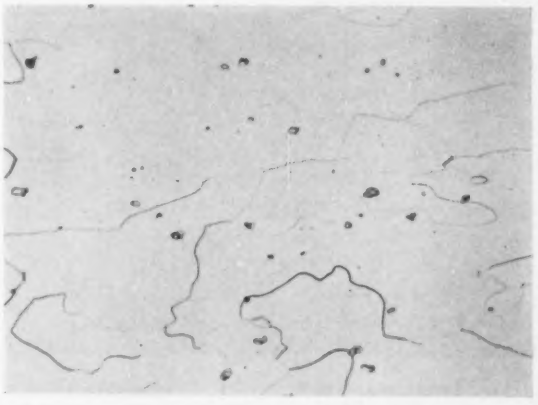

FIG. 11. Carbides in chromium containing 0.016% carbon; electrolytic etch in 10% oxalic acid. 500×.

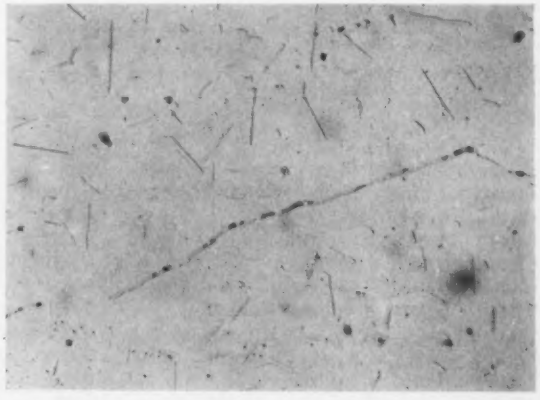

FIG. 12. As-cast structure of chromium containing 0.124% nitrogen and 0.059% oxygen. Large, light-colored Widmanstätten rods and grain boundary precipitate of nitrogen-rich phase plus gray-colored oxide inclusions; electrolytic etch in 10% oxalic acid. 500×.

inclusion phase characteristic of the sulfur addition. As shown in Fig. 13, these particles appear very similar to the oxide phase. Under direct illumination, however, the large sulfide particles have a brown color after electrolytic etching with oxalic acid, as opposed to the slate-gray color always shown by the oxide. Admittedly, visual differentiation between these phases, where either or both exist in small particle sizes or quantities, would be very difficult. However, this work indicates that the solubility of sulfur in chromium extends beyond 0.02%.

Nickel-, iron-, silicon-, and tungsten-addition alloys.—Nickel (up through 0.2%), iron (up through 0.25%), silicon (up through 0.15%), and tungsten (nominally up through 0.2%) all appeared to be soluble in chromium.

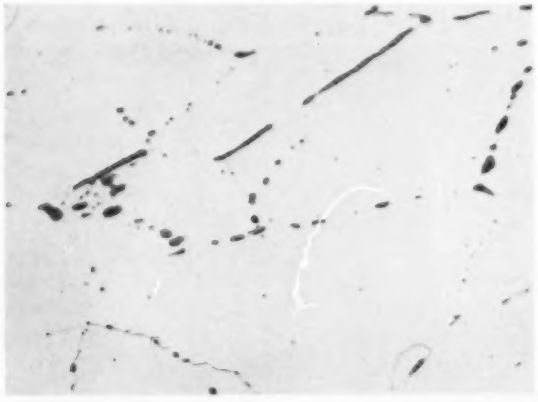

FIG. 13. Annealed structure of chromium containing, nominally, 0.22% sulfur and 0.019% oxygen. Large particles of a brown sulfur-rich phase plus small particles of oxide; electrolytic etch in 10% oxalic acid. 500×.

Correlation of Bend Ductility and Impurity Content of Chromium

All the chromium-plus-impurity element alloys which were successfully fabricated to sheet were bend tested by using the same procedure as used for bend testing the unalloyed iodide chromium. Since the impurity content of the unalloyed chromium was determined in many cases, the two sets of bend-test data together give a good idea of the effects of a number of impurity elements on the bend ductility of chromium.

Transition temperatures in both the as-fabricated and the annealed conditions and the compositions of the various lots of unalloyed chromium tested are shown in Table VI. The same information is given in Table VII for the alloys containing the deliberate impurity additions. The latter table also gives bend data for unalloyed sheet prepared from the same chromium as used for making the alloys.

From Table VI (unalloyed chromium), it appears that increasing the amounts of total metallic impurities generally increases the average transition temperature of wrought chromium sheet. Here, as in the correlation of composition with as-cast hardness, the effects of the individual metallic contaminant elements appeared equivalent and additive. The total metallic-impurity content appears to have less effect on the ductility of annealed chromium. Good bend ductility in wrought chromium can be obtained at relatively high oxygen levels. For example, the sample from Ingot R38-3, containing 190 ppm of oxygen, showed an average bend-transition temperature of 0°C. The effects of carbon, nitrogen, and sulfur are not apparent from these data on unalloyed chromium.

TABLE VI. *Composition and bend-test data for representative iodide chromium sheet samples prepared using the standard fabrication procedure*

Ingot	Composition, wt %						Fabricated bend ductility				Annealed bend ductility			
	O	N	C	S	Total metallics	Total purity	Vickers hardness	Transition range, °C: Highest brittle	Transition range, °C: Lowest ductile	Avg transition temp, °C	Vickers hardness	Transition range, °C: Highest brittle	Transition range, °C: Lowest ductile	Avg transition temp, °C
R38-3	0.0190*	<0.0050*	0.002*	0.015*	0.0100*	99.95	222	−25	−25	0	140	150	150	150
R43-1	0.0140*	<0.0003	—	—	0.0112	<99.97	211	−25	−50	−25	—	—	—	—
R49-1	0.0073	0.0010	0.002*	0.002*	0.020*	99.97	215	−25	0	0	—	—	—	—
R40-2	0.0060	<0.0020	—	—	0.020*	<99.97	209	−25	−50	−25	134	200	175	175–200
R40-1	0.0100	0.0030	0.001	—	0.020*	<99.97	213	25	0	0	138	200	225	215
R41-1	0.0074	<0.0007	0.007	—	0.021*	<99.97	205	0	−25	0	—	—	—	—
R47-1	—	—	0.005	—	0.022	<99.97	208	25	−25	0	—	—	—	—
R46-1	—	—	0.007	0.009*	0.036	<99.95	223	0	0	25	—	—	—	—
R35-1	0.0160	0.0050	—	—	0.044	<99.93	218	25	0	25	—	—	—	—
R48-1	—	—	0.005	—	0.054	<99.94	263	25	0	0–125	—	—	—	—
R37-1	0.0042*	0.0005*	—	—	0.059	<99.94	221	50	0	25	—	—	—	—
R36-1	0.0042*	0.0013*	0.002	0.011*	0.118	99.86	218	125	50	100	124	175	175	175
R27-1	0.0013*	0.0004*	0.002	0.005	0.460	99.53	236	75	25	50	—	—	—	—
R34-1	—	—	—	—	0.512	<99.49	226	100	0	75	129	200	200	200

* Analyses were taken from as-deposited chromium from which these ingots were prepared.

TABLE VII. *Bend-test data on chromium-plus-impurity base alloys*

Ingot	Alloyed Composition*, wt %	Fabricated condition				Annealed condition			
		Vickers hardness	Bend ductility			Vickers hardness	Bend ductility		
			Transition range, °C		Avg transition temp, °C		Transition range, °C		Avg transition temp, °C
			Highest brittle	Lowest ductile			Highest brittle	Lowest ductile	
R40-1	Unalloyed	213	25	0	0	138	200	225	212
R40-2	Unalloyed	209	−25	−50	−25	134	200	175	187
R40-X1	0.012 O	204	0	−50	−20	147	200	200	200
R40-X2	0.051 O	210	−50	−50	−37	152	225	250	237
R40-X3	0.075 O	207	−50	−50	−16	154	300	300	300
R40-X4	0.180 O	212	−50	−25	−30	156	275	300	287
R40-C5	0.011 C	214	50	50	60	—	—	—	—
R40-C1	0.016 C	232	50	25	55	161	200	200	200
R40-F1	0.016 Fe	216	−25	−25	−25	138	—	—	—
R40-F2	0.058 Fe	204	−25	0	0	131	—	—	—
R40-F3	0.117 Fe	214	−25	0	0	132	—	—	—
R40-F4	0.246 Fe	219	−25	−50	−25	133	—	—	—
R40-N1	0.01† Ni	214	25	25	25	—	—	—	—
R40-N2	0.055 Ni	222	0	−25	0	127	—	—	—
R40-N3	0.101 Ni	224	75	25	50	129	—	—	—
R40-N4	0.199 Ni	241	50	50	55	151	—	—	—
R40-S1	0.03 Si	206	25	0	15	144	150	150	150
R40-S2	0.07 Si	217	−50	−25	−40	141	150	175	163
R40-S3	0.07 Si	217	−50	−25	−25	144	175	200	187
R40-S4	0.15 Si	243	0	0	15	145	50	100	75
R38-3	Unalloyed	222	−25	−25	0	140	150	25	110
R38-W1	0.05† W		0	0	0	156	—	—	—
R38-W2	0.2† W		0	0	0	148	—	—	—

* See Table V for more complete analytical data on these alloys.
† Nominal compositions; all others by analysis.

The data of Table VII (chromium-plus-impurity alloys) have been plotted graphically in Fig. 14 to facilitate their interpretation. From Table VII and Fig. 14, it appears that binary additions of oxygen (up through 0.18%), iron (up through 0.246%), tungsten (nominally, up through 0.2%), and silicon (up through 0.15%) have no significant effect on the average bend-transition temperature of wrought chromium. At levels of 0.1% and above, nickel increases the bend-transition temperature by about 50°C.

Bend data on the chromium-carbon alloys show that carbon has a greater effect on ductility than any single metallic impurity. The presence of as little as 0.011% carbon results in about the same increase in transition temperature as does about 0.2% nickel for sheet tested in the as-fabricated condition.

The nitrogen level in all unalloyed chromium samples was usually less than 50 ppm, and variations in nitrogen content around this concentration could not be correlated with any properties of the metal. However, results of bend tests on a few samples of arc-melted electrolytic chromium suggest that nitrogen in the range from around 50 to 300 ppm has relatively little effect on ductility.

It was not possible to roll the ingots with sulfur additions (0.02 and 0.22% nominal), so they could not be bend tested. However, the extremely deleterious effect of sulfur on fabricability suggests that small amounts of sulfur may also be damaging to bend ductility.

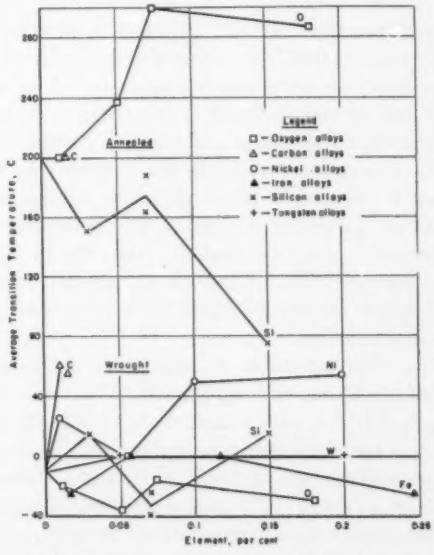

FIG. 14. Effect of various alloy additions on the bend-transition temperature of wrought and annealed iodide-chromium sheet.

Bend-test data on recrystallized samples of the oxygen alloys showed that the addition of 0.2% oxygen raised the transition temperature by about 100°C. This is in contrast to bend data on these same alloys in the wrought condition, where the oxygen content did not appear related to the transition temperature. Carbon in amounts up to 0.016% has no effect on the transition temperature of annealed chromium, in contrast to its adverse effect on the bend transition of wrought chromium. On the other hand, presence of silicon is beneficial to the ductility of annealed chromium, although it has little effect in wrought chromium. The 0.15% silicon alloy, in the annealed condition, showed the lowest average transition temperature (75°C) obtained in all of the bend tests on the recrystallized alloyed chromium samples.

Summary

This investigation has shown that both the purity and the physical condition of chromium are important factors in determining the degree of ductility at temperatures near room temperature.

By fabrication in a temperature range just below the recrystallization temperature, chromium sheet having an average ductile-to-brittle bend transition at temperatures well below room temperature can be obtained. When arc-melted iodide chromium was used, the lowest bend-transition temperature of −25°C was found for metal which contained 0.006% oxygen, less than 0.002% nitrogen, and a total of approximately 0.02% metallic elements. Carbon and sulfur analyses were not available for these specimens, but should run well below 0.015 and 0.02%, respectively. Increasing amounts of nickel (up to 0.1%) or molybdenum (up to 0.5%) above the levels normally found for these elements in the iodide chromium generally increased the bend-transition temperature. In this respect, the effects of the individual metallic contaminants present in unalloyed iodide chromium could be taken to be equivalent and additive.

Work with a number of impurity-addition alloys showed that iron (up through 0.25%), silicon (up through 0.15%), and tungsten (up through 0.2%, nominal) have no significant effect on the average bend-transition temperature of wrought chromium sheet. At levels of 0.1% and above, nickel increases the bend-transition temperature to about 50°C. Chromium containing nickel in amounts above 0.2% cannot be fabricated to sound sheet by using the procedures devised in this research.

Oxygen in amounts from 0.006 to 0.37% does not have any significant effect on the bend-transition temperature of wrought chromium. Similarly, changes in nitrogen content from 0.001 to 0.032% have no apparent effect on bend ductility. On the other hand, carbon and sulfur are both very detrimental to the hot and cold ductility of chromium. Chromium containing above about 0.015% carbon or 0.02% of sulfur cannot be rolled to sound strip. Although some small tolerance for both of these elements is indicated, chromium containing carbon in excess of 0.01% or sulfur in excess of 0.015% will not be bend ductile at room temperature.

Wrought chromium sheet exhibits marked anisotropy in its bend properties. Samples bent around an axis parallel to the rolling direction show ductile-to-brittle transition temperatures on the order of 200°C higher than do samples bent around an axis perpendicular to their rolling direction. Recrystallization tends to overcome the bend anisotropy, but invariably results in an increase in the average bend-transition temperature over that obtained on samples cut longitudinally from the wrought sheet.

Chromium in the wrought condition is extremely sensitive to notch effects. Minute surface irregularities produced by normal machine grinding or milling the edges of bend-test samples, in directions parallel to or transverse to the rolling direction, increase the transition temperature by about 50°C.

Several wrought-sheet tensile samples from material which had bend-transition temperatures well below room temperature all showed brittle fractures at stresses of 62,000 psi or less. The reason for this brittle behavior is not understood clearly, although, in view of the good bend ductility, it seems likely that this behavior is associated with a surface effect derived from machine grinding of the samples.

Acknowledgments

The authors are grateful to the Air Research and Development Command of the U. S. Air Force at Wright-Patterson Air Force Base, Ohio, for permission to publish the results of this work which was done at Battelle Memorial Institute under their sponsorship. They also wish to acknowledge the assistance of I. E. Campbell and J. M. Blocher, Jr., who directed the research on the preparation of iodide chromium, and of M. W. Mallett, C. B. Griffith, W. M. Henry, E. K. Blosser, H. R. Harris, D. P. Leiter, Jr., and F. E. Huber, Jr., of the Battelle Analytical Laboratory Staff for their invaluable contributions to this work.

Any discussion of this paper will appear in a Discussion Section to be published in the December 1955 Journal.

REFERENCES

1. W. Kroll, *Z. anorg. u. allgem. Chem.*, **226**, 23 (1935–6).
2. W. Kroll, W. F. Hergert, and L. A. Yerkes, *This Journal*, **97**, 258 (1950).
3. E. S. Greiner, *Trans. Am. Inst. Mining Met. Engrs.*, **188**, (6), 891 (1950).

4. H. B. Goodwin, R. A. Gilbert, C. M. Schwartz, and C. T. Greenidge, *This Journal*, **100**, 152 (1953).
5. E. T. Hayes, WADC Tech. Rept. 52-54, Wright-Patterson Air Force Base, Ohio (March 1952).
6. H. L. Gilbert, H. A. Johansen, and R. G. Nelson, U. S. Bur. Mines, Rept. Invest. No. 4905 (September 1952).
7. H. L. Gilbert, H. A. Johansen, and R. G. Nelson, *Trans. Am. Inst. Mining Met. Engrs.*, **5**, 63 (1953).
8. A. H. Sully, E. A. Brandes, and K. W. Mitchell, *J. Inst. Metals*, **81**, 585 (1953).
9. F. Adcock, *J. Iron Steel Inst. (London)*, **115**, 369 (1927).
10. A. Brenner, P. Burkhead, and C. Jennings, *J. Research Natl. Bur. Standards*, **40**, No. 1, R. P. 1854, 31 (1948).
11. A. H. Sully, E. H. Brandes, and A. G. Provan, *J. Inst. Metals*, **81**, 569 (1953).
12. R. I. Jaffee, L. W. Eastwood, D. J. Maykuth, R. M. Goldhoff, H. R. Ogden, J. W. Halladay, and J. G. Kura, AF Tech. Rept. No. 6515, Part 1, Wright-Patterson Air Force Base, Ohio (June 1951).
13. E. J. Ripling, *ASTM Bull.*, No. 186, 37 (December 1952).

Preparation of Titanium by Fluoride Electrolysis[1]

M. A. Steinberg, S. S. Carlton, M. E. Sibert, and E. Wainer

Horizons Incorporated, Cleveland, Ohio

ABSTRACT

Preparation of commercially pure titanium metal powder by electrolysis of K_2TiF_6 in molten NaCl is described. The process is carried out under an inert atmosphere in an all-graphite cell. Operating conditions of the electrolysis and their effect upon the metal so produced are discussed. Preparation of the K_2TiF_6 and the electrolytic procedure are completely described. The process is capable of producing metal of high purity which may be consolidated and fabricated by standard techniques as applied to metal powders. The metal is recovered by aqueous washing techniques. It may be prepared either as coarsely crystalline metal or as coarse thin metal flakes.

Introduction

One of the more conspicuous current research efforts is the attempt to develop new processes for production of titanium metal in a more economical and straightforward fashion. A large amount of this effort is concerned with electrochemical processes. One such development is described in this paper.

Three general approaches have been made to the extractive metallurgy of titanium: (*a*) thermal reduction by active metals; (*b*) thermal dissociation; and (*c*) electrolytic processes. The first of these approaches, as exemplified by the Kroll process, is limited economically by the cost of magnesium metal and $TiCl_4$ and the fact that such processes are, of necessity, batch processes. The second approach is even more severely limited by costs of materials and equipment. Notable in this respect is the Van-Arkel deBoer hot wire dissociation of the tetraiodide. Although considerable effort has been expended on refinements and improvements of existing methods, a very large portion of the research effort has gone into development of electrolytic processes. These offer prospects of inexpensive materials and continuous or semicontinuous operation.

Consideration of possible electrolytic methods and the properties of titanium metal and its salts essentially eliminates all but fused salt methods. Titanium is among those metals which are highly oxyphillic in character. Where oxygen is available, it forms an oxytitanium ion in preference to a simple metal ion. Efforts to isolate the metal from aqueous or other oxygen-containing media have produced only titanium oxides.

This particular process concerns the electrolysis of potassium fluotitanate in a melt of an alkali or alkaline earth halide. This salt of titanium is employed as the source electrolyte because it is one of the few ionic titanium salts which is stable at elevated temperature and can be obtained in an anhydrous form. Electrolysis is carried out in special cells providing an inert atmosphere to prevent oxidation of the source electrolyte and deposited titanium metal. Metal is obtained as coarse crystalline granules or as thin flakes up to 1½ in. long. Cathode deposits are recovered by aqueous techniques and consolidated by conventional powder metallurgical methods.

Ample reviews of the background of the electrolytic preparation of titanium have already been given (1–5). Of specific interest with respect to this process are previous attempts to produce pure titanium from K_2TiF_6.

Deposition of bright titanium from an electrolytic bath of K_2TiF_6, Na_2SO_4, and H_2SO_4 has been reported (6). This claim is quite doubtful, however. Electrolysis of K_2TiF_6 in a fused NaCl and KCl medium gave cathode deposits consisting essentially of reduced oxides, with only sparse evidence of a few metallic particles (7). No protective atmosphere was employed. K_2TiF_6 has been electrolyzed in a mixture of NaCl and KCl, yielding dendritic titanium crystals of undisclosed purity (8). Electrolysis was carried out at 850°C under 30–100 amp/dm² current density. This cell employed an inert atmosphere. Similar results were obtained using $TiCl_3$ and TiF_3 as the source electrolyte. Similar deposition was reported for LiCl-KCl-K_2TiF_6 at 700°C (9). This work was done in an admittedly contaminated glass system, however. A patent has been granted utilizing a bath of $TiCl_4$ in an alkali chloride, alkaline earth chloride, or mixture thereof (10). The cell is of a closed type operating at 675°C, and $TiCl_4$ is continuously added to the electrolyte. Crystalline titanium was deposited from a bath of $TiCl_3$ in

[1] Manuscript received July 6, 1954. This paper was prepared for delivery before the Chicago Meeting, May 2 to 6, 1954. It is based on a portion of the work carried out by Horizons Incorporated for the Office of Naval Research under Contract Numbers Nonr-394 (00) and 394 (01).

KCl-LiCl at 550°C (11) under hydrogen, at 1–2 v and about 6 amp/dm².

Equipment

Experimental work was carried out in inert atmosphere cells of graphite interior construction. Graphite crucibles also served as anodes. A graphite resistance element surrounding the crucible served as a heating source. The unit was essentially closed, with only a cathode entrance and charging opening being provided in the removable head. Purified argon gas was used as a cell atmosphere. Each cell took a charge of 5 lb of salts and produced up to 100 g of titanium per run. Cells of this type have been described in detail in previous papers (5, 12).

Preparation of High Purity K_2TiF_6

K_2TiF_6 may be prepared from a good grade of TiO_2 by dissolution in HF, followed by precipitation with pure K_2CO_3. Such material is subsequently water recrystallized by the following procedure.

In most cases a commercial grade of K_2TiF_6 has been obtained and only the purification step carried out.

The crude K_2TiF_6 from either source was dissolved in about 1½ gal of water/lb of K_2TiF_6 at 90°–100°C with agitation using rubber coated equipment. The solution was then filtered through Nibri-cel into a neoprene lined trough equipped with a cooling jacket.

After cooling and crystallization took place, the crystals were filtered in a polyethylene funnel or suitable filter press and the mother liquor recycled. The product, K_2TiF_6, was then vacuum dried at 85°–90°C under 2–5 cm pressure for 24–30 hr and stored in airtight containers.

This procedure enables the removal of residual TiO_2, iron, aluminum, and other minor metallic impurities. The material, as charged to the cell, contains <0.01% H_2O and <0.01% insolubles (TiO_2).

Decomposition Voltage of K_2TiF_6

An attempt was made to determine the decomposition voltage of K_2TiF_6. A small 100 g electrolytic cell coupled with an accurate current-voltage control and recorder was used for this work. Graphite electrodes were used. Voltage readings were measured as a function of current density. Extrapolation of the straight line portion of the curve to zero current gave an approximate E_D value, the exact point being determined by the point of inflection.

Results indicate a value of 1.8–2.0 at 800°C which has been experimentally verified. This curve is shown in Fig. 1.

Electrolytic Procedure

This process is essentially a straightforward fused salt electrolysis, but the elements of bath purity and exclusion of oxygen and nitrogen from both the salt bath and atmosphere determine the relative success of the process with respect to the type of metal produced. Operating variables affect the efficiency and recovery to a great extent as will be shown later.

The most satisfactory melt has been found to be a mixture of K_2TiF_6 in NaCl, and most of the work has involved this system. A typical run is carried out as follows.

A clean cell is thoroughly purged with argon gas with the crucible containing the NaCl in position. If the cell is in any manner contaminated, it is first hot evacuated until a pressure of 10–25μ is obtained and all residues are removed. This is followed by a flushing cycle with argon gas.

NaCl is then melted at 850°–900°C. After a short period to allow for volatilization of any moisture, K_2TiF_6 is charged and melted.

A pre-electrolysis is then carried out by low voltage electrolysis under the decomposition voltage of K_2TiF_6. This step removes residual moisture, iron, and perhaps other impurities. The procedure requires 5–20 amp-hr/lb of bath and is judged by a series of voltage rises which take place. When the voltage reaches 2.5–3.0 v, the procedure is terminated. Steel or graphite cathodes may be employed, but steel is preferred. The small deposits obtained are discarded. They contain appreciable amounts of iron and oxygen.

The electrolysis proper is carried out using a steel cathode supported by a steel or, preferably, a nickel shaft covered with a graphite tube. The nickel and graphite minimize corrosion due to chlorine gas.

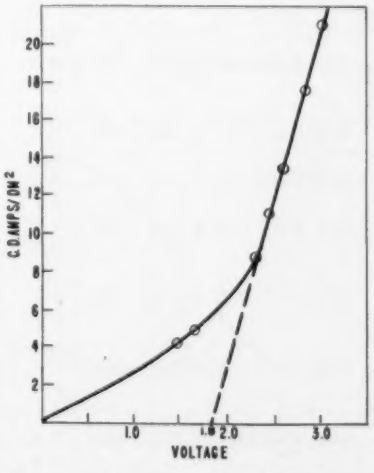

FIG. 1. Decomposition potential of K_2TiF_6, temp, 800°C, 4 runs, average value, 1.8 v.

Cathodes of cylindrical or truncated cone shape are generally employed. The steel cathode is lowered with a small voltage on it to prevent any solution of the steel in the melt. The bath temperature meanwhile is lowered to 740°–760°C. Electrolysis is then initiated at 4–6 v and 200 amp, equivalent to 400–550 amp/dm². Generally, 1 or 2 polarizations are encountered during a run requiring about a 25% cut-back in current. Electrolysis is carried out for 240–260 amp-hr on this particular cell. Chlorine gas is evolved throughout the process. The end of the run is ascertained by a voltage rise of 0.2–0.5 v when the titanium has been essentially exhausted. If the run is prolonged, sodium is produced, complicating recovery of the titanium metal.

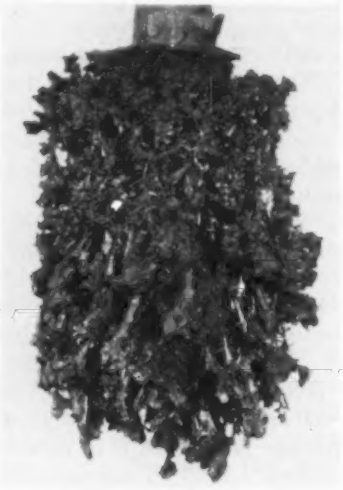

FIG. 2. Typical titanium flake cathode deposit obtained from electrolysis of K_2TiF_6.

The deposit is withdrawn from the melt under low voltage and allowed to cool either above the melt or in a sealed water-cooled chamber which may be attached to the cell.

When below 200°C, the deposit is removed. Such deposits appear as ragged salt metal agglomerates, the outer layer consisting of very coarse thin titanium flakes. Deposits contain from 40–60% metal. The interior of the deposit is coarsely crystalline metal embedded in a salt matrix. The larger flake material is essentially salt-free. A typical deposit is illustrated in Fig. 2.

The deposit is chipped from the cathode, crushed to about 20 mesh, and recovered by washing in warm water. It is then filtered and oven-dried at 40°–50°C.

Several washing steps are required to remove all salts from the metal deposits. Since the deposits contain some lower titanium halides, *p*H control is necessary to prevent precipitation of titanium hydrates which would seriously contaminate the metal powder. A final acetone or alcohol rinse is generally used to facilitate drying.

Operating and recovery data for several typical runs are given in Table I.

TABLE I. *Electrolysis of* K_2TiF_6 *in* NaCl

Run No.	Bath composition	Temp	E^*	I	Amp-hr of pre-electrolysis	Total amp-hr	Yield	Current efficiency	Remarks
		°C	v	amp			%	%	
61-68	78% NaCl 22% K_2TiF_6	715	—	150	44	330	46.2	26.9	Coarse crystals
61-73	83% NaCl 17% K_2TiF_6	730	—	200	39	295	87.5	45.0	
				150					
				100					
61-85	75% NaCl 25% K_2TiF_6	740	6.0	150	162	465	53.8	22.4	Very coarse crystals
			6.8	200					
			5.8	100					
61-109	84% NaCl 16% K_2TiF_6	755	8.0	200	92	255	87.0	51	Some crystals and platelets
			6.8	150					
61-113	85% NaCl 15% K_2TiF_6	725	5.6		52	315	76	37	Coarse platelets. Used residual salt from above run.
			6.1	100					
61-116	84% NaCl 16% K_2TiF_6	740	7.5	200	45	445	—	35	—
			6.2	150					
			5.3	100					
61-120	84% NaCl 16% K_2TiF_6	755	7.4	200	49	235	89	58	—
			6.3	150					
			5.3	100					
61-124	85% NaCl 15% K_2TiF_6	750	7.8	250	61	245	82	51	Very coarse platelets
			6.5	150					
			5.8	100					
61-127	84% NaCl 16% K_2TiF_6	800	5.8		33	243	59	37	Used residual salt from above run.
			5.6	100					

* Includes resistance of cell to crucible anode.

Process Variables

Aside from the purity of the salt bath and requirement of an inert atmosphere, process variables are also of considerable importance to the efficient operation of the fluoride process. These include K_2TiF_6 concentration, temperature, voltage, current density, and bath composition. These factors are discussed individually below.

K_2TiF_6 *concentration.*—The concentration of K_2TiF_6 in the electrolyte is one of the major contributing factors to the efficiency of the process. The amount of K_2TiF_6 present seems to determine the extent to which back reactions can interfere with deposition of titanium as metal. This may be due to the Ti-F ions, Ti^{z+} ions, or the simple F^- ion. Such reactions must fall into three general types.

$$Ti \rightarrow Ti^{z+} + xe$$

$$Ti^{2+} \rightarrow Ti^{z+} + (x - 2)e$$

$$Ti^{3+} \rightarrow Ti^{4+} + e$$

The optimum concentration for the cell used in this work has been empirically determined as 15–17 wt %. This is equivalent to a molar ratio of 1:20–23::K_2TiF_6:NaCl.

The effect of higher concentration on efficiency of the process is apparent from the data in Table I (runs 61–68 and 61–85), where a 22 and 25% concentration was used.

Electrolyte composition.—A survey of possible electrolytes was made to determine the most suitable bath composition. This included principally alkali and alkaline earth chlorides and fluorides, since a number of these could satisfy the requirement for an anhydrous oxygen-free salt medium. Initially pure K_2TiF_6 was subjected to electrolysis, but current efficiency was extremely poor as would be expected from the behavior of the K_2TiF_6 concentration variable.

Pure sodium chloride is the most satisfactory diluent from the standpoint of purity, availability, and behavior on electrolysis. This has been employed as the electrolyte in all work reported.

Alkaline earth halides are generally unsatisfactory due to the difficulty in maintaining them in anhydrous form. These are, in general, hydrates and must be vacuum dried for effective use in a process of this type. Fluorides are generally not suitable due to their relative insolubility and resultant difficulty of removal from the metal deposits. Other alkali chlorides may be used if in sufficiently pure and anhydrous form, but there is no apparent advantage to justify the higher cost of such materials over NaCl.

Various eutectic mixtures have been tried but, again, these offer no significant advantages.

Temperature.—The prime effect of temperature change is on the characteristics of the metal crystals produced. This is primarily governed by the transformation temperature of titanium (882°C). Normally an HCP structure is observed, but, above the transformation temperature, a BCC structure results. In this electrolytic procedure, electrolysis is usually carried out at 740°–760°C, whereby a hexagonal structure results. Deposits contain large hexagonal platelets and smaller hexagonal crystallites. If the temperature of the bath is greater than 830°–840°C, these large platelets do not form at all and the deposits consist essentially of a distorted cubic type of crystal. The BCC structure is not stable at normal temperatures and crystals invert to an HCP form. The fact that the change in crystal type occurs at less than 882°C is indicative that cathodes run hotter than the salt bath itself.

At bath temperatures above 800°C the current efficiency falls off, due in part to loss of titanium from the bath by $TiCl_4$ formation. At temperatures below 700°C the bath is too viscous for efficient operation. Effects of temperature on operation of the cell are illustrated by Fig. 3.

Time of electrolysis.—The time required for completion of a run is determined primarily by the starting current. This is customarily adjusted to give a current density of 400–600 amp/dm². A run on the 5 lb cell requires about 260 amp-hr to complete, or about 90 min time. Normally, 1–3 polarizations are encountered in a given run, necessitating periodic reduction in the current passed.

As would be anticipated, the least pure metal is deposited first. The average metal hardness thus decreases somewhat with the length of a given run.

Voltage.—Applied voltage is important only insofar as it is above the decomposition voltage of K_2TiF_6, about 1.8 v. With overvoltage and drop through the cell considered, a minimum voltage of about 2.6 is required to produce titanium metal.

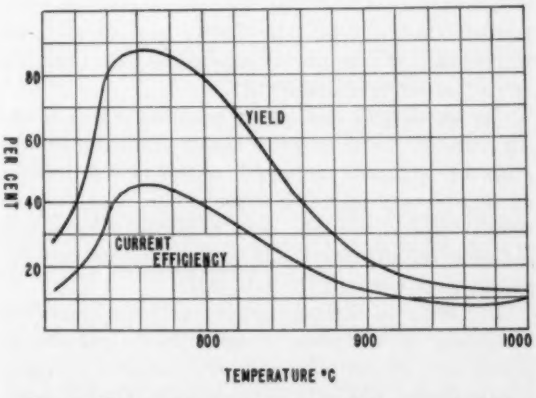

Fig. 3. Effect of temperature on efficiency and yield

TABLE II. *Current efficiency vs. cathode shape (current density)*

Run No.	Cathode shape	Cathode dimensions	Wt ratio NaCl to K_2TiF_6	Temp. °C	Amp range	Avg current density in amp/dm²	Amp-hr	% Current efficiency
64-195		Trunc. cone, ½ in. dia. × 1 in. dia. × 2 in. long	84-16	750	200-150	545-415	260	52
64-177		Bar, 1 in. × 3 in. × ⅛ in.	84-16	750	200-150	450-340	256	47
75-113		Inverse of 64-195	84-16	750	200-150	545-415	260	46
64-185		Disk, ¼ in. × 2½ in. on rod ½ in. × 2¼ in.	84-16	750	200-150	200-150	260	44
83-9		Rod ½ in. dia. × 2½ in. long	84-16	750	200-150	750-560	260	43
64-183	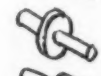	Inverse of 64-185	84-16	750	200-150	200-150	260	39
64-187	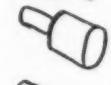	Cylinder, 3 in. dia. × 3 in. long	84-16	750	150	57	181	34
83-11		Cylinder, 1½ in. dia. × 2¾ in. long; hole ½ in. dia. × ¼ in. deep	84-16	750	200-150	190-140	267	30

All cathodes are steel on steel rods with graphite sleeves. Where more than one run was made on any type (as is the case with all), efficiencies reported are the highest of the set.

Optimum C.D. seems to range from 200-700 amp/dm² and is best from 350-550.

TABLE III. *Chemical analysis*

Sample No.	Total Ti	Carbon	Nitrogen
	%	%	%
64-183	99.8	0.102	—
64-187	99.6	0.066	—
64-191	99.8	0.06	—
75-74	99.5	—	0.004
75-80	99.5	—	0.002
75-110	99.6	0.13	0.017
75-137	99.7	0.03	—

Very high voltages of the order of 10 v are undesirable because some concurrent production of sodium metal is obtained. The decomposition voltage of NaCl is 3.15 v at 750°C, and there is no interference at nominal voltages if the bath titanium concentration is above 0.5%.

Current density and cathode geometry.—The starting current densities used varied from 50 to 750 amp/dm². There is no reliable means of determining current density once deposition starts. Also, current density is not uniform over a given cathode but depends on the particular cathode shape and resistive path through the salt bath.

A variety of cathode types has been employed consisting of cylinders, cones, disks, and strips. These were all run using uniform currents, voltages, temperatures, and bath compositions. Thus, a large range of current density resulted. It was found that higher current densities resulted in higher current efficiencies. Optimum current density seems to be in the range of 350-550 amp/dm². This is evident from Table II.

Cathode geometry is also a factor in current efficiency apart from the current density. Table II shows that the inverted truncated cone is superior to all types. An upright truncated cone did not behave as well under like conditions, presumably due to an inferior current density distribution. Strip cathodes, small cylinders, and a cylinder with disk above it behaved essentially the same. Larger cylinders gave decidedly inferior efficiencies at low current densities. Even under higher currents they do not give results equivalent to the cone cathode.

Metal Evaluation

A complete evaluation of the electrolytic titanium produced accompanied the process development.

Analysis.—Chemical analyses for titanium, carbon, and nitrogen were carried out for a large number of electrolytic titanium samples (see Table III).

Total titanium values were obtained by the Jones reductor method whereby tetravalent titanium in solution is reduced by zinc to the trivalent state and then back titrated with a ferric sulfate solution. Nitrogen was checked by the standard Micro-

Kjeldahl method, and carbon values were obtained by combustion in oxygen at 2400°F. A standard Leco Carbon Determinator was employed.

Oxygen data are not included since work to date has been done with the HCl volatilization method which has not been found to be reliable in the case of titanium. Oxygen contents are indicated to range from 0.05 to 0.10%, however. This is verified by the hardness data.

Spectrographic analyses were run on the various types of electrolytic titanium crystals. These include large flakes, coarse crystals, and impure fines which resulted from improperly controlled runs and are listed as Table IV. The only significant impurities in coarse and flake materials are iron and zirconium. Most of the iron can be eliminated by careful control in the electrolytic and recovery steps. In the case of the fine crystals, no purification electrolysis was included in the procedure accounting for the high values for Fe, Al, Mo, and V.

Screen analysis.—A large number of samples were subjected to particle size analysis. Most runs average 60–80% + 80 mesh with only 5% or less −325 mesh. Any impurities drastically reduce average particle size. Also, indications are that very high or very low current densities (>750 < 300 amp/dm²) tend to reduce particle size. Typical analyses are given in Table V.

Physical testing and metallography.—Electrolytic titanium produced by the fluoride process was continuously consolidated and arc melted to produce small ingots (usually 10 g) for physical testing. The hardness of such specimens ranges from Brinell 110–160. This corresponds to the best commercial sponge metal produced.

Hardness measurements were also carried out on a series of large flake crystals using a Tukon Hardness Tester with a 25 g load. Vickers hardness numbers of 50–70 VHN have been obtained with an average of about 55. This value is in line with values obtained for iodide titanium and is indicative of very low oxygen, nitrogen, and carbon contents.

Arc melted samples were cold rolled to varying degrees of reduction in order to determine the workability and effects on hardness and tensile strength. Edge cracking is generally first detected at 50–60% reduction. Hardness and tensile strength increase is comparable to that obtained with commercial titanium (Fig. 4). Annealing, of course, alters these curves drastically.

Some arc melted ingots were examined metallographically. Fig. 5 illustrates the typical basket weave structure of arc melted, rapidly cooled titanium. Fig. 6 is a twice arc melted specimen showing large coarse as-cast grains. Fig. 7 is a typical Widmanstätten structure with some carbide evident

TABLE IV. *Spectrographic analysis (in per cent)*

Element	Flake titanium +10 mesh	Coarse crystals −10, +80 mesh	Fine crystals −80, +325 mesh
Ti	Major	Major	Major
Si	0.001	0.002	0.001
Fe	0.005	0.05	0.15
Mg	0.001*	0.001*	0.001*
Mn	0.001*	0.001*	0.001*
Al	0.007	0.007	0.03
Mo	0.001*	0.001*	0.14
V	0.001*	0.001*	0.20
Cu	0.005*	0.0005	0.0008
Zr	0.01	0.01	0.01
Ni	0.001*	0.001	0.02
Pb	0.001*	0.001*	0.001*
Ca	0.002*	0.002*	0.002*
Cr	—	0.001*	0.001*
Total	0.0315%	0.0785%	0.5678%
Ratio	1	2.5	18

Trace amounts of Co, Cb, Ta, W, Bi, Zn.
* Less than.

TABLE V. *Particle size analysis*

Sample No.	+35	+80 −35	+100 −80	+150 −100	+200 −150	+325 −200	−325
	%	%	%	%	%	%	%
64–191	42.8	30.6	8.2	8.9	4.6	3.6	1.3
75–130	23.4	33.8	9.2	12.2	8.6	7.8	5.0
83–11	31.8	36.3	9.1	10.6	6.1	4.5	1.5
64–179	21.1	48.5	10.3	10.0	5.7	3.2	1.2

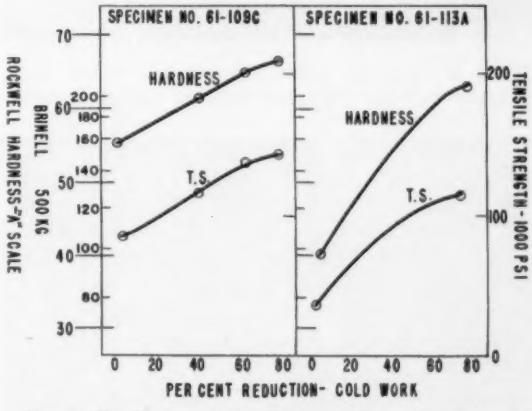

FIG. 4. Hardness and tensile strength as a function of cold reduction for two specimens of electrolytically produced titanium.

at the grain boundaries and dispersed in the structure. Fig. 8–11 illustrate the effect of annealing for various times on a 90% cold reduced ingot.

A preliminary analysis of the mechanism of this crystal growth has been done by metallographic and x-ray methods. These large platelets do not seem to have any preferential direction of growth in regard to lines of current flow. Thus, this growth must be a

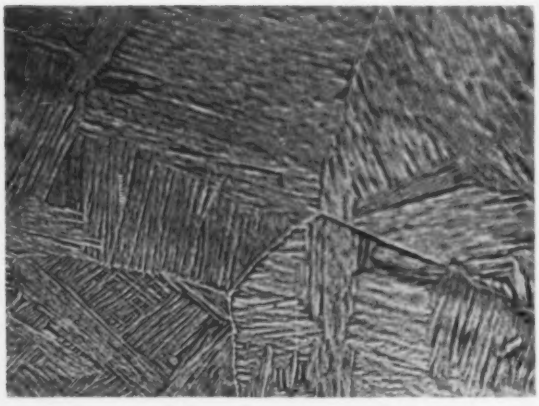

FIG. 5. Electrolytic arc melted as-cast titanium structure showing basket-weave pattern.

FIG. 6. Twice arc melted electrolytic titanium as-cast structure showing large coarse grains of high purity metal.

FIG. 7. Arc melted as-cast titanium surface, Widmanstatten structure. Electrolytically polished and etched.

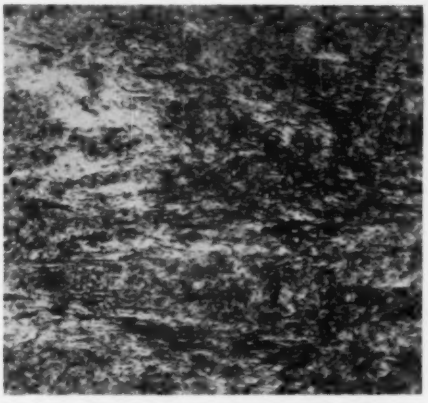

FIG. 8. Cold rolled and annealed structure of electrolytic titanium, 90% reduction, top view.

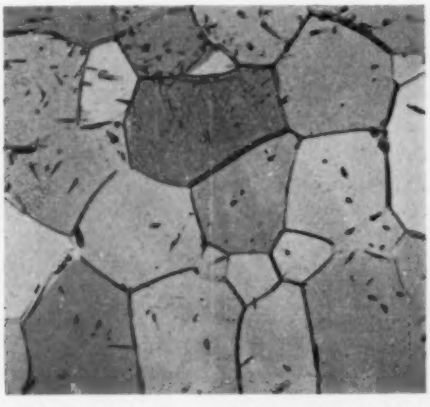

FIG. 9. Cold rolled and annealed structure of electrolytic titanium, 90% reduction, annealed at 800°C 15 min, air-cooled.

FIG. 10. Cold rolled and annealed structure of electrolytic titanium, 90% reduction, annealed at 800°C, 30 min, air-cooled.

function of the concentration gradient of Ti ions and probably also of the current density at a particular growth point.

Growth of an individual crystal, however, is determined by the specific habits of titanium. Fig. 12 illustrates some typical recovered plate crystals and the two general types found. One type has a ridge down the center parallel to the plates. In the other case, the ridge is the trace of a twin plane and

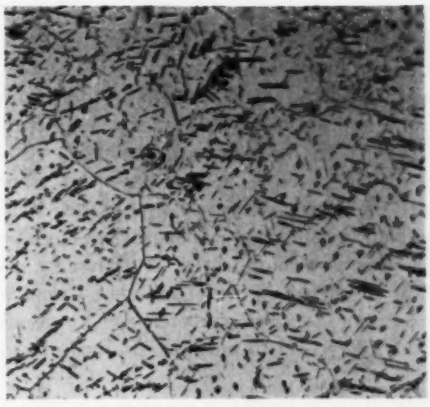

FIG. 11. Cold rolled and annealed structure of electrolytic titanium, 90% reduction, annealed at 800°C in argon atmosphere 2 hr, air-cooled.

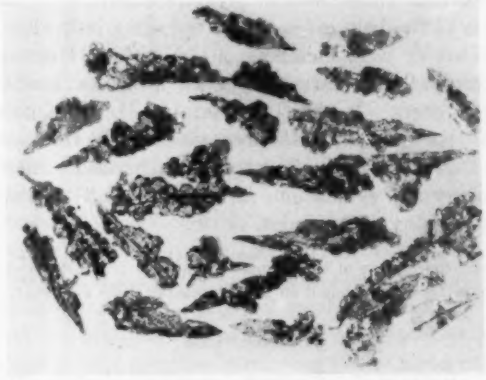

FIG. 12. Leaf-like flakes of electrolytic titanium metal showing characteristic shapes obtained. Growth twins and ribs are shown in some of the crystals.

the crystals grow as a twin with a specific angle between the two principal surfaces. All of these crystals form with their 0001 surfaces exposed, so there is no evidence of slip bands; only twins would be in evidence if deformation occurs by basal plane slip only.

The direction of crystal growth was determined by x-ray methods using Laue transmission and back reflection techniques. Molybdenum radiation at 40 kw and 20 ma was used with 2 hr exposures.

The crystals grow so that their wide surfaces are the 0001 planes; these are the minimum growth surfaces. The direction of growth from the orientation of crystals in the x-ray holder is of necessity a 2110 direction, the direction of most rapid growth.

Fig. 13 and 14 show that the large surfaces are basal plane surfaces. Growth of the layers and stacking of basal planes is clearly evident. The crystals must grow by having atoms from the electrolyte attach themselves to exposed corners in the electrolyte such that the basal plane is always

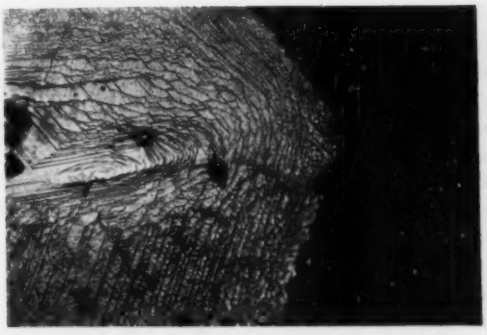

FIG. 13. Photomicrograph of electrolytic titanium crystal showing layer structure.

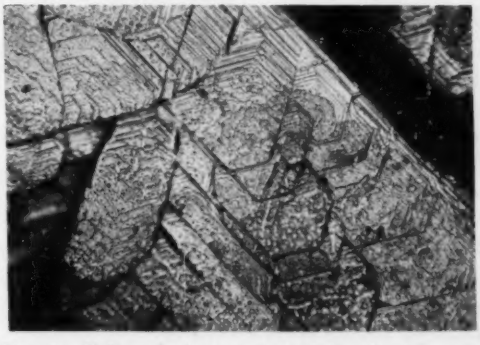

FIG. 14. Enlarged view of electrolytic titanium crystal showing well-defined layer structure and growth lines.

the surface plane. Fig. 14 illustrates the growth lines and layer structure.

DISCUSSION

A fused salt electrolytic process has been developed which is capable of yielding titanium metal of purity equivalent to commercial titanium. The process entails an electrolysis of a melt of K_2TiF_6 and NaCl under a protective inert atmosphere in closed cells. Major criteria for successful operation of the procedure include high purity reagents and elimination of container and atmosphere contamination.

Metal is obtained as a crystalline material in a salt matrix, and is recovered by carefully controlled aqueous procedures. The crystals are of three general types: (*a*) narrow flat platelets up to 1½ in. long of hexagonal structure; (*b*) coarsely crystalline hexagonal crystals of +100 mesh or greater; and (*c*) fine, less pure crystals. The latter are in very small amount under properly controlled conditions. If the temperature of operation exceeds 830°–840°C, the large platelets do not form, and deposits consist essentially of coarse crystals and dendrites of a distorted cubic structure. It is preferable from a purity standpoint to use lower temperatures.

Deposits do not consist of one crystal type alone,

although relative amounts of a given type may be controlled by adjustments of temperature, current density, and purity of the bath. The fine material is normally found adjacent to the steel cathode surface and is the least pure portion of the deposit. The large plates then grow from this crystal bed.

If significant amounts of impurities such as oxides are present, large plates do not form. The presence of even small amounts of iron as $FeCl_3$ or $FeCl_2$ is intolerable. Efficiencies are grossly reduced by a reoxidation of reduced titanium species by Fe^{3+}. Since $FeCl_3$ is volatile at the operating temperature, any iron exposed to the chlorine atmosphere can result in a continuous oxidation-reduction recycling.

It has been demonstrated that a purification electrolysis is a requisite in order to obtain maximum efficiency and purity of product. Such an electrolysis is normally carried out at 1–2 v using a graphite rod cathode. A total of 20–30 amp-hr is required for a 5 lb bath of good starting purity. When impurities, principally moisture, have been eliminated, a characteristic voltage rise occurs. A small amount of titanium plates out, but the deposit is principally iron and lower Ti oxides. A satisfactory pre-electrolysis cathode is uniformly coated with a thin layer of deposit, whereas, if a bath is severely contaminated, only the tip becomes coated.

The electrolysis is made using a steel cathode. A variety of shapes has been used, but an inverted truncated cone has been most satisfactory with respect to current efficiency and uniformity of deposit. This is presumably due to a more nearly ideal current density distribution.

Electrolysis is preferably carried out at 350–550 amp/dm^2 under 4–5 v. Very high current densities tend to decrease particle size, and lower currents offer no advantages, only slowing down the electrolysis. A temperature of 740°–760°C is preferred to give a fluid bath, maximum efficiency, and minimum tendency for impurity pick-up by metal produced. The over-all voltage must exceed 2.8 to produce metal, otherwise there is no operating limit up to the point where sodium is simultaneously liberated.

Baths may be recharged with K_2TiF_6 and run repeatedly up to a limit. There is a gradual buildup of KF and NaF in the melt and, eventually, the bath becomes sufficiently refractory and less conductive such that it is undesirable for electrolysis from a time standpoint. In addition, some of the fluorides are withdrawn with the deposit and present an extraction problem in recovery of the metal.

The process could be operated as a semicontinuous procedure, and as such would offer some advantage over existent batch processes. Materials required are readily prepared in a pure state by standard chemical techniques. The electrolysis is straightforward and, although requiring special closed cells, the design is not complicated or extremely costly. Titanium produced by this method is equivalent to or superior to present commercially available material with respect to purity and physical properties.

Acknowledgments

The authors appreciate the support of the Office of Naval Research in this work and their permission to publish these results. Acknowledgment is also made of the help given by the following individuals, who are or were members of the staff of Horizons Incorporated, in carrying out this program: process development, A. A. Topinka, Q. H. McKenna, B. C. Raynes; materials preparation, S. Cardon and D. Gollwitzer; metallography, S. Kulchar; metal recovery and evaluation, J. Wick and E. D. Fisher; photography, W. Sargent.

Any discussion of this paper will appear in a Discussion Section to be published in the December 1955 JOURNAL.

REFERENCES

1. J. Barksdale, "Titanium," p. 41–101, Ronald Press Co., New York (1947).
2. J. J. Berzelius, *Pogg. Ann.*, **4**, 1 (1825).
3. W. Kroll, *Trans. Electrochem. Soc.*, **78**, 35 (1940).
4. J. W. Mellor, "A Comprehensive Treatise on Inorganic and Theoretical Chemistry," Vol. 7, pp. 50–89, Longmans Green and Co., London (1927).
5. M. E. Sibert, Q. H. McKenna, M. A. Steinberg, and E. Wainer, *This Journal*, **102**, 252 (1955).
6. J. DeBussy, *Compt. rend.*, **36**, 540 (1853).
7. S. I. Sklylarenko and J. Lipkes, *Zhur. Priklad, Khim.*, **13**, 51 (1940).
8. A. Brenner and S. Senderoff, *This Journal*, **99**, 223C (1952).
9. P. Drossbach, *Z. Elektrochem.*, **57**, No. 7, 548 (1953).
10. Shawinigan Water and Power Co., British Pat. 678,807, May 11, 1951.
11. G. D. P. Cordner and H. W. Worner, *Australian J. Appl. Sci.*, **2**, 358 (1951).
12. M. A. Steinberg, M. E. Sibert, and E. Wainer, *This Journal*, **101**, 63 (1954).

Conductimetric and Viscometric Behavior of Lithium Bromide in 50–50 Weight Per Cent Methanol-Acetone at Temperatures within the Range 20° to −50°C[1]

LYLE R. DAWSON, RICHARD A. HAGSTROM,[2] AND PAUL G. SEARS

Department of Chemistry, University of Kentucky, Lexington, Kentucky

ABSTRACT

Conductances, viscosities, and densities, at temperatures within the range 20° to −50°C, have been determined for solutions of lithium bromide in 50–50 wt % methanol-acetone over a wide concentration range. An indirect method has been used to evaluate the limiting equivalent conductance at temperatures other than 20°C. The logarithm of the conductance-viscosity product has been found to be a linear function of the reciprocal of the absolute temperature for all solutions studied. A linear relationship has been found also between the logarithm of the equivalent conductance and the logarithm of the viscosity for all of the solutions over the temperature range studied.

INTRODUCTION

Mixed solvents frequently have some properties which are more desirable in certain respects than those of the pure constituents. Such is the case for a mixture of methanol and acetone. The mixed solvent is less viscous than methanol, thereby permitting increased ionic mobilities; it has greater dissolving power for electrolytes, and is less volatile than acetone. Since mixtures of methanol and acetone should be similar to those of methanol and methyl ethyl ketone (1), the mixed solvent furthermore should have a greater dissociating power for electrolytes than that exhibited by either methanol or acetone.

In this investigation, the conductimetric and viscometric behavior of lithium bromide in 50–50 methanol-acetone has been determined at eight temperatures within the range 20° to −50°C for eighteen solutions having molal concentrations ranging from 418×10^{-4} to 4.14. Densities of the solutions were determined also for use in the conversion of molalities to molarities and for the calculation of absolute viscosities.

EXPERIMENTAL

The anhydrous lithium bromide used in the preparation of the solutions for this investigation was a portion of that described previously (2). Both methanol and acetone were prepared by fractional distillation of 'Baker Analyzed' products after each had been refluxed for 12 hr over calcium oxide. The middle fractions, which were retained, had conductivities of 4.0×10^{-7} and 1.8×10^{-7}, respectively. The solutions were prepared by dissolving in methanol a weighed quantity of anhydrous lithium bromide contained in a tared flask. After dissolution was complete and the solution had cooled, the weight of methanol was determined and an equal weight of acetone was added to make a 50–50 solvent mixture. It was not practicable to use an initially prepared mixed solvent because the heat of solution of the lithium bromide was sufficient to cause appreciable loss of the solvent by vaporization.

Experimental procedures for measurements of the conductances, viscosities, and densities have been described adequately in previous papers (2, 3).

RESULTS

All experimental data except densities are incorporated in figures presented in this paper. Inasmuch as the tabulation of the data would be quite extensive, it has been omitted.[3]

DISCUSSION

The equivalent conductance of lithium bromide at low concentrations in 50–50 methanol-acetone is shown in Fig. 1 as a function of the square root of the concentration. Analysis of conductance data for dilute solutions at 20°C by the Shedlovsky extrapolation method (4) yielded 117.5 ohm^{-1} cm^2 and 4.8×10^{-2} for the limiting equivalent conductance and

[1] Manuscript received September 24, 1954. This paper was prepared for delivery before the Cincinnati Meeting, May 1 to 5, 1955. Based on research performed under a contract with the U. S. Army Signal Corps.

[2] Present address: Standard Oil Company, Whiting, Indiana.

[3] For tables summarizing data pertinent to the conductances, viscosities, and densities for the solutions studied, contact the Department of Chemistry, University of Kentucky.

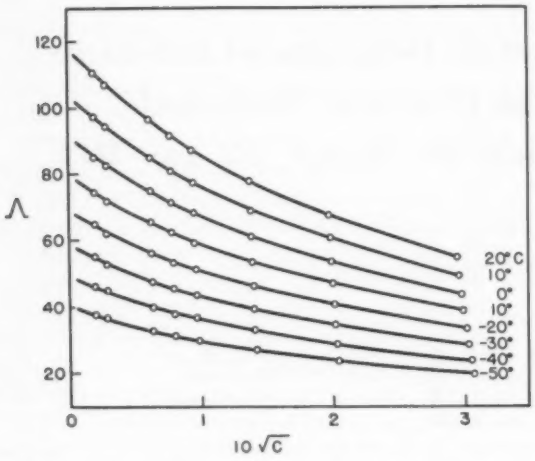

FIG. 1. Equivalent conductance of lithium bromide in 50–50 methanol-acetone.

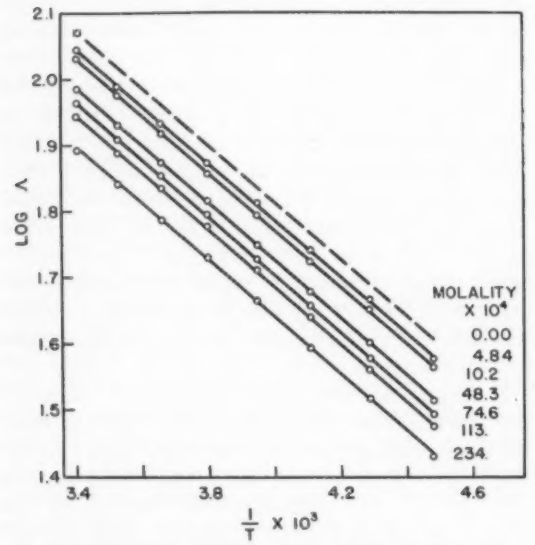

FIG. 2. Temperature dependence of the logarithm of the equivalent conductance of lithium bromide at low concentrations in 50–50 methanol-acetone.

TABLE I. *The limiting equivalent conductance and the conductance-viscosity product for lithium bromide in 50–50 methanol-acetone at temperatures within the range 20° to −50°C*

t°C	Λ_0(ohm^{-1} cm^2)	η_0(poise × 10^3)	$\Lambda_0\eta_0$
20	117.5	3.95	0.465
10	104.1	4.50	0.469
0	91.5	5.14	0.470
−10	79.7	5.93	0.473
−20	68.7	6.91	0.475
−30	58.3	8.16	0.477
−40	49.0	9.76	0.478
−50	40.3	11.95	0.482

dissociation constant, respectively, of lithium bromide in this mixed solvent. Owing to a lack of dielectric constant data, the Shedlovsky method could not be applied at other temperatures.

Plots of the logarithm of the equivalent conductance of the salt in several dilute solutions vs. the reciprocal of the absolute temperature are shown in Fig. 2. The graphs for the five lowest concentrations are linear and have equal slopes. In accordance with results reported in an earlier paper (2), it seemed reasonable to assume that a corresponding plot of the limiting equivalent conductance of lithium bromide in 50–50 methanol-acetone also would be linear and its slope would be identical with that of similar plots in the dilute range. Having available the values of Λ_0 at 20°C and the slope of the plots for dilute solutions, the point-slope method was utilized to construct a large plot of the logarithm of Λ_0 against $1/T$, from which the appropriate information was taken to calculate the limiting conductance data which appear in Table I. Conductance-viscosity products also listed in Table I are approximately constant, although an apparent trend of the product slightly decreasing with increasing temperature may be noted. Such a trend occurs when the limiting equivalent conductance increases at a slower rate than the viscosity decreases as the temperature becomes higher. The relative magnitude of the product, which is approximately 11% less for lithium bromide in 50–50 methanol-acetone than in pure methanol, is evidence that the effective size of the conducting species is greater in the mixed solvent.

The logarithm of the equivalent conductance of solutions of lithium bromide at higher concentrations in 50–50 methanol-acetone is shown in Fig. 3 as a function of the reciprocal of the absolute temperature. It may be observed that the deviation of the plots from linearity increases with increasing concentration. For comparison purposes, corresponding plots involving the viscosity instead of the conductance have been incorporated in Fig. 4. Deviation of these plots from linearity similarly becomes more pronounced with increasing concentration. Owing perhaps to cancelling effects, however, the logarithm of the equivalent conductance-viscosity product is a linear function of the reciprocal of the absolute temperature for all concentrations studied. This may be expressed mathematically as follows:

$$\log (\Lambda\eta) = A + B\left(\frac{1}{T}\right) \qquad (I)$$

where A and B are constants for a given solution representing the intercept and slope, respectively, of a plot of log $(\Lambda\eta)$ vs. $1/T$. Although graphs of this nature have not been included, data pertinent to

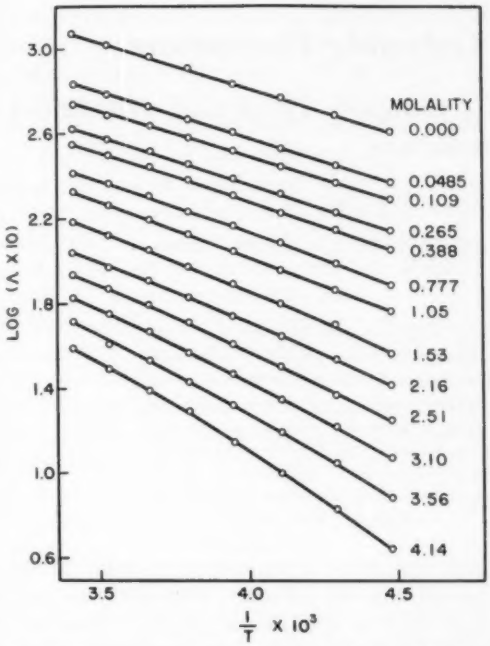

FIG. 3. Temperature dependence of the logarithm of the equivalent conductance of more concentrated solutions of lithium bromide in 50–50 methanol-acetone.

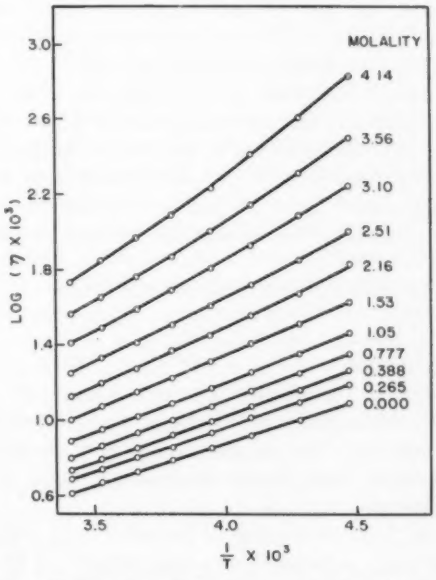

FIG. 4. Temperature dependence of the logarithm of the viscosity of more concentrated solutions of lithium bromide in 50–50 methanol-acetone.

the slopes and intercepts of such plots are listed in Table II. If the value of B were zero, equation (I) would reduce to an expression of the constancy of the conductance-viscosity product which is identical with the Walden relationship for infinite dilution. It may be noted from the data in Table II that B is never zero, but tends to increase with increasing concentration for the system under consideration.

TABLE II. *Slopes and intercepts of plots of equations (I) and (III) for solutions of lithium bromide in 50–50 methanol-acetone*

Molality	Equation (I)		Equation (III)	
	Slope	Intercept	− (Slope)	− (Intercept)
0.000	18	0.613	0.970	0.258
0.265	21	0.239	0.955	0.583
0.388	28	0.192	0.946	0.590
0.777	30	0.123	0.958	0.686
1.05	20	0.142	0.967	0.721
1.53	25	0.105	0.963	0.730
2.16	49	0.001	0.916	0.679
2.51	53	0.010	0.925	0.668
3.10	80	−0.034	0.891	0.589
3.56	102	−0.078	0.869	0.546
4.14	145	−0.177	0.866	0.514

In addition to the relationship between conductance and viscosity discussed above, it has been observed that the logarithm of the equivalent conductance is a linear function of the logarithm of the viscosity over the temperature range for each solution studied. This may be represented by a relationship between conductance and viscosity introduced by Johnston (5) which takes the following form:

$$\Lambda\eta^n = k \qquad \text{(II)}$$

where n and k are constants. Putting into logarithmic form and rearranging, equation (II) becomes

$$\log \Lambda = \log k - n \log \eta \qquad \text{(III)}$$

Hence a plot of $\log \Lambda$ against $\log \eta$ should be linear and should have a slope and an intercept of $(-n)$ and $(\log k)$, respectively. Values of $(-n)$ and $(\log k)$ taken from plots of equation (III) for various more concentrated solutions of lithium bromide in 50–50 methanol-acetone may be found in Table II.

If a value of unity for the slope in equation (III) is evidence of the complete dependence of conductance upon viscosity, the data pertinent to the slope (Table II) indicate that the dependence approaches completeness in dilute solutions.

Any discussion of this paper will appear in a Discussion Section to be published in the December 1955 JOURNAL.

REFERENCES

1. F. M. SACKS AND R. M. FUOSS, *J. Am. Chem. Soc.*, **75**, 5172 (1953).
2. P. G. SEARS, R. L. MCNEER, AND L. R. DAWSON, *This Journal*, **102**, 269 (1955).
3. P. G. SEARS, R. R. HOLMES, AND L. R. DAWSON, *This Journal*, **102**, 145 (1955).
4. T. SHEDLOVSKY, *J. Franklin Inst.*, **225**, 739 (1938).
5. J. JOHNSTON, *J. Am. Chem. Soc.*, **31**, 1010 (1909).

Mathematical Studies of Galvanic Corrosion

II. Coplanar Electrodes with One Electrode Infinitely Large and with Equal Polarization Parameters[1]

JAMES T. WABER AND MARSHALL ROSENBLUTH

University of California, Los Alamos Scientific Laboratory, Los Alamos, New Mexico

ABSTRACT

The expressions for the potential and current density distribution have been derived for the two mathematically similar corrosion problems, (*a*) tiny anodes buried in infinite cathodes, and (*b*) tiny foreign cathodic inclusions in a metal. The implication of using equal polarization parameters has been discussed. When the critical dimension of the tiny electrode becomes smaller than the polarization parameter, corrosion attack and the interfacial potential become more uniform over the galvanic cell. Figures and perspective drawings made to scale are included to illustrate the effect of polarization on the distribution of potential in the corrodent and the diminishing variation of corrosion attack.

INTRODUCTION

In a previous paper (1), the effect of polarization on the behavior of a coplanar galvanic couple was considered negligible. The present paper extends the analysis to include the effect of polarization, and deals with the corrosion behavior of an active metal which is covered by a more noble metal or film. When such barriers are slightly porous, rapid attack occurs at the tiny anodes. This attack is limited by the anodic polarization of these microcells. Another situation occurring frequently in commercial practice and pertinent to this investigation is the dissolution of a metal containing tiny foreign inclusions; in this case, the dissolution rate is regulated by polarization characteristics of the cathodes. To be consistent with the previous paper, the case of infinitesimal anodes will be discussed in detail.

Specifically, an assumption has been made which is more nearly akin to mixed anodic-cathodic control, that is, the polarization parameter,[2] $\mathfrak{P}$, as defined by Wagner (2), is assumed to be equal for both the anode and cathode.

Wagner (3) has pointed out that in many cases the IR drop in the electrolyte is relatively unimportant and that the corrosion behavior of a metal containing foreign inclusions is dictated almost exclusively by such things as the hydrogen overvoltage of the inclusions. Frumkin and Levich (4), in the case of "infinitely small" inclusions, have shown that, when it is necessary to take the ohmic potential drop into account, concentration changes within the corroding solution in the vicinity of the tiny inclusions must also be considered. That is, appreciable concentration gradients must exist in solution in order to continue the supply of hydrogen ions which are rapidly being discharged at the cathode. In the present limiting case, secular changes in electrolyte composition, as well as concentration gradients, have been ignored.

Although the case to be discussed is a finite anode buried in an infinite cathode, it will be shown below that the resulting equations are easily modified to discuss a finite cathode imbedded in an infinite anode. Wagner (5) pointed out that the latter is an important case to analyze, because of its frequent occurrence.

In accordance with Wagner's definition

$$\mathfrak{P}_i = \sigma \left| \frac{d\Delta E_i}{dJ_i} \right| \qquad [1]$$

where σ is the specific conductivity of the corrodent, ΔE_i is the overvoltage of the i-th metal or electrode, and J_i is the appropriate current density. The vertical bars denote the absolute value of the derivatives.

In a given environment, irrespective of physical dimensions, a galvanic cell may behave as though it were "macroscopic" or "microscopic" depending upon whether the critical dimension is larger or smaller than the parameter, $\mathfrak{P}$. The critical dimension, λ, is that one which affects the distribution of current density most strongly. In certain practical cases, it may be the separation of the electrodes, and in others it is the smallest dimension of one electrode.

If the resistance of the corrosive medium is high

[1] Manuscript received November 27, 1953. This paper was prepared for delivery before the Cincinnati Meeting, May 1 to 5, 1955.

[2] Herein $\mathfrak{P}$ has been used in place of Wagner's k to emphasize the fact that this parameter has the dimension of length and to avoid any possible confusion with conductivity for which k is frequently used.

or if $\mathfrak{L}$ is small in comparison to λ, then the previous analysis (1) which assumed negligible polarization is applicable. When $\lambda/\mathfrak{L}$ is large, such galvanic cells will behave as though they were macroscopic. On the contrary, under corrosive conditions that permit strong polarization of the electrodes ($\mathfrak{L}$ is large), even macroscopic elements may behave as though they had microscopic dimensions. The microscopic galvanic cells are characterized by relatively uniform distributions of current density. Wagner's treatment (2) establishes these features.

In the case under consideration, the critical dimension is a, the half width of the anode. The dependence of the maximum and the minimum anodic current densities on the ratio $a/\mathfrak{L}$ are discussed, and the qualitative results discussed above are confirmed.

Mathematical Features of the Analysis

The model to be discussed is shown in Fig. 1. A very long anode of width $2a$ is embedded in the plane of a cathode, $2c$ units wide. The authors then choose the origin to lie at the center of the anode and choose the x axis perpendicular to the long direction of the anode and the y axis perpendicular to the plane of the anode and cathode. As discussed in the previous paper (1), this arrangement has even symmetry. Without the loss of a significant amount of generality one can erect insulating walls at $x = \pm c$, that is, parallel to the length of the anode and parallel to the y axis. The insulator eliminates edge effects and permits one to concentrate on the effects occurring at the anode-cathode junction. Because of the symmetry which has been assumed, current flow parallel to the x axis does not occur in plane $x = 0$. Consequently, attention may be restricted to the first quadrant where x is positive. The electrolyte is poured in at the top and it will be assumed that it extends to $y = \infty$. Flow parallel to the Z axis is assumed to be negligibly small because of the great length of the anode as compared with its width. These features of the model permit attention to be restricted to potential and current distributions which occur in the first quadrant of the XY plane.

Thus far the model is not different from that discussed in the previous paper (1). For the present analysis, however, assume that c is infinitely larger than a. Therefore, boundary conditions must be revised. If $P(x, y)$ is potential, then

$$\lim_{y \to \infty} P(x, y) < M \qquad [2]$$

$$\lim_{x \to \infty} P(x, y) < N \qquad [3]$$

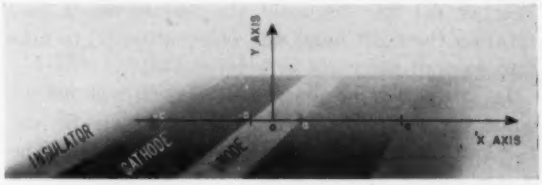

Fig. 1. Perspective sketch illustrating the geometric relation of the electrodes.

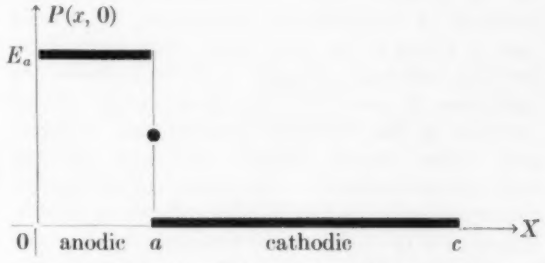

Fig. 2. Distribution of the unpolarized interfacial potential over the electrode.

where M and N are arbitrary large numbers. Since current flow at $x = 0$ and $x = c$ must not occur parallel to x axis, it is clear that

$$\left.\frac{\partial P}{\partial x}\right|_{x=0} = 0 \qquad [4]$$

$$\lim_{c \to \infty} \left.\frac{\partial P}{\partial x}\right|_{x=c} = 0 \qquad [5]$$

The anode induces a potential in the corrodent relative to the cathode. Define this difference as E_a such that

$$E_a = E_{a(0)} - E_{c(0)} \qquad [6]$$

where $E_{a(0)}$ is the potential of the anode extrapolated to zero current density and $E_{c(0)}$ is the similar potential of the cathode; using the Lewis and Randall sign convention, E_a is positive.

In the absence of polarization, the potential on the anode-cathode plane is illustrated in Fig. 2 and is proportional to the step function, $S'_a(x)$.

A further boundary condition imposed by this choice of the galvanic cell is

$$P^*(x, 0) = E_a S'_a(x) + \mathfrak{L} \left.\frac{\partial P^*}{\partial y}\right|_{y=0} \qquad [7]$$

where the infinite step function is

$$S'_a(x) = \begin{cases} 1 \\ 0 \end{cases} \quad \text{for} \quad \begin{cases} 0 \le x \le a - 0 \\ a + 0 \le x \le \infty \end{cases} \qquad [7a]$$

and where it has been assumed that

$$\mathfrak{L}_a = \mathfrak{L}_c = \mathfrak{L} \qquad [8]$$

Wagner (2) has discussed the use of the second term on the right hand side of equation [7] to take into account the effect of polarization.

In general, the values of $\mathfrak{L}_a$ and $\mathfrak{L}_c$ will not be equal because of different slopes of the anodic and the cathodic potential-current density curves. The special case $\mathfrak{L}_a$ equals $\mathfrak{L}_c$, however, is amenable to a straightforward mathematical treatment, whereas a treatment of the more general case $\mathfrak{L}_a$ is not equal to $\mathfrak{L}_c$ requires rather cumbersome numerical methods. A mathematical analysis of the special case $\mathfrak{L}_a$ equals $\mathfrak{L}_c$ has been worked out, since disregard of polarization leads to inconsistencies. In particular, if polarization is ignored, the current densities at the boundary between local cathodes and anodes become infinite, and even average values of the cathodic or the anodic current density cannot be calculated as has been shown in Part I. Results for the special case $\mathfrak{L}_a$ equals $\mathfrak{L}_c$ show the general effect of polarization. These results may also be used for a qualitative discussion of the more general case $\mathfrak{L}_a$ is not equal to $\mathfrak{L}_c$ as is shown below.

Inasmuch as there are no sources or sinks for electrons or ions within the electrolyte and since there is no space charge, the potential satisfies Laplace's equation.

Consider first the case where $\mathfrak{L} = 0$, since the resulting integrals are useful for the further analysis of the more general nonzero case which will be discussed subsequently. The mathematical features of the derivation have been discussed elsewhere (6).

Negligible Polarization

It is clear that a potential of the form

$$P(x, y) = \int_0^\infty A(n) \cos(nx) \exp(-ny)\, dn \quad [9]$$

will satisfy the two dimensional form of Laplace's equation, and have even symmetry since

$$\int_0^\infty A(n) \cos(nx) \exp(-ny)\, dn = \int_0^\infty A(n) \cos(-nx) \exp(-ny)\, dn \quad [9a]$$

This function is bounded for all positive x and y values and both x-derivatives are zero as required by [4] and [5]. The quantity $A(n)$ is unspecified in definition [9] but is chosen so that condition [7] is satisfied. The procedure for evaluating $A(n)$ is equivalent to finding the unspecified coefficients of a Fourier series. When $\mathfrak{L} = 0$ in [7], then

$$P(x, +0) = \int_0^\infty A(n) \cos(nx)\, dn = S_a'(x) E_a \quad [10]$$

Multiplying both sides of [10] by $\cos(mx)$ and integrating with respect to x one obtains

$$\int_0^\infty dn A(n) \int_0^\infty \cos(mx) \cos(nx)\, dx = E_a \int_0^\infty S_a'(x) \cos(mx)\, dx \quad [11]$$

The inner integral is equal to the Dirac delta function $\delta(n - m)$. Using its definition, one sees that

$$\int_0^\infty A(n)\delta(n - m)\, dn = \frac{E_a}{m} \sin(am) \quad [12]$$

Thus

$$A(m) = \frac{2E_a}{\pi} \frac{\sin(am)}{m} \quad [13]$$

Consequently the value of the potential is

$$P(x, y) = \frac{2E_a}{\pi} \int_0^\infty \frac{\sin(an)}{n} \cos(xn) \exp(-yn)\, dn \quad [14]$$

By employing the pertinent trigonometric identity, one obtains

$$P(x, y) = \frac{E_a}{\pi} \int_0^\infty \frac{1}{n} [\sin(a + x)n + \sin(a - x)n] \cdot \exp(-yn)\, dn \quad [15]$$

By noting that

$$\int_y^\infty \exp(-ku)\, du = \frac{1}{k} \exp(-ky) \quad [16]$$

the integrals in [15] may be simplified to

$$P(x, y) = \frac{E_a}{\pi} \int_y^\infty du \int_0^\infty [\sin(a + x)n + \sin(a - x)n] \cdot \exp(-un)\, dn \quad [17]$$

Integrating the inner integral (in n) twice by parts and solving the resulting equation for the integral one can demonstrate that

$$P(x, y) = \frac{E_a}{\pi} \int_y^\infty \left[\frac{(a + x)}{(a + x)^2 + u^2} + \frac{(a - x)}{(a - x)^2 + u^2}\right] du \quad [18]$$

The latter integral may be evaluated as

$$P(x, y) = \frac{E_a}{\pi}\left[\pi - \arctan\left(\frac{y}{a + x}\right) - \arctan\left(\frac{y}{a - x}\right)\right] \quad [19]$$

or as

$$P(x, y) = \frac{E_a}{\pi}\left[\arctan\left(\frac{a + x}{y}\right) + \arctan\left(\frac{a - x}{y}\right)\right] \quad [20]$$

By simple algebra one may verify that, as y approaches zero, P converges to E_a for x less than a and to zero for x greater than a.

A further value of performing the integration with $\mathfrak{P} = 0$ is that the corrosion current may be derived from [20], whereas the integrals derived for the more general case are difficult to evaluate at $\mathfrak{P} = 0$. This subject will be discussed in a later section.

More General Case $\mathfrak{P} \neq 0$

The required procedure is strictly analogous to that discussed above. After differentiation of [9] with respect to y and substitution of the result into [7] it may be seen that

$$\int_0^\infty [A^*(n) + n\mathfrak{P}A^*(n)] \cos(xn)\, dn = E_a S_a'(x) \quad [21]$$

where $A^*(n)$ is written to distinguish it from the function $A(n)$. The asterisk is used throughout to denote the inclusion of polarization in the argument. Proceeding as in [11] and [12] it is clear that

$$A^*(m) = \left(\frac{2E_a}{\pi}\right) \frac{\sin(am)}{m(1 + \mathfrak{P}m)} \quad [22]$$

Upon substitution of [22] into [9] and use of the trigonometric identity it follows that

$$P^*(x, y) = \frac{E_a}{\pi}\left[\int_0^\infty \frac{\sin(a + x)n}{n(1 + \mathfrak{P}n)} \exp(-ny)\, dn + \int_0^\infty \frac{\sin(a - x)n}{n(1 + \mathfrak{P}n)} \exp(-yn)\, dn\right] \quad [23]$$

This can be integrated by decomposing the fraction into a sum of two simpler fractions, namely, by noting that

$$\frac{\sin(a + x)n}{n(1 + \mathfrak{P}n)} = \left(\frac{1}{n} - \frac{\mathfrak{P}}{1 + \mathfrak{P}n}\right) \sin(a + x)n \quad [24]$$

The potentials have been evaluated from the resulting integrals and are tabulated elsewhere (7).

Evaluation of Current Density

As was discussed in the previous paper (1), the anodic current density, J_a, is defined in terms of the normal gradient evaluated at the interface. That is

$$J_a^*(x) = -\sigma \left.\frac{\partial P^*}{\partial y}\right|_{y=0} \qquad (0 \leq x \leq a - 0) \quad [25]$$

where σ is the specific conductivity. It is desirable to evaluate the current in a manner which is independent of the galvanic system under consideration. For convenience, introduce a dimensionless parameter to represent the current density. Thus

$$C_a^* = \left(\frac{-2a}{E_a}\right) \left.\frac{\partial P^*}{\partial y}\right|_{y=0} \quad [26]$$

This expression involves the potential difference of unpolarized electrodes, the critical dimension, and the normal gradient, which depends upon the geometry of the couple. Thus, C_a^* may be applied to any galvanic system, providing the polarization parameters are equal. Equations [20] and [23] are used most conveniently for calculating the normal derivative. Thus

$$-\left(\frac{2a}{E_a}\right) \frac{\partial P}{\partial y} = \frac{2a}{\pi}\left[\frac{a + x}{y^2 + (a + x)^2} + \frac{a - x}{y^2 + (a - x)^2}\right] \quad [27]$$

$$\left(\frac{-2a}{E_a}\right) \frac{\partial P^*}{\partial y} = \frac{2a}{\pi}\left[\int_0^\infty \frac{\sin(a + x)n}{(1 + \mathfrak{P}n)} \exp(-yn)\, dn + \int_0^\infty \frac{\sin(a - x)n}{(1 + \mathfrak{P}n)} \exp(-yn)\, dn\right] \quad [28]$$

Both of these expressions are simplified when $y = 0$. The integrals resulting from [28] may be evaluated by making the substitution,

$$s \equiv 1 + \mathfrak{P}n \quad [29]$$

by using [26], and the following definitions of λ and λ'.

$$\lambda \equiv (a + x)/\mathfrak{P} \qquad \lambda' \equiv (a - x)/\mathfrak{P} \quad [30]$$

Thus,

$$C_a^*(x) = \frac{2a}{\pi\mathfrak{P}} \cdot\left[\int_1^\infty \frac{\sin\lambda(s - 1)}{s}\, ds + \int_1^\infty \frac{\sin\lambda'(s - 1)}{s}\, ds\right] \quad [31]$$

Using the appropriate trigonometric identity one obtains

$$C_a^*(x) = \frac{2a}{\pi\mathfrak{P}} \cdot\left[\cos\lambda \int_1^\infty \frac{\sin\lambda s}{s}\, ds - \sin\lambda \int_1^\infty \frac{\cos\lambda s}{s}\, ds + \cos\lambda' \int_1^\infty \frac{\sin\lambda' s}{s}\, ds - \sin\lambda' \int_1^\infty \frac{\cos\lambda' s}{s}\, ds\right] \quad [32]$$

Values of the sine and cosine integrals in [32] are available (8). Using the following definitions of these integrals in their usual tabulated form

$$Si(\lambda) = \int_0^\lambda \left(\frac{\sin s}{s}\right) ds \quad [33]$$

$$Ci(\lambda) = \int_\infty^\lambda \left(\frac{\cos s}{s}\right) ds \quad [34]$$

$$-si(\lambda) = \frac{\pi}{2} - Si(\lambda) \quad [35]$$

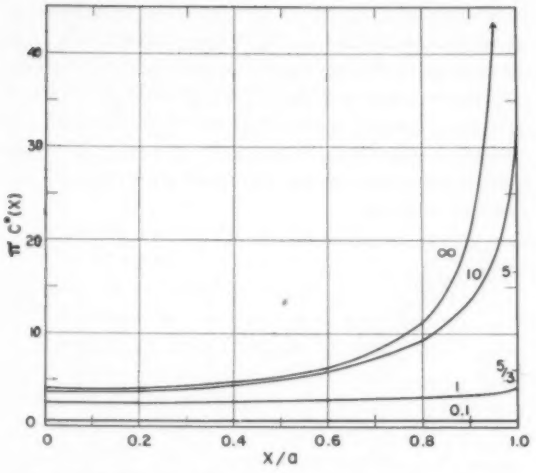

FIG. 3. Effect of polarization on the variation of anodic current density parameter. Curves are for different values of $a/\mathfrak{P}$.

TABLE I. *Values of the current density parameter as a function of* $a/\mathfrak{P}$

$a/\mathfrak{P}$	Max C_a^*	Min C_a^*	Max C_a^*/Min C_a^*
0.001	0.002002	0.001998	1.0004
0.01	0.01944	0.01936	1.0045
0.1	0.1723	0.1644	1.049
1.0	1.2540	0.7913	1.585
5/3	1.9232	1.0262	1.874
5	5.3124	1.1976	4.436
10	10.317	1.2497	8.256
100	100.318	1.2707	78.95
1000	1000.32	1.2732	785.65
∞	∞	1.2732	∞

the anodic current may be written as

$$C_a^*(x) = \frac{2a}{\pi\mathfrak{P}} [Ci(\lambda) \sin \lambda - si(\lambda) \cos \lambda - si(\lambda') \cos \lambda' + Ci(\lambda') \sin \lambda'] \quad [36]$$

Expression [36] was used to evaluate the current density for several values of $\mathfrak{P}$ and λ.

Since few tabulated values of Ci and Si are available (8) for λ greater than 20, it was necessary in some cases to employ the following complex variable relationship

$$Ci(\lambda) + i\, si(\lambda) = \frac{\exp(-i\lambda)}{i\lambda} H(i\lambda) \quad [37]$$

where the series $H(i\lambda)$ is defined as

$$H(v) \equiv \sum_{n=0}^{\infty} \frac{n!}{v^n} \quad [38]$$

This series is semiconvergent for modulus of v much greater than 1. It may be simply shown by separating real and imaginary parts that

$$Ci(\lambda) = \frac{i}{2\lambda} \cdot [H(-i\lambda) \exp(-i\lambda) - H(i\lambda) \exp(i\lambda)] \quad [39]$$

$$si(\lambda) = \frac{-i}{2\lambda} \cdot [H(-i\lambda) \exp(-i\lambda) + H(i\lambda) \exp(i\lambda)] \quad [40]$$

The maximum value of the current density parameter will occur at the anode-cathode junction and the minimum at the center of the total anode, i.e., at the origin. That is, the maximum and minimum values are

$$\text{Max } C_a^*(x) = C^*(a) \quad [41]$$

$$\text{Min } C_a^*(x) = C^*(0) \quad [42]$$

Employing a definition analogous to [26] for the case in which $\mathfrak{P} = 0$, i.e., for negligible polarization, the equivalent statements are

$$\text{Max } C_a(x) = C(a) = \infty \quad [43]$$

$$\text{Min } C_a(x) = C(0) = \frac{4}{\pi} \quad [44]$$

as can be seen from equation [27] which has been evaluated at $y = 0$. Equations [41] and [42] have been numerically evaluated for a large range of $\mathfrak{P}$ values.

It may be shown, using l'Hopital's rule that

$$\lim_{\lambda' \to 0} Ci(\lambda') \sin \lambda' = 0 \quad [45]$$

and thus [36] may be evaluated at $x = a$.

Numerical Evaluation of the Current Density Parameter

Values of the current density parameter $C_a^*(x)$ have been evaluated for three ratios of $a/\mathfrak{P}$, namely 0.1, 1, and 10. In addition $C_a(x)$ has been computed. Equation [36] was employed to evaluate $C_a^*(x)$ and equation [27] was used to obtain $C(x)$ after substituting definition [26] and setting y equal to zero. These values have been plotted and presented in Fig. 3.

From Fig. 3 it is clear that the distribution of current density becomes more uniform as $\mathfrak{P}$ increases for a fixed value of a. Or, expressed differently, the distribution approaches that characteristic of "microscopic" galvanic elements as $a/\mathfrak{P}$ becomes "microscopically" small. The maximum values of $C^*(x)$ have been added to Fig. 3 for $(a/\mathfrak{P})$ equal to 5 and to 5/3.

The results of a number of the evaluations of Max C_a^* and Min C_a^* as well as their ratio are presented in Table I. By looking at this ratio it is evident that corrosion attack is more uniform for

small values of $a/\mathfrak{L}$ than for large; that is, it is more uniform when a is microscopic in comparison with the polarization parameter.

Evaluation of Relative Potentials

Space does not permit detailed reduction of equation [23] to a form involving only tabulated functions. Waber (7) has discussed this problem in detail and obtained numerical values for four values of the ratio of $a/\mathfrak{L}$.

Perspective drawings of the potential fields for various x, y, a, and $\mathfrak{L}$ values have been prepared. In order to present such data in a form which is independent of the galvanic system under consideration, the reduced and dimensionless potential functions $P^*(x/2a,\ y/2a)/E_a$ as well as $P(x/2a,\ y/2a)/E_a$ have been plotted. These perspective views of the potential fields can be seen in Fig. 3, 4, 5, and 6.

In these drawings, the reduced potential function is plotted vertically and the reduced interfacial potential is plotted on the XY plane. The degree to which the interfacial potential has been reduced by polarization is indicated by the cross hatching. The unpolarized reduced potential is one in the anodic region and zero in the cathodic. However, polarization reduced the interfacial potential by a considerable amount. The authors have indicated the effect of polarization on the cathodic region by a different convention to indicate that this region is hidden from view by the curved potential surface. In Fig. 3, specifically, they have indicated the hidden portion of the interfacial potential by the same convention. However, in this figure the polarization has been assumed to be negligible.

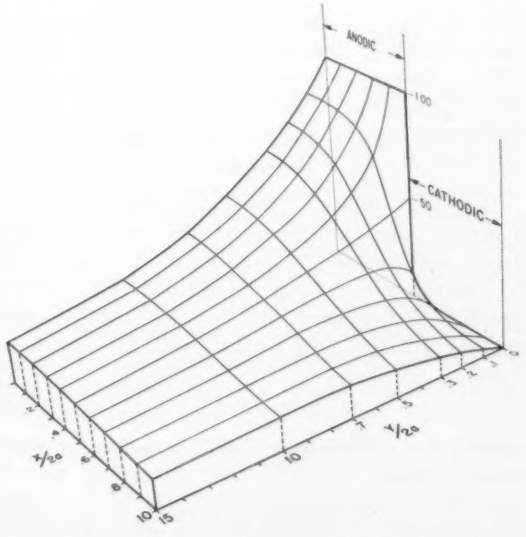

FIG. 4. Perspective scale drawing of the reduced potential function evaluated for $a/\mathfrak{L}$ equal to infinity.

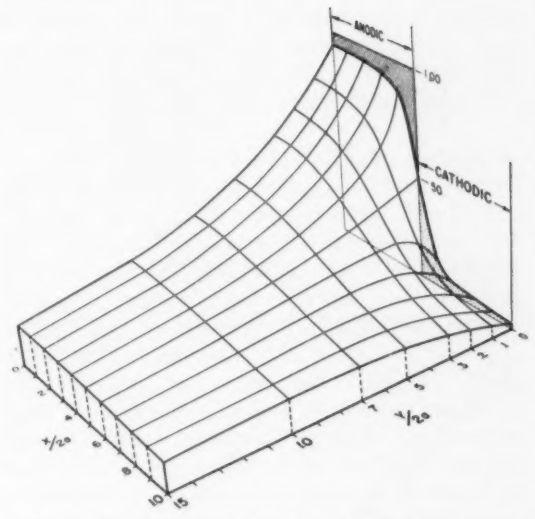

FIG. 5. Perspective scale drawing of the reduced potential function evaluated for $a/\mathfrak{L}$ equal to 10.

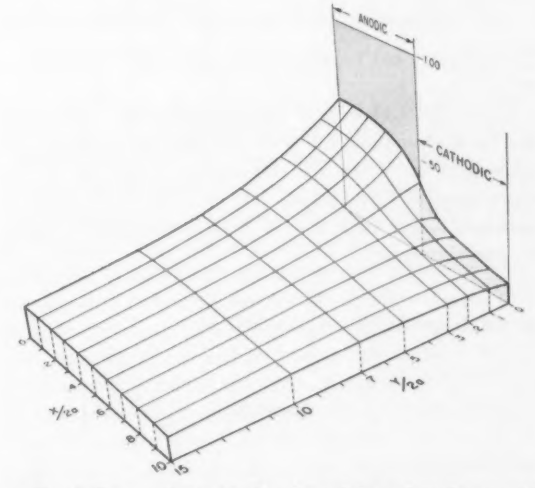

FIG. 6. Perspective scale drawing of the reduced potential function evaluated for $a/\mathfrak{L}$ equal to 1.

In Fig. 3, the reduced interfacial potential at the anode-cathode boundary, i.e., at $x/2a = 0.5$, is one-half. However, in the case of polarization, as shown by the other three figures, this potential value is less than one-half and approaches zero as $\mathfrak{L}$ becomes very large.

Evaluation of the Interfacial Potential

Variation of the potential can be computed at the electrode-liquid interfaces from the relative current distribution. Equation [26] can be substituted back into [7] to give

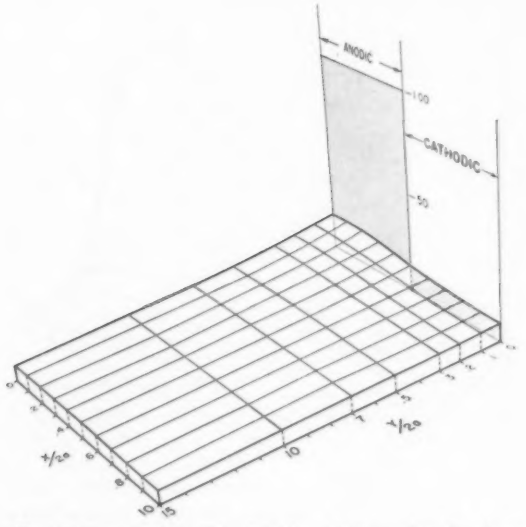

FIG. 7. Perspective scale drawing of the reduced potential function evaluated for $a/\mathfrak{P}$ equal to 0.1.

$$P^*(x, 0) = E_a S'_a(x) - \mathfrak{P} E_a C^*_a(x)/2a \qquad [46]$$

Thus, numerical values can be obtained from values of $C^*_a(x)$.

Since the cosine and sine integrals [33] and [34] are tabulated only for positive arguments (8), it is necessary to write the interfacial potential in a more general form which can be evaluated when x becomes larger than a or λ' becomes negative. Such an expression is

$$\begin{aligned} 2P^*(x, 0) = E_a \Big\{ & 1 - \frac{2}{\pi} \sin \lambda Ci(\lambda) \\ & - \cos \lambda \left[1 - \frac{2}{\pi} Si(\lambda) \right] \Big\} \\ & + E_a \nabla(x) \Big\{ 1 - \frac{2}{\pi} \sin |\lambda'| \, Ci |\lambda'| \\ & - \cos |\lambda'| \left[1 - \frac{2}{\pi} Si |\lambda'| \right] \Big\} \end{aligned} \qquad [47]$$

where $\nabla(x)$ is defined by

$$\nabla(x) = 2S'_a(x) - 1 = \begin{cases} 1 \\ 0 \\ -1 \end{cases} \text{ for } \begin{cases} x < a \\ x = a \\ x > a \end{cases} \qquad [48]$$

The interfacial potential over the anode can be evaluated by means of either [46] or [47]. Certain features of the interfacial potential have already been discussed. Further discussion has been deferred to a later section.

Consideration of an Infinitely Small Cathode

The practical cases of tiny cathodes (arising from impurities) imbedded in a large anode warrant consideration. The only modification (6) required is a shift in the potential scale so that the extrapolated potential of the unpolarized anode is taken to be zero. The cathodic width is c, and the cathodic potential, E_c, can be obtained from boundary condition [6]. Thus

$$E_c = E_{c(0)} = -E_a \qquad [49]$$

Boundary condition [7] may be written as

$$\frac{P^*(x, 0)}{E_a} = \frac{\mathfrak{P}}{E_a} \left. \frac{\partial P^*}{\partial y} \right|_{y=0} \qquad [50]$$

for the new cathodic regions, namely

$$0 \leqq x < c \qquad [51]$$

The change of sign E_a in [49] also changes the sign of P. The sign of the derivative term in [50] is not changed because the direction of flow of ions remains correct. It is clear that

$$\frac{2c}{E_a} \frac{\partial P^*}{\partial y} \text{ is } \begin{cases} < 0 \\ > 0 \end{cases} \text{ for } \begin{cases} c < x \leqq \infty \\ \text{anodic} \\ 0 \leqq x \leqq c - 0 \\ \text{cathodic} \end{cases} \qquad [52]$$

Thus the problem of tiny imbedded cathodes leads to identical equations and results, except for a change in sign of the potential.

However, the proper value of $\nabla(x)$ must be used in [47] to obtain the cathodic current density function $C^*(x)$. It may be evaluated from the expression

$$C^*_c(x) = \frac{2a}{\pi \mathfrak{P}} \left[S'_a(x) - \frac{P^*(x, 0)}{E_a} \right] \qquad [53]$$

with the condition that x is greater than a.

Some Experimental Values of Polarization Parameters

Numerical values of the polarization parameter $\mathfrak{P}$ depend upon the electrolyte as well as on the anodic and cathodic metals involved. Wagner (2) has shown how $\mathfrak{P}_c$ may be derived from Tafel's equation if hydrogen evolution and related phenomena are the predominant cathodic processes. Thus

$$\mathfrak{P}_c = \sigma\beta/J_c \qquad [54]$$

where β is a coefficient in Tafel's equation for overvoltage, namely

$$\eta = \text{constant} + \beta \log_e J_c \qquad [55]$$

One is forced in many cases to use this general expression since experimenters frequently do not

obtain polarization curves applicable to their experimental conditions.

Typical values have been calculated from the literature to indicate the order of magnitude of the polarization parameters. Using formula [54], Wagner (2) obtained an approximate value of ℓ_c from Mantzell's data. Depending on the current density ℓ_c lies in the range 0.025–0.083 cm. One may calculate from Copson's data (9) that ℓ_c lies in the range 0.81–2.41 cm.

Anodic potentials have not been extensively studied. Piontelli and Poli have systematically studied the effect of current density on the anodic dissolution of lead, tin, antimony and bismuth, copper, cadmium, thallium, and silver in a wide variety of solutions (10). Certain of their data indicate that the potential curves for anodic dissolution at moderate current densities change from a logarithmic function of current density to a linear one as the temperature of the medium increases. Thus, one may use the slope of the linear curve to evaluate ℓ_a. This has the advantage that ℓ_a is not a function of J_a and, hence, more useful values can be obtained.

Using Piontelli's data for the anodic dissolution of lead in 0.5M lead perchlorate, ℓ_a at 75°C was approximately 0.05 cm and increased to 0.14 cm at 50°C. The data for copper at 25°C dissolving in a 1M cupric perchlorate, 1M perchloric acid mixture gave ℓ_a equal to 0.3 cm.

These data indicate that test specimen anodes larger than a few inches will probably behave "macroscopically" in a wide variety of conditions if strong electrolytes are used.

Previous Studies

No experimental investigations are known to the authors in which the distribution of corrosion attack was systematically studied on systems where one electrode was very large in comparison to the other. A number of authors have studied the effects of electrolyte composition on the rate of corrosion of relatively pure metals containing intentional (or unintentional) foreign inclusions in an effort to establish the importance of local cell action. Despite the general significance of such work, it does not seem germane to the present discussion.

The most pertinent experimental study was conducted by Thornhill and Evans (11) in 1938, who investigated the variation in current flowing between a scratch line made on iron wetted with sodium bicarbonate, the concentration of which was chosen to cause rusting along the scratch but not elsewhere. However, the experimental arrangement permitted them to investigate only the horizontal gradient of potential.

The studies of Jaenicke and Bonhoeffer (12) and Daniel-Bek (13) are not pertinent to the limiting case under discussion here since the anodes and cathodes were nearly equal in size. Their thorough experimental studies will be analyzed and compared in a subsequent report.

At approximately the same time, Wagner (3) as well as Frumkin and Levich (4) were carrying on important theoretical investigations. Specifically, these authors had addressed themselves to the significant problem of the acid dissolution of a metal containing foreign inclusions, and had described the conditions under which the *IR* drop in the electrolyte was unimportant.

Frumkin and Levich (4) showed that the ohmic potential drop (evaluated for zinc containing nickel inclusions dissolving in sulfuric acid) does not exceed 13 mv if the radius of the inclusions was approximately 1 μ. Guertler and Blumenthal (14) showed experimentally that the *IR* drop was very small in two rather similar cases. As these various authors have pointed out, the corrosion of metals containing foreign inclusions is regulated by the polarization characteristics of the inclusions.

Discussion

It should be made clear that the present investigation is an idealized limiting case. The most serious limitation is that equal polarization parameters have been assumed. Not only may ℓ_a and ℓ_c be different in a given cell, but they may vary individually over the two electrodes.

As indicated above, the range of ℓ values is relatively small in any of the studies made to date. The assumption that $\ell_a = \ell_c$ is not seriously in error if the ratio of a/ℓ is either very small or very large, since in either range, fivefold changes, for instance, of this ratio do not significantly affect the interfacial potential or the current density.

The information gleaned from the two papers of Piontelli and Poli indicates that ℓ_a may be relatively insensitive to the current density and thus remain constant over a given electrode element. The current density distribution does not change very much over a tiny cathode if a/ℓ is smaller than one as shown in Table I. This in turn means that ℓ_c does not change significantly over the tiny electrode as shown by equation [54].

The question of how ℓ will vary over the infinite electrode, if it is dependent upon the current density, has not been fully investigated. One may use a qualitative argument. Since only a finite amount of cathodic current must flow which is equal in amount to the total anodic current, it is evident that J_c must decrease in size as x approaches infinity. This strongly indicates that ℓ would not be

uniform if computed from equation [54], but would increase drastically as if it were computed from measurements farther and farther away from the anode-cathode junction. Fortunately, the current distribution becomes more uniform as $a/\mathfrak{L}$ decreases; hence, this influence would tend to counterbalance any increase in $\mathfrak{L}$ due to the forced decrease in J_c. At distances several times as large as $\mathfrak{L}$, the interfacial potential and, thus, current density on the infinite electrode side of the junction become relatively uniform. Take, for example, the most drastic case shown in this paper, namely $a/\mathfrak{L} = 10$, as shown in Fig. 5, the interfacial potential decreases rapidly near the boundary. At distances of, say, $3(\mathfrak{L}/a)$ beyond the boundary, i.e., at $x/2a = 0.65$, the interfacial potential becomes rather uniform. Clearly the same is true on the anodic side for $x/2a < 0.35$. The current densities have not been evaluated on the larger electrode; however, one can clearly see the equivalent trend in the anodic current density illustrated in Fig. 3. The quantity $C^*(x)$ is relatively uniform for distances $x/a < 0.7$ for the three finite values of $a/\mathfrak{L}$.

One may summarize this much of the discussion by saying that the interfacial potential is virtually the same for the anode and the cathode if both $\mathfrak{L}_a$ and $\mathfrak{L}_c$ are much greater than the width of the small electrode. In other words, the IR drop within the corroding electrolyte between anodic and cathodic areas will be relatively insignificant under these conditions, that is, when $\mathfrak{L}$ is large in relation to a.

It is clear from inspecting the perspective drawings that the variation in potential in a direction parallel to the electrode surface is greatest at the interface between the electrode and the liquid. This variation in potential diminishes as one recedes from the interface and approaches a constant potential value at great distances. It has been shown (6) that this constant is equal to $E_a(a/c)$ for the condition $\mathfrak{L}_a = \mathfrak{L}_c$. This value has been called the potential of a composite electrode. It is evident that this potential, which is obtained with a remote reference electrode, is dependent not only on the potential difference E_a, but also on the relative proportions of anodic to cathodic material. In the present case, the composite electrode will have zero or negligible potential except in the immediate vicinity of the tiny electrode. This fact indicates the relative futility of attempting to locate individual anodic and cathodic areas by potential mapping of relatively homogeneous metal specimens. It is pertinent to the application of the rotogenerative technique as described by Francis (15) to practical problems.

Mathematically one can readily deduce these results from the expressions for the potential function. It is evident that

$$P(x, \infty) = E_a\left(\frac{a}{c}\right) = 0 \qquad [56]$$

from equation [20]. In equation [23], the integrands become zero as y approaches infinity and, thus, $P^*(x, \infty)$ becomes zero.

It is significant that the interfacial potential becomes $E_a(a/c)$ when $\mathfrak{L}$ becomes infinitely large. This has been demonstrated in a companion study (7). It is evident from equation [23] that the integrands vanish for infinite $\mathfrak{L}$. Hence, P^* approaches the value for the composite electrode, namely, zero for infinite $\mathfrak{L}$.

The potential within the electrolyte is "squeezed" between the interfacial potential $P^*(x, 0)$ and the remote potential $P^*(x, \infty)$ and, as $a/\mathfrak{L}$ becomes very small, any variation eventually vanishes. That is, any potential variation in the solution is smaller than that observed on the interface. Under conditions of strong polarization, variation of the latter becomes negligible.

The current density and the total anodic current remain finite for a given width of the anode. Consideration of tiny cathodes leads to equivalent results. This finite current density is different from calculations in which the effect of polarization is ignored. This fact justifies the present calculations in spite of the rather artificial condition of equal polarization parameters.

Summary

The distribution of current density over the anode and the distribution of potential within the electrolyte have been obtained mathematically for the condition that one electrode is infinitely large in comparison with the other, and for the condition that the polarization parameter, as defined by Wagner, is equal for both electrodes. Values of the maximum and minimum values of the current density parameter have been obtained for nine values of the parameter $(a/\mathfrak{L})$ in the range from 0.001 to 1000. In addition, detailed values of the interfacial potential and anodic current densities were calculated for three values of $(a/\mathfrak{L})$, namely, 0.1, 1, and 10. In agreement with the results of Wagner and others, the distribution of current density is more uniform for the smaller values of $(a/\mathfrak{L})$.

Acknowledgments

The authors are indebted to Max Goldstein, Jane Ingersoll, Chester Kazek, and John Ruth who assisted in evaluating the expressions and checking

the accuracy of the derivations. The friendly advice and inspiring suggestions of Carl Wagner are gratefully acknowledged.

Any discussion of this paper will appear in a Discussion Section to be published in the December 1955 JOURNAL.

REFERENCES

1. J. T. WABER, *This Journal*, **101**, 271 (1954).
2. C. WAGNER, *ibid.*, **98**, 116 (1951).
3. C. WAGNER, "Handbuch der Metallphysik," Vol. I, Part 2, p. 195, Akad. Verlagsgesellschaft Becker & Erler, K. G., Leipzig (1940).
4. A. FRUMKIN AND B. LEVICH, *Acta. Physicochim. U.R.S.S.* (in English), **18**, 325 (1943).
5. C. WAGNER, *This Journal*, **99**, 1 (1952).
6. J. T. WABER, "Mathematical Studies of Galvanic Corrosion, Part III. Effects of Polarization," AEC Document LA-1386, March 1952.
7. J. T. WABER, "Mathematical Analysis of Galvanic Corrosion, Part I. Potential Evaluations for Coplanar Electrodes with One Electrode Infinitely Large and with Equal Polarization Parameters," AEC Document LA-1651, June 1954.
8. ANON., "Tables of Sine, Cosine and Exponential Integrals," Vol. 2, Federal Works Agency, Works Project Administration for the City of New York (1940).
9. H. R. COPSON, *This Journal*, **84**, 71 (1943).
10. R. PIONTELLI AND G. POLI, *Gazz. chim. ital.*, for lead, **78**, 717 (1948); tin, **79**, 210 (1949); antimony and bismuth, **79**, 214 (1949); copper, **79**, 538 (1949); cadmium, **79**, 635 (1949); thallium, **79**, 642 (1949); silver, **80**, 107 (1950).
11. R. S. THORNHILL AND U. R. EVANS, *J. Chem. Soc. (London)*, **1938**, 614.
12. W. JAENICKE AND K-F. BONHOEFFER, *Z. physik. Chem.*, **193**, 301 (1944).
13. V. S. DANIEL-BEK, *Zhur. Fiz. Khim.*, **15**, 382 (1941); **18**, 247 (1944); **20**, 567 (1946).
14. W. GUERTLER AND B. BLUMENTHAL, *Z. physik. Chem.*, **152**, 197 (1931).
15. J. B. MCANDREW, W. N. COLNER, AND H. T. FRANCIS, Nat. Advis. Council for Aeron., Tech. Note 2523 (November 1951) 12 pp.

Discussion Section

ELECTRONIC CONFIGURATION IN ELECTRODEPOSITION FROM AQUEOUS SOLUTION

I. The Effect of Ionic Structure

E. H. Lyons, Jr. (pp. 363–375)

A. A. Vlček[1]: The rules which govern the relations of mechanism of electrode processes to structure of inorganic compounds are perhaps oversimplified in Lyons' paper. From the comparison of all experimental polarographic data on the behavior of inorganic compounds with their structure, especially their electronic configuration, it is possible to deduce the following rules.

1. It is most probable that irreversibility and overvoltage of an electrode process are not of an electrolytical, but of a chemical nature, due to a slow step in the whole electrode process, the primary electron transfer being rapid in comparison with other stages of the electrode process (in agreement with Heyrovský,[2] Libby,[3] and Lyons[4]).

2. The electrode process (reduction or deposition of a metal) can follow one of three paths:

(*a*) Direct acceptance of an electron by a free stable orbital [this occurs especially with transition metal ions with free $(n - 1)$ *d* orbitals]. If no change occurs in the structure of reacting particles after the acceptance of the electron, the electrode process is very rapid and reversible. (Only to this special case can Libby's symmetry rule and Lyons' definition of conditions for reversibility be applied.)

(*b*) Dissociation of one or more ligands resulting in loosening one or more *hybrid* orbitals by which the electron can be accepted (complexes of nontransition metal ions).

(*c*) Acceptance of the electron by a peripheral orbital (i.e., orbital higher than the orbitals occupied by electrons from ligands) with subsequent change of configuration of the particle. If this change is very slow, the particle is not reducible. This often holds for inner orbital complexes of transition metal ions which have the complete rare-gas structure, or for inert complexes of outer orbital type, especially for 6-coordinated complexes. This type of mechanism gives a specification of Lyons' rule according to which the metal is not deposited from inner orbital complexes. There are many examples of outer orbital complexes which are not reducible and of inner orbital complexes which are reducible,[5] so that Lyons' rule is not generally valid.

In addition to the three above-mentioned mechanisms there is still another possibility. It is the acceptance of the electron by a free, but not stable, inner orbital as the first step of the electrode process, with subsequent rearrangement of electron shells and ligands.

These rules are only a primary rough description of possible mechanisms of electrode processes. A detailed study of this problem, especially the influence of the stereochemistry of complexes, of external conditions (temperature, solvent, composition of solution), and of potential of electrode is in progress in the discussor's laboratory.

Agreement of the theoretical and experimental slope on logarithmic analysis of polarographic curves is by no means a proof of reversibility of the electrode reaction concerned. A reversible process has to satisfy these three conditions: (*a*) equality of the half-wave potential of the cathodic and anodic waves of the supposed electrode reaction; (*b*) agreement of this half-wave potential (extrapolated to zero ionic strength) with the normal electrolytic potential; and (*c*) agreement of the theoretical and experimental slope on logarithmic analysis of the curve.

E. H. Lyons: A number of exceptions to the rule proposed were cited,[4] and a thermodynamic basis for them was suggested. The most prominent are the six metals of the platinum group; mechanism 2*c* of Vlček appears to explain this deposition. Again, deposition of nickel from the inner orbital cyano complex at the dropping mercury electrode[6] was ascribed to the properties of the amalgam; except for "flash" deposits, deposition at a solid cathode appears to be confined to solutions also containing hexacyanoferrate (II)[7] or similar ions, a study of which is in progress in our laboratories.

Furthermore, it is not always easy to determine whether a complex ion is inner or outer orbital. According to Taube,[8] covalent (as opposed to ionic) nature of the bonds is not a reliable criterion; neither color, magnetic susceptibility, nor structure appear to be entirely trustworthy. In some instances, the free energy of the inner orbital configuration is so close to that of the outer that mobile equilibrium is established and appreciable quantities of both states are present simultaneously. Deposition of copper from the salicylaldehydediimino ion and certain others[9] may result from such a circumstance.

Besides ions characterized by rates of substitution and certain other data discussed by Taube, it is certain only that where no vacant inner orbitals exist prior to coordination, there can be no inner orbital complex. Thus, with metals such as zinc and cadmium, only outer orbital ions are formed. However, it is probable that certain structures

This Discussion Section includes discussion of papers appearing in the Journal of The Electrochemical Society, 101, No. 7–12 (July–December 1954). Discussion not available for this issue will appear in the Discussion Section of the December 1955 Journal.

[1] Polarographic Institute of Czechoslovakia, Academy of Sciences, Prague, Czechoslovakia.

[2] J. Heyrovský, *Collection*, Suppl. II, 1954. In press.

[3] W. F. Libby, *J. Phys. Chem.*, **56**, 39 (1952).

[4] E. H. Lyons, Jr., *This Journal*, **101**, 363 (1954).

[5] A. A. Vlček, *Collection*. In press.

[6] Y. P. Hokhshtein, *J. Gen. Chem. U. S. S. R.*, **7**, 2486 (1937).

[7] L. E. Stout and J. Carol, *Trans. Electrochem. Soc.*, **58**, 357 (1930).

[8] H. Taube, *Chem. Rev.*, **50**, 69 (1952).

[9] M. Calvin and R. H. Bailes, *J. Am. Chem. Soc.*, **68**, 949 (1946).

are not suitable for electrodeposition. For example, the phthalocyanine complex does not exchange zinc appreciably with the aquated ("free") ions,[10] and it may be supposed that zinc will not be electrodeposited from similar complexes having substituted groups to confer solubility. Similar considerations should apply to porphyrins, porphyrazines, and other "fused-ring" structures.[11]

Furthermore, the rule does not explain the failure of magnesium and aluminum to give deposits from aqueous solutions, although this failure would be expected from other considerations.

Nevertheless, the rule holds in so many instances as to be of general utility, particularly at solid cathodes. Thus, it led to the suggestion[4] that certain copper (II) ions are outer orbital even though of square planar configuration, a view supported only by magnetic evidence[12] the interpretation of which was not entirely clear; quite recently infrared absorption spectra[13] have shown that the ions are almost certainly outer orbital, in accordance with the rule.

A. H. Du Rose[14]: Mr. Lyons is to be commended for this presentation. More of this type of study will eventually lead to a much better understanding of electrochemical phenomena.

The statement was made that only an ultra-thin deposit of nickel could be obtained from a cyanide solution. I wonder if any nickel at all could be obtained from a very pure cyanide nickel solution. Our experience is that it cannot. If, however, a small amount of copper cyanide is added, a white deposit can be obtained, possibly because the resulting deposit is a solid solution of nickel and copper. How would the fact that nickel can be fairly easily deposited along with copper from a cyanide solution fit in with your theory?

E. H. Lyons, Jr: Our experience agrees with the remarks of Dr. Du Rose, but is not sufficiently extensive for a categorical statement that deposits cannot be obtained from pure baths. A number of such ultra-thin deposits which we have termed "flash" deposits, are doubtless alloy deposits with unrecognized impurities.

Deposition of iron, nickel, and copper as constituents of alloys from cyanide baths was reported some years ago.[15] Alloy deposits of molybdenum[16] and tungsten[17] have also been obtained, although pure deposits of these metals are unknown from any baths. Apparently in alloys the free energy of the metal is low enough so that deposition is possible. Deposition may occur because the strength of the coordinate bonds is altered by formation of heteronuclear complex ions. An investigation of this point is projected.

[10] D. C. Atkins, Jr., and C. S. Garner, *ibid.*, **74**, 3527 (1952).

[11] S. Ruben, M. D. Kamen, M. B. Allen, and P. Nahinsky, *ibid.*, **64**, 2297 (1942).

[12] P. Ray and D. N. Sen, *J. Indian Chem. Soc.*, **25**, 473 (1948).

[13] D. N. Sen, S. Mizushima, C. Curran, and J. V. Quagliano, *J. Am. Chem. Soc.*, **77**, 211 (1955).

[14] Harshaw Chemical Co., Cleveland, Ohio.

[15] L. E. Stout, O. G. Busch, and A. S. Langsdorf, *Trans. Electrochem. Soc.*, **57**, 113 (1930); L. E. Stout and J. Carol, *ibid.*, **58**, 357 (1930); L. E. Stout and C. L. Faust, *ibid.*, **60**, 271 (1931), and **64**, 271 (1933); C. L. Faust and G. H. Montillon, *ibid.*, **65**, 361 (1934).

[16] W. P. Price and O. W. Brown, *ibid.*, **70**, 425 (1936).

[17] M. L. Holt, *ibid.*, **66**, 453 (1934); *ibid.*, **71**, 301 (1937).

CORROSION OF ALUMINUM IN POTASSIUM CHLORIDE SOLUTIONS

I. Effects of Concentrations of KCl and Dissolved Oxygen

W. Beck, F. G. Keihn, and R. G. Gold (pp. 393–399)

M. E. Straumanis[18]: It is a real satisfaction to learn that all the phenomena observed during your careful work can be explained by the action of local elements.

In your numerous experiments, the presence of hydrogen peroxide could not be proven. However, the presence of this peroxide, evidently formed during corrosion processes, has been found by some other authors. How do you explain this contradiction?

W. Beck: The authors could not detect H_2O_2 under the experimental conditions already described. This is not proof that H_2O_2 is not formed during the corrosion of other metals and Al alloys under different experimental conditions.

F. A. Champion[19]: I have read with interest the paper by Beck, Keihn, and Gold. Their work adds most useful information on the subject, but it is unfortunate that some of their results have been analyzed on a false basis. They adopted the expression $w = at^n$ which Streicher observed for the dissolution of aluminum in sodium hydroxide solutions, and it is not surprising that they did not obtain a good fit with their results as indicated by the need for three slopes in their log/log plot. The asymptotic character of their w/t plots supports the expectation that the alumina film is playing a more important role in these chloride solutions. I suggest that the parameters of the exponential expression observed under such conditions[20] would provide a sounder basis for the analysis of the present results.

W. Beck: In the past many different mathematical expressions have been used to represent corrosion rates. The second part of this paper, which is concerned with the accleration of the corrosion rate of Al by the addition of H_2O_2 to KCl solutions, will discuss this corrosion rate in greater detail. The authors appreciate Dr. Champion's suggestion which will be considered in a new analysis of the results.

ELECTROCHEMICAL POLARIZATION OF ZIRCONIUM IN SODIUM CHLORIDE SOLUTION

Norman Hackerman and Olin B. Cecil (pp. 419–425)

Walter Beck[21]: The writer of this discussion was engaged in a study of the electrode potential and corrosion

[18] School of Mines and Metallurgy, Department of Metallurgy, University of Missouri, Rolla, Mo.

[19] Research Labs., The British Aluminium Co., Ltd., Chalfont Park, Gerrards Cross, Bucks., England.

[20] *Trans. Faraday Soc.*, **40**, 593 (1945); *Corrosion*, **5** (3), 92 (1949).

[21] Department of Metallurgy, Syracuse University, Syracuse, N. Y.

behavior of various borides of Zr and Mo, produced by powder metallurgy, by the American Electrometal Corporation in Yonkers, New York. He also made electrode potential measurements on pure Zr (Foote Mineral Company). Cylindrical specimens were immersed in a 0.1*N* KCl solution at 30°C under normal atmospheric conditions. In agreement with Dr. Hackerman's observations, it had been found that the potential of Zr increased very rapidly in cathodic direction during an initial period, which was short as compared with the total time of immersion of 200 hr. The potentials became stationary at −75 mv on the 1*N* $Hg2Cl_2$ scale. The electrode potential behavior of intermetallic compounds between Zr and B was completely different from that revealed by the pure Zr and was strongly influenced by the number of B atoms present in the compound.

HYDROGEN OVERVOLTAGE ON BRIGHT PLATINUM

II. *p*H and Salt Effects in Acid, Neutral, and Alkaline Solutions

Sigmund Schuldiner (pp. 426–432)

MORRIS EISENBERG[22]: If I recall correctly your H_2-overvoltage curves have shown a change to a larger slope (0.12) in alkaline solutions at current densities of about 10 ma/cm² and more. You have attempted to explain this by postulating another H_2-evolution reaction for the alkaline solutions. Wouldn't it be worthwhile to consider the effect of the concentration gradient which, for a given applied current density, would be larger in case of an alkaline solution than in case of an acidic solution. The resulting additional overpotential so-called concentration polarization can be expressed as

$$\Delta E_{\text{conc}} = \frac{RT}{n\mathbf{F}} \ln \frac{(H^+)_i}{(H^+)_o} = \frac{RT}{n\mathbf{F}} \ln \left(\frac{I_L - I}{I_i} \right)$$

where $(H^+)_i$ and $(H^+)_o$ are the H^+—concentration at electrode surface and in bulk, I_L—limiting current density, I—applied current density.

You have compared curves for acids and alkalies within the same regions of applied current densities. Since in alkalies $(H^+)_o$ and, therefore, also I_L are low, then, for a given value of I, concentration polarization would become more significant and account for progressively higher total values, hence a larger slope.

While I do not exclude the possibility that other (e.g., catalytic) effects may also be involved, in this case I would like to submit for your consideration the above argument for a possible re-examination of your data for H_2-overvoltage in alkaline solutions.

S. SCHULDINER: Dr. Eisenberg's comments are largely covered in the discussion by Stern and the reply given below. In alkaline solutions, only one hydrogen producing mechanism was postulated (water reduction).

MILTON STERN[23]: This paper is a most welcome contribution to our present growing knowledge of overvoltage phenomena. Some comments are in order both to supplement the information presented and to discuss terminology and interpretation.

[22] Stanford Research Institute, Stanford, Calif.

[23] Metals Research Labs., Electro Metallurgical Co., Niagara Falls, N. Y.

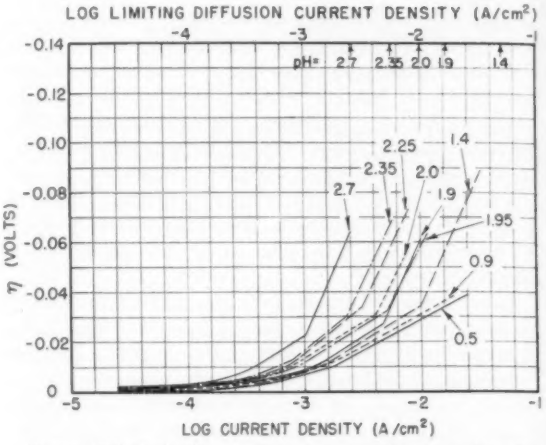

FIG. 3. Effect of *p*H on hydrogen overvoltage in acid solutions.

Since the experiments under consideration were conducted "in vigorously agitated solutions to minimize concentration overvoltage" one might assume that the use of η implies that only activation overvoltage (η_a) is involved in the reported polarization phenomena. This obviously need not be true at higher current densities, and one may estimate the current density where concentration overvoltage (η_c) will become a significant factor. For the experimental conditions used to obtain the data of Fig. 3, where the transference number of hydrogen ions may be neglected, one may use the following expression[24, 25] which relates the limiting diffusion current for hydrogen ions to their activity.

$$i_L = \frac{\eta F D}{\delta} \alpha_{H^+} \qquad \text{(I)}$$

D is the diffusion coefficient for hydrogen ions estimated here as averaging 7 (10^{-5}) cm²/sec, δ is the thickness of the diffusion layer which is approximately 0.005 cm in a vigorously stirred solution, and the other symbols have their usual meaning.

Limiting diffusion currents, so calculated for the *p*H values used, are superimposed on the original Fig. 3 and indicate that the measurements are in the range where concentration overvoltage (η_c) should be considered. The dependence of η_c on current density may be approximated[24, 25] by the following equation:

$$\eta_c = 0.059 \log \frac{i_L - i}{i_L} \qquad \text{(II)}$$

which indicates that concentration overvoltage starts to become significant when the current reaches the order of one-tenth the value of i_L.

Concentration overvoltage, which is time dependent

[24] J. N. AGAR AND F. P. BOWDEN, *Proc. Roy. Soc.*, **169A**, 206 (1938).

[25] C. W. TOBIAS, M. EISENBERG, AND C. R. WILKE, *This Journal*, **99**, 359C (1952).

upon initial application of current, can also account for the reported inconsistency of results in the *p*H range 2.7 to 7.1 where this effect would be pronounced at much lower current densities.

The hypothesis of two parallel hydrogen-producing reactions

$$(H_3O)^+ + e \rightleftarrows H + H_2O \qquad (III)$$

and

$$H_2O + e \rightleftarrows H + OH^- \qquad (IV)$$

appears to be quite sound. However, it is surprising to find a sharp, distinct change in mechanism which the author indicates takes place at the overvoltage (activation) where the Tafel slope changes abruptly from 0.029 to 0.12. Rather, one might expect deviation from Tafel behavior because of concentration overvoltage when depletion of hydrogen ions occurs. This behavior may be expressed by the relation

$$\eta = \eta_a + \eta_c = -\alpha - \beta \log i + 0.059 \log \frac{i_L - i}{i_L} \qquad (V)$$

Above the limiting diffusion current, Tafel behavior may again occur when reaction (IV) becomes controlling. Unfortunately, measurements presented on Fig. 3 at any given *p*H appear to have been stopped just short of the currents required to determine whether deviation from a slope of 0.029 truly results in another Tafel slope, or is actually that predicted when concentration polarization is considered. Placing of experimental points on Fig. 3 would be helpful in this direction. Why were the measurements not carried out to higher current densities?

Quantitative measurements[26] conducted at the Corrosion Laboratory, M.I.T., with iron and qualitative tests with smooth platinum show that deviation from Tafel behavior does occur at current densities which can be estimated from equations (I) and (II). The controlling Tafel regions for the two hydrogen-producing reactions discussed above are separated by a nonlinear region of concentration overvoltage resembling the limiting diffusion current behavior observed in polarography. Between *p*H values of 3 and 6, concentration overvoltage masks all signs of a Tafel region below the limiting diffusion current, and only one truly linear region exists.

S. Schuldiner: Experimental results given in the above paper and in part I[27] indicate a sharp change from the first to second Tafel slopes with no substantial intermediary region. Experimental points are shown in part I. The same spread of points was observed in the above paper. Current densities given in these papers represent maximum values obtainable under the experimental conditions used. This was owing to either instrumental limitations or erratic results at higher current densities.

King[28] has plotted concentration overvoltage against log current density for various solutions. His curves show that a current density range in which a 0.12 slope could be drawn would be much smaller than the actual current density ranges shown for this slope in these papers.

In the table below a typical set of data is applied to Stern's equation (II). Here the curve for *p*H 2.7 shown in the above figure (Fig. 3) was used in the calculation. The i_L, as calculated by Stern, for this case is 0.00263 amp/cm².

Current density, i (amp/cm²)	η_c (v)	$\eta_{expt.}$ (v)	$\eta_a = \eta_{expt.} - \eta_c$ (v)
0.00100	−0.012	−0.022	−0.010
0.00159	−0.024	−0.042	−0.018
0.00200	−0.037	−0.052	−0.015
0.00229	−0.053	−0.060	−0.007
0.00251	−0.079	−0.062	+0.017

These results show that after reaching a peak, the activation overvoltage, η_a, declines with increasing current density and that the calculated concentration overvoltage actually exceeds the measured overvoltages when i_L is approached. This clearly shows that equation (II) does not apply for this system.

CRYSTAL STRUCTURE AND THERMODYNAMIC STUDIES ON THE ZIRCONIUM-HYDROGEN ALLOYS

Earl A. Gulbransen and Kenneth F. Andrew
(pp. 474–480)

James C. Warf[29]: You mentioned the use of a McLeod gauge in measuring dissociation pressures. Several authors refer to the influence of traces of mercury on the dissociation pressure of hydrides, suggesting that spurious and erratic behavior may result, possibly via poisoning of the surface.[30] Is there any evidence that mercury vapor from the McLeod affected the dissociation pressure of the zirconium hydride?

E. A. Gulbransen and K. F. Andrew: Mercury vapor could have a very important influence on the pickup of hydrogen by zirconium. In the apparatus used for this study, the McLeod gauge was separated from the specimen by a liquid nitrogen cold trap. The reversible character of the dissociation process is proof for the absence of any poisoning due to mercury vapor.

DETERMINATION OF BARRIER LAYER THICKNESS OF ANODIC OXIDE COATINGS

M. S. Hunter and P. Fowle (pp. 481–485)

C. J. L. Booker and J. L. Wood[31]: The September 1954 issue carries an account by M. S. Hunter and P. Fowle of a method for the determination of the barrier layer thickness of anodic oxide coatings. This is a problem in which we are particularly concerned, and a few comments may be of interest.

The method described depends on the assumption that

[26] M. Stern, Unpublished work, Corrosion Lab., Massachusetts Institute of Technology, Cambridge, Mass.

[27] S. Schuldiner, *This Journal*, **99**, 488 (1952).

[28] C. V. King, Private communication.

[29] Department of Chemistry, University of Southern California, Los Angeles, Calif.

[30] Viallard, *Ann. Chim.*, **20**, 5 (1945); Ubbelohde, *J. Chem. Soc.*, **1950**, 1943.

[31] Sir John Cass College, Jewry St., Aldgate, England.

the current carrying characteristics of porous and barrier type coatings are comparable. Although on experimental grounds there is reason to believe that this is approximately true, two important limitations should be borne in mind. First, the effective area determining the current density flowing across a porous layer is that of the base of the pores—only a few per cent of the superficial area. Second, it is well known that the leakage current through barrier layers is highly dependent on the incorporation of impurities in the layer. In particular, the material around the bases of pores formed in acid electrolytes may differ considerably in both chemical and electrical properties from that of barrier layers prepared in neutral electrolytes.

In the course of research on the capacity of porous layers we have developed independently a number of methods providing information of the pore base dimensions. One that may be compared to that of Fowle and Hunter is as follows: the discharge current-voltage curves of a condenser with a porous aluminum oxide layer as dielectric are found to be similar to those obtained by Charlesby[32] for barrier oxide layers. In particular, the current is given by

$$i = A_+ \exp(B_+F) + A_- \sinh(B_-F)$$

where the first term refers to the ion current and the second to the electron current, and F is the field across the dielectric. This relation may also be confirmed directly. These results indicate that pore bases are comparable in conducting properties with an equivalent area and thickness of barrier oxide.

The value of F directly gives the pore base thickness, while, in principle, the pore base cross section could be determined from A_- or A_+. However, no reliable figures for these constants in the case of barrier layers are available for comparison.

As an example, for a porous layer formed by anodizing for 30 min in 17.5% v/v sulfuric acid at 17°C with a controlled current density of 40 ma/cm², the thickness of the pore bases is 85 Å. A_- is small, 0.0004 μa/cm², consistent with the small cross-sectional area of the pore bases.

M. S. Hunter and P. Fowle: The determination of barrier layer thickness from the discharge current-voltage curve of a condenser is an interesting method of establishing this dimension of anodic oxide coatings. Of particular interest is the conclusion from this work that pore bases and barrier oxide have comparable conducting properties.

We do not believe that our method of determining barrier layer thickness depends on the current carrying characteristics of the oxide, because voltage rather than current is measured, and because the effect of leakage is eliminated by first establishing the leakage current for the metal or alloy under consideration. It is true that the current carrying characteristics of the coating are important during formation of the coating when appreciable current flows but, in the case of our thickness measurement, current flow is so low as to be insignificant. Further, we do not believe that the relatively small cross-sectional area of the pores is of significance because practically no current is flowing during our measurement and, accordingly, no current density effects are involved. Both current carrying characteristics and relative pore area would be significant in a method which involved measurement of current in determining barrier thickness.

[32] Charlesby, *Proc. Phys. Soc. B*, **66**, 317, 533 (1953).

THE *p*H IN CHLORINE-CAUSTIC ELECTROLYSIS BY THE MERCURY CELL PROCESS

Lars Barr (pp. 497–506)

Patrizio Gallone[33]: This paper gives a clear theoretical demonstration of the benefits to be found in feeding mercury cells with slightly acidic brine. This is, in fact, the procedure long since adopted in de Nora mercury cell plants. In addition to the advantages shown in the paper (smaller percentages of CO_2 and H_2 in cell gas, longer anode life, practically no chlorate formation), another important benefit given by an acidic *p*H is that it is possible to keep calcium at a concentration even higher than 1 g/l without any formation of "mercury butter."

Another point I would like to take up in this important paper is the method of calculating cathodic current loss. In equation [39] that is thus derived, this loss is expressed as a function of *p*H values in the bulk of the brine and at the alkaline cathode film, respectively. Therefore, the author makes the statement that the cathodic current loss "is independent of current density." It is now to be remarked that, although theoretically correct, this statement seems to contradict experimental evidence since usually the hydrogen per cent in cell gas, i.e., cathodic current loss, decreases when current density is increased. This is because the *p*H at the cathode film is itself a function of current density; in fact, if current density is increased, although other conditions are kept equal (cell temperature, *p*H in feed brine, mercury flow rate), the *p*H at the cathode film will decrease, so that the migration of OH^- ions from the cathode will also diminish and the current efficiency will be improved, according to equation [39]. That the *p*H value at the cathode film should decrease when increasing the current density can be immediately seen from equation [36]. In fact, in order to obtain an increase in the current density, the cathode potential e_k must be depressed, even though but slightly, so that the "affinity" will be increased for all reduction reactions occurring at the cathode and, therefore, the hydrogen discharge rate will become higher. However, the hydrogen overvoltage, i.e., function $f_3(i)$ in equation [36], rises so steeply with hydrogen current density that the second term on the right side must also increase, which involves a decrease in the *p*H value at the cathode film.

Lars Barr: The remarks from Patrizio Gallone provide an interesting discussion.

Demonstrating relationship between anolyte *p*H and current efficiency should be done by investigating the relation between *p*H (composition of solution) and various current density-voltage curves at the electrode concerned.

Unfortunately, the symbol "i" in my paper refers to different current densities, which has caused a defect in

[33] Oronzio de Nora, Impianti Elettrochimici, Milan, Italy.

some equations. I am, therefore, anxious to make corrections here.

Equation [36] represents the current density (c.d.)-voltage curve of hydrogen discharge, and here i means the hydrogen c.d., which at constant total c.d. can be considered proportional to hydrogen pressure in cell gas or to $\{H_2(g)\}$ at the cathode film under equilibrium conditions. Differentiating equation [36] in order to obtain equation [37] should accordingly include differentiating $f_3(i) = a + b \ln i$. We arrive thus at equation [37] with another constant:

$$d \log \{H_2(g)\} = -(\text{a positive constant})\ d\ p\text{H}$$

In the same way there should be another positive constant than 4 in equations [24] and [25] concerning the anode.

However, the results of my calculations are not affected by these discrepancies.

Dr. Gallone's remark concerning equation [39] is correct. My remark under equation [39] was only intended to point out that the equation in question is independent of its i. Here i means total c.d.

It has been shown experimentally that cathodic current efficiency in a mercury cell increases when total c.d. is increased and approaches an asymptote near 100% efficiency.[34] This can be roughly explained by reaction [30] being reversible and reaction [32] polarized.

I think that pH at the cathode film should be a function both of loss c.d. and total c.d., loss c.d. governing the rate of feeding the film with OH^- ions, total c.d. governing the rate of emptying the film of OH^- ions. This function also contains room dimensions and concentration gradients.

Conditions at electrode films are complicated and likely to demand advanced scientific treatment.

I think, however, that Dr. Gallone has given here a good simple picture of this matter at the mercury cathode.

M. S. Kircher[35]: This paper is of considerable interest to the writer since he made a similar study on the relationship between anolyte pH and current efficiency in the diaphragm type cell.[36] The derivation of the relationships between anolyte pH and log of the activity of H_3O^+, ClO_3^-, HClO, ClO^-, Cl_2, Cl_3^-, H_2CO_3, CO_3^-, OH^-, HCO_3^-, and Cl^- and the plotting of these relationships in Fig. 1, 2, and 3 was elegantly done.

From Dr Barr's paper, one might conclude that good cell operation can be obtained by adjusting the brine pH to maintain an anolyte pH of 3, whereas it is our experience that, if cells are operated properly, a pH of approximately 3 will result. In other words, the performance of a cell depends on factors other than anolyte pH and the anolyte pH is an indication of the quality of performance.

The anolyte of either a mercury or diaphragm cell operating under steady-state conditions may be regarded as a reservoir into which OH^- ions are continuousiy being introduced and from which OH^- ions are continuously being discharged at the anode. Excepting to the extent which the OH^- ions enter into chemical reactions such as the formation of ClO_3^-, the rate of OH^- ion discharge is equal to the rate of OH^- ion feed and the $O_2 + CO_2$ content of the chlorine gas is equivalent to the OH^- ion introduced into the anolyte. The pH of the anolyte depends primarily on the character of the anode (the anolyte pH would be different if, for instance, carbon or platinum anodes were used) and, secondarily, on the rate at which OH^- ion is passing through the anolyte reservoir.

The source of OH^- ions entering the anolyte reservoir may be (*a*) the brine feed, (*b*) back migration of OH^- ion through the diaphragm (diaphragm cell), (*c*) OH^- ion formed at the mercury cathode coincident to hydrogen formation (mercury cell).

With graphite anodes and with normal operation, the pH of the anolyte of either diaphragm or amalgam cells is approximately 3 (range of 2.5–4.5), and the pH of the anolyte is practically unaffected by a change in feed brine pH from 3 to 8. Only when the acid or alkali in the feed brine is equivalent to a substantial proportion of the total current efficiency (such as 1–2%) will an appreciable effect on anolyte pH be noted.

I believe these concepts are in agreement with Dr Barr's although presented somewhat differently. I should be interested in his comments.

Lars Barr: I have read Dr Kircher's discussion with great interest. His experiences are in accordance with my own.

The purpose of my calculations is only to demonstrate the relation between anolyte pH (concentration in anolyte of certain protolytes) and current efficiency. In chlorine-caustic electrolysis such a relation must exist theoretically. This relation ought to be open to laboratory studies where all other current efficiency determining variables, e.g., anode, temperature, current density, salt concentration, are kept constant.

If in practice current efficiency is low, for instance, because of an unsuitable anode material, we cannot of course obtain good cell performance by adjusting the brine pH. Also in this case, however, the result of my calculations should be valid, i.e., with this anode material the highest possible current efficiency will be obtained below an anolyte pH of 3. In adjusting feed brine composition this anolyte could be aimed at.

FACTORS AFFECTING THE FORMATION OF ANODIC OXIDE COATINGS

M. S. Hunter and P. Fowle (pp. 514–519)

Robert Pinner[37]: The very interesting paper by M. S. Hunter and P. Fowle has recently come to my attention. One is indebted to these and other authors of the Research Laboratories of the Aluminum Company of America for much excellent work on the theory of anodic film growth on aluminum. Some comment, perhaps, is called for on their statements on p. 517 under the heading "Conditions Existing at Pore Bases." Here, the authors conclude that

[34] R. Taussig, *Trans. Faraday Soc.*, **5**, 258 (1909–10).
[35] Hooker Electrochemical Co., Niagara Falls, N. Y.
[36] R. L. Murray and M. S. Kircher, *Trans. Electrochem. Soc.*, **86**, 83 (1944).
[37] Electroplating and Metal Finishing, 85 Udney Park Rd., Teddington, Middx., England.

the dissolution rate, R, of the film at the pore base is proportional to current density, C, according to: $R = 310C$.

They base this on the assumption that dissolution rate at the barrier layer must balance film growth at this point because barrier thickness remains constant. From this the authors calculate that, in anodic oxidation of aluminum in 15% sulfuric acid, the acid concentration and temperature in the pore base must approximate 51% H_2SO_4 at bp of 128°C, in order to account for the high dissolution rate.

There is, in fact, no reason to assume a linear relation between current density and dissolution rate. Barrier thickness remains a more or less constant function of voltage, not because its growth is balanced by dissolution at the pore base, but because growth is balanced by break-through and conversion into porous type coatings.

The dissolution rate suggested by Hunter and Fowle as required to balance growth is, in fact, the dissolution rate not only of the barrier layer but also of the total coating (barrier plus porous coating) and even this only when the limiting total film thickness has been reacted. Of this total dissolution much the greater part will, of course, take place at or near the surface of the porous layer.

In view of the limited solubility of aluminum in 50% sulfuric acid and the necessarily very slow diffusion of Al ions from the pore base through the coating into the electrolyte, the very high rate of dissolution at the pore base could not be maintained at any rate, while, on the other hand, conditions for equilibrium between growth and rate of dissolution at the barrier layer only apply when no porous type of coating is formed as, e.g., in boric acid or ammonium tartrate electrolytes. It should be stated that this does not detract from the important part played by local rise in temperature inside the coating due to the dissipation of electric energy (with the heat of formation of aluminum oxide as a contributory factor). This temperature differential between electrolytes in the film and the bulk of the solution has been somewhat surprisingly ignored in many of the previous theories on anodic film growth.

M. S. Hunter and P. Fowle: The linear relationship between solution rate and current density during the formation of the porous type of anodic oxide coatings may appear to be illogical because oxide formation, which is a function of current density, is an electrochemical process; whereas, solution of oxide is primarily a chemical process. Our measurements show, however, that the thickness of oxide between the pore base and the metal (barrier thickness) remains constant once current density has reached a steady value. Since the total thickness of oxide must equal barrier thickness plus the depth of the pores, and since barrier thickness is constant, the thickness of oxide formed in any period of time must equal the amount by which the depth of the pores is increased during this same period. Thus, the linear relationship between solution rate and current density is an established fact, unreasonable as it may seem.

We are not in agreement with the explanation that the constancy of barrier thickness is the result of a balance between growth and break-through, since our concept of the mechanism of the formation of porous type coatings is based on the existence of a continuous layer of oxide in contact with the metal at all times. This has been discussed in previous papers.[38, 39]

We are somewhat puzzled by Mr. Pinner's statement that equilibrium between growth and rate of solution only applies when no porous type of coating is formed, as is the case in boric acid or ammonium tartrate electrolytes. In the formation of nonporous or "barrier type" coatings such as those formed in the electrolytes cited, rate of solution is not involved, because the prime requisite for the formation of this type of coating is that the electrolyte shall have no solvent action on the oxide. If the electrolyte can dissolve the oxide, a porous type of coating will be formed.

DIFFUSION OF HYDROGEN AND DEUTERIUM IN HIGH PURITY ZIRCONIUM

Earl A. Gulbransen and Kenneth F. Andrew (pp. 560–566)

Morris Eisenberg[40]: I feel that this is indeed a very nice piece of work. I would like to comment with one question. You said at the outset that you assumed the diffusion coefficient to be independent of hydrogen concentration. Under such conditions obviously your values represent integral average diffusion coefficients. Now wouldn't it be possible to start with specimens of various initial hydrogen contents and, by experimenting within various concentration gradients, to obtain the dependence of D on the concentration of hydrogen or deuterium in zirconium metal?

E. A. Gulbransen and K. F. Andrew: The integral average diffusion coefficients are obtained in this study for hydrogen in the δ and ϵ hydride phases and not for the α-zirconium phase. It would be very difficult to determine these coefficients as a function of concentration.

The diffusion coefficient of hydrogen in the metallic phase can be studied as a function of concentration. Thus, if one considers the removal of hydrogen at temperatures above 400°C, where the solubility in α-zirconium is appreciable, it would be possible to determine the effect of concentration. This would be an interesting study.

HIGH TEMPERATURE CRYSTAL STRUCTURE OF THORIUM

P. Chiotti (pp. 567–570)

James C. Warf[41]: Thorium metal ordinarily contains some oxide. What can you say about the constitution of this oxide in thorium at room temperature? Does the metal consist of two phases?

P. Chiotti: The thorium metal used in this investigation initially contained approximately 0.10 wt % oxygen.

[38] M. S. Hunter and P. Fowle, *This Journal*, **101**, 481 (1954).

[39] F. Keller, M. S. Hunter, and D. L. Robinson, *ibid.*, **100**, 411 (1953).

[40] Stanford Research Institute, Stanford, Calif.

[41] Department of Chemistry, University of Southern California, Los Angeles, Calif.

At room temperature the oxygen is present as ThO_2 which appears as a gray phase in the microstructure. The oxide is face-centered cubic and its lattice constant corresponds very closely to that for pure ThO_2, indicating no appreciable solubility of the metal in this compound. The solubility of the oxide in the metal is also considered to be very small or negligible at room temperature.

ANODIC BEHAVIOR OF COPPER IN HCl

Lee Stephenson and J. H. Bartlett (pp. 571–581)

N. Ibl and R. Muller[42]: We were particularly interested in this paper since we are engaged in an interferometric study of the diffusion layer at electrodes. In the course of this work some experiments were also made with Cu-anodes in 2*N* HCl which confirm the results of Stephenson and Bartlett. In the method[43] used by us a curve is obtained on the photograph which gives directly the function refractive index vs. distance from the electrode. Immediately after the electrolysis current starts to flow a refractive index continuously decreasing toward the electrode is observed, showing that a depleted layer of HCl is formed; after about 2 sec the curve of the refractive index is bent upward near the electrode surface and now exhibits a sharp minimum, indicating that a dissolution process is going on.

We would like to mention that we made quite similar observations with a Cu-anode in 2*N* H_2SO_4 (formation of a depleted layer in the first stages of the electrolysis; sharp minimum of the curve refractive index vs. distance from the electrode, when the electrolysis has been going on for more than about 2 sec). A Cu-anode in 0.6*M* $CuSO_4$, however, showed a different behavior. In this case a layer more concentrated than the bulk of the solution is formed near the electrode surface right at the beginning of the electrolysis and this situation remains the same later on, unaffected by time. Current density in both cases was 200 ma/cm².

Ralph S. Cooper[44]: In the article by Stephenson and Bartlett the total charge which has flowed during the first current plateau is expressed by a relation of the form $Q = a(i_o - b)^{-c}$, where b is given the value 0.70. In graphs of this form b is determined by adjusting it to remove the curvature in a log Q vs. log i_o plot. However, data presented in the article are too scattered to evaluate b with any degree of precision, and no distinct curvature can be observed on a log-log graph even with $b = 0$.

Recent work at this laboratory has considerably improved the reproducibility of the data with the following results: the correlation of Q with i_o is found to be dependent on the external resistance R (Fig. 1), while log Q vs. log i_I (the current during the first plateau) yields a single curve for all R. This has the same form as the earlier relation, with $b = 0.54 \pm 0.02$ (Fig. 2).

[42] Department of Physical Chemistry, Swiss Federal Institute of Technology, Zurich, Switzerland.

[43] *See* N. Ibl, Y. Barrada, and G. Trümpler, *Helv. Chim. Acta*, **37**, 583 (1954).

[44] Department of Physics, University of Illinois, Urbana, Ill.

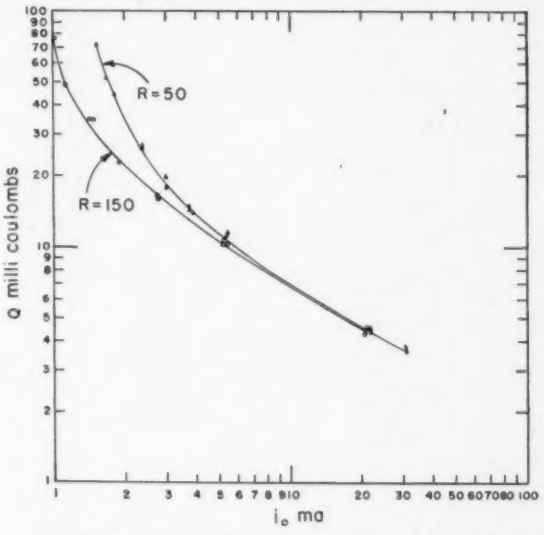

Fig. 1. Q as a function of i_o, showing R dependence.

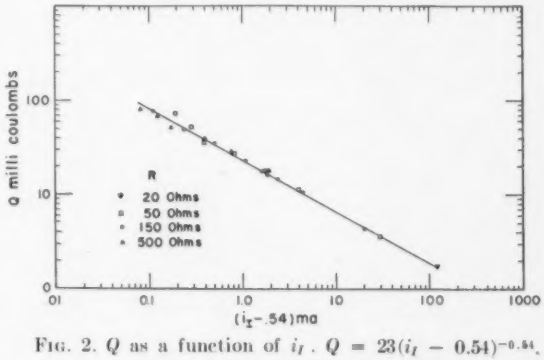

Fig. 2. Q as a function of i_I. $Q = 23(i_I - 0.54)^{-0.54}$.

In regard to the electrode reaction, theoretical calculations indicate that the reaction occurring during the first plateau is $Cu + 2Cl^- \rightarrow CuCl_2^- + e$. Details of this work will be published at a future date.

KILOGRAM SCALE REDUCTIONS OF VANADIUM PENTOXIDE TO VANADIUM METAL

Arthur P. Beard and Donald D. Crooks (pp. 597–600)

John C. R. Kelly[45]: In the powder metallurgy process, temperature at reaction centers in the reduction bomb can be computed by using Theoretical Flame Temperature methods. This calculation is verified by observing the proportion of fused beads to fine powder. This proportion varies with $CaCl_2$ content and, consequently, with the specific heat of the charge.

A. P. Beard and D. D. Crooks: A further use of the calculations of the theoretical maximum temperatures shows that the temperature in the V_2O_5 + Ca reaction should be much higher than the temperature in the V_2O_3 + Ca reaction. Therefore, better agglomeration of the

[45] Westinghouse Electric Corp., Bloomfield, N. J.

vanadium into massive pieces may be expected in the V_2O_5 reduction, and powder in the V_2O_3 reduction.

M. D. Banus[46]: What is the estimated temperature inside the liners during the reaction?

Are the high pressures which cause the explosions that burst the bombs due to the vapor pressure of Ca metal or to a gas evolved by the reaction?

A. P. Beard and D. D. Crooks: The temperature reached inside the bomb during a V_2O_5 + Ca reaction is greater than the melting point of vanadium metal (~1900°C). Calculations indicate a maximum temperature of ~3000°C. Estimated temperature inside the liners during the reaction is ~2500°C.

Explosions that burst bombs may result from the reaction mass burning through the steel bomb, because of a cracked liner or high pressures of hydrogen or nitrogen from water and ammonium ion, which were not removed during the ignition of ammonium vanadate to V_2O_5.

ROOM-TEMPERATURE DUCTILE CHROMIUM

H. Johansen and G. Asai (pp. 604-612)

Marvin L. Bromberg and Hugh B. Hix[47]: 1. Has any general relation been established between hardness and ductility?

2. Has there been found any significant difference in the properties of purified chromium prepared electrolytically and chromium prepared by chemical reduction? If there is, has any explanation been forwarded?

3. Has any evidence of a high temperature phase transformation been found?

4. Is sigma phase formation a serious problem in all Cr-Fe alloys?

H. Johansen and G. Asai: 1. If a larger tensile elongation value is to be considered as an indication of greater ductility, the softer material is more ductile. It has been shown that the ultimate tensile strength of chromium wires is increased by increased cold work. The tensile elongation has been found to decrease from 41% to 8% as the amount of cold work increases from 7% to 92%, respectively. Knoop hardness values increase from 122 to 230 for wires having no cold work and 92%, respectively.

2. No investigation of the properties of chromium produced by the magnesium reduction of chromous chloride ($CrCl_3$) has been undertaken recently and, therefore, no comparison can be made. However, there is no reason to expect any substantial differences from material prepared electrolytically.

3. No evidence of a high temperature phase transformation has been found.

4. Sigma phase formation in Cr-Fe alloys is not a serious problem here, but is certainly an item to be considered in Cr-Fe alloy work. Much work has been done here with Cr-base alloys varying in chromium content from 50 to 75%. Sigma phase formation at room temperature is very slow. Sigma phase formation during fabrication is evident but the formation is not of an extent to prevent successful working. Any sigma phase that is present in the final product is removed by heat treatment and quenching.

[46] Metal Hydrides Inc., Beverly, Mass.

[47] Pigments Department, Chemical Division, E. I. du Pont de Nemours & Co., Newport, Del.